THÈSE EN COTUTELLE PRÉSENTÉE

POUR OBTENIR LE GRADE DE

DOCTEUR DE L'UNIVERSITÉ DE BORDEAUX (UBX)

ET DE L'UNIVERSITÉ DU PAYS BASQUE (EHU/UPV)

ECOLE DOCTORALE DES SCIENCES CHIMIQUES DE L'UBX

SPÉCIALITÉ DE CHIMIE PHYSIQUE

ECOLE DOCTORALE DE BIOLOGIE MOLÉCULAIRE ET BIOMEDECINE DE L'UPV/EHU

Par Régine Dazzoni

Unravelling the role of Nuclear Membrane dynamics in the behaviour of cancer cells.

A multidisciplinary approach using cell biology, advanced imaging and biophysics

Sous la direction de Professeur Banafshé Larijani

et du Professeur Erick Dufourc

Soutenue le 19 Décembre 2019

Membres du jury:

Burkhard Bechinger, Professor University of Strasbourg, rapporteur
Michael Wakelam, Professor University of Cambridge, rapporteur
Agnès Girard-Egrot, Professor University of Lyon, examinateur
Sandrine Sagan, CNRS Research Director, Paris, Présidente
Felix Maria Goñi, Professor University of the Basque Country, examinateur
Antoine Loquet, CNRS Senior Researcher, Bordeaux, examinateur
Banafshé Larijani, Professor University of the Basque Country & University of Bath, examinateur
Erick J Dufourc, CNRS Research Director, Bordeaux & Paris, examinateur

A Aita y Ama

To my parents

A mes parents

Merci! Thanks! Gracias! Eskerrikasko!

su ayuda, amabilidad, y el sentido del humor que estaban muy importante por mi integración en este País Vasco.

Cell culture, microscopy, and molecular biology was a mystery for me before I went to Peter Parker lab. Thanks to Veronique, Gary, Marie-Charlotte et Julien for training me to all these techniques and to your availability during my thesis to answer to my questions.

J'aimerai également remercier ma collaboratrice Corinne Buré pour m'avoir fait partager son expertise de spectrométrie de masse dans la bonne humeur. Merci également pour ton implication dans l'écriture de notre article et des corrections apportées à ma thèse. Ce fut un plaisir de travailler avec toi.

Un grand merci aux membres de l'équipe d'Anthony Bouter pour m'avoir accueillie dans leur laboratoire. Flora, Céline, Coralie votre gentillesse et votre soutien m'ont énormément touché.

Cette thèse n'aurait pu se passer sans l'aide et le soutien de mes parents et amis. Merci d'avoir été présent dans les bons et mauvais moments. Un merci très spécial à mon frère qui m'a apporté une voiture après mon accident ! Un enorme gracias a los doctorandos del PiE y de Biofisika por todos los momentos que pasean juntos en el labo y fuera durante las salidas al Zua Zua, a la sidrería y también en Bilbao a comer pintxos. Me encanta también de conocer un poco de palabra vascos gracias a vosotros. Un grand merci spécialement pour toi Tifanie, ton grain de folie à égayer mes journées. Je n'oublierai jamais nos sorties surf surtout celle de Mundaka, MOUAHAHA. Mathilde, petite pipette, tu as été d'un précieux soutien et la meilleur de mes colloques ! Merci pour les petits plats chaud qui m'attendaient en rentrant du labo. Ces petites douceurs me sont allées droit au cœur. Claire et Laura merci de m'avoir accueillie chez vous à Bordeaux. Merci pour votre soutien inconditionnel et d'avoir supporté mes jérémiades sur ma thèse, d'avoir eu la gentillesse de me voir répéter mes présentations et d'avoir parcouru mes posters ! Julien, Antoine, Guillaume, Camille, Elise, Oriane, Emilien, Mark et Clémentine Merci pour les HH du jeudi soir. Même si je n'en ai pas fait beaucoup ils ont été une vrai bouffée d'oxygène ! Je n'oublie pas également mes amis parisiens qui même s'ils étaient loin m'ont toujours soutenu ! Anita, Léonore, Armelle, Margaux, Lorenzo, Aude, Emmanuelle, Arnaud, Ludovic… Merci d'être toujours là ! et promis après j'arrête mes études ! Mon petit Willy je ne t'oublie pas ! Malgré la distance on a toujours pu se voir régulièrement et ce grâce à toi ! j'ai loupé le Costa Rica mais je ne louperai pas NY promis ! J'aimerai maintenant remercier mes amis du gâtinais. Merci Léo (et sa famille) de m'avoir accueillie et de m'avoir fait partager ta passion du maraichage et de l'escalade. Ces deux activités m'ont permis de sortir la tête de l'eau quand j'en avais vraiment besoin. Merci à Charlotte, Charlie, Ian, Karouna, Lauraine pour les bons moments que l'on a partagés et pour vos encouragements.

Enfin Salim, merci d'être rentré dans ma vie tu es mon rayon de soleil. Cette thèse est maintenant terminée mais je vais regretter nos moments à travailler ensemble au coin du feu. Merci pour ton soutien ce n'est jamais facile de vivre avec une thésarde… J'attends avec impatience les bons moments que la vie nous réserve.

Maintenant merci à mes deux petits chats Goose et Saraphina pour leur douceur au quotidien !

List of abbreviations

ATP	Adenosine triphosphate
BHT	Bacteriohopanetetrol
CCTα	Choline phosphate cytidylyl-transferase
Chol	Cholesterol
CL	Cardiolipine
CMC	Critical micellar concentration
CSA	Chemical shift anisotropy
CTP	Cytidine triphosphate
DAG	Diacylglycerol
$DIOC_6$	3,3'- Dihexyloxacarbocyanine Iodide
DMEN	Dulbecco's modified eagle's medium
DMSO	Dimethylsulfoxide
DTT	Dithiotheitol
EFG	Electric field gradient
ePC	Ether Phosphatidylcholine
ER	Endoplasmic reticulum
Erg	Ergosterol
FBS	Fetal Bovine Serum
FID	Free induction decay
GUV	Giant unilamellar vesicle
H	Hexagonal phase
HEK	Humain embryonic kidney
HRP	Horseradish Peroxidase
HSQC	Heteronuclear Single Quantum Correlation
INEPT	Insensitive nuclei enhanced by polarization transfer
INM	Inner nuclear membrane
IS	Internal standard
KCl	Potassium chloride
Lα	Fluid phase
LAP	Lamina associated polypeptide
Lβ/β'	Gel phase
LBR	Lamin B receptor
Lo	Liquide ordered phase
LPA	Lysophosphatidic acid
LPC	Lysophosphatidylcholine
LPI	Lysophosphatidylinositol
LUV	Large unilamellar vesicle
MAS	Magic angle spinning
$MgCl_2$	Magnesium chloride
MLV	Multilamellar large vesicle
MRM	Multiple reaction monitoring
MS	Mass spectrometry
NE	Nuclear envelope
NERs	Nuclear envelope remnants
NMR	Nuclear magnetic resonnance
NPC	Nuclear pore complexe
NR	Nucleoplasmic reticulum
Nups	Nucleoporines
ONM	Outer nuclear membrane
PA	Phosphatidic acid
PBS	Phosphate buffered saline
PC	Phosphatidylcholine
PE	Phosphatidylethanolamine
PG	Phosphatidylglycerol
PI	Phosphatidylinositids
PIS	Precursor ion scan
PL	Phospholipids
PL	Protein ladder
POPC	Palmitoyl 2-oleoyl-sn-glycero-3-phosphocholine
PS	Phosphatidylserine
SB	Swelling buffer
SDS	Sodium dodecyl sulfate
SIT	Sitosterol
SM	Sphingomyeline
STI	Stigmasterol
SUV	Small unilamellar vesicle
TAG	Triacylglycerol
TBS	Tris buffered saline
Tm	Melting temperature
TOCSY	Total correlated spectroscopy
TPP	Triphenylphosphate
WGA	Wheat germ agglutinin

Abstract

Muscular dystrophy diseases, breast and kidney cancers are linked to malformation of the nuclear envelope (NE). Mechanisms involved in the maintenance of NE morphology are based on proteo-lipid interactions. Recently, the physical properties of specific lipids have highlighted their essential role in NE assembly process of the sea urchin model. To provide molecular insight in how the nuclear architecture is regulated, we used Mass spectrometry and Nuclear Magnetic Resonance (NMR) as quantitative methods to investigate the lipid composition and the dynamics of the NE. Nuclei extraction were performed from HEK 293T human kidney cells. A physical extraction based on pressure treatment and sucrose gradient was used and improved considerably the nuclei yield, resulting in obtaining a high quantity of intact nuclei (NE lipids) required for experiments, with a minimum of cell debris, or the ER and Golgi compartments. The nuclear lipids were then extracted from pure nuclei using a modified Folch method. Liquid-state NMR experiments showed that the NE is composed of a complex mixture of phospholipids and with phosphatitylcholine present in a higher proportion compared to other membrane organelles. Furthermore, an unusual proportion of phosphatidylinositol was found at the NE. Mass spectrometry experiments have shown that the composition of phospholipids is dominated by species with highly unsaturated chains with an average length of 34 carbons. Reconstructed nuclear lipid extract membranes were analysed by solid-state NMR and exhibit atypical physical properties. The lamellar gel-fluid phase transition temperature was found very low and broad at -10 ± 15°C, possibly due to the presence of numerous lipid species and unsaturated acyl chains. Furthermore, at 25°C, reconstructed nuclear lipid membrane was found to be more rigid than classical model membranes suggesting a larger bilayer thickness. Finally, reconstructed nuclear lipid liposomes have shown a very important prolate deformation in a magnetic field, which is unusual for biological membranes and suggests an important curvature elasticity for the membrane.

Resumen

Malformación de la membrana de núcleos esta observada en casos de distrofia muscular, así como en ciertos tipos de cáncer, como el de mama o el de riñones. Los mecanismos que intervienen en la integridad de esta membrana están controlados por las interacciones proteínas con lípidos. Hace poco, se ha demostrado que las propiedades físicas de lípidos específicos tienen una función esencial en el proceso de formación de la membrana de núcleos en el modelo del erizo del mar. Para comprender como la arquitectura de la membrana está regulada, utilizamos técnicas cuantitativas como la espectrometría de masa y la RMN para determinar la composición en lípidos de la membrana y sus propiedades dinámicas. La extracción del núcleo se realizó a partir de células renales humanas, HEK 293T. Se ha optimizado una extracción física basada en un tratamiento a presión y un gradiente de sucrosa para obtener una gran cantidad de núcleos intactos (lípidos de la membrana nuclear) necesarios para nuestros experimentos. Estos núcleos purificados incluyen un mínimo de residuos celulares, retículo endoplásmico y aparato Golgi. Después, lípidos de núcleos han sido extraídos con un método de Folch modificado. Los experimentos de RMN en líquidos mostraron que la membrana nuclear estaba compuesta de muchos tipos de fosfolípidos y de los cuales la fosfatidilcolina era el lípido principal. Además, la composición muestra una gran proporción de fosfatidilinositol en comparación con otros tipos de membranas. Experimentos de espectrometría de masa han demostrado que la membrana nuclear estaba compuesta principalmente de fosfolípidos altamente insaturados y con cadenas que contenían un promedio de 34 átomos de carbono. Los análisis por RMN del sólido realizados en membranas reconstituidas a partir de lípidos de núcleos han revelado propiedades físicas atípicas. La temperatura de transición de fase fluido-gel está muy baja y amplia (-10°C± 15°C) lo que puede venir de la presencia de muchas especies de fosfolípidos y numerosas insaturaciones. Además, a 25°C, las membranas reconstituidas están más rígidas que las membranas modelas convencionales, lo que implica que el espesor de membrana está más largo que la de membranas modelas. Al final, los liposomas de membranas reconstituidas muestran una muy importante deformación en elipsoide prolato en el campo magnético, lo que es muy atípico para membranas biológicas y sugiere una importante elasticidad de curvatura de la membrana.

Résumé

Des malformations de l'enveloppe nucléaire sont observées dans des maladies de dystrophie musculaire ainsi que dans certains types de cancer tels que le cancer du sein ou du rein. Les mécanismes impliqués dans le maintien de la morphologie de l'enveloppe nucléaire sont basés sur des interactions protéo-lipidiques. Il a été démontré récemment que les propriétés physiques de lipides spécifiques jouent un rôle dans le processus de formation de l'enveloppe nucléaire chez le modèle de l'oursin. Afin de comprendre l'implication des lipides dans la régulation de l'architecture de l'enveloppe nucléaire nous avons utilisé les méthodes quantitatives de spectrométrie de masse et de résonance magnétique nucléaire (RMN) afin d'étudier la composition lipidique et les propriétés dynamiques de l'enveloppe nucléaire. L'extraction de noyaux a été effectuée à partir de cellules humaines de rein, les HEK 293T. Une extraction physique basée sur un traitement de pression et un gradient de sucrose a été optimisée afin d'obtenir une large quantité de noyaux intacts (lipides de l'enveloppe nucléaire) requis pour nos expériences. Ces noyaux purifiés comprennent un minimum de débris cellulaires, de réticulum endoplasmique et de l'appareil de golgi. Les lipides nucléaires sont ensuite extraits en utilisant une méthode Folch modifiée. Des expériences de RMN des liquides ont montré que l'enveloppe nucléaire était composée de nombreux types de phospholipides et dont la phosphatidylcholine était le lipide majoritaire. Par ailleurs, nous avons observé une grande quantité de phosphatidilinositol en comparaison avec d'autres types de membranes. Les expériences de spectrométrie de masse ont permis de mettre en évidence que la membrane nucléaire était composée majoritairement de lipides très insaturés et de chaines comportant en moyenne 34 atomes de carbone. Les analyses de RMN du solide effectuées sur des membranes reconstituées à partir des lipides nucléaires ont permis de mettre en évidence des propriétés physiques atypiques. La température de transition de phase fluide-gel est particulièrement faible et large à -10°C ±15°C. Ce phénomène est certainement dû à la présence de nombreuses espèces de lipides et de nombreuse insaturations. Par ailleurs, à 25°C, les membranes reconstituées de lipides nucléaires sont plus rigides que des membranes modèles classiques ce qui implique une plus large épaisseur de membrane. Enfin, les liposomes de membranes reconstituées ont montré une très importante déformation en ellipsoide de type prolate, dans les champs magnétiques, ce qui est particulièrement rare pour des membranes biologiques et ce qui suggère une importante élasticité de courbure de la membrane.

Contents

Chapter I: Introduction

The Nuclear Envelope (NE) is not just a fence between the nucleoplasm and the cytoplasm; it contributes to gene expression, nuclear signal transduction, nuclear transport and protein/lipid synthesis. Its malformation is linked to diseases. The NE is a double bilayer where the Outer Nuclear Membrane (ONM) is continuous with the Endoplasmic Reticulum (ER) and the Inner Nuclear Membrane (INM) is linked to the protein lamina network. The NE shows invaginations (3, 4); these substructures called Nucleoplasmic Reticulum (NR) are defined in two types: type I is composed of the inner nuclear membrane alone and type II is composed of the double membrane of the inner and outer nuclear membranes enclosing a diffusion-accessible cytoplasmic core. These invaginations are observed especially during the telophase and the pre-metaphase of the mitosis. The role of these NRs is still unknown but the increase of its population is characteristic and used as a marker of certain case of cancer events and muscular dystrophy diseases. It has been postulated that these invaginations may play a role in the NE formation. The formation of the NE as a specific event of cellular cycle is determinant for a correct cell functioning. The study of the NE formation has led to two models; one suggesting that the ER is targeted to the chromosomes and consequently envelops them with the gaps between the tubules and sheets filled by nuclear pore complexes and the other one is a non-somatic system, where diacylglycerol (DAG), a fusogenic lipid, is used to trigger localized membrane fusion in NE reassembly. These models are not mutually exclusive but both models show that proteo-lipid interactions are at the origin of the NE formation and regulation process. Previous research into NE has focused on the protein aspect, however the role of lipids is less well understood but lately the importance of the lipid roles it has been shown and related to their physical membrane properties and fusion event. A complete proteo-lipid characterization of the NE is necessary to the NE function understanding. The description of physical membrane properties linked to the membrane lipid composition shows the importance of the role of lipid in the functioning of the membrane. My work is an attempt to reveal the NE lipid composition and link it to membrane physical properties in healthy cells in order to compare the results obtained with cancerous like cells.

In this chapter I will summarize what is known on structure and dynamics of nuclear membranes. I will finally propose an overview of my thesis and highlight the objectives in human nuclear membranes.

I.   Natural membranes

1. Structure and composition of membranes

Biomembranes are selectively permeable barriers composed of a fluid phospholipid bilayer intercalated with proteins, carbohydrates, and their complexes (2). Eukaryotic cells have an exomembrane called the

plasma membrane and endomembranes which compartmentalize cells in various organelles. These membranes are structured and composed of specific elements that promote specific properties. Membranes are often considered only as barriers, but many essential biochemical processes happen within the cell membranes, and cellular processes, such as cell signaling, cell adhesion, cell differentiation or cell death are performed by membranes and membrane proteins (5).

Various models of structure and dynamics of biomembranes have been devised. In 1935, the first model called the "sandwich model" was proposed by Danielli and Davson (6). Lipids were organized in a lipid bilayer covered by proteins like a sandwich. After some modification the mosaic fluid model was proposed during the seventies, first by Bothorel and Lussan and then by Singer and Nicolson (see Figure 1)(2, 7). The term "mosaic" illustrates the heterogeneity in space and time of the membrane. The term "fluid" means that the membrane species diffused within the membrane plane. During the last years, the model evolved especially with the discovery of lipid micro-domains called "raft" (8). These domains enriched in cholesterol and sphingolipids, indicate a high rigidity level with a specific protein composition (8-13). These particular structures are thought to provide these domains specific biological roles (8, 9, 14-16).
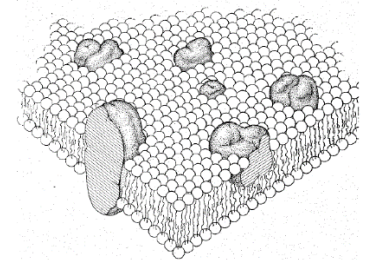
Figure 1:**Lipid and protein "fluid mosaic" model of biomembrane** structure by Singer-Nicolson (2).

2. **Biomembrane lipids**

Lipids are amphiphilic molecules shaped with a polar hydrophilic head and a hydrophobic part. They have the capability to auto-assemble in water to maximize hydrophobic and hydrophilic interactions. Frequently, they build a bilayer structure composed of an apolar part in the middle where there are no water molecules and a polar part on both sides of the bilayer in contact with the aqueous phase. There is a large quantity of lipids which have a big diversity due to polar head and hydrophobic chain combination (17, 18).
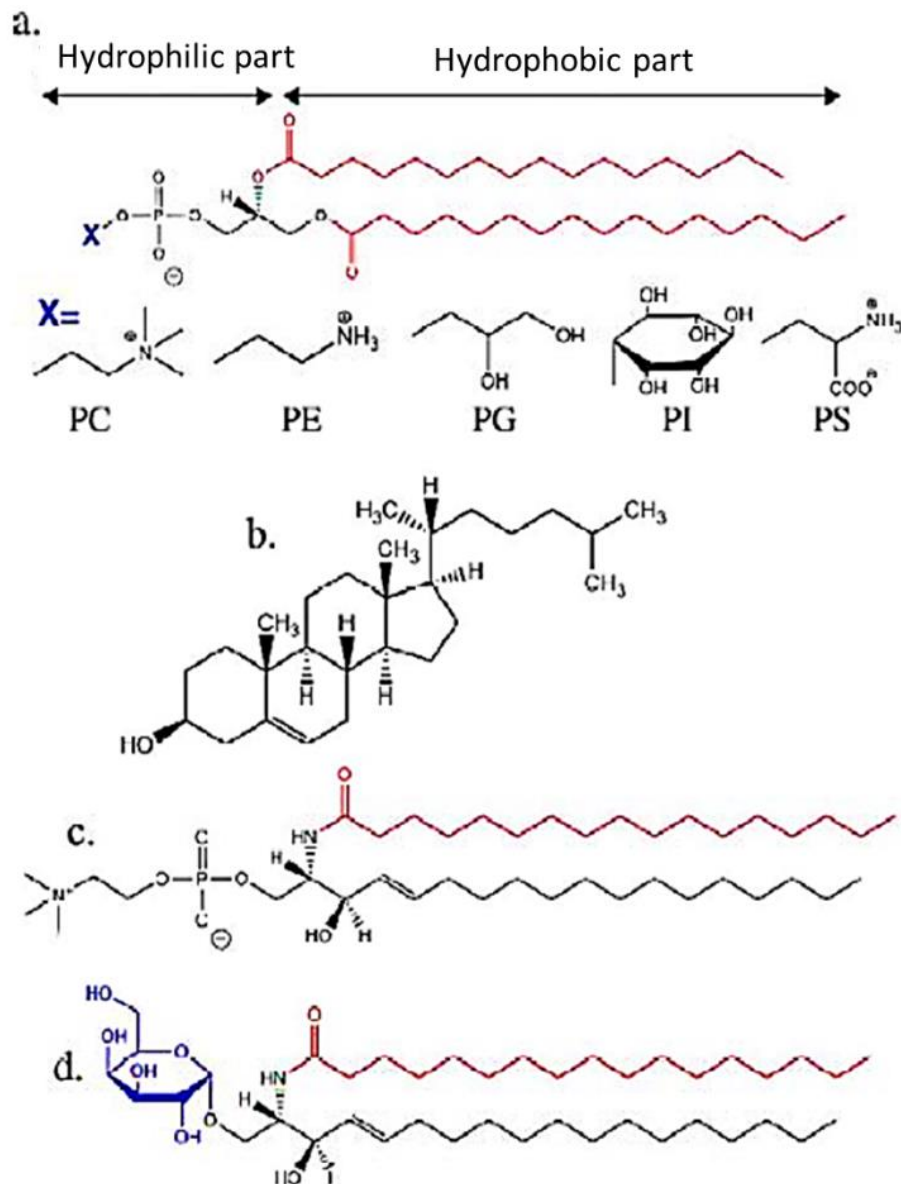
Figure 2: **Structure of several classes of membrane lipids:** phosphoacylglycerol (a.), cholesterol (b. sterol), sphingomyelin (c. sphingolipid) and galactocerebroside (d. glycolipid). Polar heads are in blue and hydrophobic part are in red. For phosphoacylglycerols, several substituent to the phosphate group: choline are possible (PC), ethanolamine (PE), glycerol (PG), inositol (PI) and serine (PS). Adapted from Vanessa Zhendre thesis (19).

1,2-diacylphosphoglyceride or phospholipids are composed of a glycerol backbone which is linked to one or two fatty acid chains by an ester link (positions 1 and 2 of the glycerol). A phosphate group is attached by an ether link to the position 3 of the glycerol. Completed by a polar group, charged or not like choline, ethanolamine, inositol… it forms the hydrophilic head of the molecule. A various number of fatty acid chains exist with a large diversity of chain length and unsaturation. This produces a large quantity of lipid types. Phospholipids are the most abundant class of lipids of biomembranes. Among prokaryotes, the most represented is phosphatidylethanolamine (PE), while among eukaryotes, the major one is phosphatidylcholine (PC) (see Table 1).

Table 1: **Lipid composition of several membranes** (% of total lipids). PE, PS, PC, PI, PG: phosphatidyl-ethanolamine, serine, choline, inositol, glycerol; CL : cardiolipin (17).

	Myelin	Erythrocyt	Mitochondr	Microsom	E. Coli
Cholesterol	25	25	5	6	0
Total	32	56	95	94	100
PE	14	20	28	17	80
PS	7	11	0	0	0
PC	11	23	48	64	0
PI	0	2	8	11	0
PG	0	0	1	2	15
CL	0	0	11	0	5
Total	32	18	0	0	0
Other	11	1	0	0	0

Steroids are made from a cyclopentanophenanthremic group with a hydroxyl group in position C3 for sterol. Cholesterol is the major sterol found in mammals. Among fungi, ergosterol is the principal sterol. This lipid class is the second class of biomembrane lipids and represents from 0 to 50% of membrane lipids. Plants usually possess more complex sterol compositions. Stigmasterol (STI) and sitosterol (SIT), two 24-ethyl sterols, are major constituents of the sterol profiles of plant species. They are involved in the embryonic growth of plants (20). Hopanoids such as bacteriohopanetetrol (BHT) are sterol surrogates of primitive bacteria (archaebacteria, cyanobacteria) that develop in very extreme conditions such as hot springs, very high deep sea pressure, highly saline water, and ice-covered lakes. They are considered as good markers of geological samples containing organic matter (21). Sphingolipids are complex lipids, derived from a sphingosine, resulting from the amidification of a sphingosine fatty acid. Some groups can be added on the first alcohol of sphingosine. Depending of the group, ceramides, phosphosphingolipids and glycosphingolipids can be found. For example, sphingomyelin (phosphosphingolipids) are from a sphingosine, link to a fatty acid by an amide link, and to a choline by a phosphodiester link (Figure 2). This lipid class is very important for vertebrates but absent in bacteria. Glycolipids constitute a group of lipids that have a sugar fixed on their polar head (figure 2). Galactolipids are derived from glycerolipids (glycerol backbone) and cerebrosides are derived from sphingolipids (sphingosine backbone).

The lipid repartition varies in function of biomembrane types within the cell and even between the outer and the inner leaflet of a membrane (see Figure 3) (17).
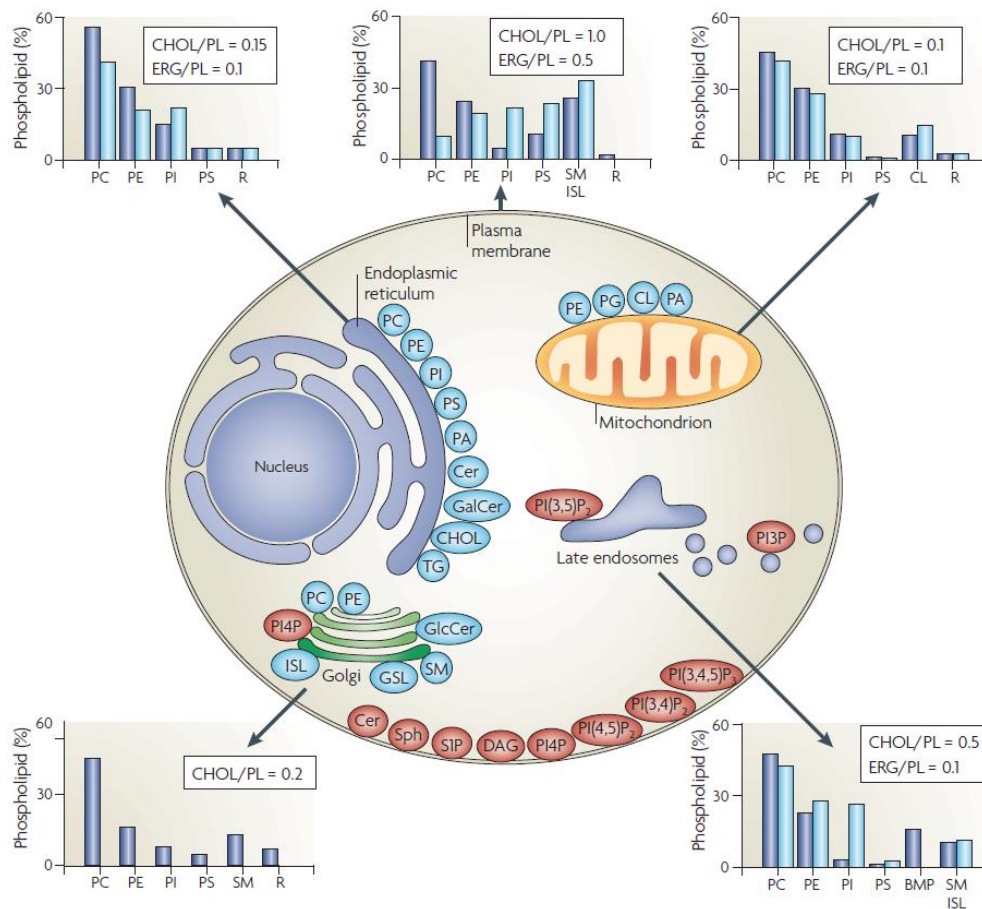
Figure 3: **The lipid composition of membranes varies throughout the cell**. Taken from (22). In dark blue: mammalian tissues, in light blue: yeast tissue. PL: phospholipids, CHOL: cholesterol in mammalians, ERG: ergosterol in yeast.

We know that the cell growth and proliferation require phospholipids as the major building block of the membrane. The synthesis of lipids occurs in the endoplasmic reticulum. The key intermediate of the pathway of TAG/DAG (triacylglucerol/diacylglycerol) and phospholipids is phosphatidic acid (PA). This synthesis is done with the addition of a fatty acyl-CoA, usually saturated, to glycerol 3-phosphate at the *sn*-1 position to produce lysophosphatidic acid. This reaction is catalyzed by glycerol 3-phosphate acyltransferase. Then a second fatty acyl-CoA, often unsaturated, is added to lysophosphatidic acid at the *sn*-2 position by acylglycerol-3-acyltransferase to form phosphatidic acid (23, 24). Phosphatidic acid can be used in the synthesis of several phospholipids by two different mechanisms. The first mechanism promotes the hydrolysis of the phosphate group from phosphatidic acid to diacylglycerol. This is done through the association of the cytosolic (phosphatidic acid phosphatase) with phosphatidic acid in the endoplasmic reticulum membrane. Diacylglycerol is used in the subsequent biosynthetic pathways for phosphatidylcholine and phosphatidylethanolamine. Diacylglycerol is also the precursor to the main storage form of energy, triacylglycerol. The second method whereby phosphatidic acid is used to synthesize additional phospholipids utilizes cytidine triphosphate (CTP) as an energy source and creates a CDP-diacylglycerol molecule. Overall, this mechanism allows for the replacement of the headgroup of

18

phosphatidic acid by other phosphate functional groups to form phosphatidylinositol, phosphatidylglycerol or cardiolipin (also known as diphosphatidylglycerol).
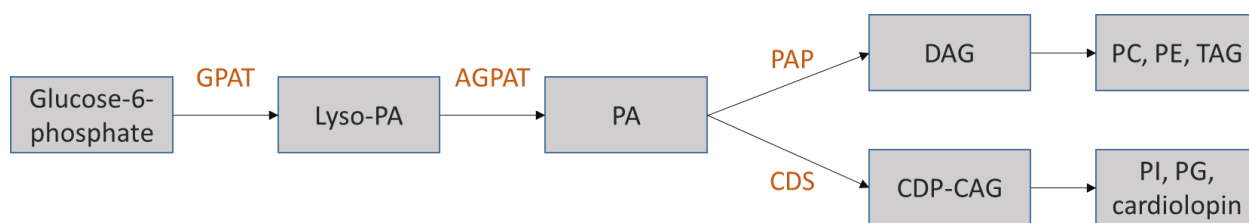
Figure 4: **Phospholipid Biosynthesis**. GPAT, glycerol 3-phosphate acyltransferase; AGPAT, acylglycerol-3-acyltransferase; PAP, phosphatidic acid phosphatase; CDS, CDP-diacylglycerol synthase; CDP: cytidine diphosphate; PA, phosphatidic acid; DAG, diacylglycerol; PC, phosphatidylcholine; PE, phosphatidylethanolamine; TAG, triacylglycerol; PI, phosphatidylinositol; PG, phosphatidylglycerol.

3. Membrane proteins

The proportion of proteins compared to lipids is very variable depending on the membrane type. In a general manner, the more the protein/lipid ratio is higher, the more the membrane will be biologically active. Membrane proteins are very important as they are 30% of expressed protein among eukaryotes. They are distributed in two groups based on their interaction with the membrane: extrinsic proteins and intrinsic proteins. Extrinsic proteins are associated to the membrane by electrostatic interaction with polar parts of lipids or other anchor proteins. They are in contact with the aqueous part. Intrinsic proteins or transmembrane proteins are associated to the membrane by hydrophobic interactions with the apolar part of lipids. These proteins can be within the membrane integrally or only partially. The large diversity of membrane proteins, as well as the lipids diversity explains that it is very difficult to describe a membrane typical composition. Indeed, depending on the cell type and the membrane type there are large variation in lipids and proteins types but also in their proportion. Furthermore, a difference in composition is also observed between the two leaflets of a membrane.

4. Role of Membranes

The first function of a membrane is to form a natural barrier between two different environments. Lipids are the principal elements required to form this protective structure. To survive, a cell needs to be protected but also needs to communicate with its environment. Cells or organelles exchange substances, information, and energy with its external environment. There are several mechanisms for molecule transport through the membrane (25). Passive diffusion is when small molecules diffuse across the membranes without any interactions. Active diffusion is when protein transport molecules across the membrane, like aquaporins for water molecules. Sometimes an input of energy is necessary, the transport is called active transport. The energy comes from the hydrolysis of an Adenosine TriPhosphate (ATP). Biological information also cross membranes. Extracellular messenger (hormone, sugar,

neurotransmitter) are used for recognizing specified membrane protein receptor. This event induces an enzymatic cascade given a specific cellular answer. Each specific membrane has its own specific receptor or transporter. Natural membranes are very complex and diverse. In order to study them, model membrane have been used to facilitate deciphering their structure and function.

II. Model membranes

In general model membrane are created by a small number of lipids to which are added membrane substances such as protein or peptide or other substances such as toxins or antibiotics if necessary. These membranes have to be representative of natural membrane and are created to be simple and easily studied by physical and chemical techniques. In order to understand better these models an explanation of the behavior of lipids in solution is necessary.

1. Lipid dispersions in water solution

During the last fifty years, several studies have shown the behavior of lipids in water. Luzzati *et al.* have studied for the first time the phase diversity of amphiphilic molecules (26). Lipids are amphiphilic molecules that were shown to self-assemble in water (27). Beyond the CMC (critical micellar concentration), lipids will associate to form lipid aggregates. The driving mechanism is minimizing the energy of contact between the hydrophobic part of lipids and water molecules (27). The shape of these structures is linked to the size of the hydrophobic and hydrophilic parts of lipids (28). Israelachvili has defined a packing parameter to describe lipid morphology (29):

$$p = \frac{v}{a_0 l_c} \qquad [1]$$

Where v is the hydrophobic volume, a_0 the optimal surface between water and the hydrophobic part and l_c the maximal length of hydrophobic tail. p is also depending on the polar charge of the lipid head and of hydrogen bond (27). According to the morphological parameter, lipids can be classified into three groups: conical, cylindrical or inverted-conical shapes (29): for p < 1, the polar head surface is more important than the hydrophobic tail. The lipid has an inverted-conical shape. To minimize water contact, this shape of lipid induces the formation of spherical micelles or cylindrical micelles. This type of shape is concerning lipids with small tail or lyso-phospholipids. This phase is rarely present in biological system (18). When 1/2 < p < 1 the shape is more cylindrical and promotes lamellar phases. In this case lipids form spontaneously multilamellar large vesicles (MLV). Most of natural membrane lipids form this kind of structure as PC, PS or PI. For p = 1, lipids have a cylindric shape. They form lipid bilayers spaced out by aqueous layers. For p > 1, the hydrophobic part is more prominent than the hydrophilic part. The lipid has a conical shape. These lipids induce inverted hexagonal phases or inverted micelles, PE can form this kind of phase.
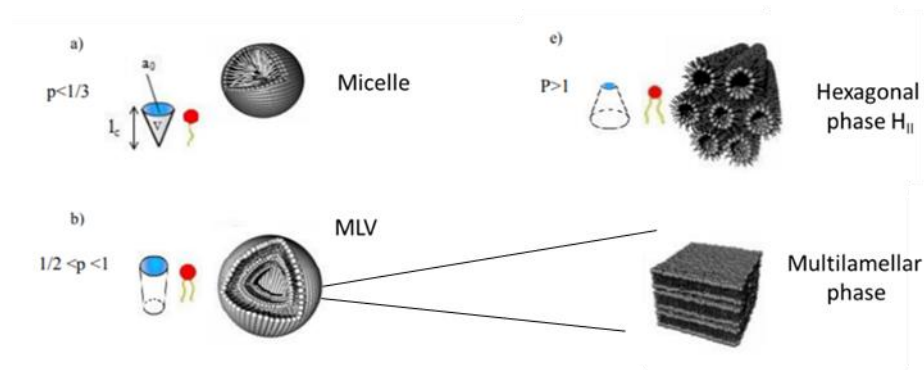
Figure 5: **The different macromolecular assemblies of lipid.** Lipids aggregate into different structures according to their packing parameter. The packing parameter (p) is the cylindrical or clonal volume of the fatty acid tail(s) (v) divided by cross section area of the polar head group (a) and the length of cylindrical or clonal volume (l). Adapted from Buchoux 2008(30). Drawings are not to scale.

In the case of a mixture of lipids more or less miscible, a mixture of phases can be observed (29). Moreover, even if the shape of lipids is important the concentration in lipids and temperature have also a great influence on the observed phase.

2. **Example of model membranes**

As we have seen above, several types of membrane models have been developed to mimic and simplify biological membranes. Micelles are often used to study membrane proteins. However, these isotropic objects do not have a lipid bilayer per say and so are not well representative of biological membranes (31-33). Multilamellar vesicles (MLVs) or unilamellar vesicles (SUVs, LUVs, GUVs) are more often used due to their simple preparation. Moreover, these objects are made of phospholipids that form one or several bilayers and so are more representative of biological membranes (31, 34-36). Therefore, these vesicles are good models to study biological membranes. Based on MLVs it is possible to create unilamellar vesicles (closer to biological membranes) by extrusion or sonication, with several sizes: few nm for SUVs (Small Unilamellar Vesicles), hundreds of nm for LUVs (Large Unilamellar Vesicles) and to some μm for GUV (Giant Unilamellar Vesicles). Recently, extracts of natural membranes have been developed in order to be closer to the physiological context. However, these model are more complex to analyze (37). In our study, we used MLVs of natural lipid extracts of nuclear membrane to mimic at best this membrane.

3. **Phase transition**

There are several types of phase transitions. The solid-solid transition, where the lipid system is changing between two solid phases. The fluid-fluid phase transition between two fluid phases and the gel-fluid transition where the lipid system changes from a solid phase to a fluid phase (38). In this thesis, we will be interested in this last phase transition, also called chain melting transition, corresponding to the

change of the static state of a lipid chain to a fluid state. Lipid tails do not behave the same at low or high temperature. When the temperature of a lipid system in lamellar phase increases we observe a change from an ordered phase or gel phase (L$_\beta$ or L$_{\beta'}$ (the apostrophe "'" means that lipid chains are tilted compared to the bilayer plane)) to a more disordered fluid phase, L$_\alpha$. In gel phase, chains are well aligned and completely extended. This is indicative of a weak mobility of lipids, leading to a static membrane behavior. In fluid phase, lipid chains are more mobile and less extended. Lipids are therefore more mobile within the membrane.
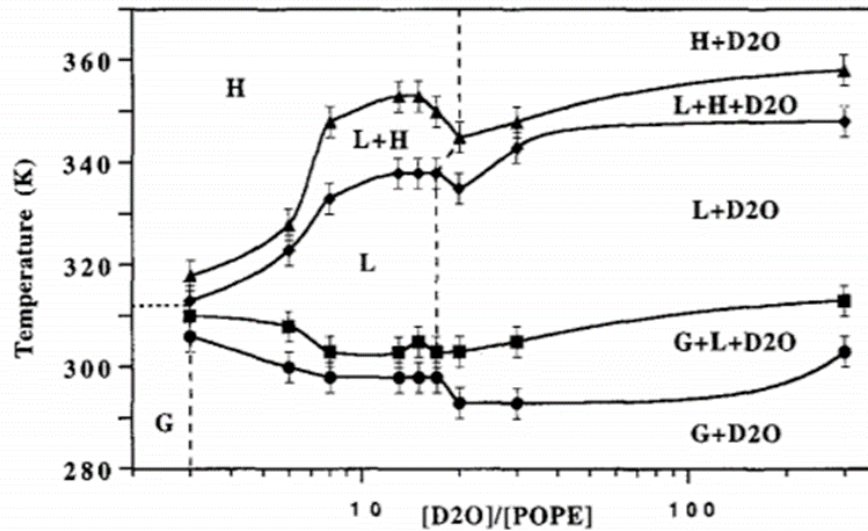
Figure 6 **Partial phase diagram of the POPE-D$_2$O system, as determined from ^{31}P and ^{2}H-NMR**. Solid curves are drawn to help reading the figure and come from interpolation between data values. Dashed lines indicate the swelling limit as obtained from ^{2}H-NMR of D$_2$0. The dotted horizontal line is also drawn to help reading the figure. Note that the water content, R$_i$, is plotted in a Log scale. Accuracy in phase boundaries is _+3 K. G: gel phase, L: fluid phase, H: hexagonal phase. Adapted from Marinov and Dufourc (39).
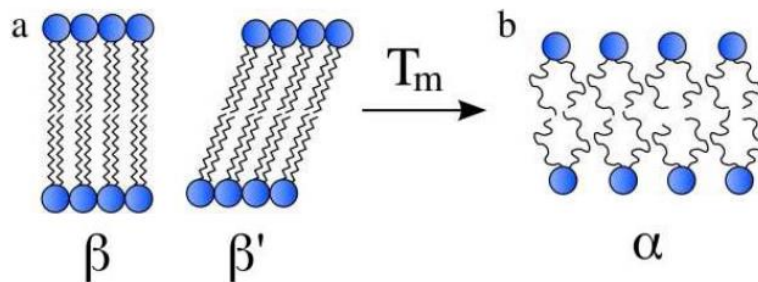
Figure 7: **Different structure of the lipid bilayer:** L$_\beta$/L$_{\beta'}$: lamellar structure in the gel phase, L$_\alpha$: lamellar structure in the fluid phase. T$_m$ is the melting temperature between the gel phase and the fluid phase. From Vanessa Zhendre thesis (19).

The melting temperature between the gel phase and the fluid phase is noted T$_m$ and is dependent on chain length, unsaturation, polar head type but also concentration of the solution in which lipids are dispersed. For example, the longer the chains, the higher the T$_m$. Moreover, if the unsaturation level is

high, T_m will decrease. Indeed, *cis*-unsaturation creates perturbations in the membrane packing and destabilizes the gel phase. There are molecules that influence the melting temperature. For example, cholesterol at more than 20% molar prevents the transition between $L_\beta/L_{\beta'}$ and L_α. In fluid phase, cholesterol increases the lipid order and in gel phase it decreases the lipid membrane packing. This situation is called liquid-ordered phase (l_O) and seems to have a role in the formation of lipid rafts. In this phase, lipids continue to diffuse within the membrane but the lipid tail are highly ordered (36, 40, 41).

The study of lipid thermotropism is important to understand some biological mechanisms. For example, Ragoonanan *et. al*, have studied the thermotropism in *G. sulfurreducens* bacteria. They have shown that a hyperosmotic shock promotes the decrease of the gel-to-liquid transition temperature, cooperativity leading to membrane disruption and lipid dissolution. Furthermore, a slow dehydration increases the T_m and decrease the phase transition cooperativity leading to fusion and vesicles formation (42).

Table 2: **Melting temperature (T_m) variation relative to chain length, unsaturation and lipid polar head**. The fist column is the number of carbon and double bond of lipid chain. Δ indicates the position of the double bond, and c means cis. PC, phosphatidylcholine; PE, phosphatidylethanolamine; PS, phosphatidylserine; PG, phosphatidylglycerol; PA, phosphatitic acid (18).

Lipids		T_m (°C)
12:0/12:0	PC	-1
14:0/14:0	PC	23
16:0/16:0	PC	41
16:0/18:1cΔ^9	PC	-36
18:0/18:0	PC	54
18:1 cΔ^9/18:1 cΔ^9	PC	-20
16:0/16:0	PE	63
16:0/16:0	PS	55
16:0/16:0	PA	67

Based on thermotropic and lyotropic properties of lipid dispersion in aqueous phase, phase diagrams of temperature/hydration have been constructed for single or mixture of lipids. Koynova and Caffrey have published an index with most of the reference diagrams (38, 43).

4. **Membrane curvature:**

Under the influence of temperature, concentration and composition, the lipid structure of model membranes can be destabilized. The presence of certain lipids may lead to the formation of intermediate

non-lamellar structures (44-47). For example, lysophospholipids such as lysophosphatidic acid (LPA) and lysophosphatidylcholine (LPC) assemble into micelle structures due to their head group being larger than their hydrophobic group. Inside a membrane, they induce positive curvatures (in red in Figure 8). Conversely, the head groups of phosphatidic acid (PA), cholesterol, phosphatidylethanolamine (PE) and DAG are small and these lipids curve negatively the membrane (in blue in Figure 8). Consequently, transitions from lamellar to non-lamellar structures can occur in mixtures with these lipids. These transitions depend on temperature, hydration (48) and lipid composition (49-51). A cylindrical inverted micelle structure can be formed for PE or DAG-containing lipid mixtures (26, 44, 46, 52). This lipid arrangement is referred to as inverted hexagonal structure, H_{II}, and can be involved in promoting fusion in model and natural membranes (53-55). Furthermore, the very high negative curvature of DAG in comparison to PA, PE and cholesterol is involved in mediating membrane fusion in a number of model and biological systems (56-58). Non-lamellar structures, although energetically unfavorable in cells, represent essential intermediates during membrane fusion. The production of negatively curved lipids that allow the formation of non-lamellar structures must therefore be highly controlled.
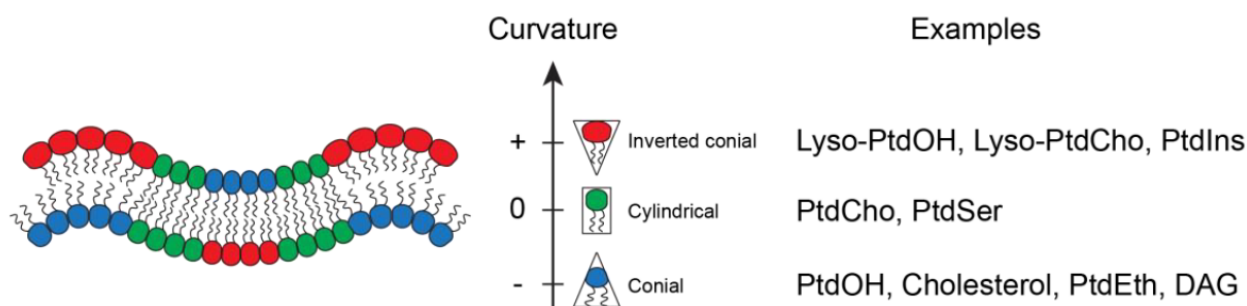
Figure 8: **The effect of lipid chemical structure on curvature preferences**. To generate membrane curvature, lipids of different spontaneous curvatures (effective shapes) are asymmetrically distributed in the two leaflets of a membrane. In mammalian cells, there is a wide variety of lipids to fulfil such function. (from Gary Chung thesis (59)).

5. **Membrane fusion**

Membrane formation involves membrane fusion processes. Although, membrane fusion mechanisms are difficult to understand, there are a number of theoretical studies on model membrane and more recently by using natural membranes that propose some models. To date, the best model to explain membrane fusion mechanism is the hemifusion model, as depicted by Figure 9. Before the fusion, membranes have to establish a contact (60-66). The initial distance between two membranes is estimated to be 10-20 nm. To initiate the contact, forces that push away the two membranes (electrostatic and hydration forces) have to be counterbalanced. Proteins are often implicated in this process by given the necessary energy to minimize the contact surface and force the membrane to be in contact and curve them locally (60-62, 64-66).
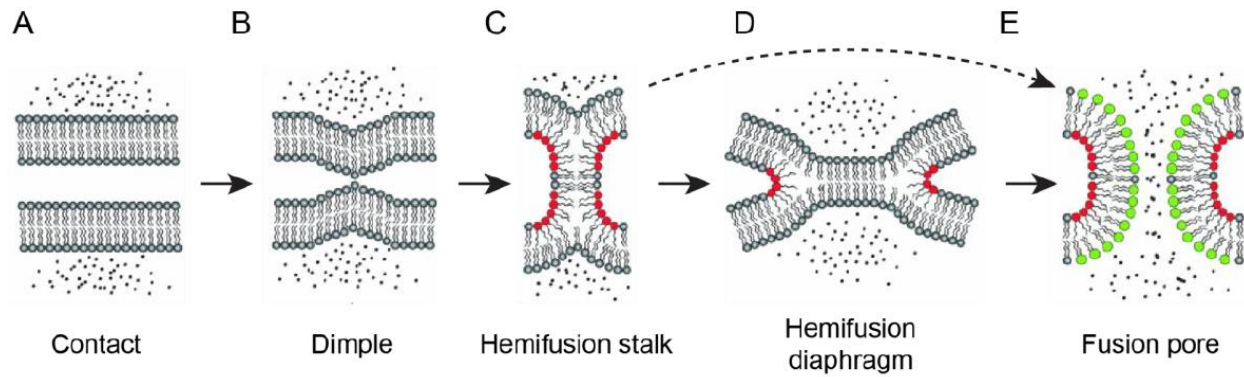
Figure 9: **Progression of membrane fusion through the hemifusion stalk.** Fusion can be dissected into multiple steps. (A) Two separate membranes approach each other and come into contact and there is a hydration barrier between the membranes. (B) Point-like protrusion, or dimple, overcomes the energetic barrier of hydration by diminishing the contacting surface area. (C) A hemifusion stalk is formed where the proximal leaflets are fused and distal leaflets remain unfused. (D) The hemifusion stalk expands and results in a hemifusion diaphragm. (E) Finally, the expanding hemifusion diaphragm becomes a fusion pore, resulting in a flow between two cellular compartments. Alternatively, the direct formation of fusion pore from hemifusion stalk has been proposed. However, theoretical calculations suggest that this is unlikely (67). Red indicates the region of negative curvature and green indicates the region of positive curvature in the hemifusion intermediates. Figure adapted from (68).

However, this process can be observed without the presence of proteins (60, 65, 69). Indeed, membrane thermic fluctuations can locally involve membrane contact. Such a process has also been observed in biological systems (70, 71). As it can be observed, the first fusion transitional step needs a high membrane curvature (65). The contact surface is equal to the polar head surface of a lipid. This configuration allows the minimization of repulsive contact forces between two membranes; as forces are proportional to the contact surface (72). Once the contact is established between the two membranes, the system can evolve in two ways. Either the system goes back to his initial state, or it forms a "stalk" (60, 62-65). The molecular structure of the "stalk" is represented in the Figure 9 The "stalk" is a local connection between two proximal monolayers of membranes that will fusion (53, 60, 61, 67). External and internal monolayer are extremely curved. The global curve of the "stalk" is negative (69). This foretells the critical role of negative spontaneous curvature lipids in fusion process. Furthermore, it has been shown recently that the formation of the "stalk" does not need as much energy than previously believed. Indeed, a fusion process has been observed with a model membrane without proteins (73).

To summarize, the hemifusion model involves the formation of highly curved fusion intermediates. This process is promoted by the presence of proteins that interact with membrane and/ or the production of lipids having a high spontaneous negative curvature. We will now present some examples that show how proteins and lipids are implicated in fusion processes.

1) Proteins role in hemifusion mechanism

Several studies have shown the involvement of proteins in different steps of the membrane fusion mechanisms (61, 63-66, 74, 75). In natural membranes, numerous scenarios are possible in order to explain the "stalk" formation and/ or the assisted protein fusion pore. Lipid modification, membrane

buckling, external scaffold and fusion coat, have been proposed, Figure 10, but their validation are still hypothetical.

We have briefly presented how proteins can promote fusion mechanisms. During the presentation of the hemifusion model it has been shown that lipids have also a role in facilitating the fusion process. Their roles are mentioned below.
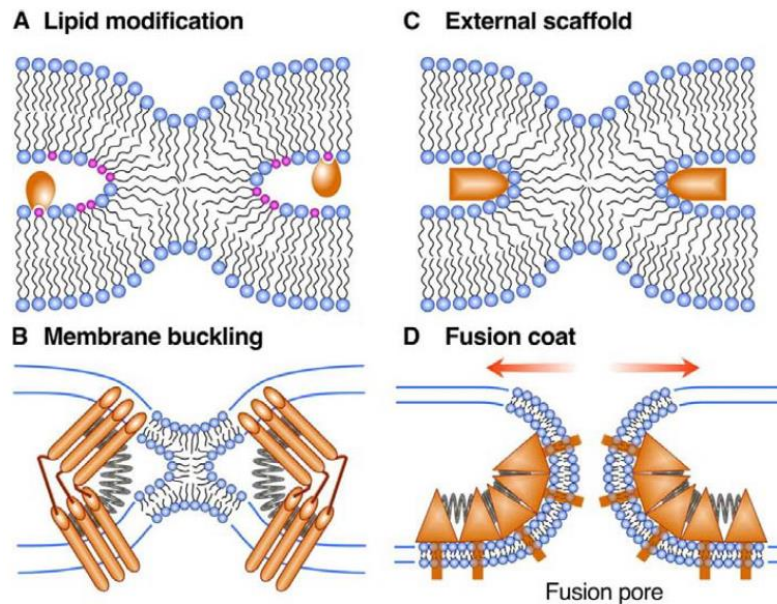
Figure 10: **Mechanisms by which fusion proteins might promote hemifusion and fusion pore development.** (A) Fusion proteins (shown as orange shapes) might change local lipid composition by generating fusogenic lipids (shown in pink) of contacting leaflets of the fusing membranes to that promoting hemifusion. (B) Folding of fusion proteins might drive hemifusion and fusion by producing bending stresses in bilayers bulged toward each other. (C) Lipids might be scaffolded onto surfaces of fusion proteins. For instance, protein scaffold located outside the hemifusion connection might present a positively charged electrostatic surface that would bind negatively charged lipids, and facilitate hemifusion and provide a handle for "pulling" the stalk open. (D) Proteins might develop a dense interconnected protein coat around the fusion site. Because of protein–protein interactions and protein shape, the protein coat has an intrinsic curvature (shown here as springs). This coat "wants" to deform the underlying lipid bilayers, thus, producing the lateral tension that drives the transition from hemifusion to opening an expanding fusion pore. Extract from (63)

2) Lipids in membrane fusion

The role of lipids in membrane fusion mechanisms can be double. First, they can promote the fusion by interacting with proteins that are involved in fusion process. These interactions can allow the recruitment and/or the activation of fusion proteins. (62-64, 76-79). Second, lipids can be engaged by their structural role in the fusion mechanism (53, 61, 63-66, 69, 78). Some lipids can promote the spontaneous curvature of a membrane and so promote or not the formation of fusion intermediates by the stabilization or the destabilization of the membrane curvature involved. Such results have been demonstrated for several lipids either in fusion mechanism models or in biological processes.

The fusion "stalk" has a negative curvature (69). Lipids that have a negative curvature such as PE, DAG, Cholesterol, could induce the formation of this fusion intermediate state. It has been observed that these lipids promote the fusion process when they are incorporated in natural membranes involved in the

26

formation of the "stalk" (proximal mono bilayer) (53, 61, 64, 69, 78). The same results have been reported on model membrane without proteins that demonstrate the specific role of these lipids in the membrane fusion. The role of lipids that have a positive curvature such as LysoPC on the "stalk" formation has been also studied. When these lipids are added to proximal membrane, it has been observed an inhibition of the "stalk" formation and so of the fusion (53, 61, 64, 65, 69, 78). The energy needed for the « stalk » formation is depending of the spontaneous curvature of membranes involved in the process (61, 65, 69). The curvature of the "stalk" is highly negative, and so lipids that have a negative curvature stabilized the "stalk" by forming a spontaneous curvature of the membrane. This phenomenon decreases the energy level of the "stalk" and promotes its formation. In the case of lipids that have a positive curvature, the membrane curvature is against that of the "stalk". The energy for the formation of the "stalk" increases and its formation in inhibited.
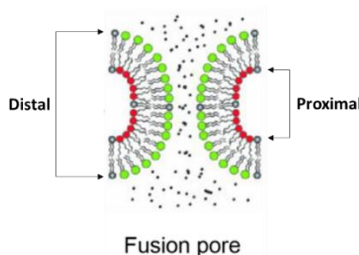
Figure 11: **Lipid shapes can influence fusion intermediate.** Lipids have to form a compact assembly to stabilize fusion intermediate. Here red lipids have a conical shape inducing a negative curvature and green lipids have an inverted conical shape inducing a positive curvature. This assembly stabilize the fusion pore. Adapted from (69)

In order to complete the fusion process, the "stalk" fusion has to evolve in a fusion pore. It has been shown that the curvature of the pore is positive (69). Contrary to the "stalk" formation, lipids with positive curvature stabilize the formation of the pore intermediate. Indeed, lipids with positive curvature promote the fusion process when they are incorporated to distal mono bilayer of membranes that have to fuse (53, 61, 64, 65, 69, 78). Furthermore, when lipids with negative curvature are introduced in these bilayer, the fusion is inhibited (53, 61, 64, 69). That is explaining that lipids with positive curvature promote a positive membrane curvature for the formation of the fusion pore. Positive curvature lipids decrease the level of energy necessary for the pore fusion and contrary to negative lipids curvature that inhibits the pore fusion formation.

III. Nuclei & Nuclear Envelope

The cell is the smallest and most fundamental unit of cell organisms. It is composed of many compartments such as the Nucleus, the Endoplasmic Reticulum, and the Golgi apparatus where proteins are encoded, maturated and where vesicles are made and used to import or translocate components outside cells. These compartments separate components with specific nature, pH or ions like the DNA in the

Nucleus. The Nucleus is the largest organelle in a cell, its average diameter is around 10 µm but can reach 20 µm in specific cells (*i.e.*, 3T3 cell line –fibroblast cells). The nucleus encapsulates the DNA in the nucleoplasm, therefore the transcriptional machinery from the cytoplasm, by a double bilayer called the Nuclear Envelope (NE). The Nuclear Envelope is composed of many types of proteins and lipids and is linked to various biological networks into the cytoplasm and nucleoplasm.
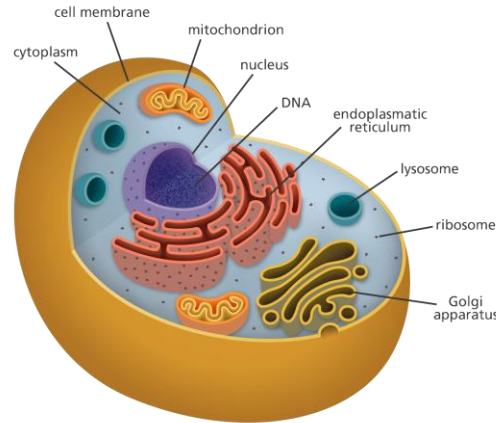
Figure 12: **General cell organization.** Credit: Genome Research Limited (80)

1. Nuclear Envelope: a complex membrane compartment

The nucleus is the largest subcellular organelle in eukaryotic cells. It was discovered by Franz Bauer in 1802. In 1851, the botanist Robert Brown, after having observed orchid cells in a microscope, described this compartment in more detail as an opaque structure and gave it the name of "aureola" or "nucleus". Since the 80's, the development of biophysical techniques have enabled a deeper description of intranuclear structures. The nucleus is a well-structured organelle and can be subdivided roughly into the nuclear envelope and the nuclear interior. The latter contains the chromatin in two states, very condensed (heterochromatin) and loosely organized (euchromatin) (81), the nucleolus, and diverse smaller structures as Cajal bodies and nuclear speckles (82). A structural nuclear network called nucleoskeleton or nuclear matrix is present into the nuclear interior and may participate to mechanical support and act as a scaffold for transcriptional complexes and other nuclear processes.

Figure 13: **Nuclear subcompartments** from (82)
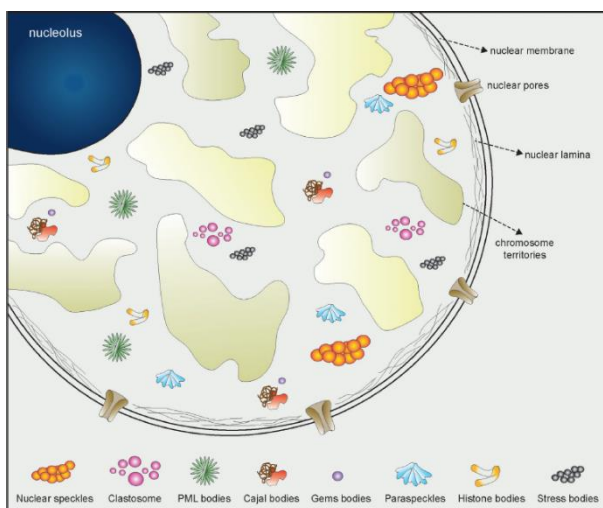
Nuclear body	Defining protein	Size (μM)	Related functions
Cajal bodies	Coilin	0.1–2	Biogenesis, maturation and recycling of small RNAs
Clastosome	19S, 20S proteasome	0.1–1.2	Sites of proteasomes, ubiquitine conjugates, and protein substrates of the proteasome
Gems nuclear bodies	SMN	0.1–2	pre-mRNA splicing
Histone body	NPAT, FLASH	0.2–1.2	Histone gene synthesis
Nuclear speckles	SRSF2, SRSF1, Malat1	0.8–1.8	Storage and recycling of splicing factors
Nuclear stress body	HSF1, HAP	0.3–3	Regulation of transcription and splicing under stress
Nucleolus	RNA Pol I machinery	0.5–8	Ribosome biogenesis
Paraspeckle	PSP1, P54NRB, PSF	0.5	mRNA regulation, RNA editing
Perinucleolar compartment	PTB, CUGBP	0.2–1	Post-transcriptional regulation of a subset of Pol III RNAs
PML bodies	PML	0.3–1	Regulation of genome stability, DNA repair, control of transcription, viral defense
Polycomb body	Bmi1, Pc2	0.3–1	Involved in polycomb proteins-mediated gene paring and silencing in Drosophila

The nucleoplasm is delimited by a double phospholipid bilayer (83, 84) called the Nuclear Envelope (NE). The two membranes are separated by an aqueous space of 30 to 50 nm, called perinuclear space (85). The Outer Nuclear Membrane (ONM) is continuous with the Endoplasmic Reticulum (ER) (86); and associated to the cytoskeletal actin network and the centrosome from where the microtubule network is organized. The Inner Nuclear Membrane (INM) is associated with the lamina network inside the nucleus (87). This network is known to contribute to the size, the mechanical stability, and the shape of the nucleus (88) but also are important for the organization of chromatin, DNA replication, and transcription (89).
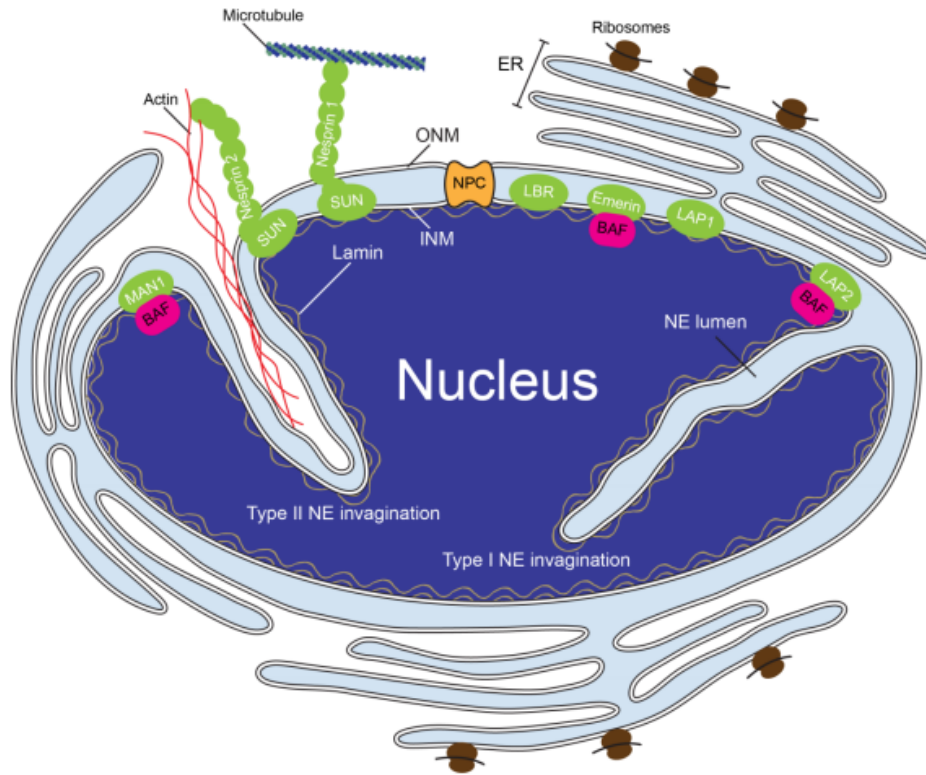
Figure 14: **The Nuclear Envelope is a complex membrane compartment**. Adapted from Gary Chang thesis.

2. Nuclear Envelope proteins

The inner and outer nuclear membranes are punctuated by Nuclear Pore Complexes (NPC), which allow bi-directional exchange of biomolecules between the nucleoplasm and the cytoplasm. NPC are massive macromolecular assemblies (around 60 MDa in yeast and 100 MDa for vertebrates) composed of multicopy about around thirty proteins called nucleoporines (Nups) (90-92).

At least 50 to 100 specific membrane proteins have been discovered by recent proteomic analyses at the Nuclear Envelope. Most of them are still incompletely characterized. Apart from NUP proteins, the NE proteins can be divided into two groups: the ONM proteins and the INM proteins. The NE proteins specifically localized in the ONM are constituted of a group of integral membrane proteins that share the small domain KASH (Klarsicht, ANC-1, Syne Homolgy). In the last decades, it has been shown that this domain can interact with Sad1p/UNC-84 (SUN)-domain proteins of the inner nuclear membrane within the periplasmic space of the NE (93, 94). Furthermore, at the ONM the nuclear envelope spectrin repeat (nesprin)-1 and -2, have been shown to directly interact with the actin cytoskeleton through their amino-terminal actin-binding domain (ABD) (95). These ONM proteins are implicated in nuclear positioning that is essential for cell polarization, pronuclear migration, and the organization of syncytia (96). The proteins that are specifically localized at the INM (97) remain largely

NPC	INM	ONM	Lamina
Nup35	LBR	Nesprin-3/ Net35	Lamin A
Nup37	Lap1	Syne/Myne/ Nesprin 1	Lamin B1
Nup43	Lap2b	Nesprin-2a and b	Lamin B2
Nup50	Emerin	Syne/ Nesprin-2G	Lamin C
Nup54	MAN1	Samp1	
Nup58/45	Nurim		
Nup62	NET8		
Nup75	NET38		
Nup88	NET56		
Nup96*	LEM2/ NET25		
Nup98*	NET9		
Nup107	NET32		
Nup133	NET37		
Nup153	Sun1		
Nup155	Sun2		
Nup160	LUMA		
Nup188	~ 60 NETs		
Nup205			
Nup214			
Nup358/ RanBP2			
Sec13R			
Seh1			
Pom121			
Ndc1			
Gp210			
Tpr			
Rae1			
Aladin			
Nlp1/hCG1			

Figure 15: **List of NE proteins**.From (1)

uncharacterized. For some of them, an interaction has been shown with Lamins and chromatin, such as Lamin B receptor (LBR), lamina-associated polypeptide (LAP) 1, LAP2, Emerin, and MAN1 (98-100). It is becoming increasingly clear that INM proteins play vital and diverse roles in nuclear function such as chromatin organization, gene expression, and DNA metabolism (101-103). Importantly, improper localization and function of INM proteins have been linked to several human diseases, which has led to considerable interest in NE biology over the last decade (104-106). In addition, ONM and INM proteins form "bridges" across the perinuclear space that might be involved in separating the two NE membrane leaflets at an even distance of 50 nm (107). These lumenal protein aqueous bridges could establish physical connections between the cytoskeleton and chromatin, which might be relevant for transcription, replication, and DNA repair mechanisms (108, 109). The final group of NE proteins constitutes the lamina, a meshwork of intermediate filaments that is composed of A- and B-type Lamins (110). Although the lamina has been shown to be critical for nuclear stability, particularly in tissues that are exposed to

mechanical forces such as muscle fibers (111), it has become clear that Lamins also play major roles in chromatin function and gene expression (89, 103, 112). Similar to INM proteins, mutations in Lamins are linked to a numerous human diseases (101, 113, 114) and to aging (112, 115), highlighting the crucial role of the NE protein network for normal cell function. In summary, the NE fulfills a critical role in shielding the genome from cytoplasmic components, but also represents a highly specialized membrane that provides anchoring sites for chromatin and the cytoskeleton (116).

3. **Nuclear envelope invagination: Nucleoplasmic Reticulum**

Nuclei have a global spherical shape with a diameter that can vary from 5 to 10 μm depending on the type of cells. Powerful visualization techniques of nuclei have highlighted the presence of NE substructures forming deep and branching invaginations inside the nucleus (4, 117, 118). Because of the resemblance with the endoplasmic reticulum, those invaginations were called Nucleoplasmic Reticulum (NR). They are classified into two classes. The type I are invagination of the INM alone and the type II is composed a double membrane invagination of the inner and outer nuclear membranes enclosing a diffusion-accessible cytoplasmic core.
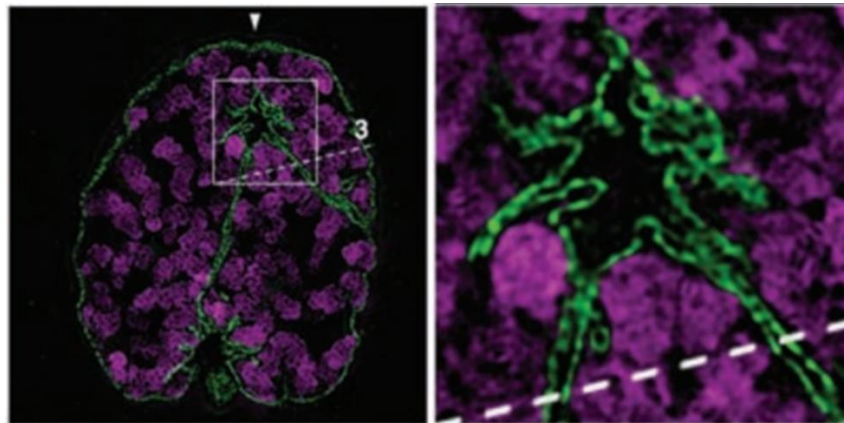
Figure 16: **Nucleus of a mitotic cell with invaginations of the NE.** Cells were immunostained with antibodies against Lamin B (in green) and DNA was stained with DAPI (in magenta). Adapted from Schermelleh et al. (2008).

The membranes of NRs resemble those of the NE. The protein composition of type I NR is more restrictive than INM with a lack of LAP2beta for example (119). Furthermore, NPC (nuclear pore complex) is only present in type II invagination. Type II NR has a stable lamina and its core contains cytoplasmic protein such as actin (4, 120-123). This can suggest a role for the NR in mechanotransduction of signal to the nucleoplasm, gene expression, RNA trafficking, and cell differentiation (124-128). NRs are reported in numerous normal and abnormal cells from plant and animal kingdom. Furthermore, type I and type II can occur alone or coexist in the same nucleus and the number of NR may vary from none to more than 10 by nucleus (4). NRs are stable and persistent but are also flexible enough to accommodate nuclear rotation or changes in morphology (129). In live cells, NRs can change on a timescale of minutes

(4). NRs seems not directly linked to the cell cycle stage but variation with state of differentiation has been described which would be consistent with a role in regulating gene expression (122, 130). The NR regulation seems to be a dynamic process that is controlled by several pathways. NRs formation can be controlled by change in phospholipid bilayer composition when CCTα (choline phosphate cytidylyl-transferase) is activated and binds to the INM. The catalytic domain of CCTα synthetize PC, which could increase the development of NRs (131, 132). Even if these substructures have been observed their roles are still unknown. Moreover, NRs are abundant in many tumor cell types including brain, breast, kidney, bladder, prostate and ovary and suggest that the NRs regulatory mechanisms are susceptible to pathological dysregulation (133-135)
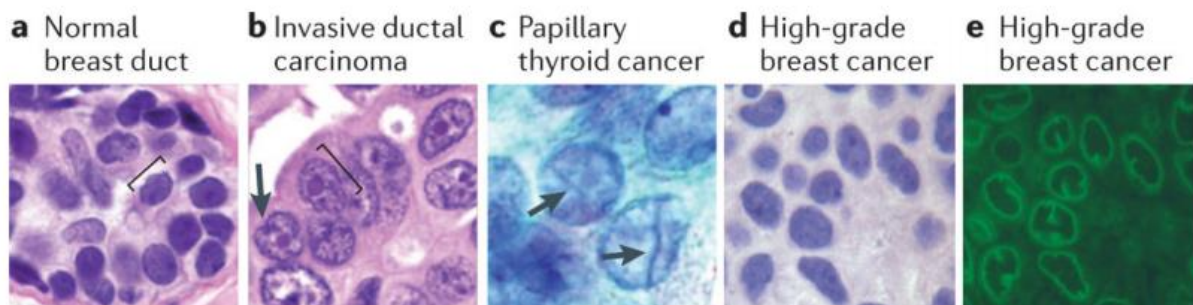
Figure 17: **Tumors relative to NE deformation**. Extract from (136) Tumors of different types show distinct morphological features, enlarged nuclei are characteristic of many cancer cells (compare the area indicated by square brackets in normal breast duct (part **a**) to invasive ductal carcinoma (part **b**)The invasive ductal breast carcinoma in part **b** shows an atypical invagination of the nucleus (indicated by an arrow). Nuclear grooves are characteristic of papillary thyroid cancer and their presence contributes to diagnosis (indicated by arrows in part **c** The enhancement of detection that is made possible with the use of immunofluorescence is illustrated in the comparison of hematoxylin and eosin staining (part **d**) versus immunofluorescence of Lamin B (part **e**) in high-grade breast cancer where we can observe nuclei invaginations.

4. **Nuclear Envelope lipids**

Lipids are an important component of cellular membranes. They are highly diverse in structure, and the distribution of different lipids and their species (membrane lipid composition) varies at the organism, cell type, organelle, membrane, bilayer-leaflet and membrane subdomain level. Understanding the biological relevance of this diversity and why there are so many lipid-related genetic diseases represent a fundamental challenge in biology. Isolated nuclear envelopes contain approximately 70 percent protein and 30 percent lipids (137, 138). Lipids and proteins of the NE are distinct from other cellular membranes but resemble the endoplasmic reticulum. Fry reports in his book(137), various NE phospholipid compositions. These results were obtained of several nuclei characterization and extraction methods of mammalian tissues but not on human cells. Results are reported in the following Table and show that the NE lipid composition is close to the endoplasmic reticulum composition and very different to that of plasma membrane. Several studies of liver nuclei have shown phosphatidylcholine (PC) to be the major PL, with lesser but still significant amounts of phosphatidylethanolamine (PE) and

33

phosphatidylinositol (PI) (139). Phosphatidylserine (PS), and sphingomyelin (SM) were detected at much lower levels. PLs were reported as 65% of NE lipids, whereas cholesterol was 10% (approximately three times that of ER); lesser amounts of other neutral lipids (cholesterol ester, DAG, triacylglycerol) were also detected (140).

Table 3: **Nuclear Envelope phospholipid composition**. [1](139), [2](141)(data from rat liver)

Tissue	PC	PE	PS+PI	SPH	LPC	CL
Bovine liver[1]	55.6±3.1	21.1±2.9	14.0±1.6	3.5±0.8	2.7±0.4	3.1±0.4
Rat liver[1]	61.8±1.0	18.3±1.0	13.9±0.2	2.5±0.3	1.4±0.4	1.4±0.3
Rat liver[1]	61.4	22.7	12.2	3.2	1.5	nd
Pig liver[1]	58.2	25.9	13.3	2.4	<1.0	nd
Calf thymus[1]	68	15	6.1	1.0	6.5	1.7
Calf thymus[1]	56.3	24.8	4.7	7.7	2.7	nd
Endoplasmic reticulum[2]	58.4	21.8	13	2.5	9.5	1.1
Plasma membrane[2]	39.3	23.3	16.7	16	1.0	1.3

Although a relatively high concentration of free fatty acids (15% of total lipid) was reported in the above-mentioned study, it is not known how much of this resulted from lysis of PLs during isolation. However, the cholesterol content was significantly below than that of plasma membranes. The study of Shindler *et al.* reports the PL composition of ONM and INM obtained by chromatography. This study shows no significant difference in PL between the total NE and the two membranes analyzed separately (142). However, it has been shown, based on filipin-sterol interaction, an unequal distribution of complexes suggesting higher cholesterol content in the ONM compared with the INM (143). On the other hand, lipid asymmetry in membranes is due to of multiple factors, including the biophysical properties linked to the ability of a lipid to cross the bilayer spontaneously, retentive mechanisms that trap lipids in one leaflet of the bilayer, and the presence of transporters that assist lipid translocation. Furthermore, Shindler *et al.* have studied the lateral mobility of the nuclear membranes. The results have shown the mobility of WGA receptors (wheat germ agglutinin) and phospholipids of the entire NE whereas the outer membrane depleted NE immobilize the INM WGA receptor or provides evidence that immobile WGA receptors are localized at the inner membrane (142). The dynamic and physical differences in the two membranes may be representative of the fact that they may serve two very different functions. Shindler suggested that the ONM may function as a communication link with the ER while the INM may offer a platform for replicating enzyme and DNA attachment or provide additional recognition information for nuclear

reassembly. NE lipids have an important function in the nucleus. Lipids maintain the membrane structure and also have an important role in signaling pathways within the nucleus. Indeed, lipid composition plays a role in membrane physical properties and the biological relevance of which is becoming clearer. For example, polyunsaturated fatty acids in glycerophospholipids increase the membrane fluidity and affect processes due to membrane deformation (144). Furthermore, the implication of lipid composition related to membrane dynamics has been studied to understand nuclear events.

5. **Nuclear Envelope events**

The formation of the NE is a specific event of cellular cycle which is determinant for correct functioning of the cell. Hence why it is important to understand the reformation on NE and mechanisms involved during its formation. In cells, during open mitosis, the NE typically breaks down at prophase and reassembles at telophase. A quite similar NE reassembly mechanism occurs in male pro-nuclear sperm formation in sea urchins and xenopus which are used as model organisms (145-149).

1) **Open mitosis**

Mitosis is the event during which the cell divides to establish two functional daughter nuclei. During this process the nuclear envelope undergoes important structural changes. (Figure 18) (150-154). Indeed, during the prophase-prometaphase step, the NE break down to reform during the telophase leading to two daughter cells. This process is called open mitosis. In yeast the breakdown of the NE is not necessary for cell division and therefore stays intact during all the mitosis processes. This case is called closed mitosis. For open mitosis, the breaking down of the NE is followed by de-polymerization of the lamina network and solubilization of nuclear pore within the cytoplasm (151-153). Mechanisms of the NE breakdown are still unknown. However, two mechanisms are proposed: the selective vesicle formation of NE for which the different membrane compartment (INM and ONM) are concerned or the whole dispersion of NE substituents within the endoplasmic reticulum (150, 152, 155, 156). At the end of mitosis, the NE is reforms around each daughter cell nuclei. In the first model, the NE formation will take place by the nuclear envelopment of the endoplasmic reticulum (ER) extension, without a fusion process (152, 155, 156). Gaps between ER extension would be filled by nuclear pores.
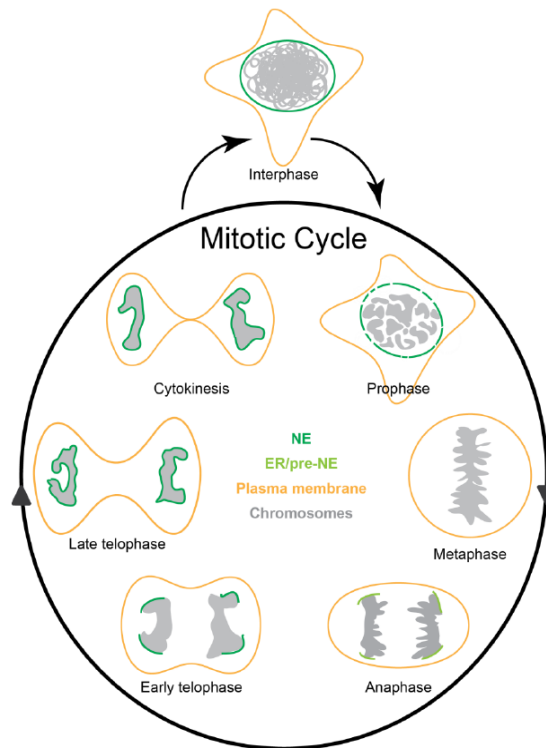
Figure 18: **NE at different mitotic stages of mammalian cells.**

The second model is based on membrane fusion either between vesicles formed during the NE breakdown or at the gap level of ER extension (68, 150, 157). In order to obtain a functional NE, nuclear pores have to be reconstituted for providing the passage of Lamins within the nucleus and to reform the lamina network (152, 155). During the last step, the nucleus will inflate to allow the chromatin de-condensation (150, 155, 156).

2) Cell free assay to study Nuclear Envelope formation

i.   Nuclear envelope formation

The nuclear envelope assembly process occurs during each mitosis. A similar process is observed during the fertilization. When the spermatozoid enters into the egg, the loss of its nuclear envelope occurs. This envelope does not have nuclear pores and so is inactive for biological mechanisms such as DNA replication and transcription. A new active envelope will have to be reformed; this process is called the male pronucleus formation process. The pronucleus formation involves several steps such as NE vesicle formation, chromatin de-condensation, vesicles docking and fusion, and nucleus swelling with Lamin importation for the lamina reformation (involving the presence of a nuclear pore). This pronucleus will then fuse with the female pronucleus to form a zygote. It has been shown that the molecular mechanism involved in this process is similar to somatic cell models (158). That is why this process can be used as a model to study NE formation of somatic cells.
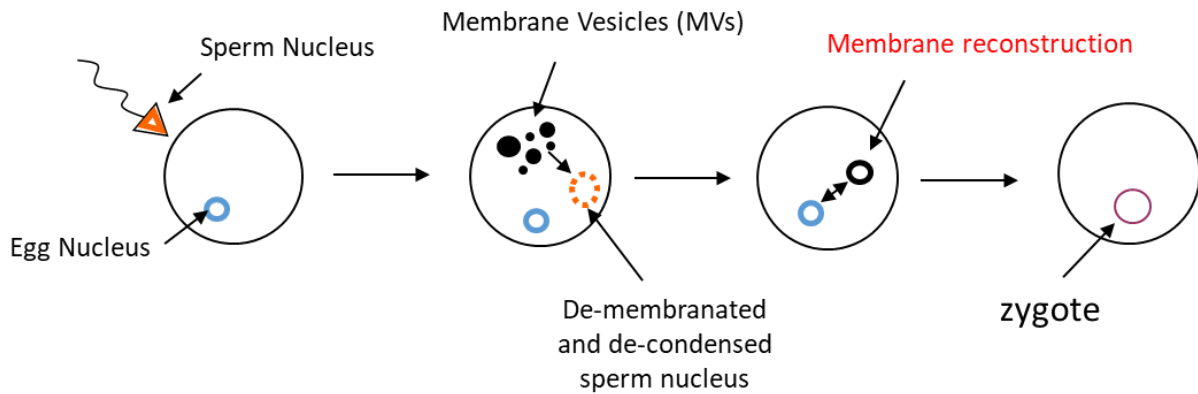
Figure 19: **Fecundation process** (70). The sperm enter in the egg. Sperms Nucleus loses its membrane when entering into the egg cell. The nucleus sperm membrane is reconstructed from membrane vesicles within the egg. Both pro nucleus fuse to form a zygote.

Among the gamete-derived cell-free extracts, the sea urchin, seems to be the most powerful because it provides the most practical (it is easy to purify a large quantity of gametes), economical and biological advantageous (68). Furthermore, sea urchin cell cycles are synchronous and the completion of the sea urchin genome (159) revealed that sea urchins conserve the human genome diversity but not its complexity.

ii.   Cell free assay mechanism

The *in vitro* NE formation is occurring in several steps: chromatin de-condensation, vesicles binding around the nucleus, vesicles fusion and nucleus swelling. (Figure 20).

Following the de-condensation of the chromatin, vesicles extracted from fertilized egg cytoplasm will bind to the nucleus after adding ATP (147, 160). This binding is polarized and begins from nuclear pole (161). Several population of vesicles have been described and two of them have a role in the NE formation: MV2 (MV2α and MV2β) and MV1 (161). These vesicles have very important differences in their shape and composition but also in their way to bind to the nucleus (Figure 20) (161). MV1 is the first and only one to bind NERs (Figure 20) (161, 162). Then MV2α and MV2β vesicles bind to MV1 and fill the nuclear surface. Following the fixation step, vesicles have to fuse with NERs to build a complete new nuclear envelope. The dynamic study of NERs has shown that these membranes are in a liquid-ordered phase (163). The liquid-ordered phase gives them a high stability for protein and chromatin interaction (163). In the cell free assay, the fusion step needs the addition of GTP (161, 162, 164). Furthermore, the fusion process is polarized (162). The fusion begins from the pole and continues around the nucleus surface
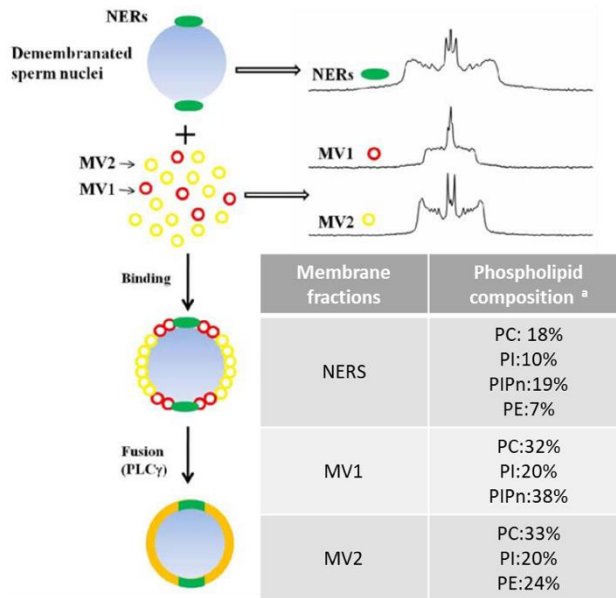
Figure 20: **NERs, MV1 and MV2 physical properties involved in the formation of the nuclear envelope. Rigid NERs are located on each pole of the sperm.** The fluid vesicles MV1 bind the NERs and MV2 vesicles with average fluidity recovered the surface of the nucleus. Then PLCγ convert PIP2 in DAG, inducing the fusion between vesicles to form the nuclear envelope. To the right, experimental ^{2}H solid NMR spectra of membrane model of NERs, MV2 and MV1. Large spectrum is corresponding to an ordered system, narrow spectrum is corresponding to a less ordered and fluid system.[a] The phospholipid composition of MV1 was characterized (161), total MV2 (MV2α+ MV2β) was characterized (165) and NERs (163). Adapted from (166)

The principal element of the fusion process are the MV1 vesicles that trigger fusion (161). The fusion is induced by the production of DAG after the hydrolysis of PI-4,5-P$_2$ by PLCγ protein. DAG has a high negative curvature that induces the formation of non-lamellar structures thus promoting fusion (58, 167). The fusion of MV1 with NERs follows with MV2 vesicles to complete the NE formation. Furthermore, the dynamic study of reconstructed MV1 vesicles has demonstrated that they are in a fluid phase due to the presence of PI. This characteristic may help for the MV1 fusion process (166). The lipid composition of MV2 is more or less that of classical natural membranes with PC, PE and Cholesterol as principal components (165). The dynamic study of reconstructed MV2 vesicles has shown that they are in a liquid-ordered phase compatible with classical natural membranes. Nuclear pores will then be formed at the NE and Lamin proteins will be imported within the nucleus (161, 168, 169).

3) Fusion model versus envelopment model

The system described above involves membrane fusion mechanism. However, in somatic cells, two mechanisms have been suggested for the NE formation, either the fusion of vesicles around the nucleus or the envelopment by extension of endoplasmic reticulum (68).
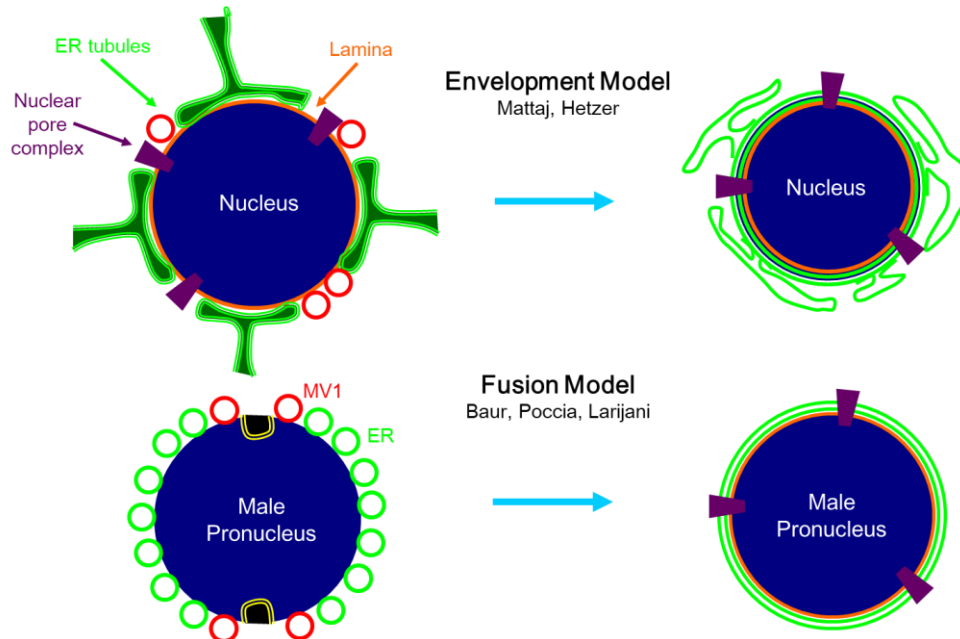
Figure 21:**Two major models of NE assembly (170).**

The second system described does not involve the fusion mechanisms (171). These two systems are often presented like completely exclusive. Nonetheless, these two systems can co-exist. Indeed, MV2 vesicles derive from ER and are under vesicular form because of the sample preparation protocol (172). In both cases, hypothesis is agreed with the fact that ER-like membranes are constituting the major component of the NE. Moreover, recently in mammalian cells it has been shown that vesicles that perhaps have MV1 characteristics, described from the Golgi have a role in ensuring the correct formation of the nuclear envelope (173). One can envisage the *in vivo* presence of vesicles similar to MV1 vesicles for fusion to occur with ER membranes by filling the ER membrane gap and complete the formation of the NE.

4) Nuclear envelope and disease

During the last decades, some dysregulation about the formation of the nuclear envelope have been correlated to numerous diseases. Until now, 24 pathologies have been associated to gene mutation of Lamins or proteins associated to the nuclear envelope. We call these diseases nuclear envelopathies (105, 111, 153, 174). Mutations of LMNA gene that is coding for Lamin A/C results in laminopathy (105, 111, 153, 174). For example, we can cite the Emery-Dreifuss muscular dystrophy, the dilated cardiomopathy or the Hutchinson-Gilford syndrome (105, 111). A mutation of the Lamin A gene can induce the leak or the absence of functional Lamin A, as the dysfunction of interaction between lamina, chromatin and the nuclear envelope leading to an abnormal nuclear envelope (105, 155). This can be observed either in the morphology of the nuclear envelope or on the chromatin organization.
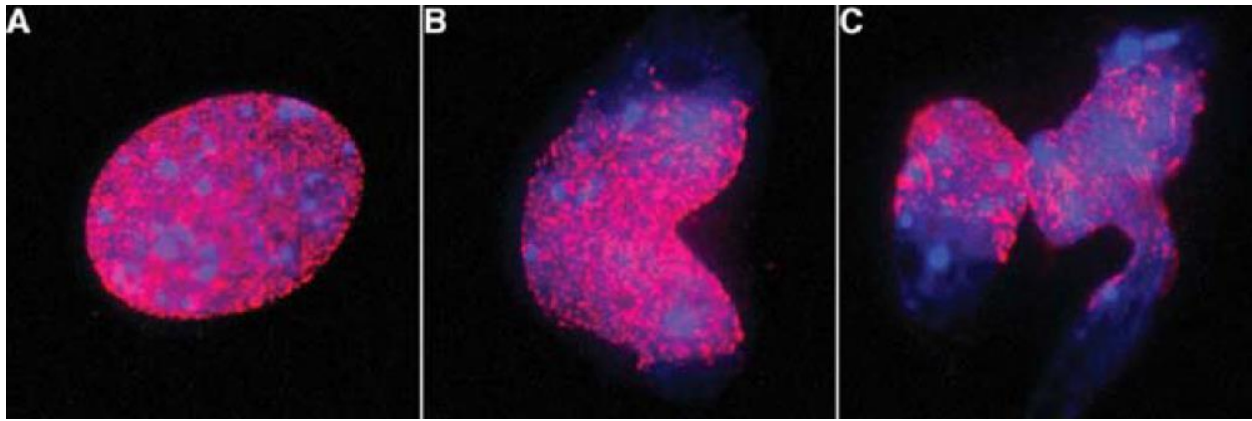
Figure 22: **Example of laminopathies nucleus. (adapted from (111)).** A: Normal nucleus. B: Nucleus that doesn't express lamin B/C. C: Nucleus of a mouse that have a cardiomyopathie. A-C: DNA in blue and nuclear pore in pink.

There are other diseases involving other nuclear membrane proteins such as LBR, LAP2 or Emerin (111, 153, 174). Several malformations of the nuclear envelope have been discovered in numerous cancers. Cancerous cells show structural changes of the nuclear envelope (133, 134, 155, 175). We can observe modifications of the nuclear shape as chromatin organization constituting the cancerous cell phenotype (133, 134, 175). These perturbations could induce the dysregulation observed in cancerous cells (175). Indeed, an abnormal nuclear envelope could disrupt the chromatin organization and the position of the genes that could degrade the genome expression (175). The formation of the nuclear envelope is a key event in the cell cycle that determine the well-functioning of the cell. The relation between pathologies and abnormal nuclear envelope is not well established (134, 175). The study of molecular mechanisms involved in the formation of the nuclear envelope appears important. This is why nuclear envelope model *in vitro* and *in vivo* have to be investigated to understand deeper the molecular mechanisms involved in the nuclear envelope formation.

IV.   Aim and objectives

As described in the Introduction, the nuclear membrane is not just a fence between two compartments but has an important biological role. The nuclear envelope is composed of proteins and lipids. Nuclear membrane proteins have been largely explored compared to nuclear membrane lipids. As lipids can influence the structure and the dynamics of natural membranes, we propose to explore the lipid nuclear membrane composition and dynamics of human cells by quantitative methods such as Nuclear Magnetic Resonance (NMR) and Mass spectrometry. In a first experimental part of my thesis I have developed a non-detergent protocol to extract nuclei from the human cell line HEK293T. Lipids were further extracted and phospholipids analyzed by liquid-state NMR and mass spectrometry (Paper submitted to the Journal Analytical Chemistry). In the second experimental part of my thesis, I investigated the dynamics of nuclear lipids reconstructed vesicles by solid-state NMR spectroscopy (Paper submitted to Nature Communications). In the last part of my thesis, I have presented the first exploration on the whole nuclear

membrane (lipids and proteins) dynamics and the first results trying to separate outer from inner nuclear membranes (ONM/INM) and determine their phospholipid composition. A conclusion will be drawn, and future directions proposed in a very last chapter. Annexes for separation techniques and references will finalize the manuscript. The Materials and Methods will be presented before the experimental results.

Chapter 2: Material & Methods

In this Chapter I will describe the materials and methods I used during my thesis. I will first present the list of buffers and reagents used, then I will present cell biology techniques used for extracting nuclei, nuclear membranes and control their purity. Finally, I will present the biophysical techniques used to analyze the integrity of nuclei and nuclear lipids composition and dynamics, such as fluorescent microscopy, Mass Spectrometry (MS) and Nuclear Magnetic Resonance (NMR).

I. Buffers and reagents

1. Materials

Liquid chromatography solvents, *i.e.*, methanol, isopropanol, acetonitrile, and chloroform, were HPLC-grade and purchased from Sigma-Aldrich (Saint-Quentin Fallavier, France). Ammonium acetate, ethylamine, formic acid, and NH_4OH solution (28.0–30.0 % NH basis) were also purchased from Sigma-Aldrich. Synthetic internal lipid standards for mass spectrometry analysis (PE 17:0/17:0, PS 17:0/17:0, PC 17:0 /17:0, PA 17:0/17:0, PI 17:0/14:1, and PG 17:0/17:0) and for NMR analysis (PA 14:0/16:1, PS 16:0/18:1, PE 16:0/18:1, PG 14:0/16:1, PC 16:0/18:1, CL 16:1/16:1, SM 14:1/14:0) were provided from Avanti Polar Lipids (Alabaster, AL, USA). $^2H_{31}$ palmitoyl, 2-oleoyl-*sn*-glycero-3-phosphocholine (POPC-$^2H_{31}$) was purchased from Avanti Polar Lipids (Birmingham, AL. USA). These starting materials were used without further purification. Deuterium-depleted water was obtained from Eurisotop (Saint Aubin, France) and solvents for liposome preparation (chloroform, methanol and ethanol) were obtained from Sigma Aldrich Chemicals (Saint Quentin Fallavier, France). Other reagent as Sucrose, $Mgcl_2$, SDS (sodium dodecyl sulfate), Tris Base, glycine, PVDF membrane, low fat milk powder, tween, HRP antibody, Hepes, KCl, DTT $DIOC_6$, Hoechst and TPP were purchased from Sigma Aldrich (Saint Quentin-Fallavier, France). Cell culture reagent, Dulbecco's Modified Eagle's Medium (DMEM), Fetal Bovine Serum (FBS) and Streptomycin/Penicillin were purchase from Invitrogen, (Carlsbad, CA. USA).

2. Buffers:

Medium for cell culture: Dulbecco's modified Eagle's medium (DMEM) high glucose, glutamax TM supplement, pyruvate, supplemented with 10% FBS and 5% Streptomycin/Penicillin.

Phosphate Buffered Saline (PBS 1%): 137 mM NaCl, 2.7 mM KCl, 10 mM Na_2HPO_4, 1.76 mM KH_2PO_4, pH 7.4

Tris Buffered Saline (TBS 1%): 150 mM NaCl, 10 mM Tris Base

Swelling Buffer (SB): 10 mM Hepes, pH 7.9, 10 mM KCl, 15 mM $MgCl_2$, 1 protease inhibitor tablet (Complete Mini, Roche) per 10 mL buffer and 5 mM DTT prior to use

S1Buffer: 0.4 M Sucrose, 15 mM $MgCl_2$

S2 Buffer: 1 M Sucrose, 15 mM $MgCl_2$

Nuclei Stock Solution: 1 M Sucrose: SB 1:1 (v/v)

Modification Buffer: 200 mM HEPES, 1 mM $MgCl_2$, 0.25 M Sucrose, pH 8.5 adjusted with NaOH.

10% SHM Buffer: 0.3 M sucrose, 10 mM HEPES pH 7.4, 2 mM $MgCl_2$, 0.5 mM $CaCl_2$. Add 2 mM DTT and protease inhibitor prior to use. 20 million nuclei/50 mL buffer.

30% SHM Buffer: 0.9 mM Sucrose, 10 mM HEPES pH 7.4, 25 mM KCl, 2 mM $MgCl_2$. Add 2 mM DTT and protease inhibitor prior to use. 2 mL requires for 20 million nuclei/50mL

Lysis Buffer: 150 mM NaCl, 50 mM Tris pH 8, 1% NP-40, 1 protease inhibitor tablet per 10 mL buffer prior to use.

4X SDS Loading Buffer: 0.01% (w/v) Bromophenol blue, 20% (v/v) Glycerol, 4% (w/v) SDS, 250 mM Tris base, pH 6.8; add 50 mM β-mercaptoethanol prior to use.

Running Buffer: 25 mM Tris Base pH 8.3, 3.5 mM SDS, 192 mM Glycine.

Transfer Buffer: 20 mM Tris, pH 8.3, 192 mM Glycine, 20 % (v/v) Methanol.

TBST: TBS 1 %, 0.1 % Tween 20.

Silanation Buffer: 3 % (v/v) Dichlorodimethylsilane in Toluene, prepared carefully under a hood.

Extraction Phase 1 (EP1): 2.5:1 (v/v) Chloroform: Methanol, supplemented with a drop of concentrated HCl.

Extraction Phase 2 (EP2): 200 mM EDTA, pellets of KOH added progressively until pH6.

Extraction Phase 3 (EP3): 200 mM EDTA, pellets of KOH added progressively until pH2.

3. **Antibodies:**

Name	Target	Species	Supplier	Cat#
Lamin B1	INM	mouse	abcam	16048
Actin Ab	Internal Control	mouse	abcam	3280
Calreticulin	ONM	mouse	abcam	22683
MAB 414	NPC	mouse	abcam	24609
H2B	DNA	mouse	abcam	52484
Anti-mouse HRP		Goat	abcam	205719

Abcam (Cambridge, UK)

4. **Fluorescent probes:**

Names	Target	λexc/λemi (nm)	Supplier	Cat#	Working dilution
Hoechst	DNA	350/461	invitrogen	H3570	1,6µM
DIOC6	Membranes	485/501	invitrogen	D273	1µM
FM 1-43FX	Membranes	473/579	invitrogen	F35355	5µg/mL

Invitrogen (Waltham, MA USA)

II. Cell Biology

1. Cell maintaining

All cell culture experiments were performed under the hood. All media, buffers, and materials were sterilized and previously autoclaved and cleaned with 70% Ethanol. Media were pre-warmed in a water bath at 37°C prior to use.

1) Cell throwing

Frozen HEK 293T cells (1.5×10^6 in 1mL FBS/DMSO, 9:1, v:v) stored in liquid nitrogen were de-frozen in a water bath at 37°C for approximately 2 minutes. All contents of the cryovial were transferred into a 15mL falcon and washed with 10 mL PBS. After being centrifuged at 200 g, during 5 minutes at 4°C, cells were transferred into a 75 mL flask containing 12 mL of pre-warmed new medium.

2) Cell passages and trypsinization

Each passage was done approximately at 80 % confluence (every 2-3 days). The old medium was removed and cells were washed carefully (HEK cells detached easily) with 10 mL of PBS 1%. 1 mL of Trypsin/EDTA was added directly to the cells to trigger the cell detachment. Then cells were diluted in 11 mL of pre-warmed new medium and transferred into a new flask containing 12 mL of pre-warmed new medium. The volume transferred is depending of the dilution required. Cells between passages 5 and 20 were used for experiments.

Container type	Number of Seeding Cells
75 mL flask	1.5×10^6
175 mL flask	3×10^6
Mattek	2.5×10^5
8 well plate	1.5×10^4

3) Cell Freezing

Cells corresponding to half of 80% confluence 75 mL flask were suspended into 1 mL of FBS/ DMSO (9:1, v:v) and transferred into a 2 mL cryovial. Cells were stored 2-3 days at -80°C and then several months in liquid nitrogen.

2. Nuclei Extraction

All processes were performed on ice to avoid sample degradation. After harvesting by trypsinization, HEK 293T cells from two 175 mL flasks of 80% confluence were incubated on ice for one hour in 10 mL of freshly prepared SB. Cells were lysed by nitrogen cavitation in a cell disruption bomb. Samples were incubated on ice at a pressure of 200 psi for 10 minutes before decompression and sample collection. Samples were centrifuged at 500 g for five minutes at 4°C to pellet the nuclei. The supernatant containing soluble cell debris was discarded. Pellets of nuclei were washed once with SB. A final purification step was done by a sucrose gradient. Nuclei were resuspended in 100 µL of SB and layered on 3 mL of solution S1 and 3 mL of S2 and centrifuged at 1000 g for 10 minutes. After discarding the supernatant, nuclei pellets were resuspended in 1mL of SB. 5 µL were transferred to 300 µL of SB for Nuclei counting and staining. Nuclei were transferred in cryovials and resuspended into Sucrose 1M in SB, flash frozen in liquid Nitrogen and stored at -80°C.

3. INM and ONM separation

The protocol was based on Schindler *et al.*, 1985(176). Nuclei were resuspended in 1 ml of modification buffer. and supplemented with 11 mM of citraconic anhydride. Following the reagent addition, the reaction mixture was centrifuged at 15,000 g at 4°C for 3 min. A pellet was formed, which was then washed with modification buffer and centrifuged.

4. Chromatin digestion

The protocol was based on Wilkie e Schirmer, 2008(177). 1-2 million nuclei were diluted in 1 mL of 10 % SHM buffer where DNase I to 10 U/mL and RNase A to 1.4 µg/mL were added. The sample was incubated during 20 min on ice and then centrifuged at 4,000g for 20 min at 4°C to pellet nuclei. The supernatant was discarded. 2-4 nuclei pellets were diluted in 1mL of 10% SHM buffer. 50 U/mL DNase I and 5 µg/mL Rnase was added and the sample was left 20 min on ice. The tube was centrifuged at 4,000 g for 20 min at 4°C. Nuclei pellets were resuspended in 10 mL of ice-cold 10% SHM supplemented with 300 mM NaCl. The solution was transferred into a round bottomed centrifuge tube and underlay with 0.15 volume of 30 % SHM. This tube was centrifuged at 6000 g for 30 min at 4°C. The digested chromatin supernatant was discarded carefully and the pellet was washed with 300 mM NaCl. The final pellet was frozen and kept at -20°C before the next experiment.

5. **Biochemistry / Molecular Biology**

For all the following tests, 100 µL of sample (cells, nuclei or membranes) were centrifuged at 500 g, 5 min, 4°C and the pellet was resuspended in 100 µL of LB. These solutions were sonicated 3 times for 4s, 1s stop at the amplitude of 7.

1) Protein quantification: BCA

The BCA Protein Assay is based on bicinchoninic acid (BCA) for the colorimetric detection and quantitation of total protein. This method used the reduction of Cu^{+2} to Cu^{+1} by protein in an alkaline medium (well known as the biuret reaction). A purple-colored reaction product is formed by the chelation of two molecules of BCA with one cuprous ion. This water-soluble complex exhibits a strong absorbance at 562 nm that is linear with increasing protein concentrations over a broad working range (20-2,000 µg/ml). The sample protein concentration was determined and reported with reference to a standards curve of the bovine serum albumin (BSA) (0.00, 0.20, 0.40, 0.60, 0.80, 1.00, 1.25, 1.50 $µg.µL^{-1}$. Samples preparation and standard curve were prepared as followed: 200 µL of a BCA mix reagent (50:1, A:B) were added to 5 µL of reference standard curve and samples in a 96-well plate. After being incubated 30 minutes at 37°C, absorbance of the plate solutions was read at 562 nm.

BCA Standard Curve Titration

$y = 0{,}2588x + 0{,}0026$
$R^2 = 0{,}9975$

[Protein Total] in $µg.µL^{-1}$
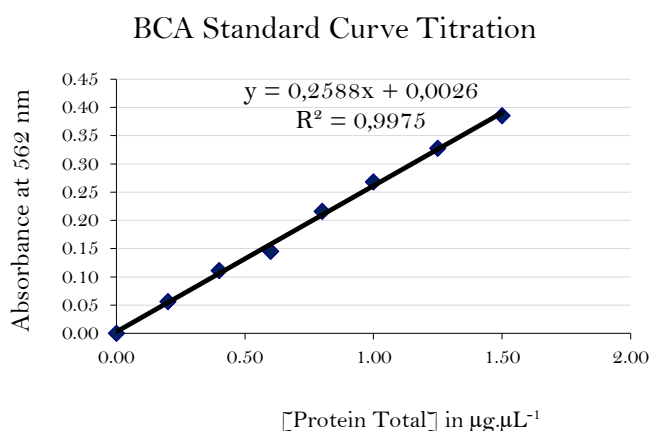
Figure 23: **Example of a BCA standard curve titration** done during the thesis

2) Chromatin quantification

DNA concentration of Cells, Nuclei and Membranes samples were estimated by UV spectroscopy using a Nanodrop system, based on acid nucleic absorbance properties at 260 nm. The sample DNA concentration was determined and reported with reference to a standards curve of Salmon DNA premade (1, 5, 50, 500, 1000, 2000 $ng.µL^{-1}$).

3) SDS PolyAcrylamide Gel Electrophoresis (SDS-PAGE)

Cells, Nuclei or Membranes samples corresponding to 10 mg proteins were mixed with 5µL of 4X SDS loading buffer and boiled for 10 minutes at 95 °C to denature proteins. Samples were loaded into a 4–12% Bis-Tris gel (Invitrogen) against a protein ladder (PageRuler Plus, Thermo Scientific). Gels were

run in a running buffer at 145 V for approximately two hours, until the dye front had reached the bottom of the gel.

4) Western Blotting

Proteins were transferred from the gel onto a PolyVinylidene DiFluoride (PVDF) membrane for Western blotting, pre-activated with methanol and followed washed by transfer buffer prior to use. Proteins were transferred using the Biorad Trans-Blot transfer apparatus. A sandwich was constructed containing (from the bottom up): four sheets of 3mm Whatman blotting paper (pre-wetted in transfer buffer), the PVDF membrane, the gel, and four more sheets of blotting paper. The whole stack was placed on the anode plate, any air bubbles were pressed out and the proteins were transferred at 400 mA for two hours. Transferred proteins were occasionally visualized by Rouge Ponceau by staining for 30 minutes with gentle shaking, followed by 30 minutes of washing steps with TBST. Membranes were blocked one hour at room temperature with 5% low fat milk powder (w/v) in TBST. Following blocking, membranes were incubated with the appropriate primary antibody in 5% (w/v) low fat milk powder in PBST at 4°C overnight. Membranes were washed twice ten minutes, and twice 5 minutes in PBST to remove the excess of primary antibody and the nonspecific binding. Membranes were subsequently incubated with HRP-conjugated secondary antibody for 1 h at room temperature in 5% (w/v) low fat milk powder in PBST, followed by four washes as above. Amersham ECL reagents were used at a ratio of 1:1 and incubated on the membrane for 3 min. The membrane was exposed for various periods of time to photographic X-ray film in a cassette and films were developed using an IGP Compact2 Developer.

III. Fluorescence Microscopy

Cells, Nuclei, and membrane fractions integrity were controlled systematically by epifluorescence after having stained by Hoechst and $DIOC_6$. For visualization, nuclei were fixed with 4% PFA after settling onto a polylysine coverslips for 1 h. 1 $\mu g.mL^{-1}$ of Hoechst and 5 μM of $DiOC_6$ were used to stain the DNA and membranes respectively. Multi Lamellar Vesicles of POPC and Nuclear Lipid Extracts were stained by 5$\mu g/mL$ FM1-43FX. Other microscopy techniques as described below were used to get more precise and specific information.

1. General considerations on Confocal microscopy

The confocal microscopy development during the late 70´s resulted in one of the major advances in optical microscopy. Specifically, fluorescence confocal microscopy allows analyzing fluorescence due to an individual thin in-focus plane of the sample, and this enables the construction of real three-dimensional (3D) images. To discard fluorescence derived from out-of-focus planes, and in contrast to common epifluorescence microscopy, confocal imaging is performed by introducing a pinhole next to the detector

that allows only fluorescence from the in-focus plane to reach the detector. Figure 24 shows a schematic picture of the central components of a fluorescence confocal microscope. Essentially, a laser beam is used as the excitation light, which is focused onto a dichroic mirror, which selects the light to be directed through an objective into a small spot within the sample. Fluorescent molecules are excited and their emitted fluorescence recovered by the microscope objective and directed across the same dichroic mirror into a pinhole that selects the emitted fluorescence to reach the photodetector.
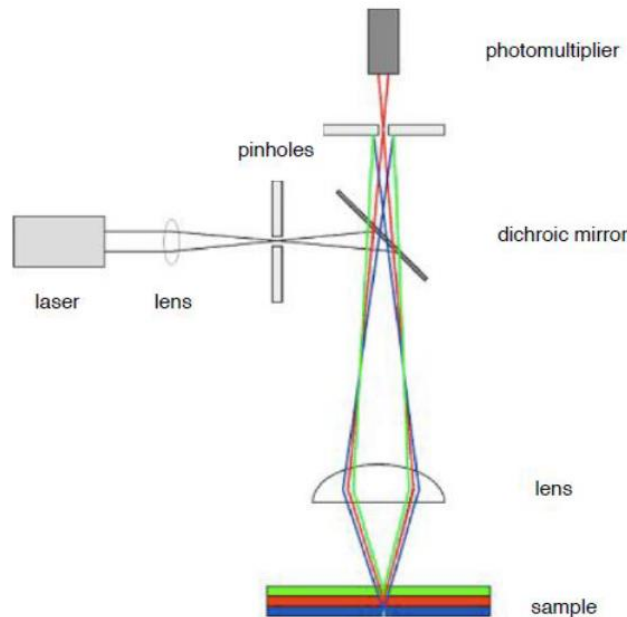
Figure 24: **Components of fluorescence confocal microscope** (From Marta G. Lete thesis,(170))

Fluorescence from the in-focus plane will go through the pinhole while out-of-focus fluorescence will be blocked. However, this is not enough to build a 3D image of the specimen being measured. For this purpose, special mirrors are introduced to scan the laser beam on the x-y plane, giving rise to a special confocal microscopy known as laser scanning confocal microscopy. In this way, by precisely controlling the z-sample movement, three dimensional images can be constructed.

2. **Sample preparation (Staining Immunofluorescence)**

Cells, Nuclei or Membrane fractions were fixed in 4% (w/v) PFA in PBS for 10 min. The cells were washed three times with 2 ml PBS and permeabilized with freshly prepared 0.5% saponin/3% fatty-acid free BSA (w/v) in PBS or TBS for 30 min where the fatty-acid free BSA was used to block the cells. Cells were washed once with PBS or TBS before primary antibody incubation. Commercial primary antibodies were diluted in 0.5% saponin/3% BSA/PBS or TBS in a 1:50 to 1:100 ratio. The primary antibody solution was added to the inner well of the MatTek dish. Unless specified in the manufacturer's protocol, cells were incubated with primary antibodies or recombinant proteins at room temperature for 1 h. After that, the primary antibody solution was aspirated and the cells were washed once with PBS or TBS. The cells were then incubated with secondary antibodies, diluted with the 0.5% saponin solution in 1:200 to 1:500

ratio, for an hour at room temperature. The secondary antibody solution was aspirated and the cells were washed once. The probed cells were kept in 2.5% (w/v) DABCO in PBS or TBS before imaging. Alternatively, cells were mounted in ~10 µl ProLong Gold antifade reagent and carefully sealed by a coverslip. If necessary, cells were incubated with Hoechst 33342 at a final concentration of 1 µg/ml for 10 min at room temperature before mounting. In every incubation step, the cells flasks were covered by aluminum foils to protect the samples from light.

3. Image processing

Images were loaded to the Image J software to improve their quality. Image J was also used to count nuclei and to defined radius of vesicles used during our NMR experiments.

IV. Mass Spectrometry

1. Lipid tandem mass spectrometry: HPLC-ESI-MS/MS

Mass spectrometry (MS) is a powerful tool for profiling a range of lipid species with a high sensitivity. After a separation by liquid chromatography according to their polarity or their size, lipids are sorted by their mass/charge (m/z) ratio. The concept of MS is to form ions from a sample, separate them based on their m/z ratio, and detect them in order to obtain a mass spectrum. A mass spectrometer is therefore composed of a source, an analyser and a detector.
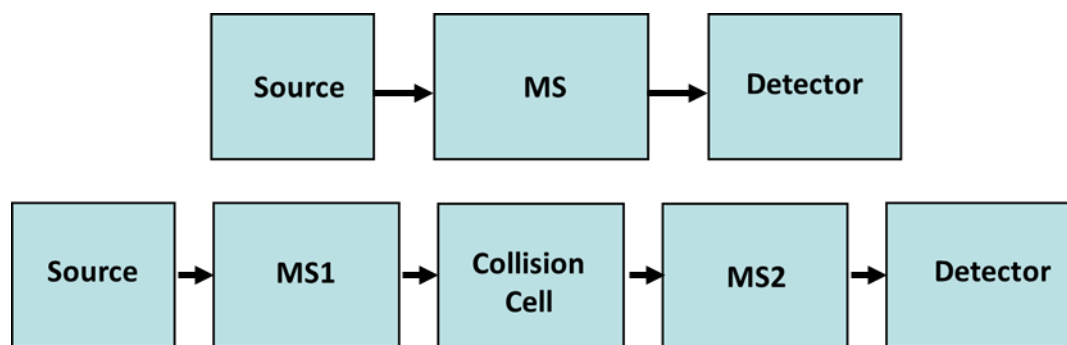
Figure 25: **Schematic representation of a mass spectrometer(top), or a MS/MS mass spectrometer (bottom)**

2. Ionization Source: ESI

The ionization source used for our experiments was an ESI (ElectroSpray Ionization) source. ESI source uses an electric field to ionize molecules in solution and a difference of potential between lenses to assist the transfer of ions from solution to a gaseous phase. Molecules are converted to ionic form by protonation or deprotonation depending on the polarity of the ionization process in the MS and the presence of charged. Within an ESI source, a continuous stream of sample solution is passed through a stainless steel, which is maintained at a high voltage (e.g. 5.5kV) relative to the wall of the surrounding chamber. A positive voltage generates positive ions and a negative voltage generates negative ions. The charged droplets, generated at the exit of the electrospray tip, pass down a pressure gradient and potential

gradient toward the analyzer region of the mass spectrometer. With the aid of an elevated ESI-source temperature and/or another stream of nitrogen drying gas, the charged droplets are continuously reduced in size by evaporation of the solvent, leading to an increase of surface charge density and a decrease of the droplet radius. Finally, the electric field strength within the charged droplet reaches a critical point at which it is kinetically and energetically possible for ions at the surface of the droplets to be ejected into the gaseous phase. The emitted ions are sampled by a sampling skimmer cone and are then accelerated into the mass analyzer for subsequent analysis of molecular mass and measurement of ion intensity.

3. The quadrupole mass analyzer

In a quadrupole mass analyzer, an assembly of 4 parallel metal rods is kept at equal distance (Figure 26).
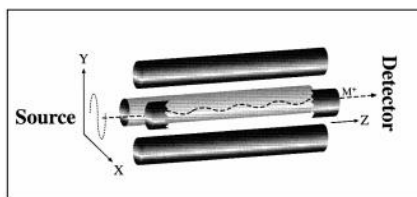
Figure 26: **Operation of a quadrupole mass analyzer**. The ion (M^+) travels from the source, through the 4 metal rods arrangement in the unique oscillating pattern, and reach the detector. Image obtained from(178).

Each pair of opposite rods is connected electrically. An equal but opposite DC voltage superimposed with a radio frequency (RF). AC voltage is applied to the diagonally placed pair of rods. The resulting electrical field causes the ions to travel forward in the z direction with oscillatory motion in the x-y plane. The amplitude of oscillation bears a unique relationship with the *m/z* ratio and can be controlled by changing the DC and RF voltages simultaneously in a pre-fixed ratio. These DC and RF voltages can be set so that amplitudes of oscillation for desirable *m/z* ratios are "stable" with the ions travelling along the z-axis without hitting the quadrupole rods, and finally reaching the detector. On the other hand, the oscillatory amplitudes of undesirable ions are large and "unstable"; they hit the metal rods, get neutralized, and fail to reach the detector.

4. Tandem quadrupole system

In a typical tandem quadrupole system, there are three quadrupoles set up in a linear fashion. The analyte ion of interest (usually called the precursor ion) is mass-selected by the first quadrupole (Q1) and allowed to collide with a collision gas (N_2 in our case) in a second RF-only quadrupole collision cell (Q2). Precursor ions are activated by collision and undergo further fragmentation. This process is known as collision-induced dissociation (CID). The daughter ions resulting from CID are related to the molecular structure of the ions and can be monitored by a third quadrupole mass analyzer (Q3) providing structural information of the molecular ions. This tandem system is commonly denoted as MS/MS.

5. The ion trap mass analyzer

In our case a linear ion trap (LIT) is used for the MS/MS experiences. LIT is a spectrometer based on four rod quadrupoles closed by two electrodes at the entrance and the exit of the cavity. They are used to trap positive or negative ions inside the quadrupole respectively by the application of a positive or a negative continue voltage. Ions are then cold by collisions with an inert gas at low pressure. They fly between the two electrodes following the z axis and oscillate in the xy plane due to the presence of a RF voltage applied on the rods. The voltage is asymmetric and allows the accumulation of ions at the extremity of the trap, increasing the sensitivity of a such system. Ions are then ejected according to their *m/z* ratio following the application of an alternative voltage on the electrodes. During tandem MS, the precursor ion is selected inside the trap where an inert gas is introduced for CID. After that, the product ions are ejected for detection. Alternatively, the product ions can be kept inside the trap and another CID reaction can be initiated and this repeated CID reaction can continue for several times (denoted as MSn in which n is the number of CID reactions). This can help differentiating molecules with similar structures.
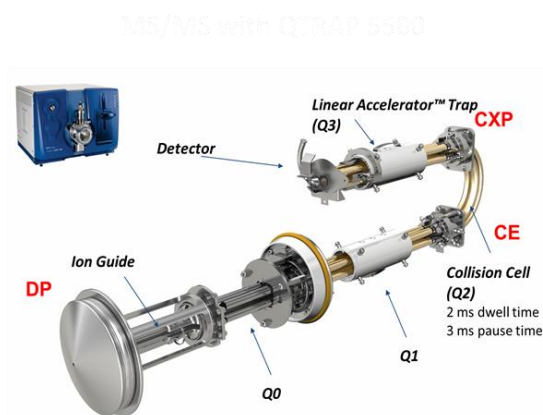
Figure 27: **Linear ion trap** used as a tandem MS/MS. Image obtained from(179)

Different potentials DP, CE and CXP located at the entrance of the source, in the collision cell and in the LIT are applied and optimized for each type of phospholipids to allow the best signal/noise ratio in spectra. The DP (De-clustering Potential) is a parameter that controls the voltage on the orifice, and which controls the ability to de-cluster ions between the orifice and IonDrive QJet ion guide. It is used to minimize the solvent clusters that may remain on the sample ions after they enter the vacuum chamber, and, if required, to fragment ions. The higher the voltage, the higher the energy imparted to the ions. If the DP parameter is too high, unwanted fragmentation may occur. The CE (Collision Energy) parameter controls the potential difference between Q1 and Q2 (collision cell). It is used only in MS/MS-type scans. This parameter is the amount of energy that the precursor ions receive as they are accelerated into the collision cell, where they collide with gas molecules and fragment. The CXP (Collision Cell Exit Potential) parameter is only used in Q3 and MS/MS-type scans, where it transmits the ions into Q3.

6. **Type of scans:**

Tandem mass spectrometry is working according to different ways. The following modes of data acquisition are commonly used in a tandem quadrupole system:

Product scan (daughter scan): Q1 is static allowing only one ion of specific m/z ratio to pass through and Q3 scans the different CID product ions. This is a "purification" step inside the MS system, eliminating complicated and time-consuming sample purification procedures prior to MS analysis. The sample purification step is sometimes necessary to provide the elimination of impurity (like salt, urea…) that prevent or avoid the ionization of the molecule of interest.

Precursor scan (parent scan): Q1 scans over a range of possible precursor ions and Q3 is static focusing on one unique product ion resulting from CID of a class of precursor ions.

Neutral loss: Both Q1 and Q3 scan together at a constant difference in m/z ratio. This is used to monitor the loss of a neutral fragment for a class of molecules from CID.

Multiple reaction monitoring: Both Q1 and Q3 are static for a pre-determined pair of precursor and product ions. This confers the highest specificity and sensitivity and is commonly used in LC-ESI-MS/MS quantification procedures.
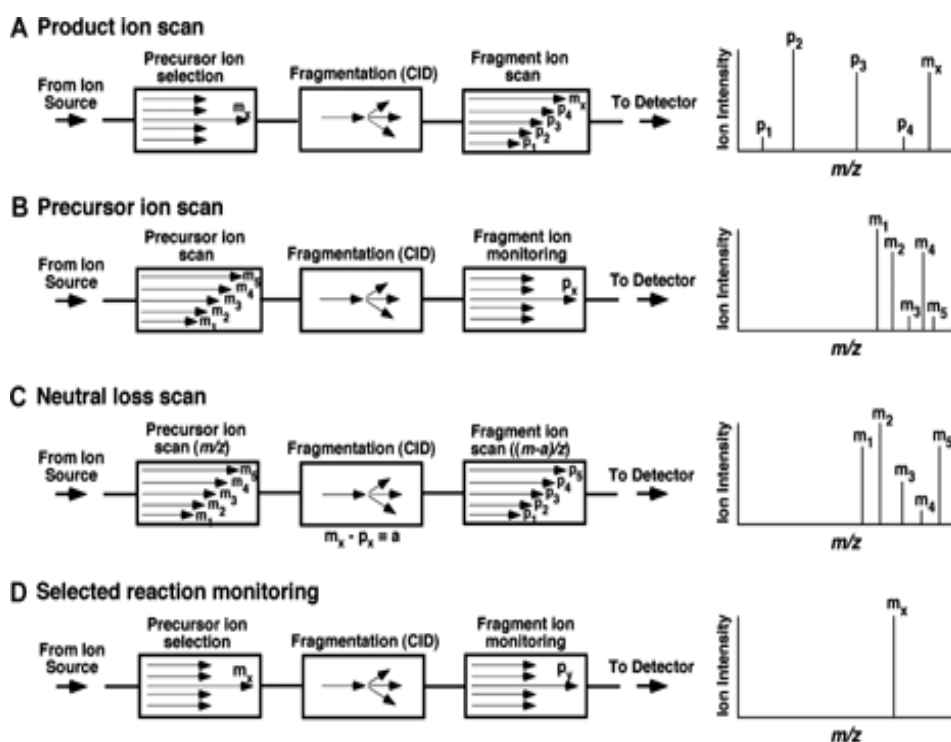
Figure 28: **Types of scan** used with a tandem quadrupole

7. **The Mass Spectrum**

The mass spectrum is a graphical display of the relative abundance of ion signals against the m/z ratios. It is a common practice that the highest signal is taken as 100% abundance and all the other signals are

expressed as a percentage of this. Fragmentation of the protonated or de-protonated molecular ions generated from ESI is generally limited, and the mass spectra are relatively simple. However, multiple-protonation of proteins and peptides occurs in the ESI process, and the ESI mass spectra might become more complicated. A first purification step by HPLC helps the interpretation along the complexity of the mass spectra.

8. **Assessment**
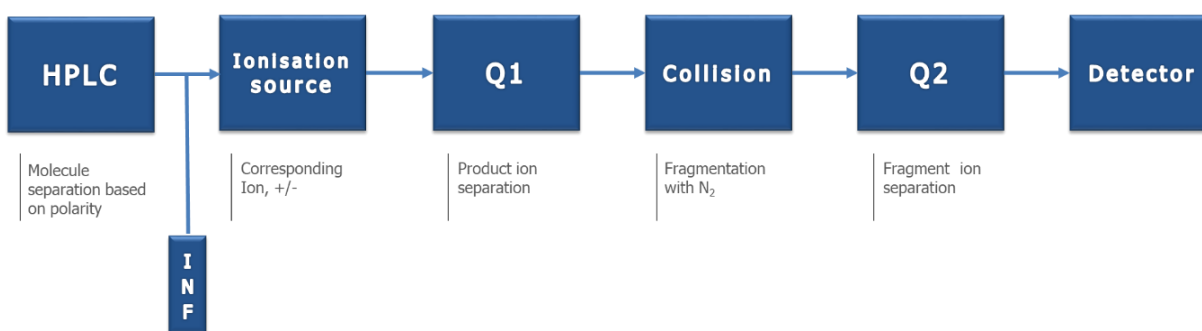
Figure 29: **Schematic view of a MS/MS experiment**

1) Nuclear Lipid Extract Study

Lipid extracts have been first analyzed by direct infusion mass spectrometry. Infusion mass spectrometry allow direct finger printing of a sample. One of the major advantage of such a fingerprint method compare to LC-MS analysis is the ability to obtain a rapid acquisition of the full range of a complex sample mass spectrum. Precursor/product ion couples were identified and used further in MRM methods to quantify all identified phospholipids. LC-MS provides multidimensional separation of lipid molecules differentially eluted by chromatography. In our study, LC-MS was done afterward. Therefore, Reversed Phase HPLC was chosen to allow the separation of phospholipids driven by the hydrophobicity of their fatty acid (FA) chains (number of double bonds and the length of FA chains).

2) Shotgun mass spectrometry

Phospholipid extracts were dissolved in $CHCl_3/CH_2OH$ (1:2, v/v) + 8 mM ammonium acetate and then centrifuged to remove the non-dissolved components. Each sample was infused into the TurboV electrospray source of a mass spectrometer model QTRAP® 5500 (Sciex, Concord, Ontario, Canada) at a flow rate of 7 µL/min. ESI- MS/MS experiments (Precursor scans) (180) were performed in the negative (PE, PS, PA, PI, PG) and positive ion modes (PC) with fast polarity switching (50 ms) and a scan rate of 200 Da/s. Nitrogen was used for the curtain gas (set to 15), gas1 (set to 20) and gas2 (set to 0). Needle voltage was set at -4,5 or +5,5 kV without needle heating. The declustering potential was either -100 V or +100 V. Calibration was achieved using an ES Tuning Mix (AB Sciex). The collision gas was nitrogen and collision energy was fixed to either -50 or 50 eV. The mass range was m/z 250–1100. MS/MS

experiments included one positive mode precursor ion scan and 54 negative mode precursor ion scans. Phospholipids species were identified using Lipid View software (v1.0, AB Sciex, Concord, Ontario, Canada).

3) Liquid chromatography mass spectrometry

LC-MS/MS (MRM mode) analyses were performed with the same mass spectrometer model QTRAP® 5500 (Sciex, Concord, Ontario, Canada) coupled to a LC system (LC-20AD XR pump, Shimatzu, Marne-la-vallée, France) and PAL HTC-xt Autosampler (CTC Analytics, Zwingen, Switzerland). Phospholipid extracts were dissolved in CH_3CN/H_2O 80/20. Analyses were achieved in the negative (PE, PS, PA, PI, PG) and positive modes (PC) with fast polarity switching (50 ms); nitrogen was used for the curtain gas (set to 20), gas1 (set to 35) and gas2 (set to 0). Needle voltage was at -4,5 or +5,5 kV without needle heating; the de-clustering potential was adjusted to +40 V and between -180V and -85 V. The collision gas was also nitrogen; collision energy was +47 eV and varied from -62 to -48 eV. The dwell time was set to 3 ms. MS/MS experiments were performed by 19 positive and 111 negative MRM scans.

Table 4: **Quantity of sample and internal standard used for mass experiments**

Sample name	Infusion sample	LC-MS/MS sample
	Quantity	Quantity
Samples	~ 0.25 mg	~ 49 pg
IS PA 17:0/17:0		10 pmol
IS PE17:0/17:0		2.5 pmol
IS PG 17:0/17:0		2.5 pmol
IS PI 17:0/14:1		2.5 pmol
IS PC 17:0/17:0		0.5 pmol

Phospholipids species were identified using Lipid View software (v1.0, AB Sciex) and the area of LC peaks were determined using MultiQuant software (v2.1, AB Sciex). Reversed phase separations were carried out at 40 °C on a Ascentis RP Amide 150×1 mm column, with 3 μm particles (Supelco, Sigma Aldrich, St Quentin Fallavier, France)). Eluent A was H_2O+0.1 % formic acid and eluent B was CH_3CN+0.1 % formic acid. The gradient elution program was: 0 min, 30 % B; 8 min, 30 % B; 10 min, 70 % B; 35–36 min, 87 % B; 37 min, 30 % B. The flow rate was 50 μL/min; 10μL sample volumes were injected.

4) Data Analysis

Precursor ions MS/MS scans were collected during 20 min infusion time to acquire tandem mass spectra for lipid identification process from nuclear lipid extract samples. The result files (*.wiff and

*.wiff.scan files) from experimental MS/MS scans, were then loaded to Lipid View in order to identify each lipid species by their product and fragment ions couple. Each fragment ions were assigned to their precursor ions and each precursor/fragment ions couple was linked to the corresponding lipid species. The resulting files were exported in *.txt and verified carefully to erase any misattribution on the Lipid Map data base (fragmentation ion data base).

Shotgun infusion experiments allowed detection of 130 lipid species (PC, EPC, PA, PE, PG, PS, PI) in the nuclear lipid extract. In order to quantify each species, MRM LC-MS were performed.
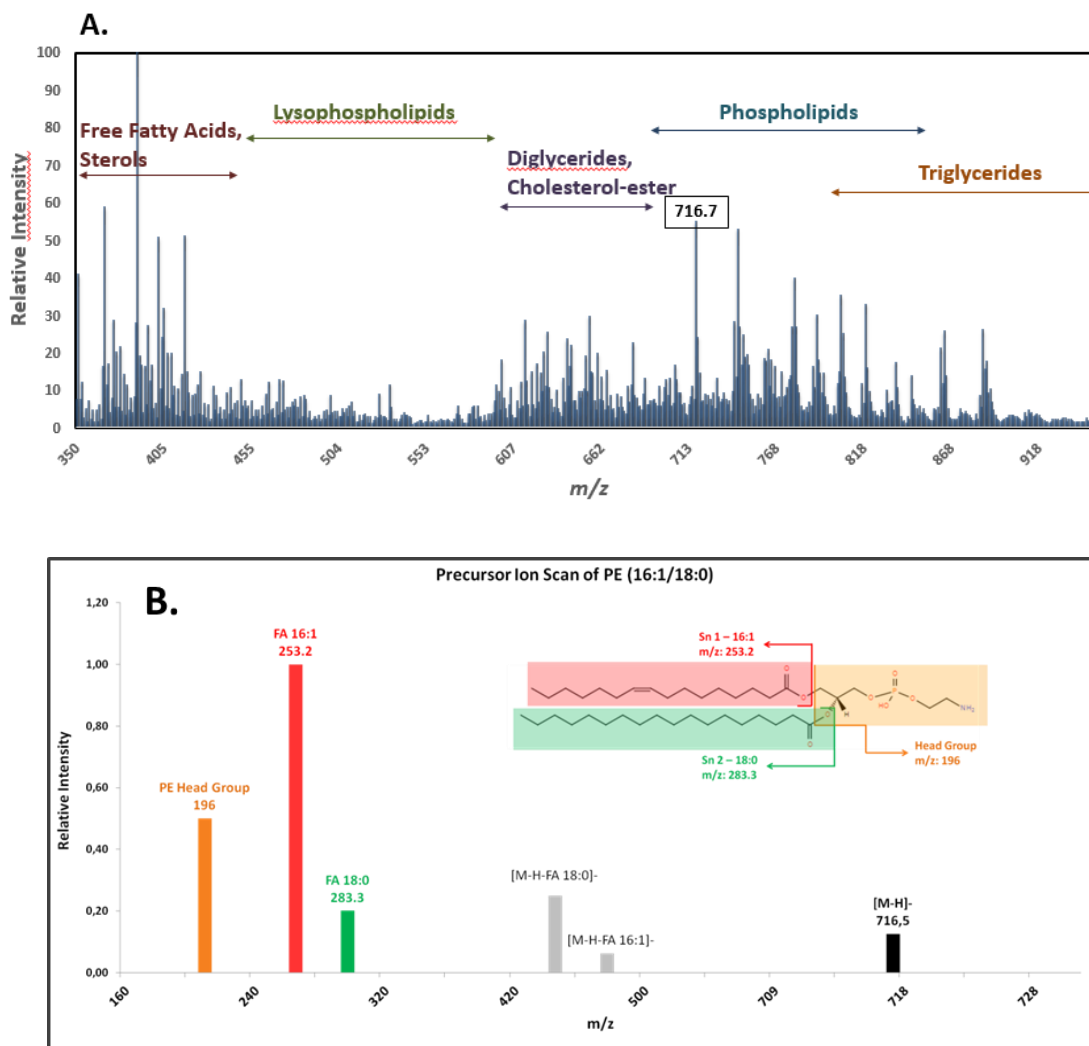
Figure 30: A. **Example of MS shotgun analysis of the nuclear lipid extract**. 0.25 mg of nuclear lipid extract were dissolved in CHCl$_3$/CH$_2$OH (1:2, v/v) + 8 mM ammonium acetate The mass spectrum was acquired in the negative ion mode in the MS mode with a mass range from *m/z* 350 to 1000. The presence of different lipid species can be observed: free fatty acids, sterols, lyso-phospholipids diglycerides, cholesterol-ester, phospholipids, triglycerides. B. The Shotgun MS/MS analysis of nuclear lipid extract generated a list of precursor ion scan (PIS) mass spectra. The mass spectrum shows PE (16:1/18:0) precursor ion scan result.

Table 5:**List of phospholipid *m/z* fragmentation results**

	Name of the different classes of phospholipids	X structure	(m/z)
Negative Ionization			
Polar Head ... Fatty Acids	Phosphatidic acid (PA)	-H	153
	Phosphatidylethanolamine (PE)	$-CH_2-CH_2-NH_3^+$	196
	Phosphatidylglycerol (PG)	$-CH_2-CH(OH)-CH_2-OH$	153
	Phosphatidylserine (PS)	$-CH_2-CH(COO^-)-NH_3^+$	153
	Phosphatidylcholine (PC)	$-CH_2-CH_2-N^+(CH_3)_3$	153
	Phosphatidylinositol (PI)		241
	FA 14:1		225,2
	FA 14:0		227,2
	FA 16:2		251,2
	FA 16:1		253,2
	FA 16:0		255,2
	FA 17:0		269,3
	FA 18:3		277,2
	FA 18:2		279,2
	FA 18:1		281,3
	FA 18:0		283,3
	FA 20:5		301,2
	FA 20:4		303,2
	FA 22:6		327,2
	FA 22:5		329,2
Positive Ionization	Phosphatidylcholine (PC,SM)	$-CH_2-CH_2-N^+(CH_3)_3$	184

5) MRM data treatment

Based on MS/MS infusion results, a MRM method *.txt file was created where precursor and fragment ions were correlated to each lipid found as well as each EC, DP and CXP correlated optimized values (applied according experimental data and literature). Lipid species were first separated based on the hydrophobicity of their FA chains. Then MS/MS experiments were done where both Q1 and Q3 were set

static for a pre-determined pair of precursor and product ions given by the infusion experiment. The areas corresponding to a species linked to a pair of precursor and product ions, were then collected, corrected with a corrected factor (based on the ionization capability of PL species) and the molar percentage of each species was calculated relatively to the corresponding PL internal standard. Global spectra for positive and negative ionization of the nuclear lipid extract are presented following.
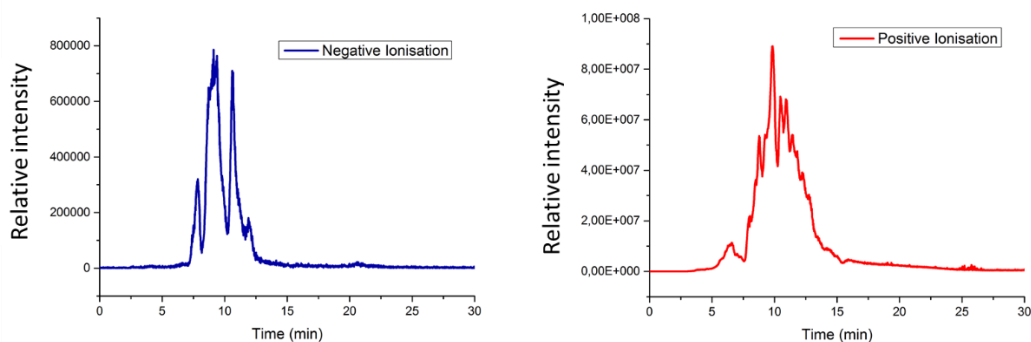
Figure 31: **HPLC chromatogram of negative and positive ionization of the nuclear lipid extract.** The spectrum of external standard shows the dispersion of pics in function of the phospholipid species.
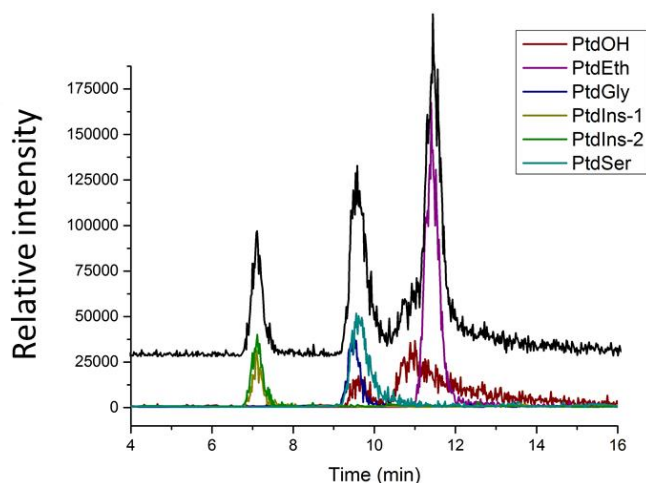
Figure 32 **HPLC chromatogram of lipid standards.**

V.   Lipid extraction

Biological samples were extracted according to a modified Folch extraction (Garnier L'homme et al, 2009; Pettitt, 2009). The 200 µL of sample were added to 4 ml of ice-cold 2.5:1 Chloroform: Methanol acidified with concentrated HCl in a glass universal. The mixture was briefly probe sonicated (Soniprep 150, MSE UK) for 10 seconds at power 22, and left on the bench for 1 hour. Samples were then filtered through a 0.22 µm Durapore membrane (Millipore) resistant to chloroform. The sample was filtered through the membrane placed on a sintered glass filter with silicone rubber stopper overhung by a borosilicate glass funnel and placed on top of a conical flask. The assembly was sealed tightly with an

aluminum clamp. Samples were collected in a specimen tube placed inside the flask. 0.2 volumes of K-EDTA were added and the sample transferred to a Chromacol screw-top vial using a Pasteur pipette and centrifuged at 800 g for 15 minutes at 4 °C. The organic lower phase was transferred to a fresh Chromacol tube and dried at 37 °C under a stream of nitrogen gas using a sample concentrator (Techne, Burlington). (Meanwhile the upper aqueous phase and the interface of denatured protein was discarded). The lipid pellet was resuspended in 100 µl (5:5:1) Chloroform: Methanol: Water and transferred to a glass sample tube insert (Alltech).

VI.   Phospholipid quantification: Fiske assay

Samples were performed in triplicate and corresponded to around 50 nmol of phosphorous lipid. A range of 0, 25, 50, 75, 100 phosphorous nmol samples were done in duplicate from 1 mM of K_2HPO_4. 500 µL of a 60% perchloric acid was added in each tube. Tubes were vigorously vortexed and introduced into a heating block at 205 °C for 45 min. Phospholipid hydrolysis achieved leaving free inorganic phosphate. Tubes were cooled down at room temperature. 4 mL of ammonium heptamolybdate solution $[(NH_4)6Mo70_2.4H_20]$ were added following by 500 µL of a 10 % Ascorbic acid solution (added while vortexing). Yellow colored solution. Tubes were introduced into a boiled water bath and leave 6 min, during this period color shift to blue. After cooled down in water the absorbance was measured at 812 nm.

VII.   Nuclear Magnetic Resonance (NMR)

Several methods exist to study and understand biological membranes. Each of them probes different properties. First liquid phase studies were done by X ray diffraction (52), then, other methods were developed for model lipid membranes in order to study other frequency ranges. Infra-red and Raman probe fast movements (10^7 to 10^{11} Hz) and RPE probe slow movements (10^3 to 10^9 Hz). Cryo-microscopy and ATM can also give other structural information. The specificity of NMR is the capacity to cover a large scale of movements from 10^{-1} to 10^{10}Hz that allow to obtain a lot of structural information. NMR is used to study structures and dynamics of membranes (scale of time from ps to s).

1. **NMR used for bio-membranes.**

Membranes are large supra-molecular structure defined as thermotropic and lyotropic liquid-crystals. These structures have anisotropic properties that vary related to space direction. In addition, their global movement are relatively slow at NMR experiment scale of time (µs). These two properties induce NMR anisotropic interactions that are expressed by large spectrum. The study of biological membrane needs similar techniques that are used to study solids by NMR.

2. Generality of Nuclear Magnetic Resonance

NMR uses a physical phenomenon that occurs for atoms that own a nonzero kinetic moment $\vec{I}$. As for electrons, nuclei turn on them self, and the nuclear spin operator $\hat{I}$ is used to describe the kinetic moment induced by this rotation. All nuclei that have a nonzero spin number have also a magnetic moment $\vec{\mu}$ that characterizes the magnetic properties of each nucleus. Nuclear spin operators are associated to those two moments by the following relation: $\hat{\mu} = \gamma\hbar\hat{I}$, where γ is the gyromagnetic ratio characteristic of each nucleus and $\hbar = h/2\pi$ with h the Planck constant. When a population of nuclear spins is placed into a static magnetic field $\vec{B}_0$, it is subjected to several interactions. These interactions are divided in two parts: external and internal $=$. External contributions are interactions between nuclei and the external environment (applied static and radiofrequency magnetic fields, field gradients) and internal contributions come from the interaction between the nucleus and the local environment (local magnetic or electronic fields within the sample). Spin nuclear coupling with their environment are described by spin nuclear Hamiltonian concept H (energy operator) developed by Abragam (181). This Hamiltonian is composed of the sum of an external coupling Hamiltonian and an internal coupling Hamiltonian: $\hat{H} = \hat{H}_{ext} + \hat{H}_{int}$.

1) Zeeman external coupling

Without magnetic field, all nuclear spins have various orientations. Magnetization is zero and all the spins have the same energy. Ina strong static magnetic field $\vec{B}_0$, spins are magnetically orientated. This phenomenon is called the Zeeman effect and results from the coupling between nuclear magnetic moment, $\vec{\mu}$ and the static magnetic field $\vec{B}_0$ (parallel to z axis in the laboratory frame of reference). This coupling is described by the Hamiltonian $\hat{H}_0$:

$$\hat{H}_0 = -\hat{\mu} \cdot \vec{B}_0 = -\gamma\hbar\hat{I}_z \cdot \vec{B}_0 \quad [2]$$

where $\hat{I}_z$ is the spin operator in z direction, parallel to $\vec{B}_0$. After solving the Schrödinger equation, the Zeeman energy is represented by the equation $E_m = -\gamma m\hbar B_0$, where m is the magnetic quantum number, which value belongs to the -I and +I interval and varied by integer steps (2I+1 values), where I is the nuclear spin number (I=1/2, I=1, I=3/2, etc…). In the presence of the static magnetic field, there is an energy magnetization effect distributed in 2I+1 energy levels that is called Zeeman effect (named by is discovered Peter Zeeman, Physics Nobel prize in 1902). Transition between energy levels is possible according to the Bohr law ($\Delta E = h\nu$) with $\Delta m = \pm 1$. A transition leads to a single resonance frequency that appears at a specific frequency ν_0.

$$\nu_0 = \frac{\gamma B_0}{2\pi} \quad [3]$$

This may be depicted by nuclear spin in precession around the principal axe of the magnetic field into laboratory frame of reference (x_L, y_L, z_L) at a specific frequency called Larmor frequency ν_0 (Larmor pulsation being $\omega_0 = 2\pi\nu_0$).
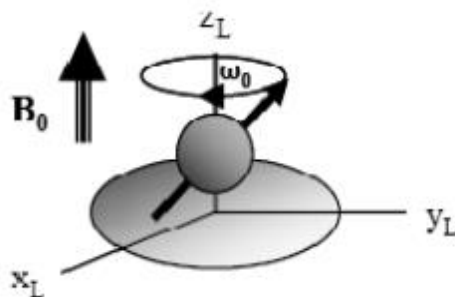
Figure 33: **Precession frequency around $\overrightarrow{B_0}$** (taken from (182)). At thermal equilibrium, nuclear spins precesses around the magnetic field axis with a ω_0 pulsation.

The frequency required to allow a transition is similar to the precession frequency of a nucleus in the magnetic field, from which it is called resonance frequency.

In the high field approximation, the Zeeman interaction prevails over other couplings (181). The quantification axis will be defined by $\vec{B}_0$ and internals coupling will be assimilated as perturbations of Zeeman energy levels.

2) Internal couplings

The Hamiltonian related to internal interactions describes the coupling between nuclear magnetic moments μ and local fields within the sample (183):

$$\hat{H}_{int} = \hat{H}_\sigma + \hat{H}_j + \hat{H}_D + \hat{H}_Q \quad [4]$$

The Hamiltonian $\hat{H}_\sigma$ is linked to the coupling between the nuclear magnetic field and the local magnetic field induced by the circulating electronic cloud of the nucleus under the effect of the static magnetic field. This interaction is also called electronic shielding and is depending on $\vec{B}_0$. Electrons are circulating around the nucleus and create a local magnetic field in the opposite sign of the global magnetic field $\vec{B}_0$ (case of diamagnetics atoms). An isolated nucleus may thus appears partially "protected" from $\vec{B}_0$ by its electrons, i.e., shielded. When these electrons are engaged in chemical bonds, the electronic density around the nucleus is decreased (or increased) and the nucleus feels in a higher (or lower) manner the global magnetic field. The nucleus appears de-shielded (or shielded).

The Hamiltonian $\hat{H}_j$ is describing the coupling between magnetic moments close through bonds of a same molecule. This interaction occurs by electrons implicated in a chemical bond. This coupling is only internal to a molecule. It's called indirect spin-spin coupling or scalar coupling and it is not depending on the $\vec{B}_0$ intensity and can be homo (like spins) or hetero nuclear (atoms of different nature).

60

The dipolar interaction $\widehat{H}_D$ is associated to the coupling that exists between two magnetic dipole $\vec{\mu}_A$ and $\vec{\mu}_B$, close to each other in space (a few Å). It is called direct spin-spin coupling and it is not depending on the magnetic field $\vec{B}_0$ but depending on the distance between nuclei A and B (it is decreasing quickly with the distance r_{AB} between nuclei). This interaction can be homo- or hetero-nuclear.

The quadrupolar interaction $\widehat{H}_Q$, appears for nuclei with nuclear spin higher than $^1/_2$. Those nuclei have a quadrupolar moment. This interaction shows the coupling between the quadrupolar moment of a nucleus and the electric field gradient (EFG). This EFG is created by the presence of external charges of the nucleus (electrons, ions, …). The quadrupolar coupling is independent of the magnetic field $\vec{B}_0$. According to the previous equation, the total Hamiltonian of a nuclear spin placed in a magnetic field can be written as:

$$\widehat{H} = \widehat{H}_z + \widehat{H}_\sigma + \widehat{H}_J + \widehat{H}_D + \widehat{H}_Q \qquad [5]$$

The strength of these interactions depends of the nucleus type, as well as physicochemical properties of the sample (liquid, solid or soft matter). Depending whether the system is of "solid" nature (internal anisotropic interactions), or "liquid" type (isotropic interactions), some components of the total Hamiltonian will dominate. The following table gives an order of magnitude in Hertz (Hz) of the energy associated with the Hamiltonians.

Table 6: **Order of magnitude in Hertz of the several Hamiltonians in solid and liquid-state systems**.

	$\widehat{H}_z$	$\widehat{H}_\sigma$	$\widehat{H}_J$	$\widehat{H}_D$	$\widehat{H}_Q$
Solid Systems	10^8	10^4 anisotropic	10^2	10^4	10^6 (I $\geq$ 1) 0 (I < 1)
Liquid Systems	10^8	10^4 anisotropic	10^2	0	0

In "liquid" systems, the contributions of dipolar and quadrupolar interactions are zero. This is due to the high dynamics of molecules in such systems (fast Brownian motions) that average to zero the orientation dependence of these interactions (*vide infra*). The same principle is applied for chemical shift anisotropy where in "liquid" systems a single isotropic contribution is obtained. The chemical shift anisotropy depending on orientation is averaged to the isotropic chemical shift.

We usually speak of Liquid-state NMR or Solid-State NMR. In Liquid-state NMR, relaxation times (times to reach the thermodynamic equilibrium) are relatively long (about several seconds). Furthermore, interactions that occur are the isotropic electronic shielding and the indirect spin-spin coupling. The spectral window for spectral detection will be relatively short (a few kHz).

In solid-state NMR relaxation times may be relatively short (reaching ms or µs for deuterium NMR of lipids). The interactions that can be observed are the chemical shift anisotropy, the dipolar coupling, and

the quadrupolar coupling for spins that are higher than $^1/_2$. This phenomenon implies detection windows much higher than in liquid NMR (a few MHz).

3. Biomembranes NMR

We consider here the case of large liposomes (several μm) undergoing very slow global motions with respect to magnetic or electric solid state interactions. In liquid-state NMR, the proton (^{1}H) is the nucleus the most used because it is naturally highly abundant and with a gyromagnetic value especially high, which makes its detection easier. However, is not really used in Solid-state NMR, unless magic angle sample spinning (MAS) at very high speed is used (*vide infra*). In lipid bilayers, there are thousands of non-equivalents protons. As the individual lines are quite large it is impossible to identify each of them. The same problem occurs with carbon-13 which in addition have low natural abundance. Again resolution can be obtained using MAS. When willing to perform broad-band Solid-state NMR of membranes other nuclei are used to study membranes by NMR such as phosphorus (^{31}P) and deuterium (^{2}H).

1) Phosphorus-31-NMR: chemical shift anisotropy (CSA)

The phosphorus is naturally present at polar heads of all phospholipids. Furthermore, natural abundance of phosphorus-31 is 100%, allowing a good detection without previous isotopic labelling. This nucleus is therefore a good candidate to probe structure and dynamics at membrane interfaces.

i. General case:

The phosphorus is a spin $^1/_2$ nucleus. The predominant interactions are thus the Zeeman effect, chemical shift anisotropy and the phosphorus/proton dipolar coupling. This last one is usually cancelled by a strong proton decoupling and will not be described below. Electrons that move around the phosphorus nucleus create a local magnetic field described with the following equation:

$$\vec{B}_{eff} = \vec{B}_0 - \sigma\vec{B}_0 = \vec{B}_0(1 - \sigma) \qquad [6]$$

where σ is the shielding tensor which can be written in its principal axis system as:

$$\begin{bmatrix} \sigma_{xx} & 0 & 0 \\ 0 & \sigma_{yy} & 0 \\ 0 & 0 & \sigma_{zz} \end{bmatrix} \qquad [7]$$

where $\sigma_{xx}, \sigma_{yy}, \sigma_{zz}$ are the principal values of the CSA tensor.

The total Hamiltonian for phosphorus-31 nuclei is written as (184):

$$\hat{H} = \hat{H}_z + \hat{H}_\sigma = -\gamma\hat{I}_z\hat{B}_0(1 - \sigma) \qquad [8]$$

ii. Lipid bilayer:

Lipids that are implicated in fluid phase bilayer structures are subject to a certain number of anisotropic movements that modified the shape of the powder spectrum (Figure 35, b and c).

Phospholipids turn rapidly on themselves and have their principal axis of rotation oriented along the molecule long axis. This fast rotation movement, co-linear to the bilayer, gives to lipids in this liquid crystal structure an axial symmetry. This converts the static tensor in a residual averaged tensor expressed in the bilayer frame of reference with the lipid long axis perpendicular to the bilayer plane (z axis):

$$\sigma = \begin{bmatrix} \sigma_\perp & 0 & 0 \\ 0 & \sigma_\perp & 0 \\ 0 & 0 & \sigma_\parallel \end{bmatrix} \quad [9]$$

Which leads after some calculations to the following observed frequency:

$$\nu(\beta) = \nu_0 \left[1 - \sigma_{iso} - \frac{2}{3} \Delta\sigma \left(\frac{3\cos^2\beta - 1}{2} \right) \right] \quad [10]$$

Where σ_{iso} is the trace of shielding tensor linked to isotropic chemical shift and $\Delta\sigma$, the anisotropy, which translates for membranes with local axial symmetry (lipids undergoing fast axial spinning in the bilayer) to $\Delta\sigma = \sigma_\parallel - \sigma_\perp$, where $\sigma_\parallel$ and $\sigma_\perp$ are the principle components of the averaged CSA tensor. The angle β representing the orientation of the local normal of a liposome with respect to the magnetic field.
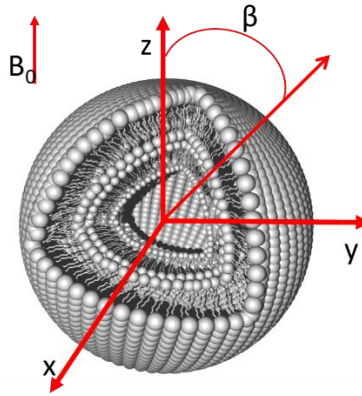
Figure 34: **Orientation of a liposome with respect to magnetic field**

Because liposomes are slowly tumbling, the spectrum is composed of an overlap of several resonance frequencies (obtained for different β angles) weighted by their distribution probability, P(β)=sinβ (spherical distribution). The less favorable orientation is obtained when $\beta = 0°$ (parallel to $\vec{B}_0$), and the most favourable is obtained for $\beta = 90°$ (perpendicular to $\vec{B}_0$). The chemical shift anisotropy can be measured on spectra by using the extreme frequencies of resonance that correspond to $\beta = 0°$ and $\beta = 90°$:

$$\Delta\sigma = \Delta\nu(90°) - \Delta\nu(0°) = \Delta\sigma_\perp - \Delta\sigma_\parallel \quad [11]$$

The phosphorus NMR lineshape gives information about the dynamics and the organization of phospholipids in membranes. The figure represents different spectral shapes obtained for lipids engaged in different types of phases. a) phospholipids as a dry powder, b) and c) of lipids organized in bilayer liposomes in gel or fluid states respect.
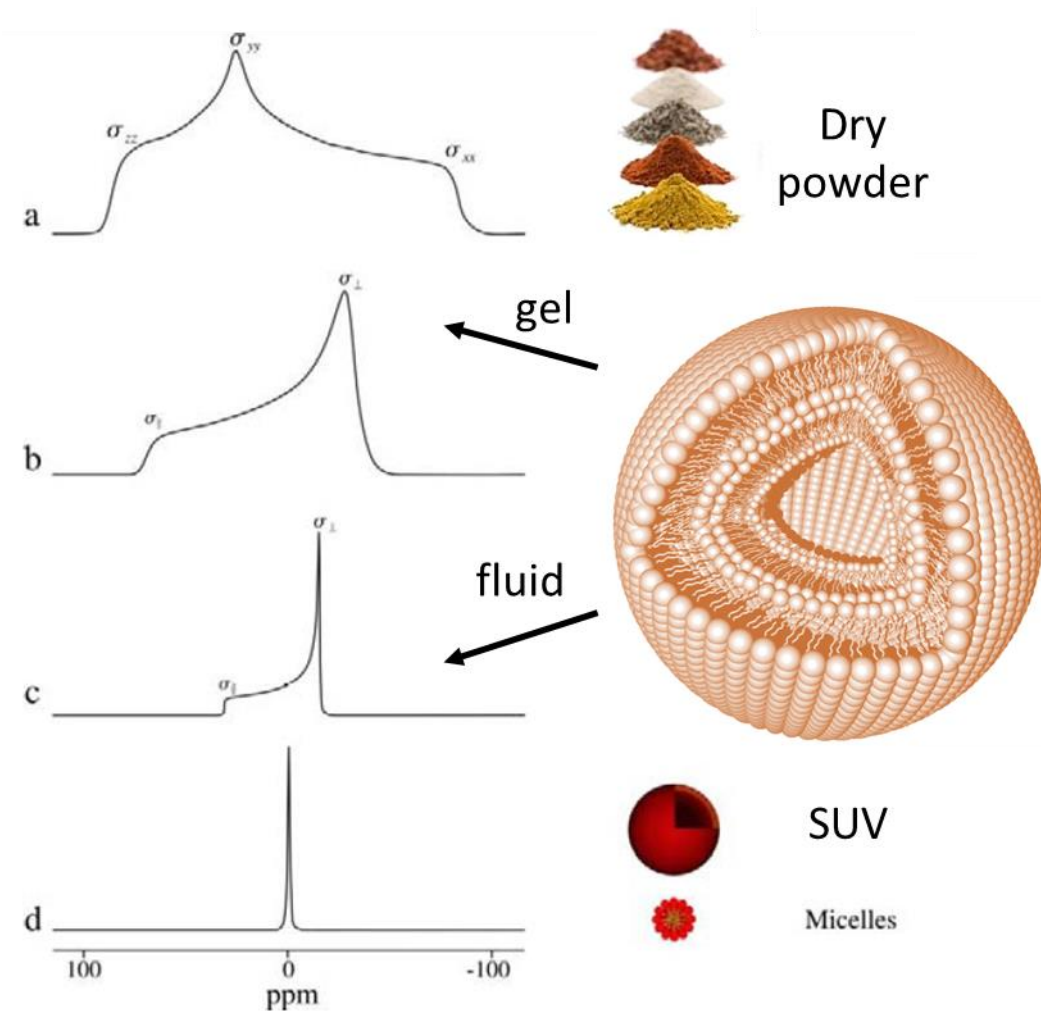
Figure 35: **Phosphorus NMR spectra as a function of lipid phases** (adapted from (185))

If lipids are engaged in small fast rotating objects (SUV or micelles), the spectrum has the form of a single isotropic line. The high dynamics of these objects induces an averaging to zero of the chemical shift shielding anisotropy. The tensor will be expressed simply with its isotropic part.

2) Wide-line deuterium-2H NMR: quadrupolar interaction

The natural abundance of deuterium is very low (0.01%) so it is necessary to use labelled lipids.

i. Generalities:

Deuterium atoms have a nuclear spin I = 1 and a quadrupolar electric moment, eQ (with e being the elementary charge of an electron and Q the quadrupolar moment of the nucleus). With this type of nucleus, the predominant internal interaction is the quadrupolar interaction, shown by the coupling between the quadrupolar moment of the nucleus and the EFG. With the laboratory as a reference, the Hamiltonian is written as follow (186):

$$\hat{H} = \hat{H}_z + \hat{H}_Q = -\hbar\omega_0\hat{I}_z + \frac{e^2qQ}{4I(2I-1)}\left(3\hat{I}_z^2 - \hat{I}^2\right)\left[\frac{3\cos^2\beta-1}{2} + \frac{\eta}{2}\sin^2\cos 2\alpha\right] [12]$$

where α and β are Euler angles of the coordinate transformation needed to express the EFG axis system into the laboratory frame of reference. eQ =Vzz, is the electric field gradient of the nucleus and η is the asymmetry parameter of EFG nearly equal to 0 for C -^{2}H bonds. Unlike phosphorus-31 there are 3 energy levels associated to this Hamiltonian and there are two transitions (with one quantum). One therefore observes two resonance lines (doublets) on the spectrum, centered on the Larmor frequency. The distance between these two lines is called the "quadrupolar splitting",Δv_Q , and is written as (after some calculations):

$$\Delta v_Q = \frac{3}{2} A_Q \left(\frac{3 \cos^2 \beta - 1}{2} \right) \qquad [13]$$

Where A_Q is the static quadrupolar coupling constant and β defines the orientation of bond C-^{2}H relative to the z-axis of the laboratory frame of reference, parallel to the magnetic field $\vec{B}_0$.
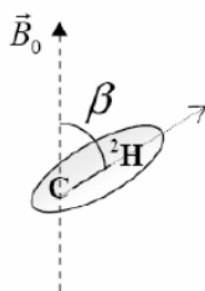
Figure 36: **Angle β between the bond C-^{2}H and the magnetic field** (extract from Loudet 2006). The grey oval is representing the EFG.

ii.   Lipid bilayer:

When lipids are engaged in a fluid phase bilayer, they are subject to many axial motions (bonds isomerizations, molecule rotations, etc…). Depending on the bilayer nature (gel or fluid) as well as the global size of the object (MLV, SUV or micelle), the appearance of the spectrum will be modulated. As for phosphorus NMR, the more the dynamics of a system increases, the more the quadrupolar interaction will decrease.
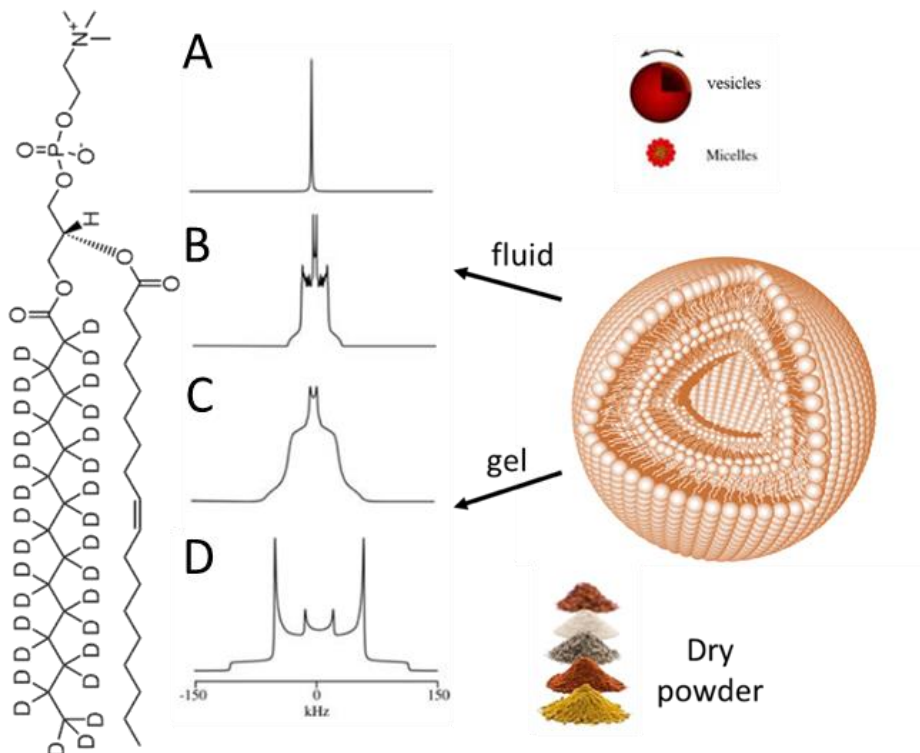
Figure 37: **Effect of molecular motions on deuterium solid-state NMR spectra profiles taken from (185).** (A) Isotropic peak characteristic of lipids in very small vesicles assimilated to molecules in the liquid phase. (B) Spectrum profile characteristic of a bilayer in the fluid phase. It results from the molecular axial rotation and oscillation. (C) Spectrum profile characteristic of a bilayer in the gel phase where axial molecular rotation are present and molecular oscillations are abolished. (D) Phospholipid in the solid-state with no molecular motion.

3) Order parameter

In order to describe membrane order and dynamics, Saupe and Seelig have introduced the Order parameter concept. This parameter is used to quantify the organization state of a system (187). The fluctuations in space and time of the C - ^{2}H bonds compared to the normal to the bilayer plane can be estimated by the order parameters S_{ii}:

$$S_{ii} = \frac{3\langle cos^2\theta_i\rangle - 1}{2} \qquad [14]$$

where, i= x, y, z are representing the axis system of the C-^{2}H bond. θ_i represent the orientation of the bond axis with respect to the normal to the bilayer (lipid axis, x', y', z'). The angular brackets stand for a time and space average.

Due to axial symmetry, $S_{zz'}$ is enough to report on system fluctuations:

$$S_{zz'} = -2s_{xx'} = -2s_{yy'} \qquad [15]$$
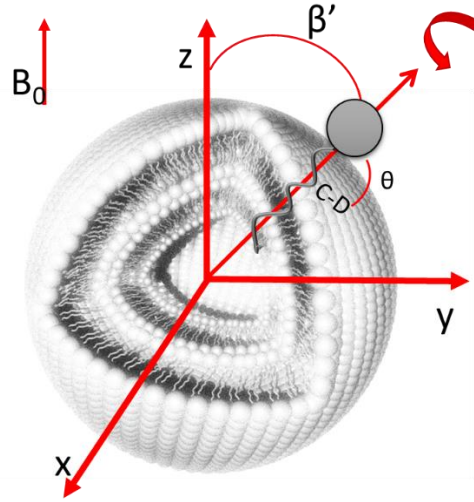
Figure 38: **Orientation of the C-D bond with respect to the magnetic field**

And the quadrupolar splitting can be expressed as:

$$\Delta \nu_Q = \frac{3}{2} A_Q \left[\frac{3 \cos^2 \beta' - 1}{2} \right] S_{zz'} \quad [16]$$

where β' corresponds to the angle between the principal z' axis of the lipid and the magnetic field $\vec{B}_0$. As the C-^{2}H bond is practically co-linear with EFG then $S_{zz'}$ can be noted S_{CD} and gives information of bond C-D (C-^{2}H) fluctuations.

$$\Delta \nu_Q = \frac{3}{2} A_Q \left[\frac{3 \cos^2 \beta' - 1}{2} \right] S_{CD} \quad [17]$$

The measurement of the quadrupolar splitting between the two most intense peaks (orientation corresponding to β'=90°) give an direct estimate of the order parameter S_{CD}:

$$\Delta \nu_Q (90°) = \frac{3}{4} A_Q S_{CD} \quad [18]$$

In a lipid membrane, the order parameter will change relative to the position of the bond along the chain. A C-D bond order profile can be represented as a function of the carbon position along the lipid chain. The Figure 39 shows a lipid order profile of ^{2}H$_{31}$-POPC MLV at 25°C. It has been shown, using selectively deuterated lipids (188) that C-D nearby the glycerol backbone have a larger quadrupolar splitting and a higher order parameter than CD at the end of the lipid chain. Furthermore, S_{CD} of the *ca.* first 5 to 6 carbon atoms are quite constant. This phenomenon is called the "plateau". This effect is due to steric constraint of hydrophilic polar head organization that restrain movement in this area. Methyl terminal S_{CD} have a lower value resulting in a higher degree of freedom (rotation around the C_3 axis).
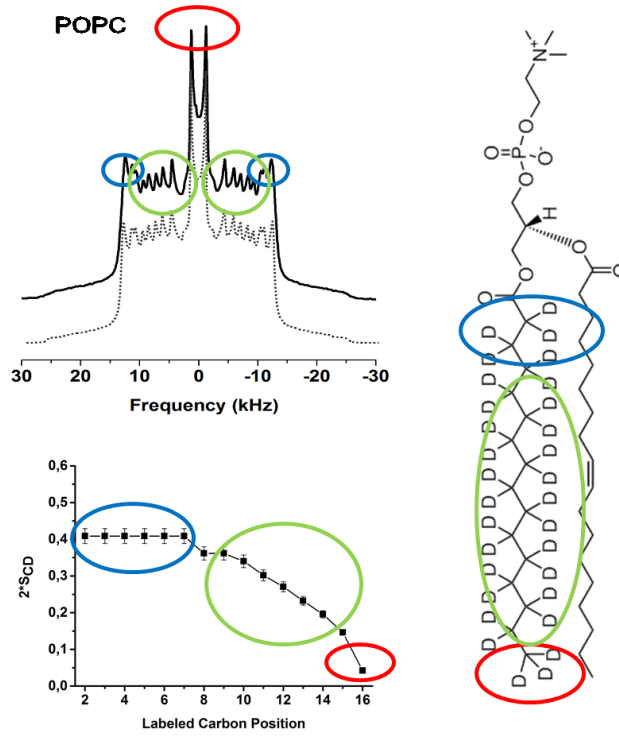
Figure 39: **Order Parameter Profile.** Top: NMR spectrum and its simulation (dotted line) of ^{2}H-POPC in MLV. Right: Molecular structure of ^{2}H$_{31}$-POPC. Bottom: order parameter profile representing S_{CD} as a function of deuterated carbon number of ^{2}H$_{31}$-POPC.

4) Liposome deformation

Lipids and proteins have a weak anisotropic magnetic susceptibility: $\Delta\chi = \chi_{//} - \chi_{\perp}$ they might therefore align in magnetic fields. Cell membranes do not usually align in weak magnetic fields, but the effect of magnetic fields on liposomes having been reconstituted with natural lipid extracts or some peculiar synthetic lipids have been reported (184, 188). This deformation phenomenon comes from a predominance of the magnetic energy that tends to align molecules parallel or perpendicular to the field (depending on the sign of $\Delta\chi$) and the curvature elastic energy which tends to stabilize the average spherical shape. Following the Helfrich theory (189, 190) one may describe the magnetically induced deformation of membrane bilayer sphere of initial radius r_0 (at the equilibrium, outside the magnetic field) to ellipsoids of revolution of semi-long and semi-short axes c and a, respectively, as the combined effects of both magnetic energy and the membrane elastic energy. The deformation happens when the membrane curvature-elastic energy E_C, is smaller than the orientation energy in the magnetic field, E_H (189, 190). If k_c is the membrane curvature-elastic modulus (in J), B_0 the magnetic field induction (in T) and $\Delta\chi = \chi_{//} - \chi_{\perp}$, the magnetic susceptibility of molecules in the membranes, then the minimization in energy leads to deformation into ellipsoids expressed as (SI system):

$$c - a \approx \frac{r_0^3 b B_0^2}{k_C} \Delta\chi \qquad [19]$$
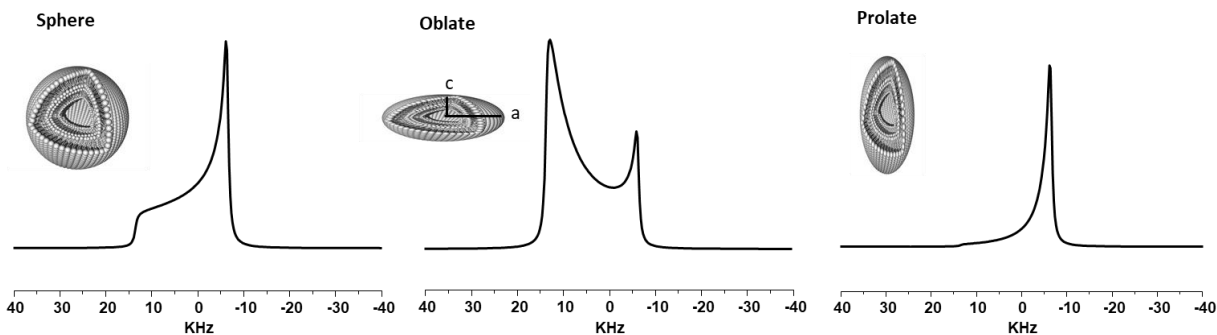
Figure 40: **Example of 31- phosphorus spectra showing the influence of vesicle deformation**. From the left to the right: spectrum of a spherical liposome (c/a=1), spectrum of an oblate liposome (c/a=0.5), spectrum of a prolate liposome (c/a=2).

Magnetic deformation will affect NMR lineshapes if in the average liposomes depart from their equilibrium spherical shape turning into prolate or oblate forms (Figure 40). This can be accounted for by lineshape simulations both for wide line ^{31}P and ^{2}H NMR. The probability distribution, $p(\beta)$, accounting for powder patterns may be written (191) as:

$$p(\beta) = \left(\frac{\sin \beta}{\left(\sin^2 \beta + (c/a)^2 \cos^2 \beta \right)^2} \right)$$
[20]

Where c/a represents the ratio between the long and short semi-axes of an ellipsoid (Figure 40).

As the difference between the ellipsoid axes (c-a) is linked to membrane elastic properties (see above), one may therefore extract the membrane elastic coefficient, k_C, from NMR lineshape simulations.

5) Magic angle sample spinning NMR (MAS-NMR)

It is possible to obtain a solid-state NMR (ssNMR) spectrum with a liquid-like resolution from a solid-state sample. This is called high-resolution ssNMR. This result is obtained by rotating mechanically the sample in a rotor orientated at 54.7° with respect to the external field.
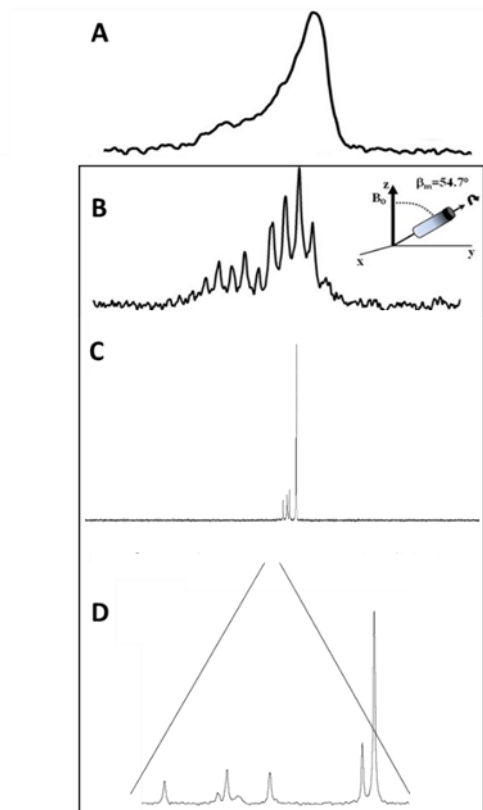
Figure 41:**Example of MAS on liposome**. A. without MAS, B.MAS at 1.4kHz, C. example of a liposome when MAS is enough to remove anisotropic interaction. D. zoom of the spectrum C.

If the rotation frequency of the sample is higher than the anisotropy of the magnetic interaction of interest, an axial symmetry will be induced around the rotor axis and the β value = 54.7° will make the term $\frac{3\cos^2\beta-1}{2}$ turn to zero. Remaining interactions will be Zeeman effect, the isotropic chemical shielding, and spin-spin indirect coupling (*i.e.*, interactions that do not bear an orientational dependence with respect to the magnetic field). These conditions will lead to liquid-like NMR experimental conditions, the sample remaining however of solid or liquid-crystal nature.

The Figure 41 represents examples of magic angle spinning (MAS) experiments for phosphorus ss-NMR. The spectrum A represents a powder pattern line shape in lipid fluid phase liposome without MAS. The spectrum B represents the same sample as in A but spinning at 1.4 kHz. We can observe spinning side bands spaced every 1.4 kHz depicting the powder pattern line shape. The Figure 41D represents a zoom of spectrum C, which is obtained by averaging to zero the anisotropy of the chemical shielding by a spinning speed greater than 8 kHz. A pseudo high resolution is then obtained.

4. NMR experiments – practical aspect

NMR experiments are based on three essential steps that give access to spin transitions between energy levels. In a first step the system has to be equilibrated. The system will be then perturbed in order to obtain an energy level transition. When the origin of the perturbation will stop, the system will relax and return in his equilibrium state, this phenomenon will be used for detection.

In order to present these different steps an example of a simple NMR experiment where the system is subject to Zeeman effect only, is presented. Then phosphorus and deuterium in membrane NMR experiments will be presented.

1) Simple case: Zeeman interaction only

   i.   Equilibrium state

A non-zero spin nucleus in a magnetic field precesses around the z axis (collinear to $\overrightarrow{B_0}$) at a Larmor frequency of $\omega_0 = \gamma B_0$. The spin distribution on different energy level (2I+1 levels) follows the Boltzmann distribution, where $\overrightarrow{M_0}$ is the resultant magnetisation of the spin distribution on energy levels.

   ii.   Perturbation

To pass from an energy level to another one ($\Delta E = h\nu$) a radiofrequency field B_1 is used. B_1 is produced by a coil (solenoid) subjected to an electric current. The frequency of this oscillating field has to be the same that the frequency of the precessing nucleus. A resonance effect will be created between the two oscillators and an energy transfer will occur between the coil and the system.
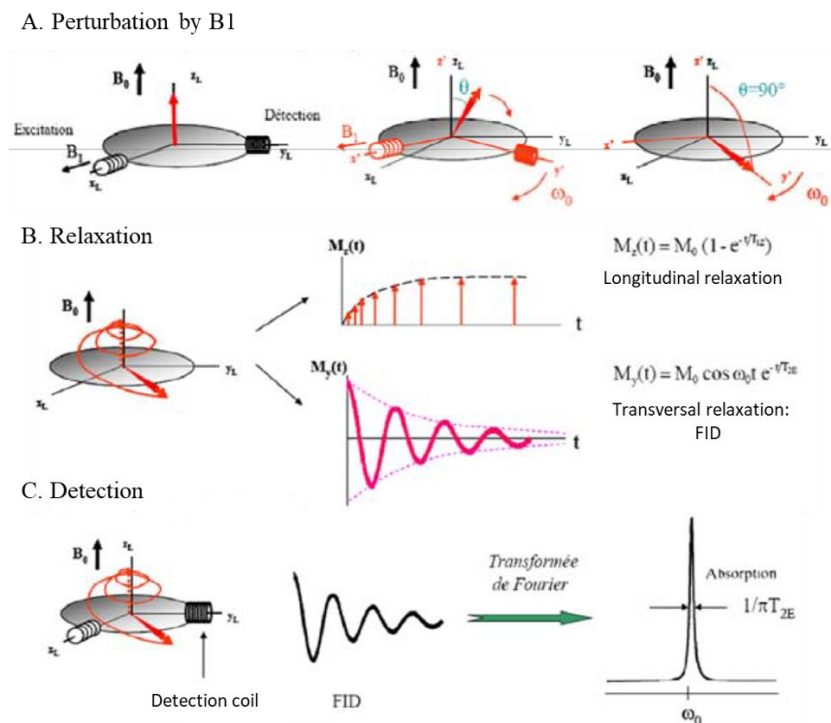
Figure 42: **Representation of perturbation and relaxation steps of a system during an NMR experiment**, from (182) xL, yL, zL represent the laboratory frame of reference and x', y', et z' represent the rotating frame of reference.

This energy input perturbs the level energy population and the resulting magnetization orientation $\overrightarrow{M_0}$ will change. Due to Larmor precession, a new spinning frame (x', y', z') has to be defined, with z' parallel to z_L of the laboratory frame of reference (xL, yL, zL). $\overrightarrow{B_1}$ is acting in this frame, along the x' axis (Figure 43). The resulting magnetization, oriented in z' initially, will be tilted by an θ angle in the y' direction:

$$\theta = \gamma B_1 \tau \qquad [21]$$

71

With τ the time during which the oscillating field $\vec{B_1}$ is applied, one uses the term pulse as the time is very short. A θ=π/2 pulse transfers the magnetization onto the x, y plane.

iii.   Relaxation and detection

The resulting magnetization is detected along the y_L axis (or the (x_L, y_L) plane). The application time of $\vec{B_1}$, τ is calculated in order to have the angle θ equal to 90°. Thereby, when the field $\vec{B_1}$ is stopped, the magnetization is oriented along y', in (x_L, y_L) plane (figure 43). Then the system will go back progressively to its original state where $\vec{M_O}$ is collinear to $\vec{B_0}$. This return to an equilibrium state is composed of a longitudinal relaxation along z_L and a transverse relaxation in (x_L, y_L) plane. The evolution of the longitudinal relaxation along z_L is an ascending exponential function (Figure 42):

$$M_z(t) = M_0(1 - e^{-\frac{t}{T_{1z}}}) \qquad [22]$$

Where T_{1z} is the longitudinal relaxation time. This time is related to thermal exchanges between spins and the system via molecular motions. This relaxation is called the spin-lattice relaxation and its study gives information about molecular motions at nanosecond scale. In the (x_L, y_L) plane, the decrease of the magnetization (transverse relaxation) occurs exponentially and is modulated by the Larmor precession. The detected signal takes the form (Figure 42):

$$M_y(t) = M_0 \cos(\omega_0 t) e^{-\frac{t}{T_{2E}}} \qquad [23]$$

T_{2E} is the transverse relaxation time. This time is linked to spin-spin interactions and gives information about slow dynamics of molecules, or their assembly, at microsecond or second time scale. The transverse relaxation phenomenon gives rise to the "Free Induction Decay" or FID. This FID is digitalized and retreated to be interpreted. This treatment is a mathematical tool called Fourier transformation that transforms a temporal signal (FID) into a frequency signal (NMR spectrum) (figure 42). The spectrum is composed of Lorentzian lines whose frequency is depending of nuclei internal couplings and their width is associated to the dynamics of molecules.

5. **Solid state NMR experiments**

Solid-state interactions and particularly quadrupolar interactions give rise to very large spectra. In the case of deuterium, the width spans hundreds of kHz. The excitation window has to be at least the same size of the largest interaction. Approximatively, the excitation window is in the range of 2/τ (with τ the radiofrequency pulse length): the smaller τ the larger excitation window. Generally, $τ_{90°}$ is equivalent to some microsecond in solid state NMR. As the consequence, the power generated for the field has to be very high (several hundred of W). These high powers induce, after impulsion, a dead time of few microseconds. During this time, it is impossible to acquire any signal; which is a serious problem in solid state NMR. As relaxation times are very short, the system can return to is equilibrium state during this

machine time forbidding any detection. In order to avoid this loss of information, echo sequences have been invented (Hahn, 1950). They are based on the refocusing of interactions. The first impulsion flips the spins at 90° and after a time τ a second impulsion (180°) is applied to refocus interactions. This treatment induces a shift of the cosinusoid maximum of τ compared to the last impulsion.
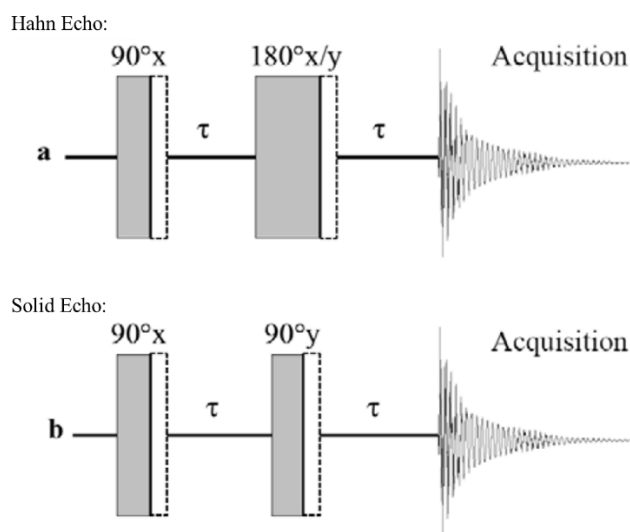
Figure 43: **NMR sequences**: a) Hahn echo, b) Solid Echo. Dotted point frames are corresponding to machine dead time.

The time τ has to be longer than the dead time but short enough to avoid the loss of signal under relaxation effects. In the case of spin I=1/2 nuclei like phosphorus-31, the Hahn echo sequence is used to refocus CSA interactions (Figure 43) (192). This sequence is not allowing the refocusing of quadrupolar and dipolar interactions. A new sequence was developed called quadrupolar echo or solid echo (Figure 43). In this case the second impulsion is equal to 90°. This sequence was used in my thesis in order to study deuterium of membrane models (193).

During my thesis, phosphorus and deuterium NMR experiments were performed on a spectrometer operating at 800MHz for protons. The software associated to the spectrometer was Bruker TopSpin version 3.5.

1) Data treatment

In order to reduce the unavoidable noise detected during NMR experiment, the FID is convoluted by a decreasing exponential e^{-LBt} (noise filtering operation). The Lorentzian Broadening, LB, can vary from tenth of Hz in liquid-state NMR to several hundred Hz in solid state NMR. This difference can be explaining by the fact that in solid state NMR the FID damping is very important leading to intrinsic very broad lines.

i. Spectral simulations

In order to validate our attributions of chemical shift anisotropy and quadrupolar interactions, phosphorus and deuterium NMR spectra simulation were done. A FORTRAN coding software has been

used, where chemical shift anisotropy or quadrupolar splittings (estimated from experimental spectra), linewidth, isotropic chemical shifts and molecular weight of spectral subcomponents can be implemented. The software calculates the corresponding FID and its Fourier transformation. The c/a parameter quantifying liposome deformations could be introduced also. Experimental and simulated spectra were then compared until correct matching was obtained (191).

ii.   Spectral moments calculation

Previously we saw that the local order of a membrane can be determined by the relation between the order parameter S_{CD} and the quadrupolar splitting Δv_Q. However, it may be difficult to measure individual quadrupolar splitting on powder spectra especially for very rigid membranes. The orientational dependence borne by solid state resonance in wide line solid state NMR may generate unresolved spectra of large frequency width. Davis and Bloom (194) have developed the spectral moments method to analyze the dynamics of non-oriented systems. A moment is a number which value is calculated from the product of spectral intensities with resonance frequencies. In lipid bilayers, and because of the axial symmetry, moments can be related to the quadrupolar splitting distribution. The first moment, M_1, of a spectrum obtained from a perdeuterated lipid chain is linked to the global measurement or the chain order parameter $\langle S_{CD} \rangle_{chain}$. This relation is written as (194):

$$M_1 = \frac{\pi}{\sqrt{3}} A_Q \langle S_{CD} \rangle_{chain} [24]$$

With A_Q is the static electric quadrupolar coupling constant.
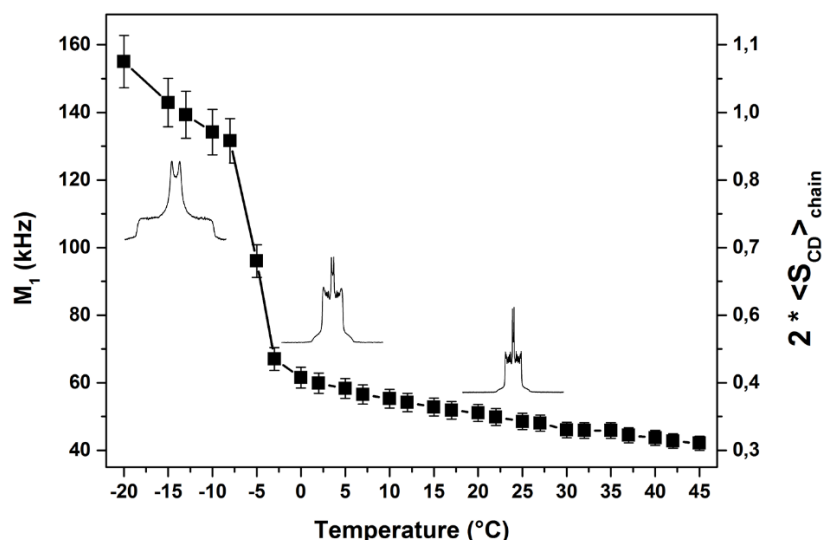
Figure 44: **M_1 calculation for ^2H POPC MLV.** Inserted traces represent selected ^2H-NMR spectra of reconstructed human nuclear lipid membrane extracts mixed with $^2H_{31}$ POPC during a thermal variation. From left to the right, example of spectra obtained at -20°C, 0°C and 25°C. From those types of spectra first spectral moments (M_1, reporting membrane fluidity) were calculated and plotted into the graph in function of thermal variation.

The calculation of the first moment in deuterium NMR will allows for instance following the global dynamics of the deuterated lipid embedded in a membrane as a function of temperature. The first moment M_1 is calculated by using a software developed in our laboratory, coded in C++ (Buchoux S., non-published). As seen of Figure 44 the sudden decrease of M_1 at -5°C is a very nice tool to detect the lamellar gel-to-fluid phase transition temperature.

6. Liquid state NMR

In the course of my thesis I needed to use also liquid-state NMR to analyze for instance the phospholipid or cholesterol composition of membranes. Liquid-state NMR is much easier that solid state NMR because anisotropic interactions are averaged to zero by Brownian motions of molecules in solution. NMR lines are dominated by isotropic chemical shifts related to σ_{iso} and indirect isotropic spin-spin coupling, J. Very classical 1D-NMR experiments have been used in the thesis as well as some specific 2D-experiments such as carbon proton and phosphorus proton correlation experiments.

The 1D ^{1}H experiment spectra were acquired to observe phospholipid chemical shift fingerprint.

The 1D ^{31}P experiment was used to quantified the total quantity of phospholipids, to characterize the phospholipid composition of nuclear lipid extract, and by the used of DMFIT software the quantity of each phospholipid was determinate by simulating ^{31}P spectrum following by the integration of each peaks.

The 2D HSQC ^{1}H-^{13}C experiment allows the correlation between ^{13}C and ^{1}H nuclei through ^{1}H-^{13}C bonds. The peak position within the spectrum describes the chemical shift of ^{1}H and ^{13}C. In the case of the 2D ^{1}H-^{31}P HSQC-TOCSY there is a magnetic transfer to all protons that have a coupling constant through 3 (^{3}J) and sometimes 4 or 5 bonds. The peak position within the spectrum describes chemical shift of ^{31}P correlated to each ^{1}H with a coupling constant ^{3}J and sometimes ^{4}J, ^{5}J or ^{6}J.

The pulse sequence used for HSQC consists of three parts (Figure 45). Preparation, evolution (t1) and mixing time. Subsequent to those the acquisition time (t2) is the time in which the FID is detected. The preparation time is composed of an INEPT (Insensitive Nuclei Enhanced by Polarization Transfer) sequence (90-180-90 on the proton channel, 180-90 on the carbon channel). The evolution takes place on the ^{13}C spin while an 180° pulse is only applied on the ^{1}H channel. In the mixing period, there is another spin echo sequence which transfers the evolved information back to ^{1}H and is detected on this channel. This is called the inverse correlation.

In the 2D experiment ^{1}H-^{31}P HSQC-TOCSY there are two evolution times that are incremented, t_1 and t_2 (the acquisition time is t_2). The HSQC pulse train is followed by the TOSCY spinlock, and a last INEPT transfer occurs before the ^{1}H detection. ^{31}P decoupling is also applied during detection.
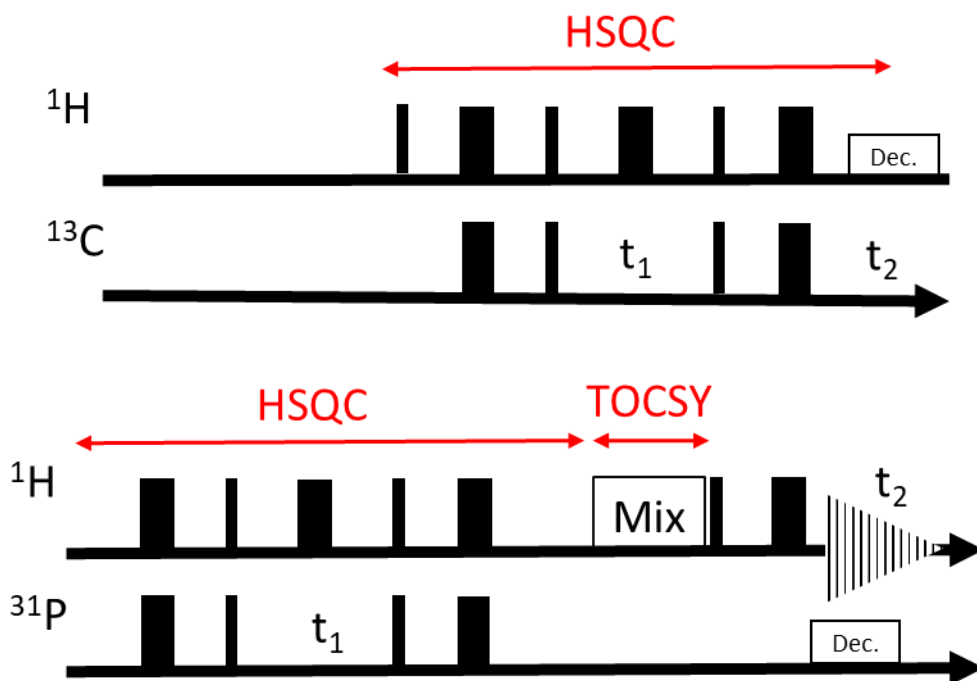
Figure 45: **Sequence representation of a ^{1}H-^{13}C-HSQC and ^{1}H-^{31}P-HSQC-TOCSY**

2D spectra are composed of 3 axes. On two of them, called F2 and F1 axis, the 1D spectra of each nucleus is plotted. The third axis is the intensity that directs out of the window plane. In HSQC spectra the signal corresponds to the contour plot of chemical shift of proton and phosphorus or carbon directly bond.
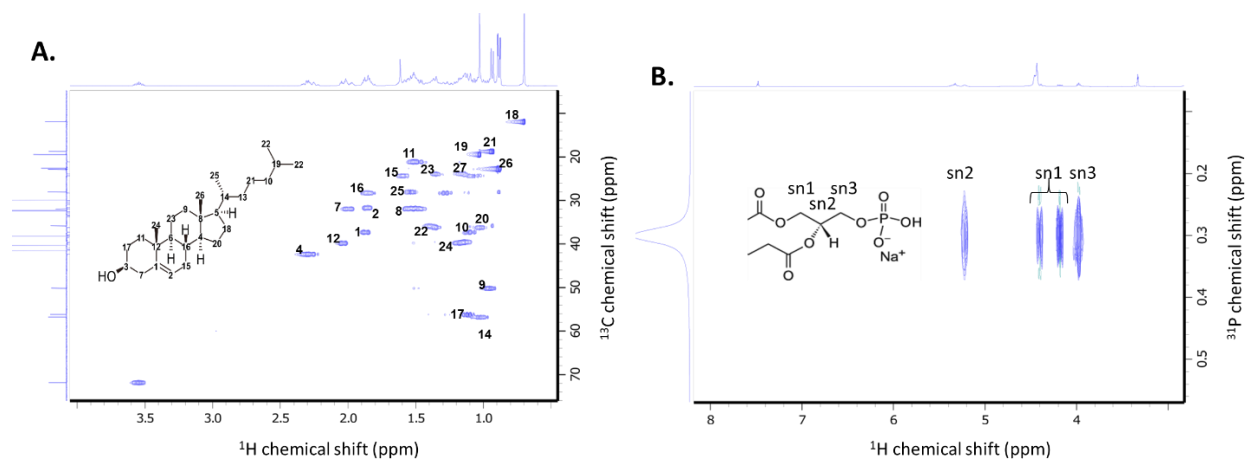
Figure 46: **Example of ^{1}H-^{13}C HSQC and ^{1}H-^{31}P HSQC-TOCSY**.A. ^{1}H-^{13}C HSQC of cholesterol. The plots are representing the correlation between carbon and proton of the same spin system in J_1. In F1 and F2 projections are represented 1D spectra in ^{13}C and ^{1}H NMR respectively. B. ^{1}H-^{31}P HSQC-TOCSY of PA (phosphatidyl acid) In F1 axis:^{31}P chemical shift, in F2: ^{1}H chemical shift. The plots are representing the correlation between phosphorus and proton of the same spin system up to ^{6}J. In F1 and F2 projection are represented 1D spectra in ^{31}P and ^{1}H NMR respectively.

VIII.   Vesicles preparation

1. MLVs preparation:

0.8 mg of POPC-^{2}H$_{31}$ were dissolved into 80 µL of MeOH/CHCl$_3$ (1:2) and added to 8 mg of nuclear lipid extract (molar ratio of ca. 1:10). The solvent was evaporated under a nitrogen gas flux. The residual lipid film was dispersed in 1 ml milliQ filtered water and lyophilized overnight. The resulting fluffy

powder was suspended into 80 μL of a 10 mM HEPES buffer (5 mM $MgCl_2$, pH 7.2, made with deuterium-depleted water) to obtain a hydration, h, of 90% (h = mass of water over the total mass of the system (phospholipids plus water)). After shaking into a vortex mixer samples were frozen in liquid nitrogen for 30 s, heated at 40 °C for 10 min in a water bath and shaken again for better sample homogeneity; this freeze-thaw-shaking cycle was repeated 3 times and the resulting milky dispersion transferred into a 4 mm diameter Zirconium rotor (80 μL, (Cortecnet, Voisins Le Bretonneux, France).

2. **SUVs preparation:**

MLVs of ^{2}H-POPC were hydrated to 98% in a minimum final volume of 1 mL and transferred into 5 mL plastic tube to be sonicated above the lipid transition temperature for at least 15 min. The pulse cycle used was 4 sec sonication followed by 6 second break, after which suspensions turned translucent. SUVs were centrifuged at 10,000 g for 10 min in order to collect any metal residue from the probe that could interfere with NMR measurements. Vesicle size was determined by dynamic light scattering: 100 nm. (195)

3. **SUVs probes incorporation:**

Nuclei were centrifuged at 500 g for 10 min at 4°C. The pellets were resuspended in a total volume of 1ml of deuterium-depleted Tris Buffer (x2) to remove as much deuterated water as possible. For probe incorporation, a probe-to-nuclei lipid molar ratio of 1.1:1 was used as taken from Garnier *et al.*(195). The mixture was kept in a water bath at 40°C for 30 min and gently agitated every 10 min to improve incorporation. Then samples were washed twice and centrifuged (500 g, 15 min, 20°C). The pellet was resuspended very gently after centrifugation. The sample was resuspended in a final volume of 80μl to be transferred to a 4 mm rotor (195).

4. **Vesicle size measurement by dynamic light scattering**

A minimum volume of 0.5 ml of SUVs was transferred into a glass tube and the correlation function acquired at different angles: 45°, 60°, 75°, 90°, 120° and 150° using an ALV/CGS-3 light scattering apparatus (Compact Goniometer System). The data were processed with an ALV Correlator Software V.3.0. The viscosity, η, and the refractive index, n, were adjusted. An average correlation time, τ_c, was measured for each angle and $1/\tau_c$ was plotted against the scattering vector, q^2, according to the equation: $1/\tau_c = Dq^2$ where D is the diffusion coefficient and $q=[4\pi n \sin(\theta/2)]/\lambda$ with θ the scattering angle and λ the laser wavelength (632.8 nm). The hydrodynamic vesicle radius is calculated from a linear fitting of the graph, $1/\tau_c = Dq^2$, using the equation $D=(k_B T)/(6\pi\eta R)$ where k_B is the Boltzman constant and T the temperature in Kelvin.

Chapter III: Nuclear membrane lipid extract characterization and quantification

As it has been explained in the introduction, the Nuclear Envelope (NE) is not just a fence between two compartments. The NE is implicated in many biological process such as gene expression, signal transduction, nuclear transport and protein/lipids synthesis (196-198). The NE is composed of two lipid bilayer: the Outer Nuclear Membrane (ONM) and the Inner Nuclear Membrane (INM). The ONM is continuous with the reticulum endoplasmic and the INM is linked to the lamina network inside the nucleus. The NE shows also some invaginations inside the nucleus called Nucleoplasmic Reticulum (NR) (3, 4). The role of such substructure is poorly known but their increase is characteristic of many diseases such as muscular dystrophy and some cancers(196-198). In order to investigate the role of NRs, information about their proteo-lipid composition has to be discovered. Previous research about NE composition have been focused on the protein aspect. We postulate that the formation of NRs is due to a proteolipid mechanism where specifics lipids may play a role in the NE deformation. In order to get more information about the NE lipid composition a nuclear extraction method has been developed and two quantitative methods, ^{31}P and ^{1}H multidimensional NMR and mass spectrometry, have been implemented to get the NE lipid composition. Results are summarized in the following chapter in a paper format submitted to the journal Analytical Chemistry.

I.   **Tandem NMR and Mass spectrometry analysis of human nuclear membrane lipids.**

Tandem NMR and mass spectrometry analysis of human nuclear membrane lipids.

Régine Dazzoni[1,3], Corinne Buré[1], Estelle Morvan[2], Axelle Grélard[1], Céline Gounou[1], Jean-Marie Schmitter[1] Antoine Loquet[1], Banafshé Larijani[2,4]*, Erick J. Dufourc[1]*.

[1]Institute of Chemistry & Biology of Membranes & Nanoobjects, UMR 5248, CNRS, Université Bordeaux, Institut National Polytechnique Bordeaux, F-33600 Pessac, France.

[2]Cell Biophysics Laboratory, Ikerbasque Basque Foundation for Science, Instituto Biofísika (CSIC, UPV/EHU) and Research Centre for Experimental Marine Biology and Biotechnology (PiE), University of the Basque Country (UPV/EHU), Spain

[3] Institut Européen de Chimie et Biologie, University of Bordeaux, INSERM, CNRS (UMS 3033- US 001), 2 rue Escarpit, Pessac 33600, France

[4] Cell Biophysics Laboratory, Centre for Therapeutic Innovation & Department of Pharmacy and Pharmacology, &

Department of Physics, University of Bath, Bath, United Kingdom

S Supporting Information

ABSTRACT: The human nuclear membrane is composed of a double bilayer; the inner membrane being linked to the protein lamina network and the outer nuclear membrane continuous with the endoplasmic reticulum. Nuclear membranes can form large invaginations inside the nucleus whose role are poorly known. Although most of the protein identification has been determined, their lipid composition remains largely undetermined. In order to understand the mechanical and dynamic properties of nuclear membranes we investigated their lipid composition by two quantitative methods, ^{31}P and ^{1}H multidimensional NMR and mass spectrometry using internal standards. We also developed a non-detergent nuclei extraction protocol allowing to produce milligram quantities of nuclear membrane lipids. We found that the nuclear membrane lipid extract is composed of a complex mixture of phospholipids with phosphatidylcholines present in large amounts. Negatively charged lipids, with high amounts of phosphoinositides were also present. Mass spectrometry confirmed the phospholipid composition and

provided further information on acyl-chain length and unsaturation. Lipid chain lengths range between 30 to 38 carbon atoms (two chains summed up) with a high proportion of 34 carbon atom length for most species. PI lipids have large amounts of chain length with 36-38 carbons. Independent of the chain length unsaturations were highly elevated with 1 to 2 double bonds per lipid species.
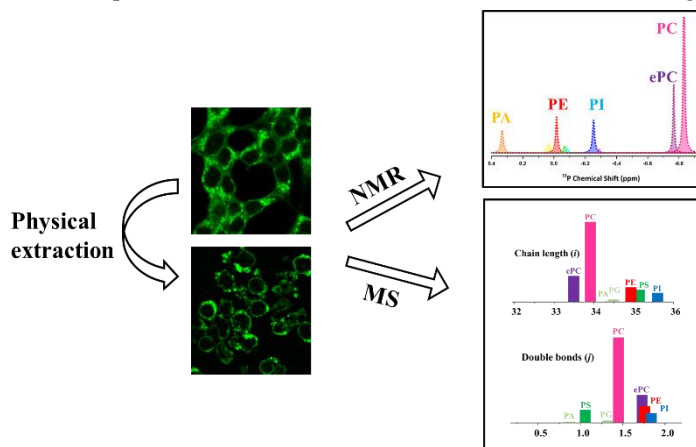
In human cells, the Nuclear Envelope (NE) is not just a barrier between the nucleoplasm and the cytoplasm; it contributes to gene expression, nuclear signal transduction, nuclear transport and protein/lipid synthesis. Its malformation is concomitant with various pathologies (1-3). The NE is a double bilayer where the Outer Nuclear Membrane (ONM) is continuous with the Endoplasmic Reticulum (ER) and the Inner Nuclear Membrane (INM) is linked to the lamina network maintaining DNA within the nucleus. The NE shows large invaginations of submicrometric size; these substructures are called Nucleoplasmic Reticulum (NR) (4, 5). Their role is still unknown but their increase is related to various dysfunctions and often used as a marker of cancerous conditions and muscular dystrophy (1-3). Previous research of the NE focused on the protein aspect and the role of lipids was much less understood. However, very recent results, using sea urchin nuclear membranes as a model, have demonstrated that remodeling/fusion of the nuclear envelope required both

proteins and lipids. Specific lipids such as phosphoinositides, cholesterol and diacylglycerol were identified in large amounts and were shown to have a role in modulating nuclear membrane dynamics during NE assembly process (6, 7). In particular, high levels of phosphoinositides were shown to counterbalance the stiffening effect of cholesterol by providing very fluid membranes despite the high cholesterol content (7, 8). It was proposed that these unusual membranous properties were due to this lipid composition and that the membrane domain with this unusual composition may have a role in chromosomal interactions. It was postulated that such processes might happen in human nuclear membranes, possibly during NE invagination, but to date there has been little information on the lipid composition of the whole human nuclear membrane.

This lack of information resides in several factors: i) nuclei extraction is difficult. Salt extraction, ball-type homogenizers, and detergent methods are mostly used for breaking down the plasma membrane. The most commons methods used to extract membrane proteins from tissues rely on detergents, that is to say, some lipids may be solubilized using such an approach (9) and therefore not detected. ii) Semi-quantification of lipid content is often obtained using Mass Spectrometry (MS) which is very sensitive and requires only a few nanograms of membrane lipids. However, quantification necessitates the use of internal standards, which must possess the same ionizing properties as natural lipids. These standards for lipids have sometimes a limited availability or do not exist. iii) On the other hand, NMR is a non-invasive technique intrinsically quantitative, by definition, but often requires relatively important quantities of sample (hundreds of micrograms at best). Whereas NMR will provide the nature of lipids, especially phospholipids, MS will be able to determine chain lengths and unsaturation states.

The goal of our study is to develop a method capable of purifying human nuclei by a non-detergent method and produce large quantities of human nuclear membrane lipids. We therefore "broke" the cells by using a physical pressure provided by a nitrogen gas bomb apparatus. In order to quantitatively determine the nature, chain length and degree of unsaturation of lipids, both NMR and MS were developed together.

Materials and methods

Materials. Cell culture reagent, Dulbecco's Modified Eagle's Medium (DMEM), Fetal Bovine Serum (FBS) and Streptomycin/Penicillin were purchase from Invitrogen, (Carlsbad, CA. USA). Lipids for NMR and lipid standards for mass spectrometry quantification (PE 17:0/17:0, PS 17:0/17:0, PC 17:0 /17:0, PA 17:0/ 17:0, PI 17:0/14:1, and PG 17:0/17:0) were purchased from Avanti Polar Lipids (Birmingham. AL. USA) and used without further purification. Solvents (chloroform and methanol) were obtained from Sigma Aldrich Chemicals (Saint Quentin-Fallavier, France). Other reagent as Sucrose, $MgCl_2$, SDS (sodium dodecyl sulfate), Tris Base, glycine, PVDF membrane, low fat milk powder, tween, HRP antibody, Hepes, KCl, DTT $DIOC_6$, Hoechst and TPP were purchased from Sigma Aldrich (Saint Quentin-Fallavier, France).

Nuclear extraction. Nuclei purification without use of detergent was performed following a protocol from Blobel & Potter and Domart (6, 9) that we optimized for human membrane lipids (supplementary Fig.1). All operations were

performed on ice to avoid sample degradation. After harvesting by trypsinization, HEK 293T cells grown at 80% confluence into two 175 mL flasks were incubated on ice for one hour in 10 mL of freshly prepared swelling buffer, SB (10 mM Hepes, pH 7.9, 10 mM KCl, 15 mM $MgCl_2$, 1 protease inhibitor tablet (Complete Mini, Roche) per 10 mL buffer and 5 mM DTT prior to use). Cells were lysed by nitrogen cavitation in a cell disruption bomb (Parr Instrument Company, Illinois, USA): samples were incubated on ice at a pressure of 200 psi (13.8 bar) for 10 minutes before rapid decompression and sample collection. Samples were centrifuged at 500 g, 4°C, for five minutes to pellet nuclei. The supernatant containing soluble cell debris was discarded. Pellets of nuclei were washed once with SB. A final purification step was performed using a sucrose gradient. Nuclei were resuspended in 100 μL of SB and layered on 3 mL of solution S1 (0.4 M Sucrose, 15 mM $MgCl_2$) and 3 mL of S2 (1 M Sucrose, 15 mM $MgCl_2$) and centrifuged at 1000 g for 10 minutes. After discarding the supernatant, nuclei pellets were resuspended in 1mL of SB. 5 μL were transferred to 300 μL of SB for Nuclei counting and staining. Nuclei were transferred into cryovials and resuspended into Sucrose 1M in SB, flash-frozen in liquid Nitrogen and stored at -80°C for further use.

Fluorescence imaging microscopy. Cells and nuclei were placed on a poly-lysine coated MatTek dish (Cultureware, Ashland, MA., USA) and stained with $DiOC_6$ (2 mM) and Hoechst 33343 (2 mg/ml) to assess the efficiency of nuclei isolation. Cells were visualized under an inverted confocal microscope with a high-efficiency spectral detector (Leica TCS SP5; Leica Microsystems, Manheim, Germany). A 63-fold glycerol immersion, N.A. 1.3 objective was used, and the images were collected and analyzed with the LAS AF software (Leica MicroSystems, Manheim, Germany). The $DiOC_6$ dye, used for staining all membranes, was excited at 488 nm using an argon laser and its emission was in the 504-661 nm range. The Hoechst dye, used to stain DNA, was excited at 405 nm using a pulsed diode laser and its emission was at 283-436 nm range. Nuclei were visualized under an inverted microscope, Olympus IX81, equipped with U-MINIBA2 fluorescence cube (470- to 490-nm bandpass excitation filter, 505-nm dichroic mirror, 510- to 550-nm bandpass emission filter) and UPlan FLN 60×/1.25 oil-objective lenses (or an equivalent fluorescence microscopy system). All experiments were performed at room temperature (ca. 20°C).

Electrophoresis. Cells and nuclei samples corresponding to 20 μg proteins (obtained by Bradford (10)) were mixed with 5μL of 4X SDS (Sodium Dodecyl Sulfate) loading buffer and boiled for 10 minutes at 95 °C to denature proteins. Samples were loaded into a 4–12% Bis-Tris gel (Invitrogen, Carlsbad, CA. USA) against a protein ladder (PageRuler Plus, Thermo Scientific, Carlsbad, CA. USA). Gels were run in a running buffer (25 mM Tris Base pH 8.3, 3.5 mM SDS, 192 mM Glycine) at 145 V for approximately two hours, until the dye front had reached the bottom of the gel.

Western blotting. We used the classical method based on Towbin and coworkers (11). Proteins were transferred from the gel onto a PolyVinylidene DiFluoride (PVDF) membrane for Western blotting, pre-activated with methanol and subsequently washed by a transfer buffer (20 mM Tris, pH 8.3, 192 mM Glycine, 20 % (v/v) Methanol)) prior to use. Proteins were transferred using the Biorad Trans-Blot transfer apparatus. The proteins were transferred at 400 mA for two hours. Membranes were blocked one hour at room temperature with 5% low fat

milk powder (w/v) in TBST (TBS: Tris Buffered Saline 1 %, 0.1 % Tween 20). Following blocking, membranes were incubated with the appropriate primary antibody in 5% (w/v) low fat milk powder in PBST (PBS: Phosphate Buffered Saline 1 %, 0.1 % Tween 20) at 4°C overnight. Membranes were washed (in low fat milk powder in PBST) to remove the excess of primary antibody and the nonspecific binding. Membranes were subsequently incubated with HRP (horseradish peroxidase)-conjugated secondary antibody for 1 h at room temperature in 5% (w/v) low fat milk powder in PBST, followed by 5% (w/v) low fat milk powder in PBST washing steps. Amersham ECL reagents were used at a ratio of 1:1 and incubated on the membrane for 3 min. Protein were revealed under a chemiluminescent system (Thermo Scientific, Carlsbad, CA. USA).

Lipid extraction. Lipids were extracted from nuclei samples using a modified Folch extraction method (12). Nuclei were added to 4 mL of acidified (HCl) chloroform:methanol (2.5:1), sonicated and filtered. After addition of 0.2 volumes of K_4EDTA (0.02 M, pH 6), samples were centrifuged at 800 g. The lower phase was retained and dried down at, 55°C, under nitrogen gas. Phospholipid concentration was determined by a Fiske Assay resulting on an indirect measurement of inorganic phosphates released from extracted lipids (13). Phospholipid characterization and quantification were provided by liquid-state ^1H and ^{31}P NMR and mass spectrometry as described below.

Sample preparation for liquid-state NMR. 4 mg of lipid extract dried under N_2 were resuspended in milliQ (Millipore, Billerica, MA., USA) filtered water, flash frozen with liquid N_2 and lyophilized overnight. The "fluffy" powder was dissolved into 450 μL of $CD_3OD/CDCl_3$ (1:2). 30 μL of EDTA 0.02 M/D_2O pH 6 were added to chelate potentially present paramagnetic ions (14). This solution was placed into a 5-mm diameter glass tube (Cortecnet, Voisins Le Bretonneux, France). 50 μL of CD_3OD /$CDCl_3$ (1:2) containing 2 μmol of the external standard TPP (Triphenylphosphate) were sealed into in a coaxial insert tube that was placed into the 5-mm diameter glass NMR tube for proton (^1H) and Phosphorus-31(^{31}P) NMR quantification. Mixture of phospholipids corresponding to PG: 8%, PA: 8%, CL:6%, PE: 18%, SM: 4%, PS:5%, PI: 6%, LPC:4%, PC: 41% and dissolved in chloroform-methanol 2:1, 0.02M EDTA-D_2O, pH 6 as described above.

NMR spectroscopy. Liquid-state ^1H- and ^{31}P-NMR experiments were carried out on a Bruker Avance III-HD 400 MHz SB spectrometer (Wissembourg, France) equipped with a 5mm broadband SmartProbe at 25°C. ^{31}P-NMR spectra were acquired at 161.98 MHz by using a one-pulse sequence with proton decoupling during the acquisition ($\pi/2$ pulse width of 8 μs, recycling delay of 10 s, acquisition time of 4s, spectral window of 54 ppm and between 80 and 1024 scans). ^1H-NMR spectra were acquired at 400.13 MHz using a single pulse sequence ($\pi/2$ pulse width of 10μs, recycling delay of 2s, acquisition time of 2s, spectral window of 20 ppm and 48 scans). Two-dimensional experiments were performed at 400.13 MHz using a HMQC-TOCSY 2D-sequence (15, 16) used to identify/assign chemical shifts for various phospholipids. Acquisition parameters: recycle delay of 2s, ^1H and ^{31}P 90 $\pi/2$ pulse widths of respectively 10 and 8μs, acquisition time of 0.3s, 64 transients, 9 and 3 ppm spectral widths in proton and phosphorus dimensions respectively, 2k

data points for the F2 dimension and 64 data points for the F1 dimension, transfer delays corresponding to a 7 Hz proton-phosphorus coupling constant and an additional 100 ms DIPSI mixing period for protons after the HMQC step.

NMR data treatment and spectral simulations. Liquid state ^1H and ^{31}P NMR spectra were processed using the Bruker TopSpin software. All peaks in 1D-^{31}P NMR spectra were integrated and converted into molar quantities by comparison with the external standard triphenylphosphate, and the whole spectrum was integrated to obtain the total quantity of Phospholipids. The quantity of each of the phosphorus-containing lipid types was determined by simulating ^{31}P liquid-state NMR spectra with the DMFIT software (17). 2D-NMR maps were used as phospholipid fingerprints to confirm their chemical shift assignment (Supplementary Fig. 3 and Table 1). Identification was based on head group ^1H-^{31}P cross peaks for most intense peaks and to chemical shift comparison to literature for smaller resonances (18).

Mass spectrometry. Phospholipid extracts (0.25 mg) were dissolved in 800 μL of $CHCl_3/CH_2OH$ (1:2, v/v) + 8 mM ammonium acetate and then centrifuged to remove the non-dissolved components. Each sample was infused into the TurboV electrospray source of a mass spectrometer model QTRAP® 5500 (Sciex, Concord, Ontario, Canada) at a flow rate of 7 μL/min. ESI-MS experiments were achieved in the negative (PE, PS, PA, PI, PG) and positive (PC) ion modes in the mass range m/z 350-1000. ESI- MS/MS experiments (Precursor Ion scans, supplementary Fig.2) were also performed in the negative and positive ion modes with fast polarity switching (50 ms) and a scan rate of 200 Da/s. Nitrogen was used for the curtain gas (set to 15), gas1 (set to 20) and gas2 (set to 0). Needle voltage was set at -4,5 or +5,5 kV without needle heating. The declustering potential was either -100 V or +100 V. Calibration was achieved using an ES Tuning Mix (Sciex, Concord, Ontario, Canada). The collision gas was nitrogen and collision energy were fixed to either -50 or 50 eV. The mass range was m/z 250-1100. MS/MS experiments included one positive mode precursor ion scan and 54 negative mode precursor ion scans. Phospholipids species were identified using Lipid View software v1.0 (Sciex, Concord, Ontario, Canada).

Liquid chromatography mass spectrometry (LC-MS/MS, MRM mode) analyses were performed with the same mass spectrometer model QTRAP® 5500 (Sciex, Concord, Ontario, Canada) coupled to a LC system (LC-20AD XR pump, Shimatzu, Marne-la-Vallée, France) and PAL HTC-xt Autosampler (CTC Analytics, Zwingen, Switzerland). Phospholipid extracts (50 pg) were dissolved in 30 μL of CH_3CN/H_2O 80/20 and internal lipid standards were added (PA: 10 pmol, PC: 0.25 pmol, PE, PG, PI: 2.5 pmol). Analyses were achieved in the negative (PE, PS, PA, PI, PG) and positive ion modes (PC) with fast polarity switching (50 ms); nitrogen was used for the curtain gas (set to 20), gas1 (set to 35) and gas2 (set to 0). Needle voltage was at -4.5 or +5.5 kV without needle heating; the de-clustering potential was adjusted to +40 V and between -180V and -85 V. The collision gas was also nitrogen; collision energy was +47 eV and varied from -62 to -48 eV. The dwell time was set to 3 ms. MS/MS experiments were performed by 19 positive and 111 negative MRM scans. Phospholipids species were identified using the same software and the area of LC peaks was determined using MultiQuant

software v2.1 (Sciex, Concord, Ontario, Canada). Reversed phase separations were carried out at 40 °C on an Ascentis RP Amide 150×1 mm column, with 3 μm particles (Supelco, Sigma Aldrich, St Quentin Fallavier, France). Eluent A was H_2O+0.1 % formic acid and eluent B was CH_3CN+0.1 % formic acid. The gradient elution program was: 0 min, 30 % B; 8 min, 30 % B; 10 min, 70 % B; 35–36 min, 87 % B; 37 min, 30 % B. The flow rate was 50 μL/min; 10μL sample volumes were injected. Quantitative determination of lipid species (%mol) was accomplished by normalizing to the peak area of injected lipid standards.

Results

Nuclei Purification.

A physical extraction protocol based on nitrogen cavitation was chosen to extract nuclei (6, 9). As described in Materials & Methods, HEK 293T cells were placed in a hypotonic buffer to be swollen and then placed in a nitrogen cavitation bomb for plasma membrane disruption. As the pressure is controlled in the cavitation bomb the resulting plasma membrane disruption is more reproducible than using a Dounce homogenizer. To improve the extraction ratio and the integrity of extracted nuclei the protocol was modified. $MgCl_2$ and DTT concentrations of the swelling buffer, were increased (*ca.* 15 mM of $MgCl_2$ and 5 mM of DTT) to stabilize DNA (19) and membranes (20), respectively. Intact nuclei were recovered and purified by a sucrose gradient/centrifugation step. Using this protocol modification, we could recover, after the purification step, 30% of intact nuclei from the initial number of cells.
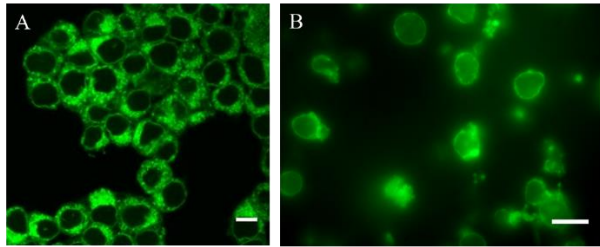
	Nuclei
% Extraction	30%
Protein concentration	10.5 mg/10^8 nuclei
PLipid quantity	4 mg/10^8 nuclei
DNA	10mg/10^8 nuclei

Fig. 47. Non-detergent Nuclei extraction. A. HEK 293T cells stained by DiOC$_6$ and visualized by a confocal instrument equipped with a x60 objective: all membranes were stained. B. Nuclei extracted by a non-detergent treatment and observed by an epi fluorimeter microscope equipped with a x100 objective. Nuclei were stained by DiOC$_6$. Nuclear membranes surrounding nuclei were mainly visualized. Scale bar: 10 μm.

Cells and nuclei were visualized by fluorescence microscopy using the DiOC$_6$ dye that specifically stains membranes (green, Fig. 1). We observe (Fig. 1A) all membranes of HEK cells: the plasma membrane surrounding the cell, the Endoplasmic Reticulum (ER) in the cytoplasm compartment and the nuclear membrane enclosing the chromatin. After the nitrogen cavitation bomb treatment and sucrose gradient we assessed the "purity" of extracted nuclei: absence of plasma membrane and ER membranes and presence of nuclear membranes (Fig. 1B). Nuclei were intact and nuclear membranes appeared complete.

As the outer nuclear membrane is continuous with the ER, a small proportion of ER membranes was nonetheless observed; as it was minor no further removal was performed.

Using Bradford (10) analysis, the protein concentration, for 10^8 nuclei, was estimated to be 10.5 mg. The chromatin concentration was also investigated as described in Materials & Methods, and for 10^8 nuclei, 10 mg of DNA was determined.

The "purity" of nuclei was controlled by western blot experiments as described in Materials & Methods (Supplementary Fig. 2). As a control, entire cells were also subjected to blotting. Cells fraction exhibit the presence of cytoplasmic proteins such as Tubulin, Actin and GAPDH (D-glyceraldehyde-3-phosphate dehydrogenase). Nuclei fractions are exempted of cytoplasmic protein and exhibit an enrichment of nucleus protein such as Lamins and Nuclear Pore Complex proteins (NPC). A small proportion of Actin is nonetheless detected in the purified fraction of nuclei and may be due to the ER contamination or to the presence of actin in the nucleoplasm.

Lipids were extracted from the nuclei membrane samples by a Folch method as described in the Materials & Methods. The phospholipid amount was measured by ^{31}P NMR experiment: 4 mg of phospholipids were extracted from 10^8 nuclei. (*vide infra*).

NMR determination of lipid content. Fig. 2 shows a 1D ^{31}P-NMR spectrum with a classical series of isotropic lines that were assigned to individual phospholipids. As NMR spectra were acquired in quantitative conditions, *i.e.*, waiting 14s in between successive accumulating scans, the amount of each phospholipid in the extract was obtained by integrating the surface area under the spectral peaks. Spectral simulation was performed using the DMFIT software to perform the quantification by Gaussian integration (see spectral simulations of 1D ^{31}P-NMR spectra, Fig. 2). Spectral areas were normalized with respect to the TPP external reference of a known concentration. We determined the total quantity of phospholipids in the extract: 4 mg.
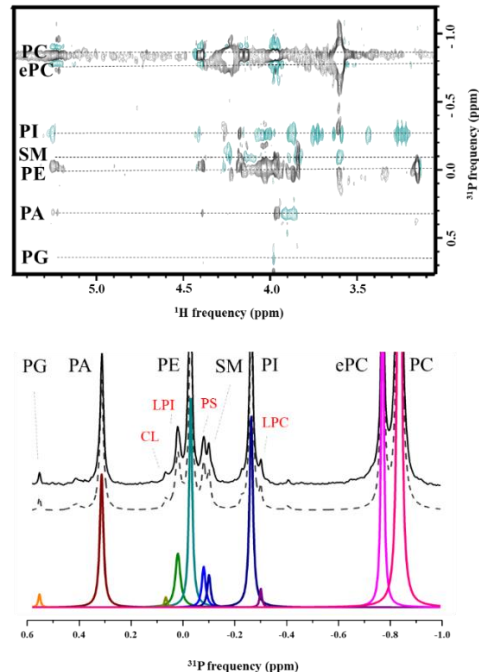
The phospholipid assignment was performed with the help of 2D NMR experiments. ^{1}H-^{31}P HMQC-TOCSY NMR experiments provided a map of heteronuclear [1]H-^{31}P cross-peaks that was utilized as fingerprints for phospholipid head group determination (Fig. 2 top). This map led to proton chemical shifts along the horizontal axis and to phosphorus-31 chemical shifts along the vertical axis. The 2D map led to identification of phosphatidylcholine (PC), ether-phosphatidylcholine (ePC), phosphatidylinositol (PI), sphingomyelin (SM), phosphatidylethanolamine (PE), phosphatidic acid (PA) and phophatidylglycerol (PG). The minor peaks that appeared in the 1D ^{31}P NMR spectrum (Fig. 2 bottom, solid line) did not give cross-peaks in the 2D map due to much more demanding S/N conditions and could not be assigned. Literature values obtained for individual phospholipids were used (21, 22). However, as there were some variance in chemical shifts (Table 1) we also decided to run NMR experiments for individual standard species available commercially. We also mixed all standard lipids in the same sample as chemical shifts in the mixture may differ from individual chemical shifts. The sample representing the mixture of standards contained PG, PA, CL, PE, SM, PS, PI, LPC, PC was also analyzed. Table 1 represents all ^{31}P-NMR chemical shifts for phospholipids obtained from literature and from NMR experiments on individual standards, mixture of standards and the lipids from human nuclear membranes. Details of 2D experiments for individual lipid standards and mixture of standards are available in supplementary materials (Supplementary Fig. 3 and Table 1). Three more lipid species were assigned, lyso-phosphatidylinositol (LPI), phosphatidylserine (PS) and lyso-phosphatidylcholine (LPC). It is worth noting that there were marked differences in chemical shifts for individual lipid standards and in the mixture, indicating a mixture effect. An eleventh lipid species was tentatively assigned to cardiolipin (CL).

Table 7. [31]P chemical shifts for hNE lipids

Lipid Species	Ref 1[a]	Ref 2[b]	Isolated standards[c]	Mixed standards[d]	NLE[e]
ePC	-0.77	nd	nd	nd	-0.77
PC	-0.84	-0.84	-0.84	-0.84	-0.84
PG	0.52	0.47	0.48	0.58	0.57
PA	0.25	0.23	0.30	0.34	0.33
CL	0.18	0.13	0.18	nd	0.06
LPI	0.10	nd	nd	nd	0.03
PE	-0.01	0.04	-0.08	-0.04	0.03
PS	-0.05	0.00	-0.08	-0.11	-0.06
SM	-0.09	-0.07	-0.10	-0.09	-0.10
LPC	-0.28	-0.28	-0.30	-0.29	-0.22
PI	-0.37	-0.36	0.10	-0.20	-0.20

Black letters in lipid species column stand for assignments obtained directly from the human nuclear lipid membrane extract whereas letters in italics stand for assignments made in comparison with literature and experiments on lipid standards.

Quantification of lipid species by NMR. The phospholipid quantification was performed from the 1D ^{31}P-NMR spectrum of the human nuclear membranes lipid extract as it had quite an elevated S/N ratio and was acquired under quantitative conditions, *i.e.*, with sufficient waiting time in between successive scans. Fig. 2 illustrates this method. The ^{31}P spectrum lineshape was simulated using the DMFIT software, each peak being fitted by a Gaussian lineshape to account for sample heterogeneity. The trace below, the experimental spectrum (dashed line) demonstrates the quasi-perfect matching between experimental and simulated spectra. In Fig. 2 the individual lines with their respective area are shown with colors to distinguish lipid species. The area under each peak was normalized with respect to the external TPP reference present in the capillary tube and reported in supplementary Table 2 and plotted in Fig.3. The accuracy of the method was estimated to be 1%. The sum of all lipid areas (100%) represents a total of 4 mg of phospholipids. Phosphatidylcholines (PC) dominated the lipid extract with ca. 63%. Negatively charged lipids were present at ca. 24% with half of them being phosphatidylinositides (PI). Phosphatidylethanolamines (PE) were present at 9%.
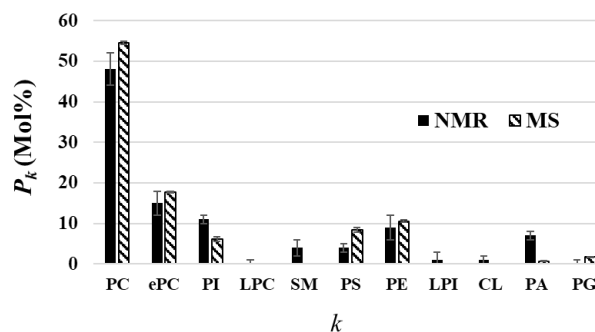
Fig. 3 Nuclear lipid extract phospholipid composition. P_k: proportion of lipid types (k). k: PC, ePC, LPC, PE, PS, PA, PG, PI, LPI, SM, CL (100% = sum of all lipid types detected by each technique). The NMR quantification is based on the simulation/integration of NMR lines of the ^{31}P-NMR spectrum of the human nuclear membranes lipid extract. Figures represent mol% of phospholipids. Results represent the average over three samples. Total phospholipid mass of 4 mg (100%). Mass spectrometry quantification was obtained by MRM (Multiple Reaction Monitoring) experiments on the same lipid extract using injected lipid standards (see text). Results stand for the average over two samples.

Mass spectrometry of human nuclear membranes lipid extract. Mass experiments on nuclear lipid extracts were

performed in order to confirm the phospholipid content and to characterize the acyl chain length and the presence of unsaturation. Human Nuclear Membranes Lipid extracts were first analyzed by direct infusion mass spectrometry, a technique that provides at a glance a direct lipid fingerprint of a sample (Fig. 4).

The shotgun infusion mass spectrometry experiment shows the presence of a complex mixture of lipids composed of free fatty acids and sterols, lysophospholipids, diglycerides and cholesterol esters, phospholipids and triglycerides (23). Although the technique is not quantitative *per say* and despite the complexity of the mass spectrum, one may nonetheless state that phospholipids show a high intensity in the negative ion mode compared to the other lipids and thus represent the most important class of lipids in the sample, with mass range from *m/z* 650 to 850. Very long chain free fatty acids have also a high intensity with mass ranging from *m/z* 350 to 450. This intensity can be explained by the strong ability to ionize endogenous free fatty acid in the sample and also by the presence of fatty acid derived from degradation of other lipids. Lysolipids were also present in the mass range *m/z* 450-600. Diglycerides and cholesterol esters are found around *m/z* values ranging from 600 to 700 and triglycerides from *m/z* 750 to 1000.
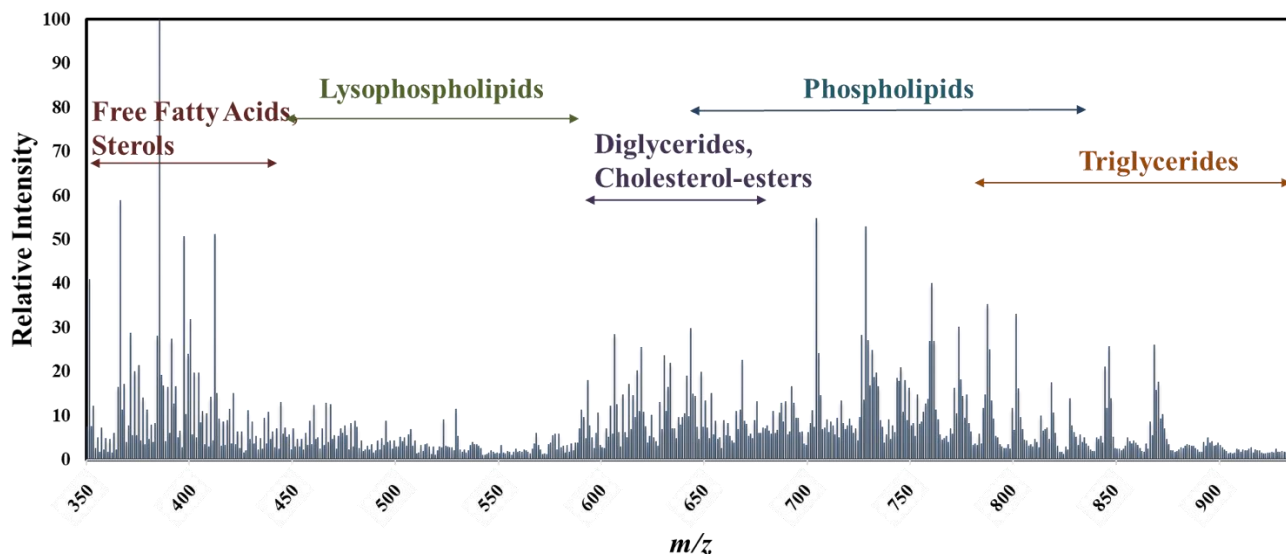
Fig. 4. Mass spectrum (shotgun method) of the nuclear lipid extract determines the lipid landscape. 0.25 mg of nuclear lipid extract were dissolved in $CHCl_3/CH_2OH$ (1:2, v/v) + 8 mM ammonium acetate. The mass spectrum was acquired in the negative ion mode in the MS mode with a mass range from *m/z* 350 to 1000. The presence of different lipid species can be observed: free fatty acids, sterols, lysophospholipids, diglycerides, cholesterol-esters, phospholipids, triglycerides.

One of the major advantages of such a fingerprint method compared to LC-MS analysis is the ability to obtain a rapid acquisition of the full mass range of a complex sample. Because phospholipids were the dominant species in the human nuclear membrane lipid extract we focused our analysis on phospholipid composition. A direct mass spectrometric analysis of the nuclear lipid extract was achieved in the precursor ion scan mode in order to determine the different phospholipid species. In this mode, PCs were identified by a loss of a fragment ion at m/z 184 in the positive ion mode, corresponding to the polar head group. All the other PLs were analyzed in the same way but in the negative ion mode (54 precursor ion scans)) and were identified by their fatty acid chains losses. A Table of 130 MRM transitions corresponding to 85 phospholipids was established and used in the MRM method for quantification with internal standards. Reverse Phase HPLC was chosen to allow the separation of phospholipids driven by the acyl chain (number of double bonds and chain length), and with little contribution to their head group. The area under the peak in RPLC corresponding to a precursor/fragment ions transition was measured and correlated to a given phospholipid. For each phospholipid species, all the peak areas were summed and normalized with internal standards allowing a relative quantification in mol%. In this way, two different samples coming from different nuclei preparations were analyzed and results were averaged giving a relative quantification of each PL species in the sample.

The phospholipid molar composition is reported in supplementary Table 2 and plotted in Fig. 3 for comparison with NMR results. The phospholipid composition found by mass spectrometry globally agrees with that found by NMR. PC lipids are found at *ca.* 72%, negatively charged lipids at *ca.*17 % and PE lipids *ca.* 10 %. Because our MS experiments were not optimized for Lysophospholipids, CL and SM detection, we did not report figures for these species. It is noteworthy that MS and NMR show some discrepancies in evaluating negatively charged lipid species, especially PI and PA. This phenomenon can be accounted for by specific conditions to achieve a RPLC analysis in a single run for all phospholipids: some compromises had to be made and notably a compromise on the pH of eluents, *i.e.*, the conditions for LC analysis were not optimum for the detection of PA. Moreover, some adsorption of PA and PI on different parts of the LC system (tubing) may be considered to explain the finite differences between NMR and MS.

Mass spectrometry analysis of phospholipid chain length.

From the results obtained by MRM, the phospholipids were identified with their two fatty acid chains (supplementary Table 3). To compare the results, we added the number of carbon and unsaturation of the two fatty acid chains for each phospholipid to obtain a global identification of PL (Fig. 5). We observed that a majority of phospholipids with the sum of both hydrocarbon chains lengths representing 34 carbons was found, followed by 32 and 36 carbon lengths. We plotted in Fig. 5 the lipid chain length distribution according to the nature of phospholipid head group. The PC and PE profiles have a wide chain length distribution ranging from 30 to 40 carbon atoms, with 32, 34 and 36 carbon length representing ca. 90 % of the distribution. Conversely, ether PCs have a narrow distribution with chain lengths of 32 and 34 carbons. The PI profile is dominated by long chains from 32 to 38 carbons, with that at 38 representing *ca.* 20%. PA, PS and PG lipids have distributions with major lengths of 34 and 36 carbons.
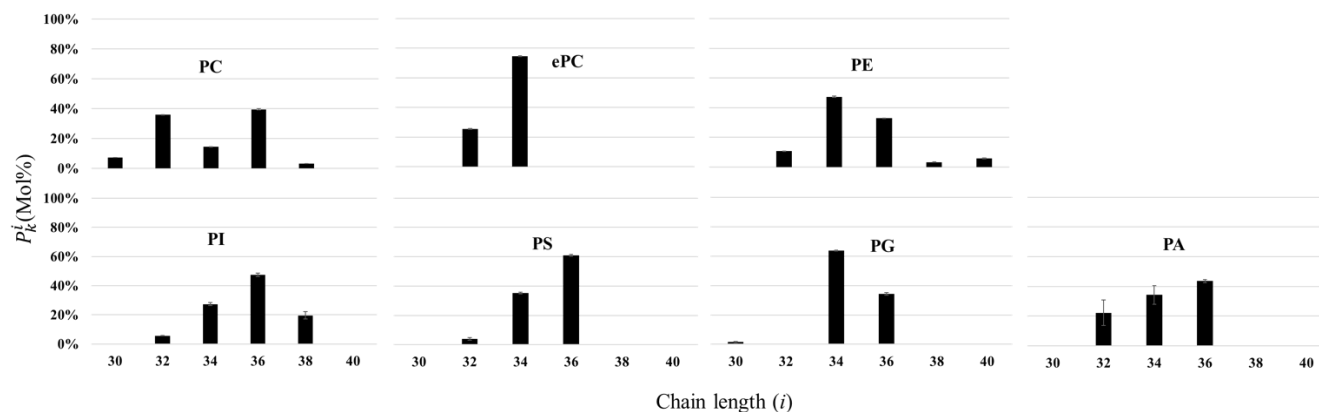
Fig. 5. Distribution of phospholipids according to their chain length (*sn*-1 and *sn*-2 chain length are summed up) obtained by reversed phase liquid chromatography-mass spectrometry in MRM mode. P_k^i: proportion of lipid chain length, i, for the k lipid type. $i = 30, 32, 34, 36, 38, 40$. Experimental conditions: 50 pg of lipid extract were dissolved in CH_3CN/H_2O 80/20 and internal lipid standards were added (PA: 10 pmol, PC: 0.25 pmol, PE, PG, PI: 2.5 pmol). Mol% are obtained by normalization to the peak area of internal lipid standards. Error bars are obtained from standard deviation, n=2 independent experiments.
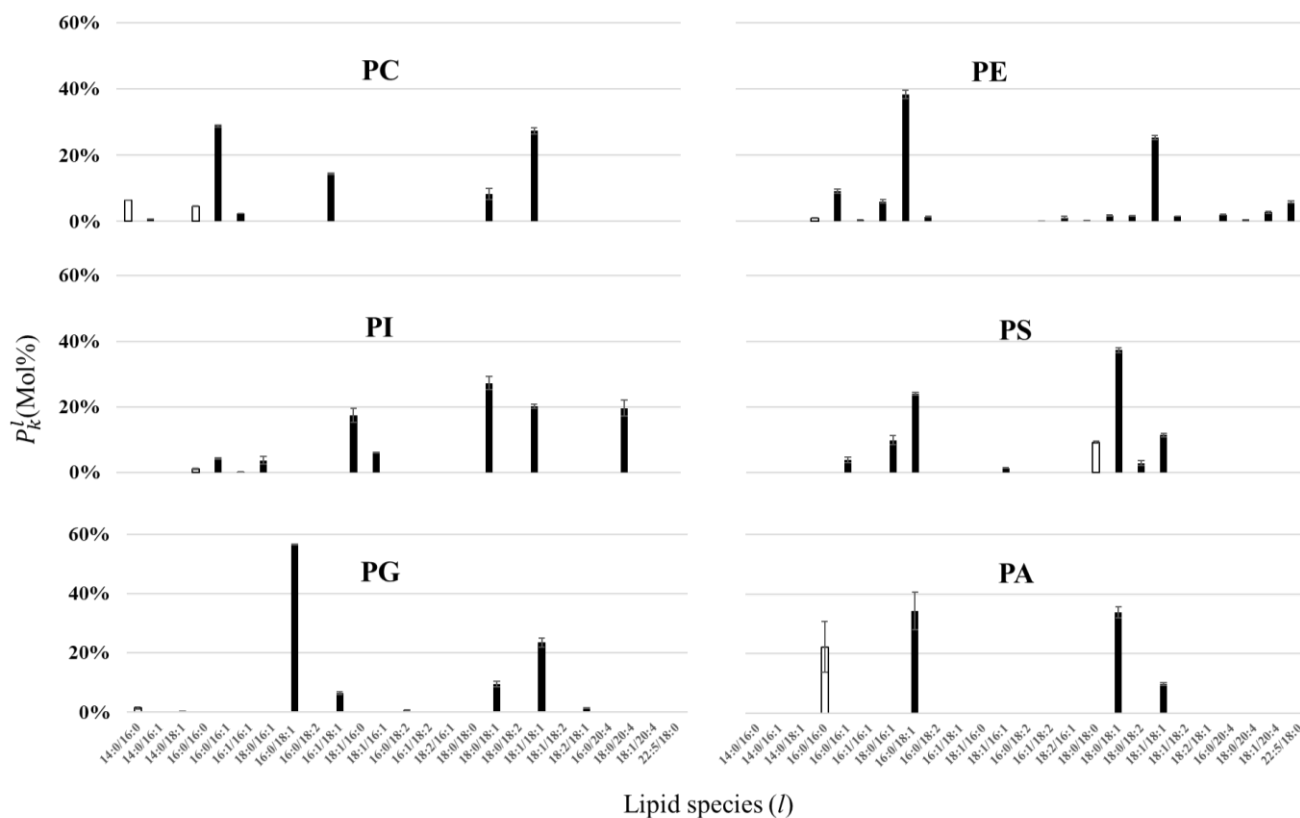
Fig. 6. Distribution of *sn-1/sn-2* chain length and unsaturation according to phospholipid type, k, as obtained by reversed phase liquid chromatography-mass spectrometry in MRM mode (see text). P_k^l: proportion of lipid species (l) for the kth lipid type. l: *sn-1/sn-2*. Experimental conditions: 50 pg of lipid extract were dissolved in CH_3CN/H_2O 80/20 and internal lipid standards were added (PA: 10 pmol, PC: 0.25 pmol, PE, PG, PI: 2.5 pmol). Mol% were obtained by

normalization to peak area of internal lipid standards Error bars were obtained from standard deviation, n=2 independent experiments. Saturated chains (white bars), unsaturated chains (black bars).

Mass spectrometry analysis of lipid unsaturation.

Fig. 6 represents the distribution of fatty acid chains in *sn-1* and *sn-2* positions and unsaturation composing each phospholipid denoted *x:j/y:m* where *x* and *y* stand for the number of carbons and *j/m* the number of double bonds. The attribution rule for *sn-1* and *sn-2* positions was as follows: for PI, PA, and PS phospholipids, the intensity of the *sn-1* carboxylate anion peak was equal or higher than the intensity of the *sn-2* carboxylate anion peak (*sn-1≥sn-2*) (24, 25), and for PE and PG, the intensity of the *sn-2* carboxylate anion peak was higher than the intensity of the *sn-1* carboxylate anion peak (sn-2>sn-1) (24, 26). Filled black bars represent fatty acid chains having one or more double bond. At first sight a striking information comes from this figure. Unsaturation dominate the hydrocarbon chains, there were only a few lipids having both chains saturated and only to a small extent, the most important being PA with 20% of (16:0/16:0) chains. In general, each phospholipid type was represented by two or three phospholipid species, *l*. PC is composed of around 30% of 16:0/16:1 and

18:1/18:1 and 15% of 16:1/18:1, PS 37% of 18:0/18:1 and 25% of 16:0/18:1, PG 55% of 16:0/18:1 and 25% of 18:1/18:1, PE 40% of 16:0/18:1 and 25% of 18:1/18:1 and PA was composed of 35% of 16:0/18:1 and 18:1/18:0, and 25% of 16:0/16:0. Interestingly, PI was composed of a majority of long chains with numerous unsaturation, 27% of 18:0/18:1, 20% of 18:1/18:1 and 18:0/20:4. Furthermore, it is noteworthy that only 7% are unsaturated in *sn*-1, whereas 65% were unsaturated in *sn*-2 and 28% of species were unsaturated both in *sn*-1 and *sn*-2. The species 18:1/18:1 were present in all lipid types.

From results obtained by MRM, the proportion of phospholipid type, *k*, bearing *j*=1,2, … double bonds can be represented, $P_k^j = \sum_l P_{k,l}^j$, with $P_{k,l}^j$ = proportion of phospholipid species (*l*) containing *j* double bonds (summed over the *sn-1* and *sn-2* chains). Fig. 7 shows that PS, PG, PA lipids had in average 1 double bond per lipid, PC, ePC and PE have 1.6 and PI lipids had 1.9 in average. This clearly indicated that the lipids from the human nuclear membranes were highly unsaturated.
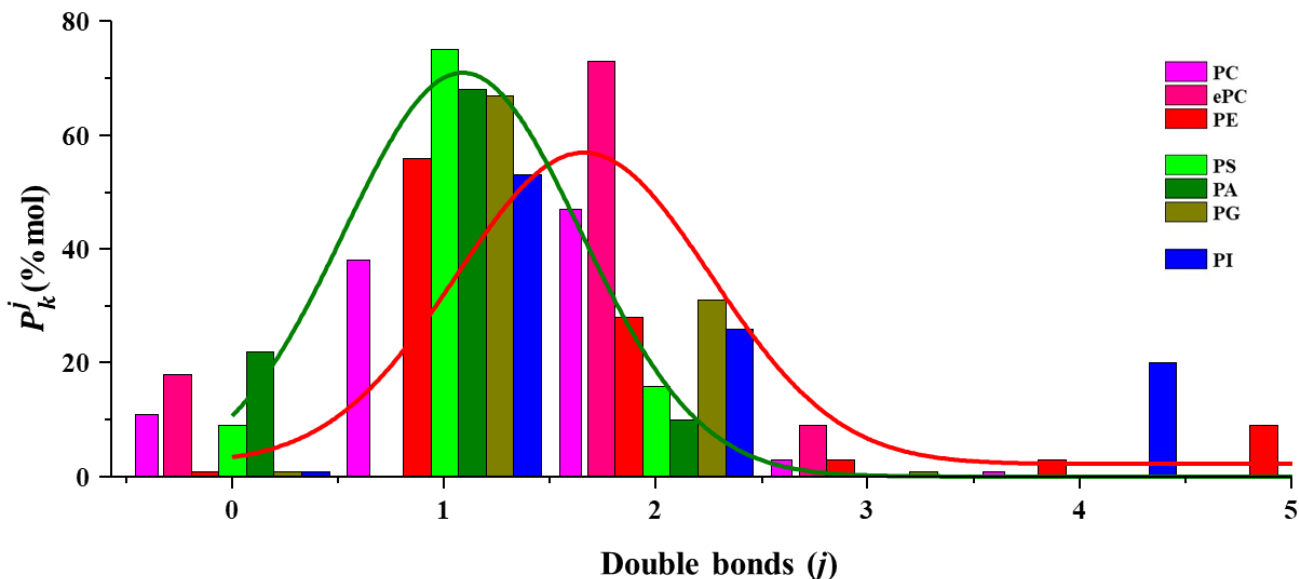
Fig. 7. Distribution of the number of double bonds per lipid type, obtained by reversed phase liquid chromatography-mass spectrometry in MRM mode. P_k^j: Proportion of lipid types, *k*, containing *j* double bonds. Colors stand for individual species (variations in green for PS, PA and PG, variations in red for PC and PE and blue for PI). A gaussian curve was tentatively fitted on the distribution with maxima around 1.0 for PS/PA/PG, 1.6 for PC/PE. For PI no gaussian fit was possible but the weighted average is 1.9.

Discussion.

Human nuclear membrane is composed of a double bilayer, that has a special topology with invaginations inside the nucleoplasm. The present work proposes a new method to purify and quantitatively analyze by combining both NMR and mass spectrometry the lipid part of the nuclear envelope that may account for such phenomena. The paper first reports an isolation method capable of producing large quantities of human nuclear membrane lipids in a detergent-free approach and demonstrates by NMR and mass spectrometry together

that the nuclear membrane lipid extract is composed of a complex mixture of phospholipids with phosphatidylcholines present in large amounts. Negatively charged lipids, with high amounts of phosphoinositides, and phosphatidylethanolamines are also present in notable quantities. Of great interest is the finding of lipids with an elevated quantity of double bonds that may impact the fluidity of the entire membrane. These findings will be discussed in the and some possible biological implications will be proposed.

A new methodology to analyze lipids from natural membranes.

Purification of membrane lipids is often based on methods that are used to extract proteins from membranes, *i.e.*, make use of detergents that have an amphiphilic structure allowing to stabilize by their surfactant properties the hydrophobic core of proteins in solution. This structure is very similar to that of lipids that are also by essence amphipathic and lipids may be solubilised using such a procedure. The physical approach, pressure explosion of cells that we modified from the paper of Blobel & Potter (9) and Domart *et al.*(6), appears quite efficient to isolate nuclei with their surrounding membranes from the rest of the cell and cell organelles. This method allows the isolation of milligram scale nuclear membrane lipids from 10^8 cells. With such quantity of lipid, liquid-state ^{31}P/^{1}H NMR can be performed quite easily, even 2D NMR can be achieved. Use of internal reference allows direct quantification of phospholipids. 11 lipid classes could be detected, namely, PC, ePC, PE, SM, CL, PG, PI, PA, PS and lysolipids such as LPC and LPI. This is more than what has been reported from literature for similar membranes (supplementary Table 4). Mass spectrometry could also be implemented in a quantitative way using lipid standards. It is worth mentioning that MS is a relative measuring method because molecules with different structures and charges may ionize in the mass spectrometer chamber very differently and therefore lead to misleading peak intensities. The use of commercially available internal standard phospholipids (17:0/17:0 PE, PS, PC, PA, (17:0/14:1), PI, PG) aided in the quantification of these classes of lipids. The close agreement with ^{31}P/^{1}H-NMR data confirms the quantification, although a small variance is detected, especially for PA that may be partially interacting with the tubing and columns of the MS apparatus. Unfortunately, we could not find standards for lysolipids, ePC, CL and SM, which limited the comparison between the two methods.

PC, PE and PI dominate the phospholipid composition of the human nucleus membrane.

In most cells the membranes of intracellular organelles may have very different lipid compositions as it is shown in supplementary Table 4. Plasma membranes, such as in human Erythrocytes, are typically enriched in PC (25-40% of phospholipids), PE (20-30%) and SM (15-25%), other species are below 15%. They also elevated levels of cholesterol (25% of total lipids) except for membranes of E. Coli, Mitochondria and Microsomes where cholesterol is absent or in very small amounts. Unfortunately, there is little data on nuclear membranes to compare with our work. We nonetheless extracted data on ER, which is continuous with nuclear membranes, and Golgi from rat kidney/liver and sea urchins (Supplementary Table 4). Data on ER membranes show larger amounts of PC (40-55%) whereas PE are found in similar quantities. There is considerable variability for SM (2-20%) and for PI (2-25%). Nuclear membranes from our work show the greatest amount of PC (63%) and very moderate amounts of PE (9%). SM is almost absent (4%) and phosphoinositide lipids are in important quantities (12%). Interestingly, such a lipid species is considered as a signaling agent (27) and a potential membrane disordering (7) and membrane-inducing curvature agent. Indeed, PI(4,5)P$_2$ can be hydrolyzed by PLCγ to DAG (Diacylglycerol), which is known to have a high negative membrane curvature and could be at the origin of the formation of nuclear membranes invaginations (28, 29).

Nuclear membrane lipids have moderate chain length but are largely unsaturated.

Lipid chain lengths range between 30 to 40 carbon atoms (two chains summed up) with a high proportion of 34 carbon atom length for most species, *i.e.*, C16:C18 chain length in average. This may be better visualized by plotting the normalized chain length according to lipid type proportions ($P_k L_i$) as found by MS, in which L_i is the average chain length, $\sum \left(P_k^i \times i\right)$, (Fig. 8A). The C34 chains length dominate the distribution for all species except for PI lipids that have near 36 carbon atoms on average. In a previous paper (30) we have shown that such a chain length distribution corresponds to an average membrane thickness of 4.5 nm, which is relatively thin considering that we may have ca. 20% cholesterol in the membrane (30). Of note, PI lipids have large amounts of longer chain length with 36-38 carbons but as they are greatly unsaturated (*vide infra*) they shrink (by conformational disorder) to the thickness imposed by dominant PC lipids. We can postulate that the presence of important amounts of phosphoinositides may compensate the stiffening effect of cholesterol (31, 32) as it has already been found in the case of nuclear membrane remnants in the apical side of sea urchin male pronuclear membrane (8). The normalized degree of unsaturation according to lipid type proportions ($P_k D_j$) of human nuclear membranes lipid extracts can also be represented in the same way. D_i is the average number of double bonds ($D_j = \sum P_k^j \times j$), (Fig 8B). We found *ca.* 1.5 double bonds, in average, for each of the lipids in the membrane. Such an amount is very elevated and may confer special properties to the membrane (*vide infra*). It has indeed been shown that the more double bonds in the bilayer the lower the elastic modulus of the membrane (33).
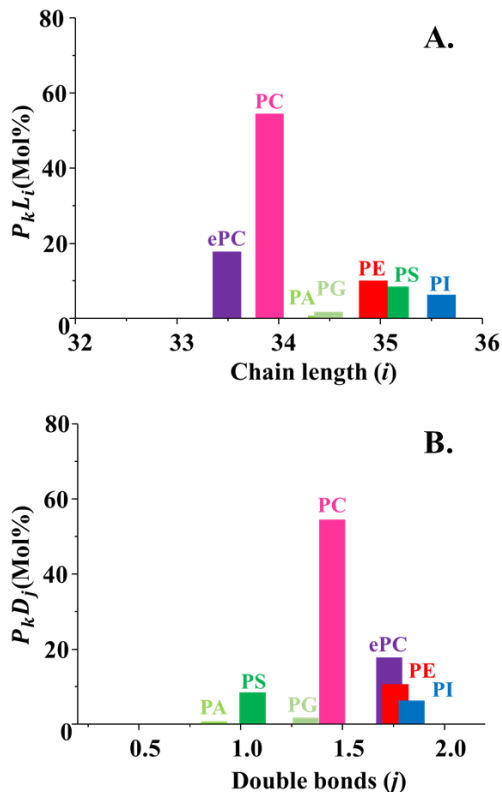
Fig. 8. **Normalized view of chain length** (P_kL_i) **and unsaturation number** (P_kD_j) **for the entire membrane**. P_k is the proportion of lipid types, k= PC, PE, … as determined by MS, with the average chain length, $L_i = \sum(P_k^i \times i)$ with i the chain length, $i = 30, 32, 34, 36, 38, 40$ detected, and the average number of double bonds $D_j = \sum P_k^j \times j$, with j standing for the number of double bonds. A) Distribution of phospholipids according to their chain length (sum of 2 chains) and B) unsaturation.

A phospholipid composition favoring the nuclear membrane invaginations?

The main findings of our work indicate that PC lipids dominate the composition of phospholipids in the human nuclear membranes extracted from embryogenic kidney cells. They have moderate chain length and bear a lot of unsaturation. Phosphoinositides are also present in high amounts with longer chains and have even more double bonds per species. This situation is quite unique, to our knowledge, because plasma membranes or other organelles show the presence of marked amounts of sphingolipids, cardiolipin, or phosphatidylserine lipids; none of these are found in important amounts in hNM. At this level of the discussion we must nonetheless bear in mind that free fatty acids cholesterol, cholesterol esters, lysolipids, diglycerides and triglycerides were also found in the hNM but to a lesser extent. Is it therefore reasonable to assume that the main physicochemical properties of the membrane may be imprinted by the

phospholipids (mostly PC and PI) and drive the mechanical properties of the nuclear membrane towards a very fluid double bilayer. The presence of cholesterol that is well known to regulate membrane dynamics (32) would in principle stiffen fluid-phase membranes.

This is where phosphoinositides may be essential: in addition to be signaling lipids, they are fluidizing agents that may counteract the effect of cholesterol providing the membrane with a very fluid double bilayer, despite elevated amount of sterols. Evans and coworkers demonstrated that short acyl chains and double bonds lead to small elastic modulus of the membrane (33). In other words, this means that large out of membrane plane undulations are favored by low elastic moduli. We measured by solid state NMR that the hNM are 100 times more elastic than plasma membranes(30). This means that globally the nuclear membranes of our study intrinsically possess the high deformability needed to stabilize the micrometric-size invaginations in the DNA core. Although important this is not enough to explain the appearance of invaginations in some locations within the nuclear membranes. There may be local events that induce high point of curvature within membranes, such as those possibly produced by DAG that is present in the lipid composition or may be obtained from PI lipids using naturally present phospholipases. Care must however be taken because membrane proteins may play an important role in curving membranes or modifying the mechanical properties of the membrane. The dynamics of whole nuclear membranes is investigated in our laboratory.

Conclusion.

In order to understand the role of human nuclear membranes and their specific topology named invaginations, we developed a non-detergent nuclei extraction protocol allowing to produce milligram quantities of nuclear membrane lipids. We further developed specific NMR and mass spectrometry to quantitatively investigate their lipid composition. The two techniques provide very similar results, NMR being able to quantitate at the mg scale every lipid species bearing a phosphorus atom. Mass spectrometry can also bring the same information provided there is an internal lipid standard that can be added to the lipid mixture. Unfortunately, there is not enough lipid standards for all lipid species but most of species can be determined by this method. The nuclear membrane lipid extract is composed of a complex mixture of phospholipids and with phosphatidylcholines present in large amounts. Negatively charged lipids, with high amounts of phosphoinositides, and phosphatidylethanolamine were also detected in noticeable quantities. Additionally, their high level of unsaturated fatty acid acyl chains might account for rendering the membrane very fluid and hence

deformable, for human nuclear membrane invaginations to be formed.

ASSOCIATED CONTENT

Supporting Information

Table of contents

Sup. Fig. 1: Schematic view of the nuclear extraction protocol.
Sup. Fig. 2: Nuclei extraction protocol controlled by western blot.
Sup. Fig. 3: NMR Phospholipid assignment of a mixture of reference lipids.
Sup. Fig. 4: Example of precursor ion scan spectra of acyl chain.
Sup. Table 1: 1H and 31P NMR chemical shift of phospholipids.
Sup. Table 2: Nuclear lipid extract phospholipid composition by NMR and MS.
Sup. Table 3. Phospholipid species classified according to their chain length and unsaturation number.
Sup. Table 4. Lipid and Phospholipid composition in membranes of different tissues.
The Supporting Information is available free of charge on the ACS Publications website as a PDF file.

AUTHOR INFORMATION

Corresponding Author

*Correspondence should be addressed to Erick J. Dufourc (e.dufourc@cbmn.u-bordeaux.fr or erick.dufourc@cnrs-dir.fr), or to Banafshé Larijani (banafshe.larijani@ikerbasque.org)

Author Contributions

The manuscript was written through contributions of all authors. All authors have given approval to the final version of the manuscript.

ACKNOWLEDGMENT

REFERENCES

1.   Fischer AH, Bardarov S, Jiang Z. Molecular aspects of diagnostic nucleolar and nuclear envelope changes in prostate cancer. J Cell Biochem. 2004;91(1):170-84.
2.   Fischer AH, Taysavang P, Jhiang SM. Nuclear envelope irregularity is induced by RET/PTC during interphase. Am J Pathol. 2003;163(3):1091-100.
3.   Sarkar D, Emdad L, Lee SG, Yoo BK, Su ZZ, Fisher PB. Astrocyte Elevated Gene-1: Far More Than Just a Gene Regulated in Astrocytes. Cancer Res. 2009;69(22):8529-35.
4.   Fricker M, Hollinshead M, White N, Vaux D. Interphase nuclei of many mammalian cell types contain deep, dynamic, tubular membrane-bound invaginations of the nuclear envelope. Journal of Cell Biology. 1997;136(3):531-44.
5.   Fricker M, Hollinshead M, White N, Vaux D. The convoluted nucleus. Trends in cell biology. 1997;7(5):181.
6.   Domart MC, Hobday TMC, Peddie CJ, Chung GHC, Wang A, Yeh K, et al. Acute Manipulation of Diacylglycerol Reveals Roles in Nuclear Envelope Assembly & Endoplasmic Reticulum Morphology. PLoS One. 2012;7(12):14.
7.   Zhendre V, Grelard A, Garnier-Lhomme M, Buchoux S, Larijani B, Dufourc EJ. Key Role of Polyphosphoinositides in Dynamics of Fusogenic Nuclear Membrane Vesicles. PLoS One. 2011;6(9).
8.   Garnier-Lhomme M, Byrne RD, Hobday TMC, Gschmeissner S, Woscholski R, Poccia DL, et al. Nuclear Envelope Remnants: Fluid Membranes Enriched in STEROLS and Polyphosphoinositides. Plos One. 2009;4(1):12.
9.   Blobel G, Potter VR. Nuclei from Rat Liver - Isolation Method that Combines Purity with High Yield. Science. 1966;154(3757):1662-&.
10.   Bradford MM. Rapid and Sensitive Method for Quantitation of Microgram Quantities of Protein Utilizing Principle of Protein-Dye Binding. Anal Biochem. 1976;72(1-2):248-54.
11.   Towbin H, Gordon J. Immunoblotting and Dot Immunobinding - Current Status and Outlook. Journal of Immunological Methods. 1984;72(2):313-40.
12.   Larijani B, Poccia DL, Dickinson LC. Phospholipid identification and quantification of membrane vesicle subfractions by P-31-H-1 two-dimensional nuclear magnetic resonance. Lipids. 2000;35(11):1289-97.
13.   Fiske CH, Subbarow Y. The colorimetric determination of phosphorus. J Biol Chem. 1925;66(2):375-400.
14.   Sotirhos N, Herslof B, Kenne L. Quantitative-Analysis of Phospholipids by P-31-NMR. J Lipid Res. 1986;27(4):386-92.
15.   Bax A, Davis DG. MLEV-17-Based Two-Dimensional Homonuclear Magnetization Transfer Spectroscopy. Journal of Magnetic Resonance. 1985;65(2):355-60.
16.   Bax A, Griffey RH, Hawkins BL. Correlation of Proton and N-15 Chemical-Shifts by Multiple Quantum NMR. Journal of Magnetic Resonance. 1983;55(2):301-15.

17.   Massiot D, Fayon F, Capron M, King I, Le Calve S, Alonso B, et al. Modelling one- and two-dimensional solid-state NMR spectra. Magnetic Resonance in Chemistry. 2002;40(1):70-6.

18.   Edzes HT, Teerlink T, Valk J. Phospholipid Identification in Tissue-Extracts by 2-Dimensional P-31-H-1 NMR-Spectroscopy with Isotropic Proton Mixing. Journal of Magnetic Resonance. 1991;95(2):387-95.

19.   Wilkie GS, Schirmer EC. Purification of nuclei and preparation of nuclear envelopes from skeletal muscle. Methods in molecular biology (Clifton, NJ). 2008;463:23-41.

20.   Scott RE, Maercklein PB. Effect of Dithiothreitol on Plasma-Membrane Intramembranous Particle Topography in Balb-C 3t3 and Simian Virus-Transformed 3t3 Cells and Plasma-Membrane Vesicles. Journal of the National Cancer Institute. 1980;65(2):415-9.

21.   Kaffarnik S, Ehlers I, Grobner G, Schleucher J, Vetter W. Two-Dimensional P-31,H-1 NMR Spectroscopic Profiling of Phospholipids in Cheese and Fish. J Agric Food Chem. 2013;61(29):7061-9.

22.   Meneses P, Glonek T. High-Resolution P-31 NMR of Extracted Phospholipids. J Lipid Res. 1988;29(5):679-89.

23.   Gao XL, Zhang QB, Meng D, Isaac G, Zhao R, Fillmore TL, et al. A reversed-phase capillary ultra-performance liquid chromatography-mass spectrometry (UPLC-MS) method for comprehensive top-down/bottom-up lipid profiling. Analytical and Bioanalytical Chemistry. 2012;402(9):2923-33.

24.   Hsu FF, Turk J. Charge-driven fragmentation processes in diacyl glycerophosphatidic acids upon low-energy collisional activation. A mechanistic proposal. J Am Soc Mass Spectrom. 2000;11(9):797-803.

25.   Hvattum E, Hagelin G, Larsen A. Study of mechanisms involved in the collision-induced dissociation of carboxylate anions from glycerophospholipids using negative ion electrospray tandem quadrupole mass spectrometry. Rapid Commun Mass Spectrom. 1998;12(19):1405-9.

26.   Hsu FF, Turk J. Studies on phosphatidylglycerol with triple quadrupole tandem mass spectrometry with electrospray ionization: Fragmentation processes and structural characterization. J Am Soc Mass Spectrom. 2001;12(9):1036-43.

27.   Larijani B. Protein and lipid signaling in membrane fusion: nuclear envelope assembly. Signal transduction. 2007;7:142-53.

28.   Byrne RD, Gamier-Lhomme M, Han K, Dowicki M, Michael N, Totty N, et al. PLC gamma is enriched on poly-phosphoinositide-rich vesicles to control nuclear envelope assembly. Cellular Signalling. 2007;19(5):913-22.

29.   Barona T, Byrne RD, Pettitt TR, Wakelam MJO, Larijani B, Poccia DL. Diacylglycerol induces fusion of nuclear envelope membrane precursor vesicles. Journal of Biological Chemistry. 2005;280(50):41171-7.

30.   Dazzoni R, Grelard A, Morvan E, Bouter A, Applebee CJ, Loquet A, et al. Unprecedented deformation of human Nuclear Envelopes in magnetic field: is membrane elasticity driving membrane invaginations? submitted. 2019.

31.   Dufourc EJ, Smith ICP. A detailed analysis of the motions of cholesterol in biological-membranes by H-2-NMR relaxation. Chemistry and Physics of Lipids. 1986;41(2):123-35.

32.   Dufourc EJ. Sterols and membrane dynamics. J Chem Biol. 2008;1(1-4):63-77.

33.   Rawicz W, Olbrich KC, McIntosh T, Needham D, Evans E. Effect of chain length and unsaturation on elasticity of lipid bilayers. Biophysical Journal. 2000;79(1):328-39.

II. Supplementary information: Tandem NMR and Mass spectrometry analysis of human nuclear membrane lipids.

Supplementary information to:

Tandem NMR and mass spectrometry analysis of human nuclear membrane lipids.

Régine Dazzoni[1,2], Corine Buré[1], Estelle Morvan[3], Axelle Grélard[1], Céline Gounou[1], Jean-Marie Schmitter[1], Antoine Loquet[1], Banafshe Larijani[2*], Erick J. Dufourc[1*].

[1]Institute of Chemistry & Biology of Membranes & Nanoobjects, UMR 5248, CNRS, Université Bordeaux, Institut National Polytechnique Bordeaux, F-33600 Pessac, France.

[2]Cell Biophysics Laboratory, Ikerbasque Basque Foundation for Science, Instituto Biofísika (CSIC, UPV/EHU) and Research Centre for Experimental Marine Biology and Biotechnology (PiE), University of the Basque Country (UPV/EHU), Spain

[3]Institut Européen de Chimie et Biologie, University of Bordeaux, INSERM, CNRS (UMS 3033- US 001), 2 rue Escarpit, Pessac 33600, France

*Correspondence should be addressed to Erick J. Dufourc (e.dufourc@cbmn.u-bordeaux.fr or erick.dufourc@cnrs-dir.fr), or to Banafshé Larijani (banafshe.larijani@ikerbasque.org)

Table of contents

Supplementary Figure 1: Schematic view of the nuclei extraction protocol. Nuclei purification without use of detergent was performed following an optimized protocol from Blobel & Potter[1]. All processes were performed on ice to avoid sample degradation. After harvesting by trypsinization, HEK 293T cells from two 175 mL flasks grown at 80% confluence were incubated on ice for one hour in 10 mL of SB (10 mM HEPES, pH 7.9, 10 mM KCl, 15 mM $MgCl_2$, 1 protease inhibitor tablet (Complete Mini, Roche, Mannheim) per 10 mL buffer and 5 mM DTT prior to use) freshly prepared. Cells were lysed by nitrogen cavitation in a cell disruption bomb. Samples were incubated on ice at a pressure of 200 psi for 10 minutes before decompression and sample collection. Samples were centrifuged at 500 g for five minutes at 4°C to pellet the nuclei. The supernatant containing soluble cell debris was discarded. Pellets of nuclei were washed once with SB. A final purification step was completed by a sucrose gradient. Nuclei were resuspended in 100 µL of SB and layered on 3 mL of solution S1 (0.4 M Sucrose, 15 mM $MgCl_2$) and 3 mL of S2 (1 M Sucrose, 15 mM $MgCl_2$) and centrifuged at 1000 g for 10 minutes. After discarding the supernatant, nuclei pellets were resuspended in 1mL of SB. 5 µL were transferred to 300 µL of SB for Nuclei counting and staining. Nuclei were transferred in cryovials and resuspended into Sucrose 1M in SB, flash frozen in liquid Nitrogen and stored at -80°C, for further use.
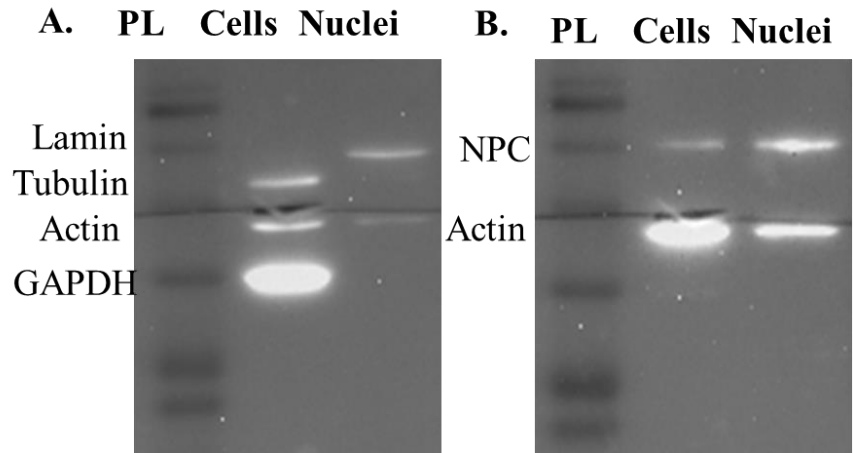
Supplementary Figure 2. Nuclei extraction protocol controlled by western blot. Cells and nuclei corresponding to 20 μg of proteins were added in respective wells. After the migration, Lamin, Tubulin, Actin GAPDH and NPC primary antibody were detected using an HRP secondary antibody and revealed by chemiluminescence. Tubulin and GAPDH are proteins specific of the cytoplasm compartment and are found exclusively in cells protein extract. Lamin and NPC are enriched in the nuclei protein extract. PL: protein ladder.
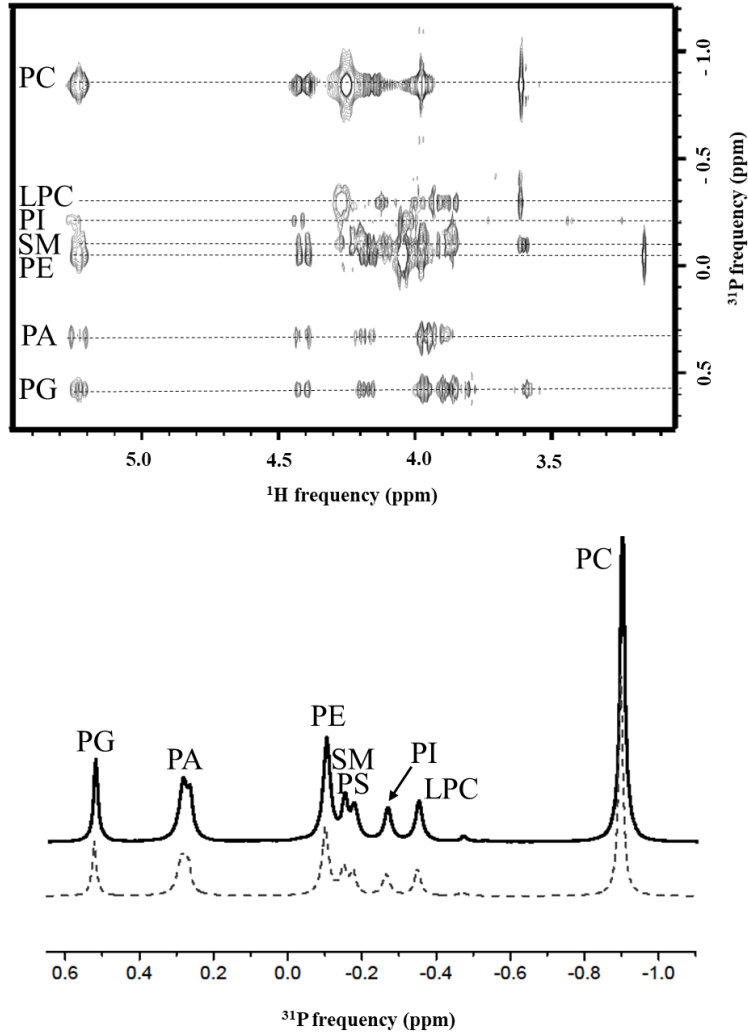
Supplementary Figure 3: NMR Phospholipid assignment of a mixture of reference lipids. Mixture of phospholipids corresponding to PG: 8 mole %, PA: 8%, CL:6%, PE: 18%, SM: 4%, PS:5%, PI: 6%, LPC:4%, PC: 41% and dissolved in deuterated chloroform-methanol 2:1, 0.2M EDTA-D$_2$O, pH 6. Top : 2D ^{1}H-^{31}P HMQC-TOCSY, assignment was performed based individual HMQC of each phospholipid on literature chemical shifts (1D) for those having a weaker trace on the 2D experiment. The transfer delay was adjusted to correspond to a 7 Hz average proton-phosphorus coupling constant. The other parameters were a recycle delay of 2s, ^{1}H and ^{31}P 90 π/2 pulse widths, 10 and 8µs, acquisition time 0.3s, 384 scans, 9 and 3 ppm spectral widths in proton and phosphorus dimensions, respectively, 2K data points in F2 dimension and 64 data points in F1 dimension. Bottom, 1D ^{31}P-NMR with proton decoupling, acquisition conditions: number of scans = 2048, recycling delay = 10s, Lorentzian filtering = 1 Hz. The dotted line below the experimental phosphorus spectrum represents the simulated spectrum using the DMFIT software [2]. All ^{31}P and ^{1}H chemical shifts are referenced respectively relative to PC = - 0,84 ppm and residual solvent peak at 3,31ppm. Peak line shape was approximated by a Gaussian line. PC: phosphatidylcholine, LPC: Lyso-phosphatidylcholine, PI: Phosphatidylinositol, SM: Sphingomyelin, PS: Phosphatidylserine, PE: Phosphatidylethanolamine, PA: Phosphatidic Acid, PG: Phosphatidylglycerol.
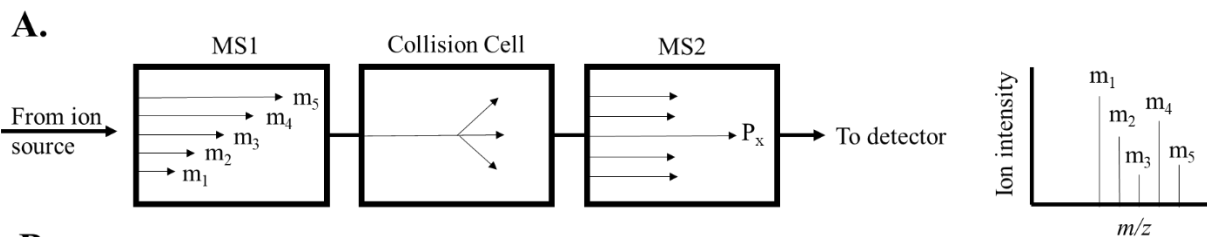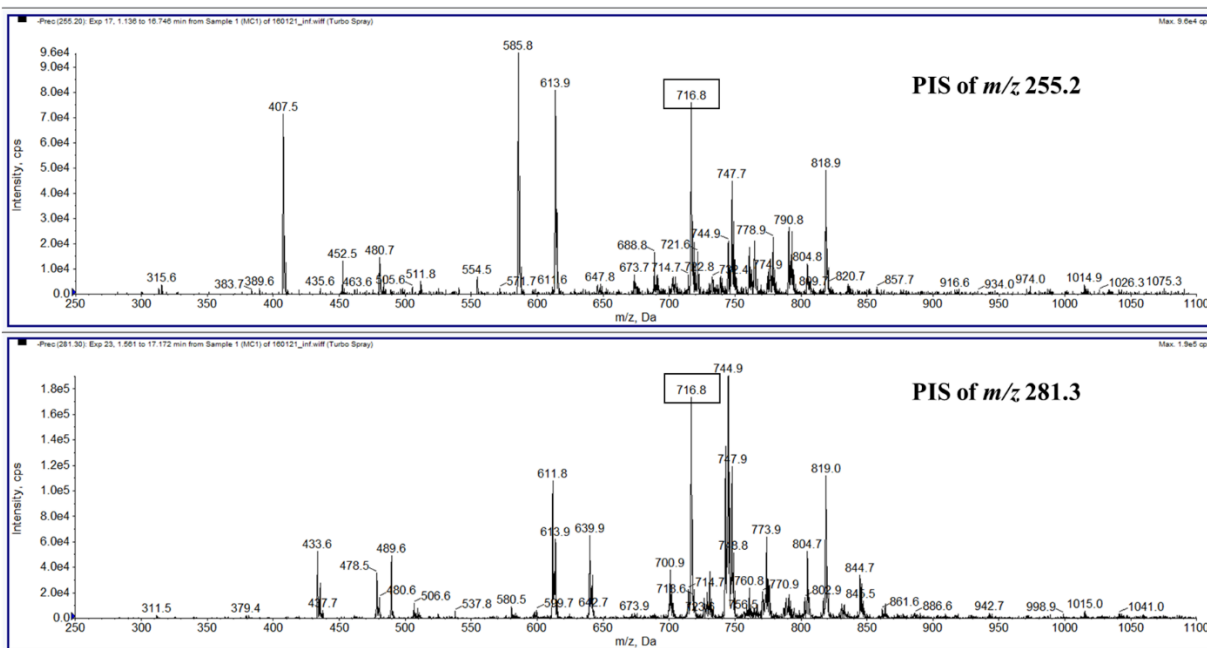
i. **Supplementary Figure. 4. precursor ion scan mode and example of PIS mass spectra of acyl chain**. A. Ions that arrived in the first analyzer MS1 (quadrupole) were scanned over a wide mass range of possible precursor ions. Then, ions were fragmented in the collision cell. The second analyzer MS2 (quadrupole) is focusing on one unique product ion resulting from CID of one or several precursor ions. This MS/MS mode is called precursor ion scan (PIS). B. Shotgun MS/MS analysis of nuclear lipid extract (~0.25mg) dissolved in $CHCl_3/CH_2OH$ (1:2, v/v) + 8 mM ammonium acetate. This analysis generated a list of precursor ion scan (PIS) mass spectra. The PIS mass spectrum on the top shows all lipids that lost a 16:0 acyl chain (at *m/z* 255.2) and the PIS mass spectrum at the bottom represents all lipids that lost a 18:1 acyl chain (at *m/z* 281.3). In this example, a peak is occurring in both spectra at *m/z* 716.8 representing PE 16:0/18:1.

Supplementary Table 1: ^{1}H and ^{31}P chemical shifts of phospholipids
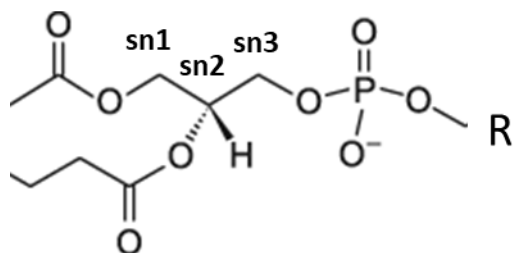
PC, Phosphatidylcholine (16:0/18:1)
1-palmitoyl-2-oleoyl-*sn*-glycero-3-phosphocholine

	Individual Standard	Standard in mixture	Nuclear Lipid Extract
	Glycerol backbone		
-CH$_2$ *sn*-1	4.36; 4.12	4.39; 4.14	4.38; 4.13
-CH *sn*-2	5.20	5.21	5.20
-CH$_2$ *sn*-3	4.00	3.96	3.95
	Head group		
-O-C<u>H</u>$_2$	4.26	4.23	4.22
-O-CH$_2$-C<u>H</u>$_2$	3.60	3.59	3.58
-N$^+$-(C<u>H</u>$_3$)$_3$	3.19	-	3.19
^{31}P	-0.84	-0.84	-0.84

LPC (16:0)
1-palmitoyl-2-hydroxy-sn-glycero-3-phosphocholine

	Individual Standard	Standard in mixture	Nuclear lipid extract
	Glycerol		
-CH$_2$ *sn*-1	4.13; 4.35	4.09	Nd
-CH *sn*-2	5.21	Nd	Nd
-CH$_2$ *sn*-3	4.02	Nd	Nd
-O<u>H</u>	Nd	Nd	Nd
	Head group		
-O-C<u>H</u>$_2$	4.28	Nd	Nd
-O-CH$_2$-C<u>H</u>$_2$	3.61	3.59	Nd
-N$^+$-(C<u>H</u>$_3$)$_3$	3.19	Nd	Nd
^{31}P	-0.30	-0.29	-0.22

PI (16:0/ 18:2)
L-α-phosphatidylinositol
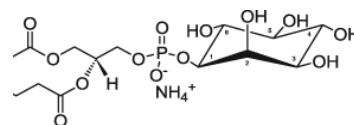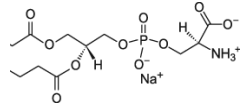
Glycerol			
	Individual Standard	Standard in mixture	Nuclear lipid extract
-CH$_2$ *sn*-1	4.40; 4.16	4.40; 4.14	4.39; 4.16
-CH *sn*-2	5.23	5.23	5.24
-CH$_2$ *sn*-3	4.02	4.01	4.01
Head group			
-C$_1$H - m	3.88	Nd	3.85
-C$_2$H-OH - t	4.14	Nd	Nd
-C$_3$H-OH - t	3.39	3.42	3.41
-C$_4$H-OH - t	3.62	Nd	3.59
-C$_5$H-OH - t	3.22	Nd	3.22
-C$_6$H-OH - t	3.76	Nd	3.72
^{31}P	-0.10	-0.21	-0.26

SM
Egg SM, (16:0/16:0) –
Hexadecanoyl Sphingomyelin
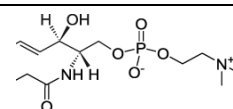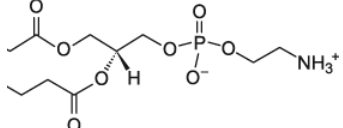
Glycerol			
	Individual Standard	Standard in mixture	Nuclear lipid extract
-C$_\square$H$_2$ *sn*-1	4.14; 3.92	4.10; 3.91	4.10; 3.94
-C$_\square$HNHCOR *sn*-2	3.91	3.84	3.82
-C $_\gamma$H(OH)CH=CH *sn*-3	4.02	Nd	Nd
-C $_\gamma$H(OH)CH=CH	5.40	Nd	Nd
-C $_\gamma$H(OH)CH=CH	5.68	Nd	Nd
Head group			
-O-CH$_2$	4.25	4.25	4.22
-O-CH$_2$-CH$_2$	3.58	3.60	3.58
-N$^+$-(CH$_3$)$_3$	3.18	Nd	Nd
^{31}P	-0.10	-0.09	-0.10

PS (16:0/18:1)
1-palmitoyl-2-oleoyl-*sn*-glycero-3-phospho-L-serine
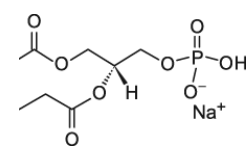
	Glycerol		
	Individual Standard	Standard in mixture	Nuclear lipid extract
-CH$_2$ *sn*-1	4.14; 4.36	Nd	Nd
-CH *sn*-2	5.18	Nd	Nd
-CH$_2$ *sn*-3	3.95	Nd	Nd
	Head group-		
-O-CH$_2$-CH(NH$_3^+$)COO$^-$	4.22; 4.19	4.23; 4.18	Nd
-O-CH$_2$-CH(NH$_3^+$)COO$^-$	3.92	3.95	Nd
^{31}P	-0.08	-0.11	-0.06

PE (16:0/18:1)
1-palmitoyl-2-oleoyl-*sn*-glycero-3-phosphoethanolamine
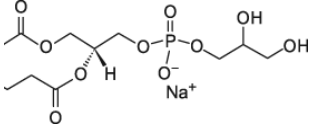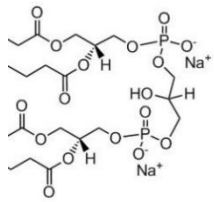
	Glycerol		
	Individual Standard	Standard in Mixture	Nuclear lipid extract
-CH$_2$ *sn*-1	4.36; 4.14	4.39; 4.15	Nd
-CH *sn*-2	5.21 / 5.19	5.21	Nd
-CH$_2$ *sn*-3	4.03 /3.99	4.03	4.02
	Head group		
-O-CH$_2$	3.99 /4.02	3.96	3.95
-O-CH$_2$-CH$_2$	3.09 /3.08	3.14	3.14
-NH$_3^+$	Nd	Nd	Nd
^{31}P	-0.08	-0.04	0.02

PA (16:0/18:1) –
 L-α-phosphatidic acid (Egg, Chicken) (sodium salt)

	Glycerol		
	Individual Standard	Standard in mixture	Nuclear lipid extract
-CH$_2$ *sn*-1	4.35; 4.16	4.39; 4.17	Nd
-CH *sn*-2	5.20	5.22	Nd
-CH$_2$ *sn*-3	3.97	3.95	Nd
^{31}P	0.30	0.34	0.33

PG (14:0/14:0) 1,2-dimyristoyl-*sn*-glycero-3-phospho-(1'-rac-glycerol) (sodium salt)			
Glycerol			
	Individual Standard	Standard in mixture	Nuclear lipid extract
-CH$_2$ *sn*-1	4.37; 4.15	4.39; 4.15	4.37;
-CH *sn*-2	5.20	5.21	5.22
-CH$_2$ *sn*-3	3.99	3.95	3.94
Head group			
O-CH$_2$-CH	3.90	3.87	3.89
-CH-OH	3.75	3.78	Nd
CH-CH$_2$-OH	3.57	3.57	3.88
^{31}P	0.48	0.58	0.57

Cardiolipin (18:1/18:1) 1',3'-bis[1,2-dioleoyl-*sn*-glycero-3-phospho]-*sn*-glycerol			
Glycerol			
	Individual Standard	Standard in mixture	Nuclear lipid extract
-CH$_2$ *sn*-1	4.36; 4.14	Nd	Nd
-CH *sn*-2	5.20	Nd	Nd
-CH$_2$ *sn*-3	4.01	Nd	Nd
Head group			
-CH-OH	3.89	Nd	Nd
-CH$_2$-OH	3.97	Nd	Nd
^{31}P	0.17	Nd	0.06

The table is representing ^{1}H and ^{31}P phospholipid chemical shifts (ppm, reference Kaffarnik *et al*[3] for ^{1}H and Kaffarnik *et al*[3], Glonek *et al*[4] for ^{31}P) of individual standards, standard in a mixture of standard lipids and nuclear lipid extract. Individual lipids (~1 mg), mixture of phospholipids (27 mg, PG: 8 mole %, PA: 8%, CL:6%, PE: 18%, SM: 4%, PS:5%, PI: 6%, LPC:4%, PC: 41%) and Nuclear lipid extract (4 mg) were dissolved in deuterated chloroform-methanol 2:1, 0.02M EDTA-D$_2$O, pH 6. Assignment was accomplished using ^{1}H-^{31}P HMQC-TOCSY experiments on each phospholipid, on the mixture and the extract. The transfer delay was adjusted to correspond to a 7 Hz average proton-phosphorus coupling constant. The other parameters were a recycle delay of 2s, ^{1}H and ^{31}P 90 π/2 pulse widths of respectively 10 and 8μs, acquisition time of 0.3s, between 128 and 384, 9 and 3 ppm spectral widths in proton and phosphorus dimensions, respectively, 2K data points for the F2 dimension and 64 data points for the F1 dimension. All ^{31}P and ^{1}H

chemical shifts are referenced respectively relative to PC = - 0.84 ppm and residual solvent peak at 3.31ppm. Nd: not determined.

Supplementary Table 2. Nuclear lipid extract phospholipid composition by NMR and MS.

Lipid species	NMR[a]	MS[b]
PG	0±1	1.7±0.1
PA	7±1	0.7±0.1
CL	1±1	Nd
LPI	1±2	Nd
PE	9±3	10.6±0.3
PS	4±1	8.4±0.5
SM	4±2	Nd
LPC	0±1	Nd
PI	11±1	6.2±0.6
ePC	15±3	17.8±0.2
PC	48±4	54.5±0.4

[a]The NMR quantification is based on the simulation of NMR lines of the ^{31}P-NMR spectrum of the human nuclear membranes lipid extract. Figures represent mol% of phospholipids. Results represent the average over three samples. Total phospholipid mass of 4 mg (100%)

[b]Mass spectrometry quantification is obtained by MRM (Multiple Reaction Monitoring) experiments on the same lipid extract (see text). Results stand for the average over two samples. Nd: not determined.

PC: phosphatidylcholine, ePC: ether-phosphatidylcholine, PI: phosphatidylinositol, SM: sphingomyelin, PE: phosphatidylethanolamine, PA: phosphatidic acid, PG: phophatidylglycerol, LPI: lyso-phosphatidylinositol, PS: phosphatidylserine, LPC: lyso-phosphatidylcholine, CL: cardiolipin.

Supplementary Table 3. Phospholipid species classified according to chain length and unsaturation

Lipid species	PC	ePC	PI	PS	PE	PA	PG
30:0	6±1%	nd	nd	nd	nd	nd	2±1%
30:1	1±1%	nd	nd	nd	nd	nd	nd
32:0	5±1%	18±1%	1±1%	nd	1±1%	22±9%	nd
32:1	29±1%	nd	4±1%	4±1%	9±1%	nd	0±1%
32:2	3±1%	8±1%	0±1%	nd	1±1%	nd	nd
34:1	0±1%	nd	22±1%	34±1%	44±1%	34±6%	57±1%
34:2	14±1%	65±1%	6±1%	2±1%	1±1%	nd	7±1%
34:3	nd	9±1%	nd	nd	1±1%	nd	nd
36:0	nd	nd	nd	9±1%	0±1%	nd	nd
36:1	8±2%	nd	27±2%	37±1%	2±1%	34±2%	9±1%
36:2	27±1%	nd	20±1%	14±1%	27±2%	10±1%	24±2%
36:3	3±1%	nd	nd	nd	2±1%	nd	1±1%
36:4	1±1%	nd	nd	nd	2±1%	nd	nd
36:6	0±1%	nd	nd	nd	nd	nd	nd
36:8	0±1%	nd	nd	nd	nd	nd	nd
38:2	3±1%	nd	nd	nd	nd	nd	nd
38:4	nd	nd	20±2%	nd	1±1%	nd	nd
38:5	nd	nd	nd	nd	3±1%	nd	nd
38:6	0±1%	nd	nd	nd	nd	nd	nd
40:5	nd	nd	nd	nd	6±1%	nd	nd

Nd: Not detected

Distribution of phospholipids according to their chain length and unsaturation, obtained by reversed phase liquid chromatography-mass spectrometry in MRM mode. 50 pg of lipid extract were dissolved in CH_3CN/H_2O 80/20 and internal lipid standards were added (PA: 10 pmol, PC: 0.25 pmol, PE, PG, PI: 2.5 pmol). Mole % are obtained by normalization with respect to the peak area of internal standards. Analyses were achieved with RPLC-MS/MS (MRM mode) in the negative (PE, PS, PA, PI, PG) and positive ion modes (PC, ePC). The collision gas was nitrogen; collision energy was +47 eV and varied from -62 to -48 eV according to phospholipids species. In bold are highlight the most prominent species. Results stand for the average over two samples. Lipid abbreviations as in supplementary Table 2.

Supplementary Table 4. Lipid and Phospholipid composition in membranes of different tissues.

A) Lipid composition of several membranes (mol % of total lipids). PE, PS, PC, PI, PG: phosphatidyl-ethanolamine, serine, choline, inositol, glycerol; CL : cardiolipin[5]

	Myelin	Erythrocyte	Mitochondrion	Microsome	E. Coli
Cholesterol	25	25	5	6	0
Total Phospholipids	32	56	95	94	100
PE	14	20	28	17	80
PS	7	11	0	0	0
PC	11	23	48	64	0
PI	0	2	8	11	0
PG	0	0	1	2	15
CL	0	0	11	0	5
Total sphingolipids	32	18	0	0	0
Other	11	1	0	0	0

B) Phospholipid composition (mol % of total phospholipids) of related membranes vs. our results on human nuclear membranes.

Phospholipid species	Endoplasmic Reticulum			Golgi		Plasma Membrane			Nuclear Envelope
	Rat Kidney[a]	Rat Liver[a]	Sea Urchin[b]	Rat Kidney[a]	Rat Liver[a]	Rat Kidney[a]	Rat Liver[a]	Human Ery-throcyte[c]	HEK 293T[d]
PC	**38.4**	**54.0**	**38.5**	**52.1**	**49.6**	**34.2**	**39.7**	25	**48.0**
ePC	Nd	Nd	Nd	Nd	Nd	Nd	Nd	Nd	**15.0**
PE	**22.7**	**20.2**	**29.0**	**23.1**	**19.6**	**32.9**	**23.5**	30	9.0
PI	1.7	9.3	**23.61**	7.1	**12.2**	1.9	7.8		**11.0**
PIP	Nd	Nd	1.19	Nd	Nd	Nd	Nd		Nd
PIP2	Nd	Nd	0.6	Nd	Nd	Nd	Nd	6	Nd
PIP3	Nd	Nd	1.9	Nd	Nd	Nd	Nd		Nd
PA	0.7	0.6	0.1	0.7	0.4	0.5	0.5		7.0
PS	11.1	2.7	5.4	5.4	5.6	8.4	9.1	15	4.0
PG	Nd	Nd	Nd	Nd	Nd	Nd	Nd	Nd	0.0
SM	**19.7**	2.3	Nd	6.7	7.6	**14**	**16.1**	**24**	4.0
CL	0.0	1.0	Nd	0	1.2	3.7	1.0	Nd	1.0
LPI	Nd	Nd	Nd	Nd	Nd	Nd	Nd	Nd	1.0
LPC	4.0	8.8	Nd	3.6	1.4	4.0	1.0	Nd	0.0
LPE	1.6	1.0	nd	0.3	1.6	0.5	1.3	Nd	Nd

[a]Zambrano et al [6]. [b]Also called MV2, from Collas et al [7]. [c]Zachowski[8] [d]This paper. In bold are highlighted the 3 most prominent species. Nd: not detected/reported. Lipid abbreviations as in supplementary Table 2.

References

1   Blobel, G. & Potter, V. R. Nuclei from Rat Liver - Isolation Method that Combines Purity with High Yield. *Science* **154**, 1662-&, doi:10.1126/science.154.3757.1662 (1966).

2   Massiot, D. *et al.* Modelling one- and two-dimensional solid-state NMR spectra. *Magnetic Resonance in Chemistry* **40**, 70-76, doi:10.1002/mrc.984 (2002).

3   Kaffarnik, S., Ehlers, I., Grobner, G., Schleucher, J. & Vetter, W. Two-Dimensional P-31,H-1 NMR Spectroscopic Profiling of Phospholipids in Cheese and Fish. *Journal of Agricultural and Food Chemistry* **61**, 7061-7069, doi:10.1021/jf4021812 (2013).

4   Meneses, P. & Glonek, T. High-Resolution P-31 NMR of Extracted Phospholipids. *Journal of Lipid Research* **29**, 679-689 (1988).

5   Schechter. *Biochimie et Biophysique des Membranes : Aspects structuraux et fonctionnels.* . (Masson, 1990).

6   Zambrano, F., Fleischer, S. & Fleischer, B. Lipid-Composition of Golgi Apparatus of Rat-Kidney and Liver in Comparison with other Subcellular Organelles. *Biochimica Et Biophysica Acta* **380**, 357-369, doi:10.1016/0005-2760(75)90104-6 (1975).

7   Collas, P. & Poccia, D. Distinct egg membrane vesicles differing in binding and fusion properties contribute to sea urchin male pronuclear envelopes formed in vitro. *Journal of Cell Science* **109**, 1275-1283 (1996).

8   Zachowski, A. Phospholipids in animal eukaryotic membranes - transverse asymmetry and movement. *Biochemical Journal* **294**, 1-14 (1993).

III. Conclusion

In order to have a better view the role of human nuclear membranes and their specific substructure named invaginations, we developed a powerful non-detergent nuclei extraction protocol allowing to produce milligram quantities of nuclear membrane lipids. Then we developed NMR and mass spectrometry experiments to quantitatively investigate the nuclear membrane lipid composition. The two techniques led to very similar results, NMR being able to quantitate at the mg scale every phospholipid species bearing a phosphorus atom. Mass spectrometry can also bring the same information by using internal lipid standards that can be added to the lipid mixture. Unfortunately, there is not enough lipid standards for all lipid species but most of species can be covered with this method. It is found that the nuclear membrane lipid extract has a typical phospholipid composition compare to other types of cellular membranes and is composed of a complex mixture of phospholipids, with phosphatidylcholines present in large amounts. Negatively charged lipids, with high amounts of phosphoinositides, and phosphatidylethanolamine were also detected in noticeable quantities. We found in addition a very unsaturated lipid part of the membrane. We wonder that this specific lipid composition leads to specific dynamic membrane properties. In order to study such parameters, we performed solid-state NMR experiments on reconstructed nuclear lipid vesicles and analyses their dynamic properties in the following chapter.

Chapter IV: Nuclear membrane dynamics properties

Nuclear cells are surrounding by a membrane called the Nuclear Envelope (NE). This membrane is composed of a double bilayer which the Outer Nuclear Membrane (ONM) is continuous with the endoplasmic reticulum and the Inner Nuclear Membrane is linked to the lamina network inside the nucleus. The NE is not just spherical but form invaginations called Nucleoplasmic Reticulum (NR)(3, 4) inside the nucleus. In order to understand the role of such substructure, an overview of proteolipid composition of NR in necessary to explore. As seen in the Chapter III, we developed a non-detergent nuclei extraction protocol allowing to produce milligrams quantities of nuclear membrane lipids. We further developed liquid-state NMR and Mass spectrometry experiments to quantify the lipid composition. It has been found that the nuclear membrane lipid extract is composed of a complex mixture of phospholipids and with phosphatidylcholine is present in large amount. Negatively charged lipids, with a high amount of phosphoinositidids and phosphatidylethanolamine were also detected in notable quantities. We found in addition a very unsaturated lipid part. We wonder that if this specific lipid composition has an effect on membrane dynamics which can play a role in the formation of NRs. We performed ^{31}P and ^{2}H solid-state NMR experiments in order to investigate nuclear membranes dynamics of nuclear lipid extract reconstituted vesicles. Results are presenting in this chapter in a paper form submitted to Nature Communications.

I. **Unprecedented deformation of human Nuclear Envelopes in magnetic field: is membrane elasticity driving membrane invaginations?**

Unprecedented deformation of human Nuclear Envelopes in magnetic field: is membrane elasticity driving membrane invaginations?

Régine Dazzoni[1,2], Axelle Grélard[1], Estelle Morvan[3], Anthony Bouter[1], Christopher J. Applebee[2], Antoine Loquet[1], Banafshé Larijani[2,4*], Erick J. Dufourc[1*]

[1]Institute of Chemistry & Biology of Membranes & Nanoobjects, UMR5248, CNRS, Université Bordeaux, INP-Bordeaux, F-33600 Pessac, France.

[2]Cell Biophysics Laboratory, Ikerbasque Basque Foundation for Science, Instituto Biofísika (CSIC, UPV/EHU) and Research Centre for Experimental Marine Biology and Biotechnology (PiE), University of the Basque Country (UPV/EHU), Spain

[3]Institut Européen de Chimie et Biologie, UMS3033, CNRS, Université Bordeaux, INSERM (US001), 2 rue Escarpit, Pessac 33600, France

[4]Cell Biophysics Laboratory, Centre for Therapeutic Innovation & Department of Pharmacy and Pharmacology, & Department of Physics, University of Bath, Bath, United Kingdom

Key words: Membrane elasticity and fluidity, human Nuclear Envelope, Phospholipids, Solid-state NMR, fluorescence microscopy.

* Correspondence should be addressed to Erick J. Dufourc (e.dufourc@cbmn.u-bordeaux.fr or erick.dufourc@cnrs-dir.fr) or to Banafshé Larijani (bl666@bath.ac.uk)

ABSTRACT

Human nuclear membrane (hNM) invaginations are believed to be crucial in fusion, fission and remodeling of cells and present in many human diseases. There is however little knowledge, if any, about their lipid composition and dynamics. We therefore isolated nuclear envelope lipids from human kidney cells, analyzed their composition and determined the membrane dynamics after resuspension in buffer. It was found that the hNM lipid extract was composed of a complex mixture of phospholipids, with large amounts of phosphatidylcholines, phosphoinositides (PI) and cholesterol. hNM dynamics was followed by solid-state NMR and revealed that the lamellar gel-to-fluid phase transition occurs below 0°C, reflecting the presence of many lipid unsaturation. Fluidity is higher than in plasma membranes, illustrating the dual action of Cholesterol (ordering) and PI lipids (disordering). The most striking result was however the large magnetic field-induced membrane deformation allowing to determine the membrane bending elasticity, a property related to hydrodynamics of cells and organelles. Human Nuclear Lipid Membranes were found to be at least two orders of magnitude more elastic than classical plasma membranes, suggesting a physical explanation for the formation of nuclear membrane invaginations.

Cell nuclei are known to have a quasi-spherical shape at rest with a diameter that may vary from 5 to 10 µm depending on the cell type. Their envelope is composed of a double lipid bilayer, the inner and outer nuclear membranes (NM), and the nuclear lamina. The lamina play an important role in structure, stability, and gene regulation and consist of a dense network of proteins underlaying the inner membrane [1]. Inner and outer NM join at the nuclear pores and enclose a perinuclear space that is continuous with the endoplasmic reticulum (ER), providing a reservoir of membrane material that may be used during nuclear deformation. Powerful imaging techniques highlighted the presence of nuclear envelope substructures forming invaginations inside the nucleus [2]. These invaginations have been called Nucleoplasmic Reticula (NR). NRs are reported in numerous normal and abnormal cells from the plant and animal kingdom. NRs are particularly abundant in many tumor cell types including brain, breast, kidney, bladder, prostate and ovary and suggest that the NRs regulatory mechanisms are susceptible to pathological dysregulation [3,4]. However, and to the best of our knowledge, their role is still unknown. The appearance of this specific morphology inside the nucleus suggests that NRs may have a role in mechano-transduction of signal to the nucleoplasm, gene expression, RNA trafficking, and cell differentiation [1,5]. NRs are stable and persistent but are also flexible enough to accommodate nuclear rotation or changes in morphology [6]. In live cells, NR may change on a timescale of minutes [2]. The NR regulation appears to be a dynamic process that may be controlled by several pathways. NR formation might be controlled by changes in phospholipid bilayer composition when choline phosphate cytidylyl-transferase (CCTα) is activated. This enzyme synthetizes phosphatidylcholines (PC), which might play a role in modifying the human nuclear membrane (hNM) mechanical properties and promote the development of invaginations [7]. Unlike for model marine organisms hNM dynamics has not been investigated yet. Larijani et al. [8] have shown the conserved membrane fusion mechanism in sea urchins and that both proteins and lipids are strong requirements for such a process [9]. In the sea urchin model, an elevated heterogeneity has been reported for such nuclear membranes and high amounts of cholesterol and phosphoinositides (PI) were found. Fluid properties have been nonetheless reported, offering an alternative to the present paradigm that cholesterol-enriched membranes are rigid membranes [10]. To complement these findings the essential role of diacylglycerol as both a second messenger and a modulator of membrane dynamics in the formation of the nuclear membrane has also been demonstrated [9].

To the best of our knowledge, a detailed characterization of the lipid composition and physical properties of the human nuclear membranes by a non-invasive methodology has not been reported. One of the most precise, quantitative and non-invasive methods for studying physical properties of natural membranes, such as composition, dynamics and morphology, is NMR spectroscopy [11-13]. Phosphorus, proton and carbon liquid-state NMR were chosen to probe phospholipid composition, whereas phosphorus and deuterium solid-state NMR have been used to monitor the physical properties (fluidity, elasticity) of human nuclear membranes. In order to provide enough material for NMR, nuclei needed to be purified using a non-detergent method. In the past, the use of detergents for purifying nuclei from mammalian cells has led to misinterpretations of function, localization and composition of the "nuclear lipids" [14,15]. Based on existing procedure [16] we therefore implemented a non-detergent method for purifying nuclei from Human Embryonic Kidney (HEK) 293T cells (Fig. 1). Lipids were extracted from quasi-pure nuclei with minimum contamination from the endoplasmic reticulum.

Using various types of advanced liquid-state and solid-state NMR experiments we report herein the atypical lipid composition and physical properties of human Nuclear Membrane. The most striking result is however the observation of a significant deformation of the reconstructed nuclear lipid membrane in magnetic fields. In addition, we show that such a deformation is directly linked to a very high nuclear membrane elasticity, which was found to be two orders of magnitude more elastic than that of plasma lipid membranes. We finally discuss the biological implications in terms of membrane invaginations.

Results

Purification of large amounts of human Nuclear Membrane lipids using a non-detergent method.

The method published by Blober & Potter [16] was optimized and used to recover mg-scale lipid membranes without detergents. Human Embryonic Kidney (HEK) 293T cells were grown as described in Materials & Methods. They were visualized using Hoechst and $DiOC_6$ dyes that specifically bind to nuclei and membranes as respectively seen in blue and green in Fig. 1A, using fluorescence microscopy. $DiOC_6$ staining shows all membranes of HEK cells: the plasma membrane surrounding the cell, the Endoplasmic Reticulum (ER) filling the cytoplasm compartment and the nuclear membrane enclosing the decondensed chromatin stained by the Hoechst reagent. Nuclei were thus submitted to a nitrogen gas cavitation action provided by a cell disruption bomb apparatus. Fig. 1B attests the efficiency of the method: the plasma membrane is absent; nuclei are intact and nuclear membranes appear complete. As the outer nuclear membrane is continuous with the ER, a small proportion of ER membranes is nonetheless observed attached to nuclei. As it is minor no further removal has been performed. Lipids were then extracted from the nuclei as described in the Materials & Methods section. The yield is quite important: from ca. 10^8 nuclei, 4 mg of human nuclear membrane lipids (dry weight) could be recovered.
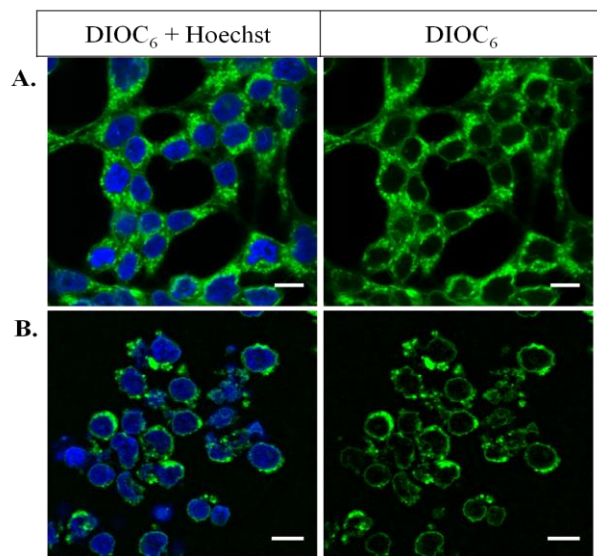
Fig. 1: Nuclei purification efficiency by the nitrogen gas cavitation method. HEK 293T Cells (A) and cells treated by the cavitation method (B). Staining by $DiOC_6$ (1µM, green) to visualize membranes, and by Hoechst (1µM, blue), binding specifically to chromatin and imaging the nuclei interior. Images have been acquired by an inverted confocal instrument with a 63-fold water immersion objective. Excitation wavelengths of $DiOC_6$ and Hoechst were respectively 488nm and 405nm; emission ranges are of 504-561nm for $DiOC_6$ and of 436-483nm for Hoechst. Scale bars: 10µm.

Human Nuclear Membranes are mainly composed of phosphatidylcholines, phosphoinositides and cholesterol.

Lipid extracts were solubilized and the solution transferred into a 5mm diameter NMR tube to be analyzed by liquid-state ^{1}H-,^{13}C- and ^{31}P-NMR. The phosphorus 1D spectrum shows a classical series of isotropic lines that can be assigned to individual phospholipid species (supplementary Fig. 1, bottom). As NMR spectra were acquired under quantitative conditions, the amount of each phospholipid in the extract was obtained by integrating the surface area under the spectral peaks (see spectral simulations of 1D ^{31}P-NMR spectra, supplementary Fig. 1). Spectral areas were normalized with respect to the internal reference of known concentration. We thus determined the total quantity of phospholipids in the extract, from 107×10^6 nuclei, 4 mg of phospholipids were extracted. Results are reported in Table 1. Phosphatidylcholines (PC) dominate the lipid extract with *ca.* 60%. Negatively charged lipids were present at *ca.* 25% with more than half of them being phosphoinositides (PI). Phosphatidylethanolamines (PE) were present at 9%. ^{31}P-NMR chemical shifts globally agree with literature values obtained from individual species. There was however some variance with negatively charged lipids that were very sensitive to pH[17]. Another source of variance was due to the fact that chemical shifts of lipids in a complex natural mixture may slightly vary from those reported from individual synthetic species (Table 1). The identification of most of the main lipids was nonetheless secured using 2D NMR (^{1}H-^{31}P correlation, supplementary Fig. 2). Of interest is also the presence of Cholesterol that has been detected using 2D-NMR (^{1}H-^{13}C correlation, supplementary Fig. 1 and 3), and also the presence of numerous unsaturation in the lipid chains (5.3 to 5.4 ppm).

Phospholipid[a]	^{31}P-chemical shift (ppm) from literature	^{31}P-chemical shift hNM (ppm)[c]	% mol[d]
TPP (reference)		-17.95	
PC	-0.84±0.01	-0.84±0.01	**46±4**
EPC	-0.78±0.01	-0.77±0.01	**15±2**
LPC[e]	-0.28±0.04	-0.22±0.01	0±1
PI	-0.36±0.03	-0.20±0.06	**11±1**
SM	-0.07±0.03	-0.10±0.01	3±2
PS[g]	-0.05±0.01	-0.06±0.01	4±1
PE	0.04±0.10	0.03±0.01	9±2

LPI[e]	0.10±0.04	0.03±0.01	4±1
CL[g]	0.18±0.01	0.06±0.01	1±1
PA	0.23±0.04	0.33±0.02	6±1
PG[f]	0.47±0.01	0.57±0.01	0±1

TABLE 1. Quantification of phospholipid species in human nuclear membranes (hNM) by liquid-state NMR

[a]TPP: Triphenylphosphate (internal reference), PC: phosphatidylcholine, EPC: ether phosphatidylcholine, LPC: lysophosphatidylcholine, PI: phosphatidylinositol, LPI: lysophosphatidylinositol SM: sphingomyelin, PS: phosphatidylserine, PE: phosphatidylethanolamine, CL: cardiolipin, PA: phosphatitic acid, PG: phosphatidylglycerol.

[b]Chemical shifts of individual phospholipids in the MeOD/CDCl$_3$ (from Kaffarnik *et al.* and Meneses & Glonek [18,19]). Average over the 2 reference values. Reference H$_3$PO$_4$ (0 ppm).

[c] Chemical shifts of individual phospholipids in the nuclear lipid extract mixture (4 mg of phospholipids solubilized in of 500 μL of MeOD/CDCl$_3$ (1:2) + 30 μl of 0.2 M EDTA-D$_2$O pH 6). Chemical shifts were referenced with respect to the internal standard TPP: -17.95ppm [18], assignment was performed with ^{1}H-^{31}P 2D NMR (supplementary materials). Values in the column represent the average over 3 different sample extractions over a period of one year.

[d]Molar lipid content in the extract as determined from simulated spectra using the DMFIT software (see Materials and Methods and supplementary Fig. 1). Figures represent the average over 3 NMR sample preparations. Bold stand for the most abundant species.

[e]Only detected once among 3 samples. Assignment by comparison with literature values.

[f]Only detected once among 3 samples.

[g]Assignment by comparison with literature values.

Nuclear lipid membranes are fluid below 0°C

Lipid extracts were mixed with deuterated POPC (10:1 molar ratio) and rehydrated for membrane thermotropic and dynamics studies. Spherical liposomes (multilamellar vesicles, MLV) of 0.9 μm average diameter was readily detected by optical microscopy indicating that the lipid extract was capable of reforming lipid bilayers (supplementary Fig. 4). The hydrated lipid extract was analyzed between -20°C to 45°C by solid-state ^{2}H-NMR. As a control, spectra for pure ^{2}H$_{31}$-POPC MLV were also recorded. Selected spectra are shown in the Figure 2A, the spectra for the entire temperature variation are shown in supplementary Fig. 5. ^{2}H$_{31}$-POPC spectra reflect the classical thermotropic behavior of MLVs: uniaxial lamellar fluid phase (also known as, L_α, or liquid-disordered, *ld*) above 0°C with well-resolved quadrupolar doublets, the largest width being ≈ 26 kHz, with marked shoulders at ca. 52 kHz, and below very wide ^{2}H-NMR spectra of approximately 120 kHz width, which was typical of C-^{2}H$_2$ groups no longer undergoing chain and segment isomerization. These were features characteristic of a lamellar gel phase, also known as $L_{\beta\prime}$, or solid-ordered phase, *so*, [20]. These features in fluid and gel phases reflect a random distribution of local bilayer normals with respect to the magnetic field, *i.e.*, "powder" or spherical distribution of bilayer

115

membranes typical of slowly tumbling micrometer-size spherical liposomes [20-22]. This thermal behavior is completely reversible (Fig. 2). Reconstituted nuclear membrane vesicles, labelled with $^2H_{31}$-POPC, led to a fluid phase spectrum at 25°C. The width ($\approx$ 30 kHz) was wider than for pure POPC MLV, indicating that the lipid probe was sensing a more rigid membranous environment. Cooling down to -20°C led to a composite spectrum with broad features of approximately 120, 35 kHz and an unresolved broad central peak. This indicated a heterogeneous lamellar phase with rigid parts but also with more dynamic portions. Increasing the temperature to 0°C led to an almost fluid phase spectrum with broad features detected near 110 kHz. Increasing further to 25°C resulted in a well-resolved spectrum consisting of several doublets. In this case the spectrum has lost the "powder" type distribution, *i.e.*, the "shoulders" at *ca.* 60kHz were absent. This event suggests a deformation/orientation of the reconstituted membrane vesicles in the magnetic field (*vide infra*).
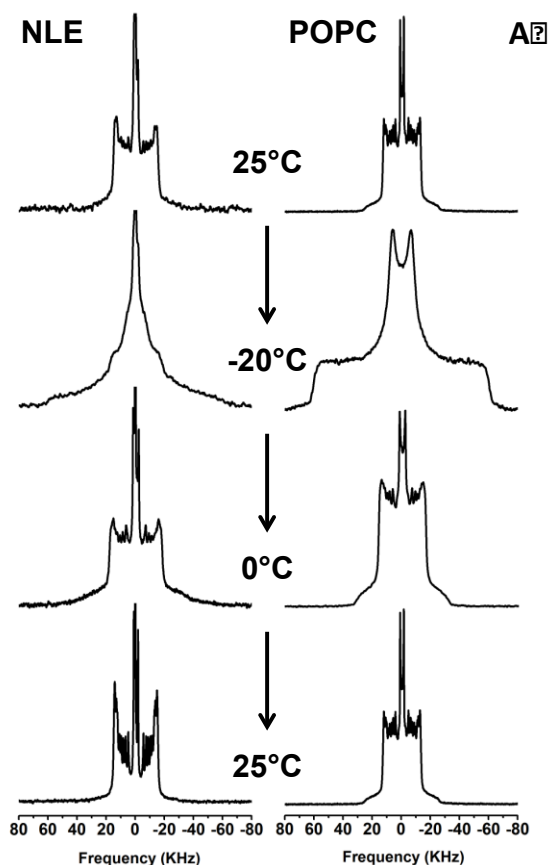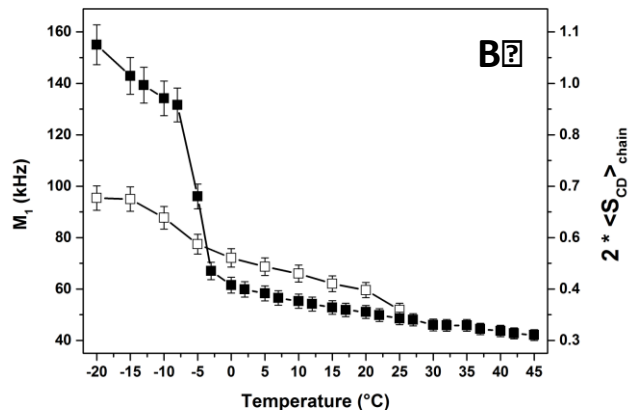
Fig. 2- Thermotropism of hNM lipid extract membranes and POPC controls. A) Selected ^{2}H-NMR spectra of reconstituted human nuclear lipid membrane extracts (NLE) mixed with ^{2}H$_{31}$-POPC and pure ^{2}H$_{31}$-POPC (POPC) vesicles during a thermal variation (25°C down to -20°C and back) and recorded after temperature stabilization. Spectra were obtained after Fourier transformation of solid-echo type experiments accumulated for 2-18k transients. The entire thermal variation is shown in supplementary Fig. 3. Details for experimental parameters and data treatment are found in the methods section. **B)** Thermal variation of the first spectral moment (reporting membrane fluidity), M$_1$, from ^{2}H-NMR spectra of Figure 2A and supplementary Fig. 3 of reconstituted NLE (□), and control POPC vesicles (■). The double y-axis plots twice the fatty acid chain order parameter to depict rigid chains (solid-ordered membranes) when $2\langle S_{CD}\rangle_{chain} = 1$ and fully disordered systems (liquid-like) when $2\langle S_{CD}\rangle_{chain} = 0$.

The temperature behavior of hydrated lipid systems can be further quantified by calculating the first spectral moment, M_1, [20,23]. M_1 is directly proportional to the average chain order parameter, $\langle S_{CD}\rangle_{chain} = \sqrt{3}M_1/\pi A_Q$, with A_Q being the static quadrupolar coupling constant [24]. The chain order parameter is a direct measure of the state of order/disorder of the membrane: $2\langle S_{CD}\rangle_{chain} = 1$ for totally rigid systems and 0 for liquid systems. Fig. 2B shows both M_1 and $2\langle S_{CD}\rangle_{chain}$. At low temperatures, POPC model membrane reached $2\langle S_{CD}\rangle_{chain}$ values near 1 confirming the rigid nature of the hydrophobic membrane core. A sharp order-disorder transition occurs at T$_m$ = -5 ± 2°C due to the onset of various molecular processes [25]. The chain ordering slowly decreased when the temperature was increased above T$_m$ also indicative of the liquid disordered state. In contrast, the reconstituted nuclear membrane vesicles did not reach a complete ordered state at the lowest temperature. Their phase transition was broad and occurred between -15°C to 0°C. Chain ordering in the fluid phase was greater than that observed with pure POPC vesicles except above 25°C where both systems show similar fluidity.

Spectral simulations reveal ordering and vesicle deformability.

For fluid phase temperatures (*e.g.*, 25°C) a minute description of chain ordering may be obtained from ^{2}H-NMR spectra. Figure 3A shows both experimental and calculated spectra for ^{2}H$_{31}$-POPC and reconstituted

nuclear membrane vesicles labelled with $^2H_{31}$-POPC. The palmitic chain contains 14 methylene (C-$^2H_2$) labelled positions and one C-$^2H_3$. The methyl terminal doublet was assigned as the smallest and the most intense peak [22]. Only 8 other splittings were detected from the experimental spectra indicating that there are several magnetically and dynamically equivalent positions. Simulations allowed to accurately determine splitting values (in kHz) with a high accuracy. Assigning a doublet to a labelled position, k, relied on comparisons with values from the literature and using mean-field theories [21]. Figure 3B illustrates the carbon-deuterium order parameter (S_{CD}) profile as a function of the labelled carbon position, k, after converting quadrupolar doublets into order parameters ($\left|\Delta v_Q^k\right| = \frac{3}{4}A_Q S_{CD}^k$). A typical behavior was detected with elevated values for positions 2 to 8-10 and a marked decrease towards the chain end, *i.e.*, the bilayer center. This reflected the well-known gradient of order parameters with increased rigidity near the interface and an almost liquid-like environment at the center of the membrane. The reconstituted nuclear membrane vesicles have a similar ordering profile but are clearly more ordered than pure POPC. Ordering information can be correlated to bilayer thickness by considering that the more motion present in the bilayer core the shortest, in average, are the hydrophobic chains [22,26]. At 25°C the value for the bilayer thickness of pure POPC was 42.8Å. 44.2Å were obtained for reconstituted nuclear membrane vesicles respectively (Supplementary Table 1). The difference is small but notable. This could be due to the presence of cholesterol that has been shown to increase membrane ordering and hence membrane thickness [23].
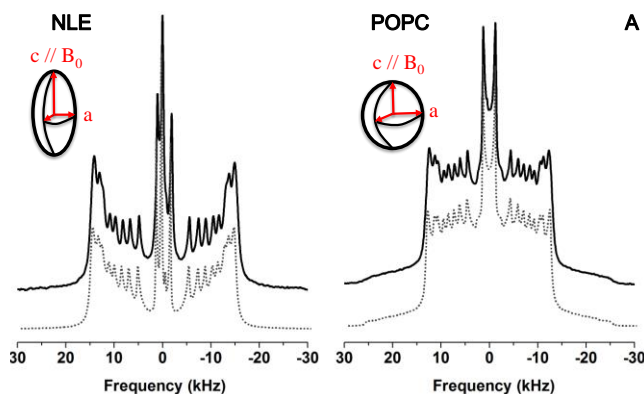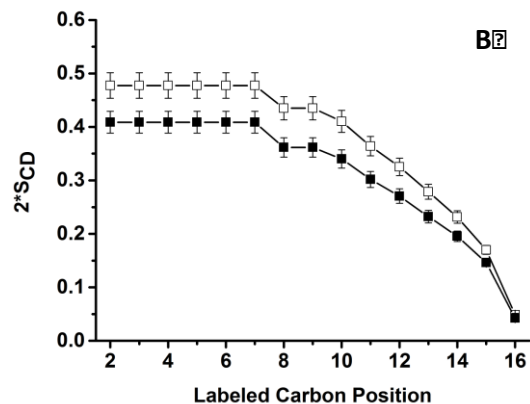
Fig. 3 - Simulations of deuterium solid state spectra reveals ordering and deformability. **A)** Experimental and simulated (dotted line) ^{2}H spectra of reconstructed membrane vesicles and control POPC vesicles as obtained at 25°C. Same experimental parameters as in Fig. 2. Simulated spectra were calculated as described in Materials & Methods. Inserts (ellipsoid and sphere) depict the deformation that is obtained from simulations, c/a = 3.0 for NLE and 1.0 for POPC. c and a are the long and short semi-axes with c being aligned with the B_0 magnetic field direction. **B)** Plot of S_{CD} order parameters as a function of the labelled carbon position, k, along the palmitoyl acyl chain ($k=16$, chain end, $k=2$, membrane interface). Accuracy in order parameters is 0.5%.

Spectral simulations were performed by considering a distribution of bilayer orientations, θ, with respect to the magnetic field as in an ellipsoid of revolution: $p(\theta) \sim \frac{sin^2\theta}{sin^2\theta + \frac{c}{a}cos^2\theta}$ [27], where c/a represents the ellipsoid long axis to short axis ratio [27]. c/a values were varied until a correct agreement was obtained between experimental and calculated spectra (Figure 3A). c/a was found near 1.0 for POPC (almost no deformation) and close to 3.0 for reconstituted nuclear membrane vesicles. This indicated a large prolate deformation of the initially spherical vesicles. Inserts in Figure 3A (ellipsoid and sphere) depict the deformation that was obtained from simulations, with c being aligned with the B_0 magnetic field direction.

^{31}P-NMR reveals enhanced deformability of NLE vesicles.

The liposome deformation that was pointed out by deuterium NMR was further investigated by wide line ^{31}P-NMR. Selected spectra are shown in Fig. 4 together with POPC control liposomes obtained through the same temperature variations and magnetic conditions (the entire temperature variation is shown in supplementary Fig. 6). POPC illustrates a classical "powder" spectral profile indicating a random or spherical distribution of bilayer normals in the field (*i.e.*, non-oriented samples). This line-shape is independently obtained at initial conditions and after having been to low temperatures and back. The reconstituted nuclear membrane vesicles show prominent differences between the initial spectrum taken at 25°C and the final one recorded after the temperature variations in the magnetic field. The left hand side

119

shoulder almost disappeared and the spectrum looks like an oriented sample spectrum as could be obtained by placing lamellar lipid membranes onto glass plates and orienting the plate normal perpendicular to the field [25]. Such a spectrum may be accounted for by a huge liposome deformation into an ellipsoid prolate with short and long axes, *a* and *c* (Figure 4 diagrams), such as *c/a* > 1.
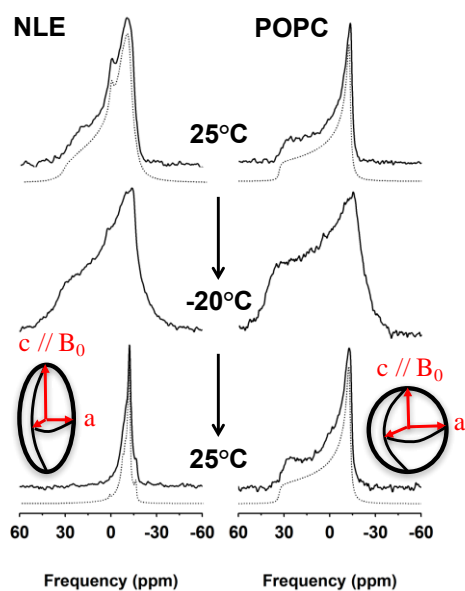
Fig. 4- Temperature-dependent ^{31}P-NMR spectral lineshapes and simulations of nuclear lipid extract membranes and POPC vesicles.

Selected ^{31}P-NMR spectra (solid lines) of reconstituted nuclear lipid membrane extracts (NLE) and POPC vesicles during a thermal variation (25°C down to -20°C and back) and recorded after temperature stabilization. Spectra were obtained after Fourier transformation of Hahn-echo type experiments accumulated for 300 to 7000 transients. The entire thermal variation is shown in supplementary Fig. 4. Details for experimental parameters and data treatment are found in the methods section. Simulated spectra (dotted lines) were calculated as described in Materials & Methods. Inserts (ellipsoid and sphere) depict the deformation that is obtained from simulations, *c/a* = 3.0 for NLE and 1.0 for POPC. *c* and *a* are the long and short semi-axes with *c* being aligned with the B_0 magnetic field direction.

This was in complete accordance with what has been observed by deuterium NMR (*vide supra*); the samples were however slightly different; this one was without insertion of the deuterated lipid reporter. As the same deformation values (*c/a*) were found from deuterium and phosphorus NMR on different samples this strengthens the observation of a huge magnetic field effect on lipid nuclear membranes.

Magic angle spinning abolishes magnetic field induced vesicle deformation. The magnetic field induced liposomes deformation in general occurs when the magnetic energy for orienting molecules in the field overcomes the curvature elastic energy of liposomes [28] (Supplementary Information). These two energies can be counterbalanced using a third one, the mechanical energy related to rapid rotation of the sample at the magic angle (54.7°), as it is often performed in solid state NMR. In the present experiment, the sample, once the initial spherical liposomes (Fig. 5A) were deformed into prolate ellipsoids (Fig. 5B) by slowly increasing the temperature from -20°C back to 25°C, was submitted to a moderate spinning rate of 1.4 kHz (1400 rotor rotations per second), Fig. 5C at 25°C. The pattern obtained was made of spinning side bands, spaced by 1.4 kHz, which map out the intensities of the initial powder pattern spectrum (Fig. 5A).
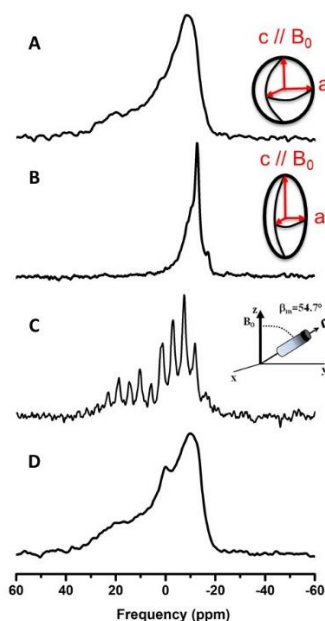
Fig. 5- Annihilation of magnetic field-induced vesicle deformation by Magic Angle sample Spinning (MAS) as detected by ^{31}P-NMR.

A) "Powder" spectrum obtained at 25°C just after sample preparation and scheme of a sphere indicating a spherical distribution of bilayer normals. **B)** Oriented-like spectrum at 25°C, after placing the sample in the magnetic field at low temperatures and returning back to 25°C. The insert depicts the prolate deformation of vesicles with a *c/a* semi-axes ratio of 3. **C)** Same as B) except for magic angle sample spinning at 1400 rotor rotations per second (1.4 kHz). Spinning side bands spaced every 1.4 kHz depict the powder pattern line shape, *i.e.*, loss of deformation. **D)** Spectrum obtained at 25°C just after stopping MAS showing the recovery of a powder pattern lineshape similar to **A)**. All spectra were obtained with the same acquisition parameters (as in Fig. 4).

After stopping the sample rotation, a static ^{31}P-NMR spectrum was acquired (Fig. 5D), showing the characteristics of a powder distribution, with $c/a \approx 1.0$ (simulation not shown). One has the clear evidence that magnetic field induced deformation could be destroyed by rapid rotation of the sample at the magic angle. Interestingly, the deformation phenomenon was reversible, *i.e.*, the same field-induced prolate deformation could be obtained by submitting the sample to the same thermal variations in the magnetic field, without MAS. Cooling down to -20°C and stepwise increase in temperature to 25°C lead to the oriented like spectra of Fig. 5B (not shown).

DISCUSSION

The purification of lipids from mammalian nuclear envelopes and their reconstitution into liposomes has brought several new and interesting findings that can be summarized as follows. 1) The phospholipid composition is dominated by phosphatidylcholines, with remarkable amounts of negatively charged lipids and cholesterol. 2) Reconstituted nuclear membrane vesicles are fluid at ambient temperatures and enter into a gel-like solid ordered phase below 0°C. Their membrane is more ordered (more rigid) than that of classical POPC membranes. 3) Reconstituted nuclear membrane vesicles are greatly deformed by magnetic field suggesting a highly deformable lipid membrane. These findings will be discussed sequentially and finally related to the propensity of large membrane invaginations that are observed for nuclear membranes.

The lipid composition that was analyzed by liquid state ^{1}H, ^{13}C and ^{31}P-NMR shows that PC lipids represent more than 60 mol% of the phospholipid composition. Of interest, negatively charged lipids are present in large proportions, including phosphoinositides, PI, that amount ca. 15%. The presence of large amounts of PC lipids clearly accounts for the easy formation of micrometer-size liposomes when the lipid extract is rehydrated. It is indeed known, after Isaelashvili [29], that PC lipids have, in average, a cylindrical shape that favors the flat lamellar topology at the nanometer scale and hence the stabilization of bilayer membranes. ^{1}H-NMR also indicates the presence of numerous unsaturation, which account for a low lamellar gel-to-fluid phase transition temperature (*vide infra*). It is interesting to compare our results to those obtained on sea urchins nuclear membrane extracts [30,31]. There are three nuclear envelope membrane precursors, MV1, MV2 and NER. MV1 and NER are precursor membranes that are highly enriched rich in PI. The nuclear envelope remnants (NER) are rich in cholesterol. These nuclear envelope precursors are responsible for the initiation of nuclear envelope formation during the male pronucleus formation. Their lipid composition globally resembles the male pronucleus membrane precursors with a small variance in the quantity of PI lipids that appears in slightly lesser amount. It is however worth mentioning that non-silanized glassware

was used in our study which may tend minimizing the detection of negatively charged species. Our results show that the hNM is enriched in PC, PE, PI and cholesterol and suggest that the NE lipid composition is globally similar to ER (endoplasmic reticulum) lipid membrane composition [32,33]. The presence of cholesterol is similar to the high levels of cholesterol in NER of the sea urchin [10]. The membrane domain is located at the acrosomal and centriolar fossae of the sperm and remains during the formation of the male pronucleus formation [34]. These are the membranous regions that have a role in chromosomal organization. We suggest the resemblance of the lipid composition, especially in the cholesterol levels, in sea urchin NERs and the NRs may lead to the similarity of their function in the chromosomal organization both in non-somatic and somatic cellular models. The outer nuclear membrane (ONM) is continuous with the ER [35] therefore it is not too surprising finding similar lipid compositions. As Larijani and coworkers have shown that unsaturated fatty acid chained phosphoinositides are promoters of membrane disordering, their detection in mammalian nuclear membranes militates in favor of very dynamic membranes. [10]

Depending on their function, natural membranes may show very different thermotropic properties. It is recognized that the lipid membrane may be in a certain state of fluidity to perform its function [23,36]. For instance, the transition from an ordered state to a more disordered one in human erythrocytes has been found to occur at *ca.* 20°C [37]. On the other hand *Mycoplasma Laidlawii* membranes and lipid extracts show transition temperatures near 40°C [38] whereas *E. Coli* lipid extracts have been shown to transit from 20 to 40°C depending on the fatty acid that was supplemented in the growing medium [39]. Extremophile *Archaea* grow at very high temperature, near very hot water sources, and show to be rather fluid above 80-90°C [40]. Our finding concerning the reconstituted nuclear membrane vesicles indicate that the gel-to-fluid phase transition occurs near -10°C and has a breadth of ca. 20°C. Even at the lowest temperature investigated, -20°C, the system is not completely in the solid-ordered state. This is remarkable and bound to the presence of many charged phospholipids and of unsaturation in the hydrocarbon chains. A more complete determination of chain length and unsaturation per lipid species is currently under way by mass spectrometry in our laboratories.

In addition to having a low transition temperature, reconstituted lipid nuclear membrane vesicles have been found to be slightly thicker than pure POPC membranes at ambient temperatures and up to 40°C. We suggest that this is related to the presence of cholesterol in the lipid composition. Sterols are indeed known to increase membrane ordering in the fluid phase [11,27]. The membrane ordering and thickness are however much less important than in membranes containing large amounts of sterols (30% and above), such as the

plasma membrane. This suggests than the reconstituted nuclear membrane vesicles have increased stability but remain extremely fluid. We propose that the fluidity is bound to the presence of invaginations in the nuclear membranes, a more fluid membrane will help in stabilizing these large nuclear membrane deformations that can penetrate deeply inside the nucleus (see below).

One of major findings in our work is that the reconstituted nuclear membrane vesicles of initial spherical shape can be remarkably deformed by a high magnetic field (18.8T) into elongated ellipsoidal prolates. Magnetic alignment of proteins or lipids has already been reported [41-44]; it is in general very small as biological molecules have a very weak magnetic susceptibility, χ. However, molecules and cells may contain paramagnetic species, like iron ions, of high χ that will allow behaving as small orienting magnets. Lipid magnetic susceptibility anisotropy, $\Delta\chi$, is in general very small (-10^{-7}, dimensionless) and so lipids do not show orienting properties in solution. However, lipids under the form of liposomes may present cooperative orienting properties, the bulk magnetic susceptibility being the sum of the molecular susceptibilities. Seelig [44] has first reported that liposomal lipid extracts could be oriented in magnetic fields, and Helfrich [28] had long ago worked out the physics of magnetic-induced deformation of liposomes: under thermal equilibrium, liposomes are spherical in average and may be deformed when the magnetic orienting energy is greater than the membrane curvature elastic energy. Spherical liposomes are then deformed into prolate or oblate ellipsoids, of semi axes c and a. The extend of deformation is expressed as c-a and energy minimization leads to, in the SI system (see supplementary information):

$$c - a \approx -f\frac{r_0^3\Delta\chi b B_0^2}{\mu_0 k_C} \qquad (1)$$

Where r_0 (in m) is the initial radius of spherical liposomes, b (in m), the bilayer thickness, B_0 (in Tesla, T = kg.s^{-2}.A^{-1}), the magnetic field intensity, k_C the apparent elastic energy modulus (in Joules, J = kg.m^2.s^{-2}) and $\Delta\chi = \chi_\parallel - \chi_\perp$, the anisotropy (dimensionless) of the magnetic susceptibility of molecules in the membrane. f and μ_0 are constants of value 1/18 and $4\pi\times10^{-7}$ (in kg.m.s^{-2}.A^{-2}), respectively. $\Delta\chi$ is in general negative, e.g. -4.10^{-7} for dimyristoylphosphatidylcholine, (DMPC) [45], for lipids having saturated or unsaturated chains. This will lead to c-a > 0 and to a prolate deformation as observed for nuclear lipid extracts. From the spectral simulation c/a was found close to 3.0 and calculating c-a, a value of 0.63 μm was obtained, which represents a substantial deformation of the initial spheres of radius r_0 = 0.45 μm. In equation (1) all variables are known or measurable, except for $\Delta\chi$ and k_C. In other words, the deformation scales as $\Delta\chi/k_C$ and may increase because the membrane elastic modulus (of the order of 10^{-19} J) decreases

or the anisotropy of the membrane magnetic susceptibility, $\Delta\chi$, increases. $\Delta\chi$ values are very difficult to determine and have been scarcely measured up to now; there are debates about the accuracy in their determination. In case of lipid mixtures, it will be the weighed sum of the molecular magnetic susceptibilities of each of the lipid species. Borowske & Helfrich [45] nonetheless reported a value for egg lecithin membranes: $-0.28.10^{-8}$ cgs units, which translates in the SI system as $\Delta\chi_{SI} = 4\pi\Delta\chi_{CGS} = -3.5.10^{-7}$. By making the rough hypothesis that the magnetic susceptibility anisotropy in reconstituted human nuclear membrane vesicles and in egg lecithin are similar one may calculate the corresponding elastic modulus: k_C $\approx 0.03.10^{-19}$ J. This value may be compared to some reliable values for DMPC in the presence of various amounts of cholesterol [46], k_C (DMPC) $= 1.27.10^{-19}$ J and k_C (DMPC + 30mol% CHOL) $= 3.07.10^{-19}$ J. It therefore appears that the membrane elasticity modulus of nuclear membranes is very small meaning that membrane undulations are very much favored. Figures seem to indicate about 2 orders of magnitude more elastic membranes compared to plasma-like membranes. Of course, this conclusion must be taken with care as we hypothesized a similar magnetic susceptibility for nuclear lipid membranes and egg lecithin membranes. However, the difference in elasticity is so elevated that it cannot be compensated by large variations in $\Delta\chi$.

The most striking result of our study is the finding of very fluid and highly deformable nuclear lipid membrane. To our knowledge this is the first time that such measurements of physical parameters have been made. We believe that their special lipid composition, PC lipids, charged lipids, including PI lipids, cholesterol and a high concentration of chain unsaturation is at the origin of such phenomena. The elasticity of lipid nuclear membranes is much more important than that usually reported for plasma lipid membranes. This indicates that the nuclear lipid membrane bears this intrinsic property that would lead to large membrane fluctuations (undulations, hydrodynamic deformations, etc.), in the absence of membrane proteins and lamina proteins present in the nucleus. The time scale that is usually reported for large scale membrane undulations ranges from milliseconds to several seconds. Our results can be linked with the fact that NE has to promote fusion events and/or nuclear invaginations. Even if these results are based on natural membrane lipids without proteins we may conjecture that a such lipid composition is one of the requirements to promote the formation of nuclear invaginations, that is to say, the lipid matrix has the intrinsic property to deform almost at will. Of course, such a dynamic membrane has to be bound to other proteins to prevent unwanted undulations; invaginations would be the result of lipid membrane plasticity and special protein anchoring. Although, nuclear invagination functions are still under investigation, there

is primarily evidence of their involvement in calcium signaling, gene expression and transport [47-50]. Furthermore, it has been shown that lipid synthesis and modification enzymes occurs within nuclei, together with independent nuclear phosphoinositide and diacylglycerol pools, [47-50]. In addition, it has been reported that the morphology of nuclear invaginations can change on a timescale of 5 minutes [51], a time scale that is close to that observed for hydrodynamics modes for membrane undulations reported herein. Such a dynamic structure suggests that its formation is regulated and that the mechanisms of regulation could be linked to nuclear invaginations function and composition. From our results, we postulate that the lipid composition of the nuclear envelope is involved in the formation of such substructures. It has also been reported that in some pathologies nuclear invaginations morphology is altered suggesting that nuclear invaginations are susceptible to be pathologically dysregulated. By extension we may postulate that the dysregulation of the lipid composition could lead to abnormal membrane structure and could be involved in various pathologies.

MATERIALS & METHODS

Chemicals. Cell culture reagent, Dulbecco's Modified Eagle's Medium (DMEM), Foetal Bovine Serum (FBS) and Streptomycin/Penicillin were purchased from Invitrogen, (Carlsbad, CA. USA). $^2H_{31}$ palmitoyl, 2-oleoyl-*sn*-glycero-3-phosphocholine (POPC-$^2H_{31}$) was purchased from Avanti Polar Lipids (Birmingham, AL. USA). These starting materials were used without further purification. Deuterium-depleted water was obtained from Eurisotop (Saint Aubin, France) and solvents for liposome preparation (chloroform, methanol and ethanol) were obtained from Sigma Aldrich Chemicals (Saint Quentin Fallavier,

France).

Human Nuclear Membranes Purification Nuclei purification without use of detergent was performed following a protocol that we optimized from Blobel & Potter [16]. Details will be published elsewhere. Typically, human Embryonic Kidney (HEK) 293T cells were grown on tissue culture dishes in DMEM supplemented with FBS and Streptomycin/Penicillin). After harvesting by trypsinization, cells were incubated in a hypotonic buffer and then lysed by nitrogen cavitation in a cell disruption bomb (Parr Instrument Company, Il. USA). This method prevents alteration of membrane lipid composition as could happen using a classical detergent protocol. Nuclei were purified with a sucrose gradient. Nuclei were further labelled with $DiOC_6$ (1 µM) and Hoechst 33343 (1.6 µM) and observed by confocal fluorescence microscopy to assess the efficiency of nuclei isolation.

Fluorescence imaging microscopy.

Cells and nuclei were placed on polylysine-coated MatTek dishes. (Cultureware, Ashland, MA. USA) and visualized under an inverted confocal microscope with a high-efficiency spectral detector (Leica TCS SP5; Leica Microsystems, Manheim, Germany). A 63-fold glycerol immersion, N.A. 1.3 objective was used, and the images were collected and analyzed with the LAS AF software (Leica Microsystems, Manheim, Germany). $DiOC_6$ was excited at 488 nm using an argon laser and its emission was collected in the 504-661 nm range. Hoechst was excited at 405 nm using a pulsed diode laser and its emission was collected in the 283-436 nm range. All experiments were performed at room temperature (*ca.* 20°C).

Lipid extraction. Lipids were extracted from nuclei samples using a modified Folch extraction [31]. Nuclei were added to 4 mL of acidified chloroform:methanol (2.5:1), sonicated and filtered. After addition of 0.2 volumes of K_4EDTA (0.2 M, pH 6), samples were centrifuged at 800 g. The lower phase was retained and dried down completely at 55°C, under nitrogen gaz. Phospholipid concentration was determined by a Fiske assay resulting in an indirect measurement of inorganic phosphates released from extracted lipids [51]. Phospholipid characterization and quantification were provided by liquid-state ^{31}P NMR as described below.

Sample preparation for liquid-state NMR. 4 mg of lipid extract dried under N_2 were resuspended in milliQ (Millipore, Billerica, MA) filtered water, flash-frozen with liquid N_2 and lyophilized overnight. The fluffy powder was dissolved into 450 µL of $MeOD/CDCl_3$ (1:2). 30 µL of EDTA 0.2 M/D_2O pH 6 was added to chelate residual paramagnetic ions [52]. The lipid extract solution (450 µL) was poured into a 5-mm diameter glass tube (Cortecnet, Voisins Le Bretonneux, France) together with a sealed 1 mm reference tube

containing 50 µL of MeOD/CDCl$_3$ (1:2) with 2 µmol of the internal standard TPP (Triphenylphosphate) for proton (^{1}H) and Phosphorus-31(^{31}P) NMR quantification.

Sample Preparation for solid-state NMR. 0.8 mg of POPC-^{2}H$_{31}$ were dissolved into 80 µL of MeOH/CHCl$_3$ (1:2) and added to 8 mg of nuclear lipid extract (molar ratio of ca. 1:10). The solvent was evaporated under a nitrogen gas flux. The residual lipid film was dispersed in 1 ml milliQ filtered water and lyophilized overnight. The resulting fluffy powder was suspended into 80 µL of a 10 mM HEPES buffer (5 mM MgCl$_2$, pH 7.2, made with deuterium-depleted water) to obtain a hydration, h, of 90% (h = mass of water over the total mass of the system (phospholipids plus water)). After shaking into a vortex mixer samples were frozen in liquid nitrogen for 30 s, heated at 40 °C for 10 min in a water bath and shaken again for better sample homogeneity; this freeze-thaw-shaking cycle was repeated 3 times and the resulting milky dispersion transferred into a 4 mm diameter Zirconium rotor (80 µL, (Cortecnet, Voisins Le Bretonneux, France).

NMR spectroscopy. Liquid-state ^{1}H- ^{13}C- and ^{31}P-NMR experiments were carried out on a Bruker Avance III-HD 400 MHz SB spectrometer (Wissembourg, France) equipped with a 5mm broadband SmartProbe at 25°C. ^{31}P-NMR spectra were acquired at 161.98 MHz by using a one-pulse sequence with proton decoupling (π/2 pulse width of 8 µs, recycling delay of 10 s, acquisition time of 4s, spectral window of 54 ppm and between 80 and 1024 summed aquisitions). ^{1}H-NMR spectra were acquired at 400.13 MHz using a single pulse sequence (π/2 pulse width of 10µs, recycling delay of 2s, acquisition time of 2s, spectral window of 20 ppm and 48 scans). Two-dimensional experiments were performed at 400.13 MHz using a HSQC-TOCSY 2D-sequence [53] used to identify/assign chemical shifts for various phospholipids. The ^{1}H-^{31}P HSQC-TOCSY 2D-map was obtained with transfer delays corresponding to a 7 Hz proton-phosphorus coupling constant and an additional 50 ms DIPSI mixing period for protons after the HSQC step. The other parameters were a recycle delay of 2s, ^{1}H and ^{31}P 90 π/2 pulse widths of respectively 10 and 8µs, acquisition time of 0.3s, 48 scans, 9 and 10 ppm spectral widths in proton and phosphorus dimensions, respectively, 2K data points for the F2 dimension and 176 data points for the F1 dimension. The ^{1}H-^{13}C HSQC (Heteronuclear Single-Quantum Correlation) experiment allows to obtain a 2D heteronuclear chemical shift correlation map between directly-bonded ^{1}H and ^{13}C. The polarization transfers are obtained via INEPT blocks and proton-carbon coupling constant of 145 Hz was used. The other parameters were a recycle delay of 1.5s, ^{1}H and ^{13}C 90 π/2 pulse widths of respectively 10µs for both, acquisition time of 0.14s, 24 scans, 18 and 165 ppm spectral widths in proton and carbon dimensions, respectively, 2K data points for the F2 dimension and 256 data points for the F1 dimension. Solid-state ^{31}P and ^{2}H NMR were performed on a

Bruker Avance III 800 MHz SB spectrometer (Wissembourg, France) equipped with a dual H/X 4-mm MAS probe. ^{31}P-NMR spectra were acquired at 323.96 MHz by using a proton decoupled Hahn-echo pulse sequence [54]. Typical acquisition parameters were as follows: spectral window of 200 kHz, $\pi/2$ pulse width of 5.4 µs, interpulse delay of 40 µs and recycle delay of 5 s. Typically 5k scans were accumulated. Phosphorus chemicals shifts were calibrated relative to H_3PO_4 (85% in H_2O, 0 ppm). Magic angle sample spinning (MAS) was accomplished on some samples, a spinning rate of 1.4 kHz was applied and the [1]H-decoupling-one-pulse sequence used with the following parameters: [31]P $\pi/2$ pulse width of 5.4 µs, recycling delay of 5 s, acquisition time of 40.9 ms, spectral window of 100 kHz and 100 scans, proton decoupling at 10W power. ^{2}H-NMR spectra were acquired at 122.82 MHz by means of a quadrupolar echo pulse sequence [55], with a spectral width of 500 kHz, a $\pi/2$ pulse width of 4.5 µs, a 40 µs interpulse delay and a recycle delay of 2 s. Typically, 10-50 k scans were recorded depending on temperature. The reference for solid-state deuterium powder patterns was set to zero and the position of the carrier arbitrarily placed in the middle of the symmetric pattern. A Lorentzian noise filtering of 100-500 Hz was applied prior Fourier transformation from the top of the echo signal. Quadrature detection was used in all cases. Samples were allowed to equilibrate at least 30 min at a given temperature before the NMR signal was acquired.

Optical microscopy and size of liposomes. POPC and reconstituted nuclear membrane vesicles were added in an 8-wells plate (Lab-Tek[TM], Nalc Nunc International) diluted 3-fold in order to be observed by microscopy. Liposomes were let settle down for 24h ensuring that all liposomes were in the same focal plane. DIC (Differential Interference Contrast) and Epifluoresence imaging were processed using an IX81 (Olympus) microscope. For Epifluorescence imaging, liposomes were stained by the dye FM 1-43 (N-(3-Triethylammoniumpropyl)-4-(4-(Dibutylamino) Styryl) Pyridinium Dibromide) diluted one hundred times. Particle size analysis was performed with the Image J software [56] from DIC images obtained with a 60 fold oil objective. A size histogram was constructed based on 4 DIC images containing a total of 3000-3600 objects. A gauss function was used within the Origin Pro 9 Software (OriginLab, Northampton, MA) in order to obtain the mean diameter of vesicles. Mean diameters are 0.9±0.4 µm for reconstituted nuclear membrane vesicles and of 1.0 ±0.4 µm POPC vesicles (supplementary Fig. 4).

NMR data treatment and spectral simulations.

Liquid state ^{1}H-, ^{13}C- and ^{31}P-NMR spectra were processed using the Bruker TopSpin software. All peaks in 1D-^{31}P NMR spectra were integrated and converted into molar quantities by comparison with the internal standard triphenylphosphate (TPP), and the whole spectrum was integrated to obtain the total quantity of Phospholipids (see supplementary Fig. 1). The quantity of each of the phosphorus-containing lipid species

was determined by simulating ³¹P liquid-state NMR spectra with the DMFIT software [57]. 2D-NMR maps were used as phospholipid finger prints to confirm their chemical shift assignment. Identification was based on head group ¹H-³¹P cross peaks according to literature [57]. For wide-line solid-state NMR, spectral moments allow to quantitate spectral changes as function of temperature and were calculated according to Dufourc [23] and Davis [20] using a FORTRAN code developed by Erick Dufourc and implemented in a user-friendly routine, NMRFriend, by Sébastien Buchoux [58]. Wide-line solid-state NMR spectra were simulated by calculation in the time domain (as free induction decays) and then Fourier transformed. Individual components are built from experimental estimates of chemical shielding anisotropies ($\Delta\sigma$) or quadrupolar splittings ($\Delta\nu_Q$), isotropic chemical shifts and individual line-widths (line-width is considered constant throughout the pattern). Small variations are allowed to match with sharp experimental features on spectra. For lipids containing perdeuterated chains, weights for individual C^2H_2 or C^2H_3 depend on the number of deuterons per labelled carbon position; the individual time dependent signals are then added accordingly leading after Fourier transformation to the multicomponent spectrum. Such a simulation leads to individual quadrupolar splittings, $\Delta\nu_Q^k$, for labelled carbon positions, k, and subsequently to S^{CD} order parameters in bilayer membranes [20]: $S_k^{CD} = 4\Delta\nu_Q^k/3A_Q$. Order Parameters can be used to calculate the average length of a lipid molecule in terms of a sum of chain, glycerol backbone and head-group average lengths [26]: $\langle L_{lipid} \rangle = \langle L_{chain} \rangle + \langle L_{gly} \rangle + \langle L_{head} \rangle$ (See supplementary information, Table 1). Liposome deformation leading to non-spherical distributions of bilayer normals with respect to the magnetic field was taken into account by introducing in the simulation the ellipsoidal orientation dependence, $p(\theta) \sim \dfrac{sin^2\theta}{sin^2\theta + \frac{c}{a}cos^2\theta}$, where θ is the orientation of bilayer normal with respect to the magnetic field direction and *c* and *a* the ellipsoid axes [27,28]. The simulation program for wide line spectra has been developed in FORTRAN code by Erick Dufourc and implemented in a user-friendly graphical interface (Microsoft .NET) for Windows platforms by Arnaud Grélard. The program is available on demand.

References

1   Houben, F., Ramaekers, F. C. S., Snoeckx, L. & Broers, J. L. V. Role of nuclear lamina-cytoskeleton interactions in the maintenance of cellular strength. *Biochim. Biophys. Acta-Mol. Cell Res.* **1773**, 675-686, doi:10.1016/j.bbamcr.2006.09.018 (2007).

2   Fricker, M., Hollinshead, M., White, N. & Vaux, D. The convoluted nucleus. *Trends in cell biology* **7**, 181, doi:10.1016/s0962-8924(97)84084-6 (1997).

3   Fischer, A. H., Bardarov, S. & Jiang, Z. Molecular aspects of diagnostic nucleolar and nuclear envelope changes in prostate cancer. *J. Cell. Biochem.* **91**, 170-184, doi:10.1002/jcb.10735 (2004).

4   Fischer, A. H., Taysavang, P. & Jhiang, S. M. Nuclear envelope irregularity is induced by RET/PTC during interphase. *Am. J. Pathol.* **163**, 1091-1100, doi:10.1016/s0002-9440(10)63468-2 (2003).

5   Hu, S. H., Chen, J. X., Butler, J. P. & Wang, N. Prestress mediates force propagation into the nucleus. *Biochem. Biophys. Res. Commun.* **329**, 423-428, doi:10.1016/j.bbrc.2005.02.026 (2005).

6   Ji, J. Y. *et al.* Cell nuclei spin in the absence of lamin B1. *J. Biol. Chem.* **282**, 20015-20026, doi:10.1074/jbc.M611094200 (2007).

7   Gehrig, K., Lagace, T. A. & Ridgway, N. D. Oxysterol activation of phosphatidylcholine synthesis involves CTP:phosphocholine cytidylyltransferase alpha translocation to the nuclear envelope. *Biochem. J.* **418**, 209-217, doi:10.1042/bj20081923 (2009).

8   Larijani, B. & Poccia, D. L. in *Annual Review of Biophysics* Vol. 38 *Annual Review of Biophysics* 107-124 (Annual Reviews, 2009).

9   Domart, M. C. *et al.* Acute Manipulation of Diacylglycerol Reveals Roles in Nuclear Envelope Assembly & Endoplasmic Reticulum Morphology. *PLoS One* **7**, 14, doi:10.1371/journal.pone.0051150 (2012).

10   Garnier-Lhomme, M. *et al.* Nuclear Envelope Remnants: Fluid Membranes Enriched in STEROLS and Polyphosphoinositides. *PLoS One* **4**, 12, doi:10.1371/journal.pone.0004255 (2009).

11   Dufourc, E. J. Sterols and membrane dynamics. *Journal of chemical biology* **1**, 63-77, doi:10.1007/s12154-008-0010-6 (2008).

12   Gamier-Lhomme, M. *et al.* Probing the dynamics of intact cells and nuclear envelope precursor membrane vesicles by deuterium solid state NMR spectroscopy. *Biochim. Biophys. Acta-Biomembr.* **1768**, 2516-2527, doi:10.1016/j.bbamem.2007.06.004 (2007).

13   Uzureau, P. *et al.* Mechanism of Trypanosoma brucei gambiense resistance to human serum. *Nature* **501**, 430-+, doi:10.1038/nature12516 (2013).

14   Chamberlain, L. H. Detergents as tools for the purification and classification of lipid rafts. *FEBS Lett.* **559**, 1-5, doi:10.1016/s0014-5793(04)00050-x (2004).

15   Valtierra, F. X. S., Mateos, M. V., Aveldano, M. I. & Oresti, G. M. Sphingomyelins and ceramides with VLCPUFAs are excluded from low-density raft-like domains in differentiating spermatogenic cells. *J. Lipid Res.* **58**, 529-542, doi:10.1194/jlr.M072595 (2017).

16   Blobel, G. & Potter, V. R. Nuclei from Rat Liver - Isolation Method that Combines Purity with High Yield. *Science* **154**, 1662-&, doi:10.1126/science.154.3757.1662 (1966).

17   Estrada, R., Stolowich, N. & Yappert, M. C. Influence of temperature on P-31 NMR chemical shifts of phospholipids and their metabolites I. In chloroform-methanol-water. *Anal. Biochem.* **380**, 41-50, doi:10.1016/j.ab.2008.05.007 (2008).

18   Kaffarnik, S., Ehlers, I., Grobner, G., Schleucher, J. & Vetter, W. Two-Dimensional P-31,H-1 NMR Spectroscopic Profiling of Phospholipids in Cheese and Fish. *J. Agric. Food Chem.* **61**, 7061-7069, doi:10.1021/jf4021812 (2013).

19   Meneses, P. & Glonek, T. High-Resolution P-31 NMR of Extracted Phospholipids. *J. Lipid Res.* **29**, 679-689 (1988).

20   Davis, J. H. The Description of Membrane Lipid Conformation, Order and Dynamics by 2H-NMR. *Biochimica Et Biophysica Acta* **737**, 117-171, doi:10.1016/0304-4157(83)90015-1 (1983).

21   Douliez, J. P., Leonard, A. & Dufourc, E. J. Restatement of Order Parameters in Biomembranes - Calculation of C-C Bond Order Parameters from C-D Quadrupolar Splittings. *Biophys. J.* **68**, 1727-1739, doi:10.1016/s0006-3495(95)80350-4 (1995).

22   Seelig, J. Deuterium Magnetic-Resonance - Theory and Application to Lipid-Membranes. *Q. Rev. Biophys.* **10**, 353-418, doi:10.1017/s0033583500002948 (1977).

23   Beck, J. G., Mathieu, D., Loudet, C., Buchoux, S. & Dufourc, E. J. Plant sterols in "rafts": a better way to regulate membrane thermal shocks. *Faseb J.* **21**, 1714-1723, doi:10.1096/fj.06-7809com (2007).

24   Burnett, L. J. & Muller, B. H. Deuteron Quadrupole Coupling Constants in 3 Solid Deuterated Paraffin Hydrocarbons-C2D6, C4D10, C6D14. *J. Chem. Phys.* **55**, 5829-&, doi:10.1063/1.1675758 (1971).

25   Dufourc, E. J., Mayer, C., Stohrer, J., Althoff, G. & Kothe, G. Dynamics of Phosphate Head Groups in Biomembranes - Comprehensive Analysis Using P-31 Nuclear-Magnetic-Resonance Lineshape and Relaxation-Time Measurements. *Biophys. J.* **61**, 42-57, doi:10.1016/s0006-3495(92)81814-3 (1992).

26   Douliez, J. P., Leonard, A. & Dufourc, E. J. Conformational order of DMPC sn-1 versus sn-2 chains and membrane thickness: An approach to molecular protrusion by solid state H-2-NMR and neutron diffraction. *J. Phys. Chem.* **100**, 18450-18457, doi:10.1021/jp961220v (1996).

27   Pott, T. & Dufourc, E. J. Action of Melittin on the DPPC-Cholesterol Liquid-Ordered Phase - A Solid-State 2H-NMR and P-31-NMR Study. *Biophys. J.* **68**, 965-977, doi:10.1016/s0006-3495(95)80272-9 (1995).

28   Helfrich, W. Lipid Bilayer Spheres - Deformation and Birefringence in Magnetic-Fields. *Phys. Lett. A* **A 43**, 409-410, doi:10.1016/0375-9601(73)90396-4 (1973).

29   Israelachvili, J. N., Marcelja, S. & Horn, R. G. Physical Principles of Membrane Organization. *Q. Rev. Biophys.* **13**, 121-200, doi:10.1017/s0033583500001645 (1980).

30   Collas, P. & Poccia, D. Distinct egg membrane vesicles differing in binding and fusion properties contribute to sea urchin male pronuclear envelopes formed in vitro. *J. Cell Sci.* **109**, 1275-1283 (1996).

31   Larijani, B., Poccia, D. L. & Dickinson, L. C. Phospholipid identification and quantification of membrane vesicle subfractions by P-31-H-1 two-dimensional nuclear magnetic resonance. *Lipids* **35**, 1289-1297, doi:10.1007/s11745-000-0645-4 (2000).

32   Griffiths, G., Back, R. & Marsh, M. A Quantitative-Analysis of the Endocytic Pathway in Baby Hamster-Kidney Cells. *Journal of Cell Biology* **109**, 2703-2720, doi:10.1083/jcb.109.6.2703 (1989).

33   Zambrano, F., Fleischer, S. & Fleischer, B. Lipid-Composition of Golgi Apparatus of Rat-Kidney and Liver in Comparison with other Subcellular Organelles. *Biochimica Et Biophysica Acta* **380**, 357-369, doi:10.1016/0005-2760(75)90104-6 (1975).

34   Collas, P. & Poccia, D. Lipophilic organizing structures of sperm nuclei target membrane vesicle binding and are incorporated into the nuclear-envelope. *Developmental Biology* **169**, 123-135, doi:10.1006/dbio.1995.1132 (1995).

35   Watson, M. L. The Nuclear Envelope - Its Structure and Relation to Cytoplasmic Membranes. *Journal of Biophysical and Biochemical Cytology* **1**, 257-&, doi:10.1083/jcb.1.3.257 (1955).

36   Dufourc, E. J. The role of phytosterols in plant adaptation to temperature. *Plant signaling & behavior* **3**, 133-134, doi:10.4161/psb.3.2.5051 (2008).

37   Cullis, P. R. & Dekruyff, B. P-31 NMR-Studies of Unsonicated Aqueous Dispersions of Neutral And Acidic Phospholipids - Effects of Phase-Transitions, P2H and Divalent-Cations on Motion In Phosphate Region of Polar Headgroup. *Biochimica Et Biophysica Acta* **436**, 523-540, doi:10.1016/0005-2736(76)90438-7 (1976).

38   Chapman, D. Phase-Transitions and Fluidity Characteristics of Lipids and Cell-Membranes. *Q. Rev. Biophys.* **8**, 185-235, doi:10.1017/s0033583500001797 (1975).

39   Esfahani, M., Barnes, E. M. & Wakil, S. J. Control of Fatty Acid Composition in Phospholipids of Escherichia-Coli . Response to Fatty Acid Supplements in a Fatty Acid Auxotroph. *Proc. Natl. Acad. Sci. U. S. A.* **64**, 1057-&, doi:10.1073/pnas.64.3.1057 (1969).

40   Ulrih, N. P., Gmajner, D. & Raspor, P. Structural and physicochemical properties of polar lipids from thermophilic archaea. *Appl. Microbiol. Biotechnol.* **84**, 249-260, doi:10.1007/s00253-009-2102-9 (2009).

41   Diller, A. *et al.* Bicelles: A natural 'molecular goniometer' for structural, dynamical and topological studies of molecules in membranes. *Biochimie* **91**, 744-751, doi:10.1016/j.biochi.2009.02.003 (2009).

42   Prosser, R. S., Hwang, J. S. & Vold, R. R. Magnetically aligned phospholipid bilayers with positive ordering: A new model membrane system. *Biophys. J.* **74**, 2405-2418, doi:10.1016/s0006-3495(98)77949-4 (1998).

43   Raffard, G., Steinbruckner, S., Arnold, A., Davis, J. H. & Dufourc, E. J. Temperature-composition diagram of dimyristoylphosphatidylcholine-dicaproylphosphatidylcholine "bicelles" self-orienting

in the magnetic field. A solid state H-2 and P-31 NMR study. *Langmuir* **16**, 7655-7662, doi:10.1021/la000564g (2000).

44   Seelig, J., Borle, F. & Cross, T. A. Magnetic-Ordering of Phospholipid-Membranes. *Biochimica Et Biophysica Acta* **814**, 195-198, doi:10.1016/0005-2736(85)90437-7 (1985).

45   Boroske, E. & Helfrich, W. Magnetic-Anisotropy of Egg Lecithin Membranes. *Biophys. J.* **24**, 863-868, doi:10.1016/s0006-3495(78)85425-3 (1978).

46   Meleard, P. *et al.* Bending elasticities of model membranes: Influences of temperature and sterol content. *Biophys. J.* **72**, 2616-2629, doi:10.1016/s0006-3495(97)78905-7 (1997).

47   Bootman, M. D., Fearnley, C., Smyrnias, I., MacDonald, F. & Roderick, H. L. An update on nuclear calcium signalling. *J. Cell Sci.* **122**, 2337-2350, doi:10.1242/jcs.028100 (2009).

48   Lui, P. P. Y., Kong, S. K., Kwok, T. T. & Lee, C. Y. The nucleus of HeLa cell contains tubular structures for Ca2+ signalling. *Biochem. Biophys. Res. Commun.* **247**, 88-93, doi:10.1006/bbrc.1998.8649 (1998).

49   Malhas, A., Lee, C. F., Sanders, R., Saunders, N. J. & Vaux, D. J. Defects in lamin B1 expression or processing affect interphase chromosome position and gene expression. *Journal of Cell Biology* **176**, 593-603, doi:10.1083/jcb.200607054 (2007).

50   Paytubi, S. *et al.* ABC50 Promotes Translation Initiation in Mammalian Cells. *J. Biol. Chem.* **284**, 24061-24073, doi:10.1074/jbc.M109.031625 (2009).

51   Fiske, C. H. & Subbarow, Y. The colorimetric determination of phosphorus. *J. Biol. Chem.* **66**, 375-400 (1925).

52   Sotirhos, N., Herslof, B. & Kenne, L. Quantitative-Analysis of Phospholipids by P-31-NMR. *J. Lipid Res.* **27**, 386-392 (1986).

53   Bax, A. & Davis, D. G. MLEV-17-Based Two-Dimensional Homonuclear Magnetization Transfer Spectroscopy. *J. Magn. Reson.* **65**, 355-360, doi:10.1016/0022-2364(85)90018-6 (1985).

54   Rance, M. & Byrd, R. A. Obtaining High-Fidelity Spin-1/2 Powder Spectra in Anisotropic Media - Phase-Cycled Hahn Echo Spectroscopy. *J. Magn. Reson.* **52**, 221-240, doi:10.1016/0022-2364(83)90190-7 (1983).

55   Davis, J. H., Jeffrey, K. R., Bloom, M., Valic, M. I. & Higgs, T. P. Quadrupolar Echo Deuteron Magnetic-Resonance Spectroscopy in Ordered Hydrocarbon Chains. *Chem. Phys. Lett.* **42**, 390-394, doi:10.1016/0009-2614(76)80392-2 (1976).

56   Schindelin, J. *et al.* Fiji: an open-source platform for biological-image analysis. *Nat. Methods* **9**, 676-682, doi:10.1038/nmeth.2019 (2012).

57   Massiot, D. *et al.* Modelling one- and two-dimensional solid-state NMR spectra. *Magnetic Resonance in Chemistry* **40**, 70-76, doi:10.1002/mrc.984 (2002).

58   Buchoux, S. *et al.* Surfactin-triggered small vesicle formation of negatively charged membranes: A novel membrane-lysis mechanism. *Biophys. J.* **95**, 3840-3849, doi:10.1529/biophysj.107.128322 (2008).

I. Supplementary information: Unprecedented deformation of human Nuclear Envelopes in magnetic field: is membrane elasticity driving membrane invaginations?

Supplementary Information to the article

Unprecedented deformation of human Nuclear Envelopes in magnetic field: is membrane elasticity driving membrane invaginations?

Régine Dazzoni[1,2], Axelle Grelard[1], Estelle Morvan[3], Anthony Bouter[1], Christopher J. Applebee[2], Antoine Loquet[1], Banafshé Larijani[2*], Erick J. Dufourc[1*]

[1]Institute of Chemistry & Biology of Membranes & Nanoobjects, UMR5248, CNRS, Université Bordeaux, Institut National Polytechnique Bordeaux, F-33600 Pessac, France.

[2]Cell Biophysics Laboratory, Ikerbasque Basque Foundation for Science, Instituto Biofísika (CSIC, UPV/EHU) and Research Centre for Experimental Marine Biology and Biotechnology (PiE), University of the Basque Country (UPV/EHU), Spain

[3]Institut Européen de Chimie et Biologie , University of Bordeaux, INSERM, CNRS (UMS3033-US001), 2 rue Escarpit, Pessac 33600, France

* Correspondence should be addressed to Erick J. Dufourc (e.dufourc@cbmn.u-bordeaux.fr or erick.dufourc@cnrs-dir.fr), to Antoine Loquet (a.loquet@iecb.u-bordeaux.fr) or to Banafshé Larijani (banafshe.larijani@ikerbasque.org)

Contents
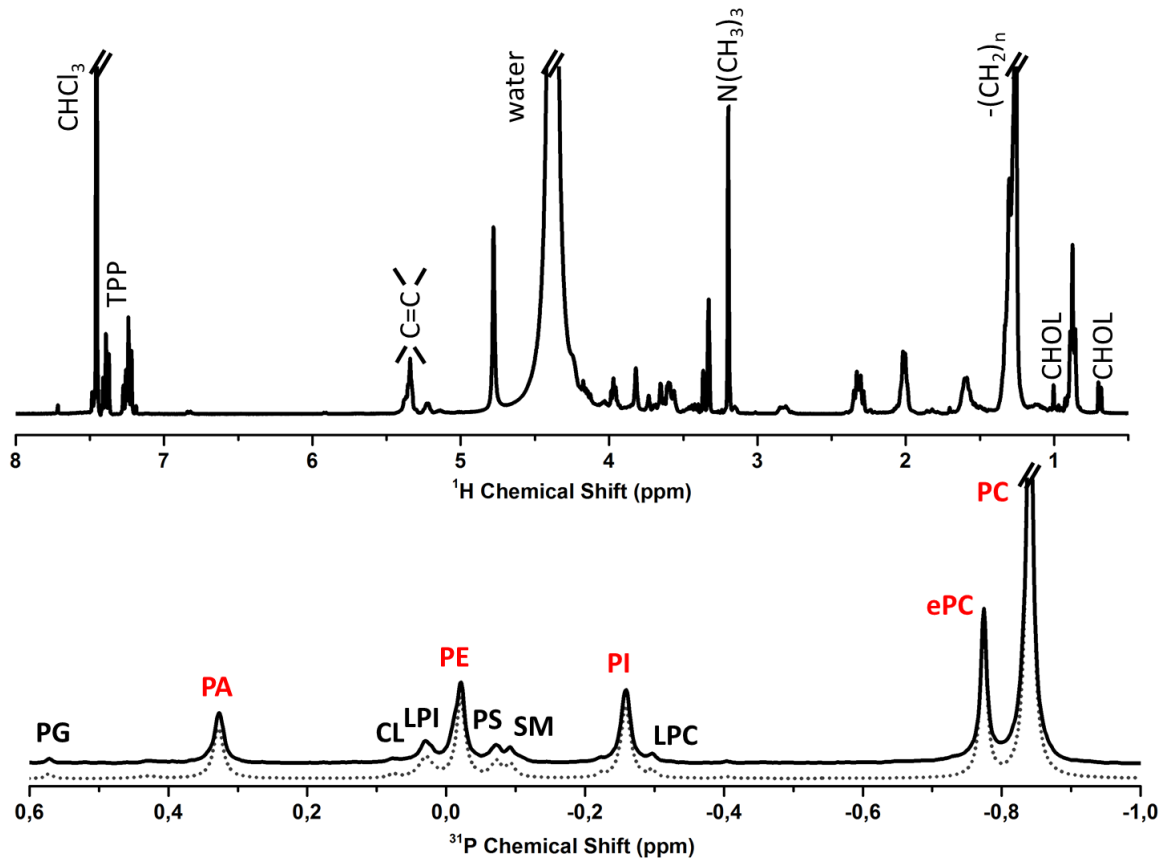
Supplementary Fig. 1. **NMR quantification of phospholipids in human nuclear membranes.** Liquid-state ^{31}P-NMR (bottom) & ^{1}H-NMR (top) spectra of human Nuclear Membrane Lipids corresponding to 4 mg of phospholipids dissolved in chloroform-methanol 2:1, 0.2M EDTA-D_2O, pH 6. Phospholipids assignments were based on ^{31}P chemical shift from Meneses & Glonek and Kaffarnic *et al.*[1,2], and also from ^{1}H-^{31}P 2D experiments (Fig. 2 below). TPP: triphenylphosphate (external reference) was used as a standard for chemical shift and concentration (see main text), PC: phosphatidylcholine, EPC: ether phosphatidylcholine, LPC: lysophosphatidylcholine, PI: phosphatidylinositol, LPI: lysophosphatidylinositol SM: sphingomyelin, PS: phosphatidylserine, PE: phosphatidylethanolamine, CL: cardiolipin, PA: phosphatitic acid, PG: phosphatidylglycerol. Red labels stand for secured assignment using 2D NMR and black labels represent assignments by comparison with literature. ^{31}P acquisition conditions: number of scans = 1024, recycling delay = 10s, Lorentzian filtering = 1 Hz. The dotted line below the experimental phosphorus spectrum represents the simulated spectrum using the DMFIT software [3]. Peak lineshape was approximated by a Gaussian line to account for experimental inhomogeneity (water dispersions). The area below each peak is reported in Table 1 of main text as a percentage of the total area. On the proton spectrum (top), labels stand for straightforward chain, chain unsaturation (5.3 and 5.4 ppm) and head group assignment using literature, CHOL labels highlights characteristic CH_3 resonances of cholesterol (further evidences for cholesterol resonances are see in the 2D spectrum of Fig. 3). Number of scans: 48 with a recycling delay of 2 s and a Lorentzian filtering of 0.3 Hz. Very intense peaks were cut in the vertical expansion to show details on lower intensity peaks.
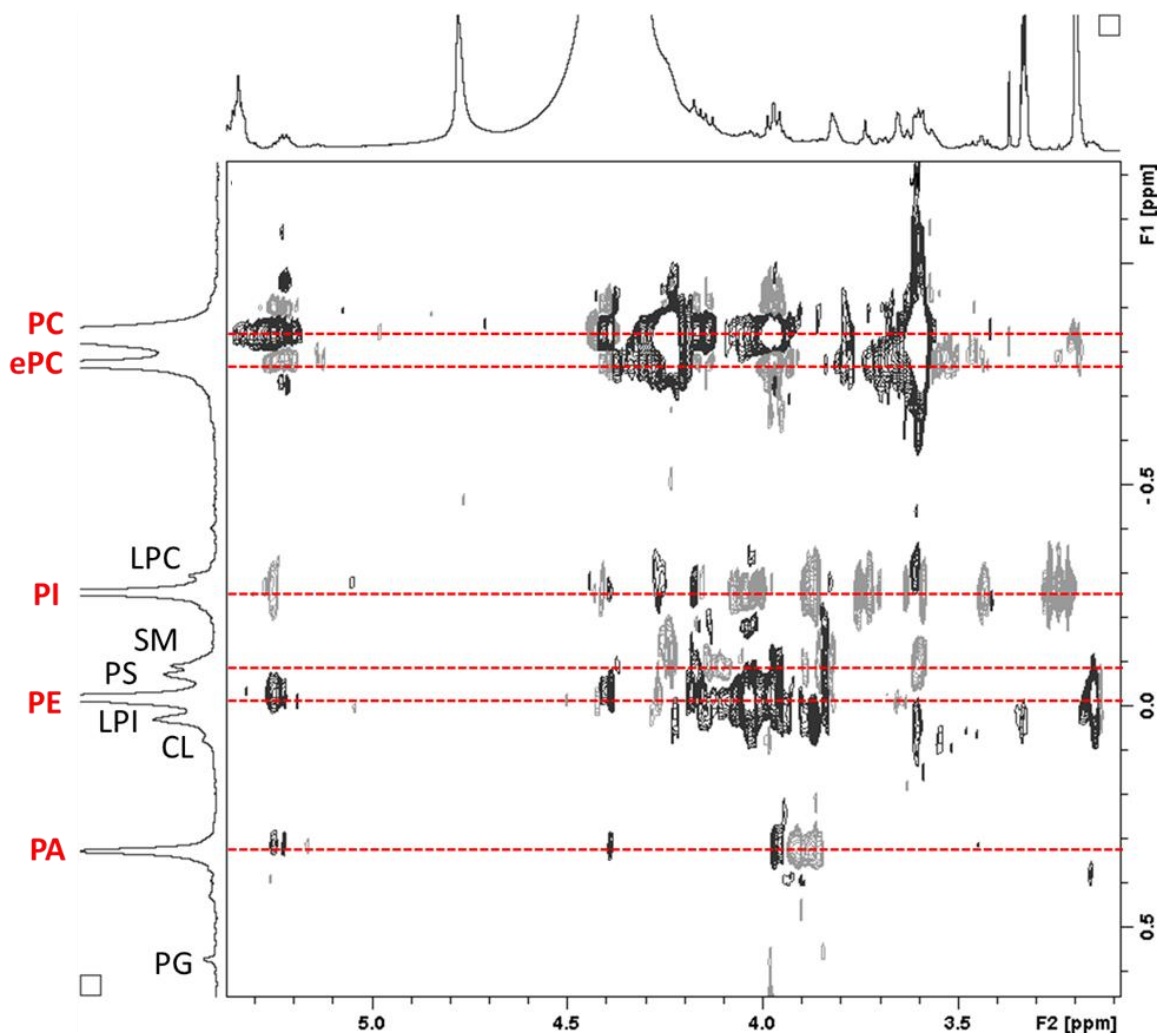
Supplementary Fig. 2. **Assignment of lipid species.** Liquid-state ^{1}H-^{31}P HSQC-TOCSY 2D map of Nuclear Membrane Lipids corresponding to 4 mg of phospholipids dissolved in chloroform-methanol 2:1, 0.2M EDTA-D$_2$O, pH 6. The transfer delay was adjusted to correspond to a 7 Hz average proton-phosphorus coupling constant. The other parameters were a recycle delay of 2s, ^{1}H and ^{31}P 90 $\pi/2$ pulse widths of respectively 10 and 8µs, acquisition time of 0.3s, 48 scans, 9 and 10 ppm spectral widths in proton and phosphorus dimensions, respectively, 2K data points for the F2 dimension and 176 data points for the F1 dimension.

PC: phosphatidylcholine, EPC: ether phosphatidylcholine, LPC: lysophosphatidylcholine, PI: phosphatidylinositol, LPI: lysophosphatidylinositol SM: sphingomyelin, PS: phosphatidylserine, PE: phosphatidylethanolamine, CL: cardiolipin, PA: phosphatitic acid, PG: phosphatidylglycerol. Red labels stand for secured assignment using this map and black labels represent assignments by comparison with literature [1,2,4,5].
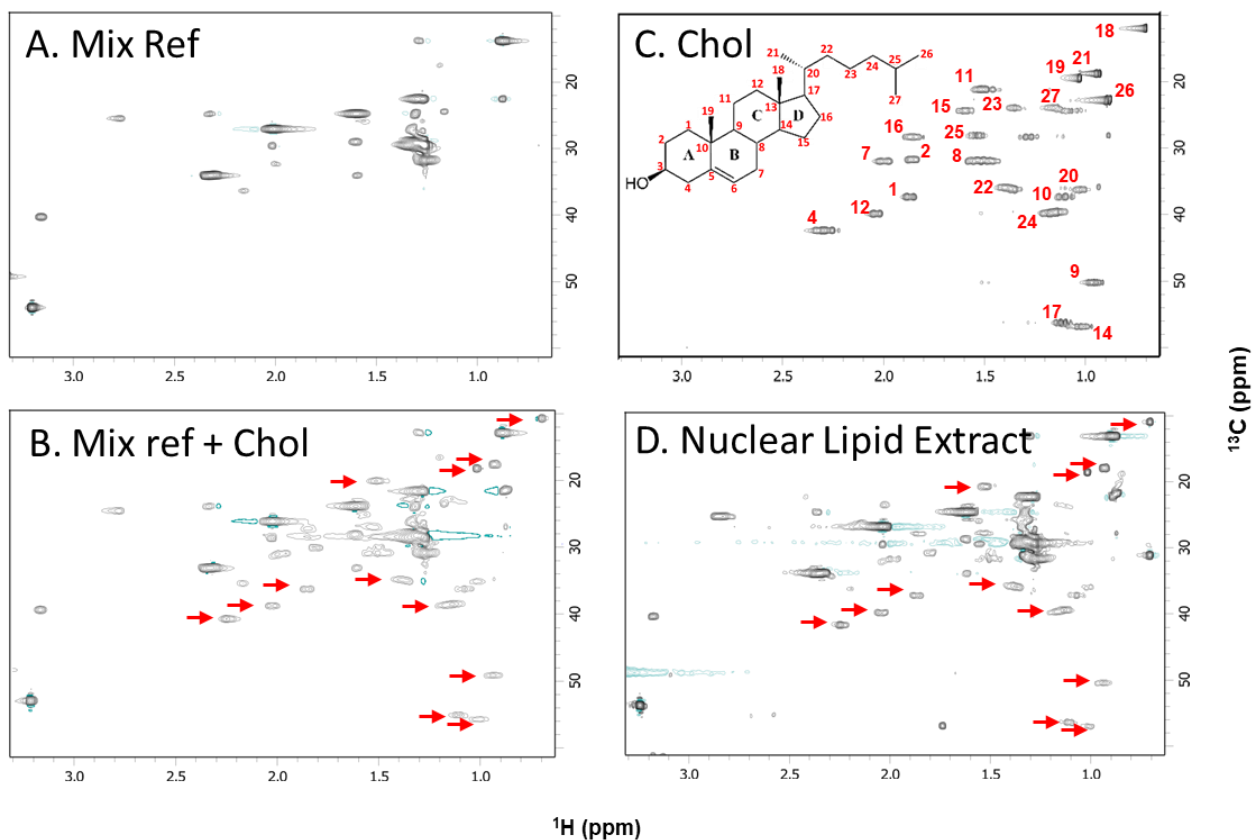
Supplementary Fig. 3: **Identification of cholesterol in the Nuclear Lipid Extract.**

A) ^{1}H-^{13}C HSQC 2D experiment of a mixture of phospholipid references (PG: 8 % mole, PA: 8 %, CL: 6 %, PE: 18 %, SM: 4 %, PS: 5 %, PI: 6 %, LPC: 4 %, PC: 41 %) dissolved in CDCl$_3$:CD$_3$OD. B) ^{1}H-^{13}C HSQC 2D experiment of the same mixture of phospholipid references with cholesterol (ca. 20% with respect to the total phospholipid amount). Red arrows highlight cholesterol resonances on comparing with Fig. 3C. C) ^{1}H-^{13}C HSQC 2D experiment on cholesterol dissolved in CDCl$_3$:CD$_3$OD; insert shows its chemical structure with carbon numbering; assignment of cholesterol ^{1}H-^{13}C correlations (numbers corresponding to carbons) was based on the SDBSweb[6] D) ^{1}H-^{13}C HSQC 2D experiment of 4 mg of the nuclear lipid extract. Red arrows highlight cholesterol resonances on comparing with Fig. 3C and 3B.

Acquisition parameters: The transfer delays were set to correspond to 145 Hz as an average for the proton-carbon coupling constant. The other parameters were a recycle delay of 1.5s, ^{1}H and ^{13}C 90 π/2 pulse widths of respectively 10µs for both, acquisition time of 0.14s, 16 to 96 scans depending on the concentration of each sample, 18 and 165 ppm spectral widths in proton and carbon dimensions, respectively, 2K data points for the F2 dimension and 256 data points for the F1 dimension.
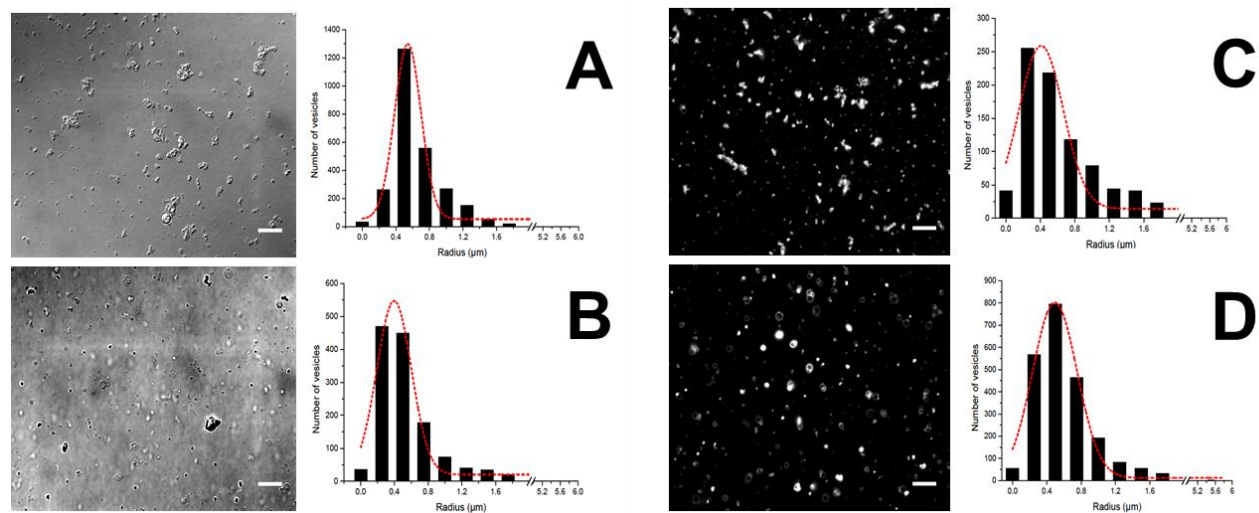
Supplementary Fig. 4. **Size determination for Nuclear Lipid Extract (NLE) Vesicles and POPC MLV**. POPC vesicles (A/C) and NLE vesicles (B/D) as used for solid state NMR experiments were diluted 1000 times in a HEPES buffer (10 mM, 5mM $MgCl_2$, pH7.2). Images were obtained by Differential Interference Contrast (DIC), (A/B), and epifluorescence, (C/D), microscopy with a magnification x 60 after staining vesicles with the FM1-43 probe (5ng/µL). Vesicles radii were obtained using the Image J software and size distributions are reported on the right-hand side of the corresponding image. A Gaussian fitting (dotted red line) was performed using OriginPro Software. 3000 and 3600 vesicles were respectively analysed for POPC and NLE respectively; mean diameters are 0.9±0.4 µm for NLE vesicles and of 1.0 ±0.4 µm for POPC vesicles.
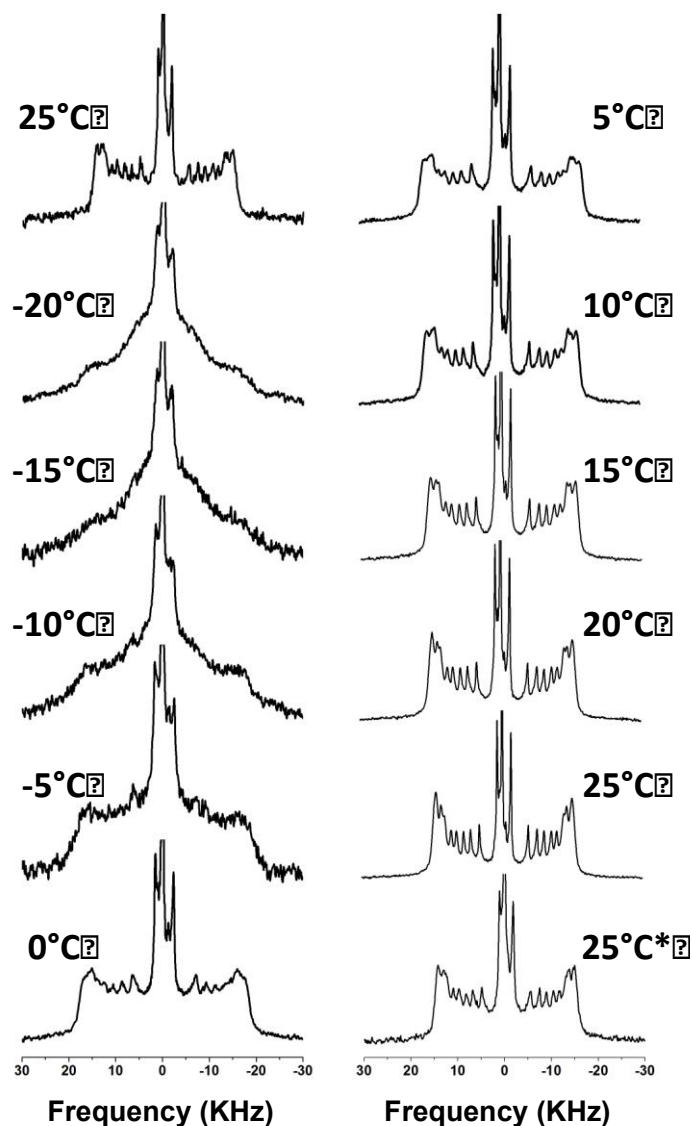
Supplementary Fig. 5. **Thermal variation of deuterium solid-state NMR spectra.** ^{2}H-NMR spectra of reconstituted nuclear lipid membrane extracts (NLE) vesicles doped with 10% deuterated POPC during a thermal variation (25°C down to -20°C and back, from left top to right bottom) and recorded after temperature stabilization. Spectra were obtained after Fourier transformation of solid-echo type experiments accumulated for 10 to 50 k transients, Lorentzian line filtering of 100 to 500 Hz. Details for experimental parameters and data treatment are found in the methods section. The lower right spectrum (asterisk) was obtained after spinning the sample at the magic angle (1.4 kHz) and let the system stabilize at 25°C after stopping MAS.

25°C   25°C

-20°C $\beta_m = 54.7°$

-10°C   25°C*

0°C

60   40   20   0   -20   -40   -60
Frequency (KHz)

60   40   20   0   -20   -40   -60
Frequency (KHz)
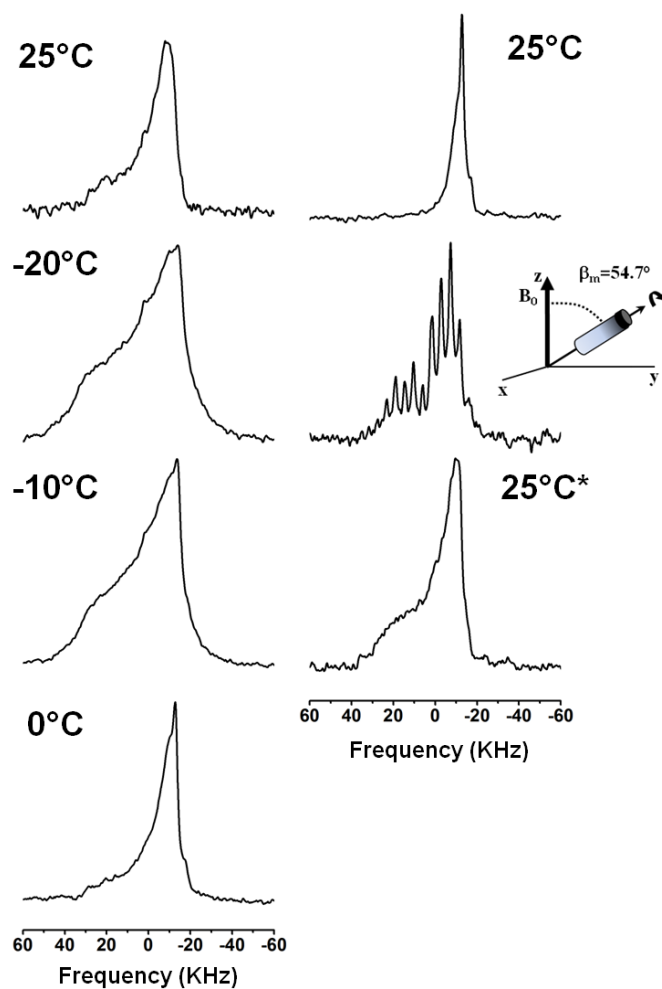
Supplementary Fig. 6. **Thermal variation of ^{31}P-NMR spectra.** ^{31}P-NMR spectra of reconstituted nuclear lipid membrane extracts (NLE) during a thermal variation (25°C down to -20°C and back, from left top to right top) and recorded after temperature stabilization. Spectra were obtained after Fourier transformation of Hahn-echo type experiments accumulated for 0.3 to 7k transients, Lorentzian line filtering of 300 Hz. Details for experimental parameters and data treatment are found in the methods section. Middle spectrum on right column was acquired at 25°C under magic angle sample spinning at 1.4 kHz and shows a spinning side band pattern picturing the "powder-like" pattern (*i.e.*, destruction of magnetic alignment as seen on the above spectrum). The insert aside the spectrum depicts the MAS set up, the rotor spinning at an angle of 54.7° with respect to the magnetic field. The lower right spectrum (asterisk) was obtained after spinning the sample at the magic angle (1.4 kHz) and let the system stabilize at 25°C after stopping MAS.

Supplementary Table 1. **Chain order parameters from ^{2}H-NMR spectra**. Experimental quadrupolar splittings, order parameters and bilayer thickness calculation for NLE containing ^{2}H$_{31}$-POPC and for pure ^{2}H$_{31}$-POPC liposomes, at 25°C.

#C	NLE			POPC		
	$\Delta\nu_Q{}^a$	$S_{CD}{}^b$	$S_{CC}{}^c$	$\Delta\nu_Q{}^a$	$S_{CD}{}^b$	$S_{CC}{}^c$
2	29.60	-0.236	0.230	25.60	-0.204	0.195
3	29.60	-0.236	0.242	25.60	-0.204	0.213
4	29.60	-0.236	0.230	25.60	-0.204	0.195
5	29.60	-0.236	0.242	25.60	-0.204	0.213
6	29.60	-0.236	0.230	25.60	-0.204	0.195
7	29.60	-0.236	0.242	25.60	-0.204	0.213
8	27.10	-0.216	0.230	22.65	-0.180	0.195
9	27.10	-0.216	0.201	22.65	-0.180	0.166
10	25.45	-0.203	0.230	21.30	-0.170	0.195
11	22.75	-0.181	0.175	18.90	-0.151	0.145
12	20.50	-0.163	0.187	16.95	-0.135	0.156
13	17.50	-0.139	0.139	14.55	-0.116	0.114
14	14.50	-0.116	0.140	12.25	-0.098	0.118
15	10.70	-0.085	0.091	9.15	-0.073	0.077
16	3.05	-0.024	0.079	2.65	-0.021	0.069
$S_{mol}{}^d$	0.75			0.7		
$L_{chain}{}^e$	13.7			13.0		
b^f	44.2			42.8		

^{a}Obtained from spectral simulations of figure 2A of main text and represents the splitting for orientations of bilayer normals at 90° to the magnetic field, accuracy is better than 0.5 %. Assignment was based on literature [7,8]. Positions 2-9 could not be separated.

^{b}Calculated from $\Delta\nu_Q$ using the equation $\Delta\nu_Q^k = \frac{3}{4}A_Q S_{CD}^k$ from [9] with $A_Q = 167$ kHz [10]. Accuracy is 0.5 %.

$^{\text{c}}$Calculated from S_k^{CD} using the recurrent equation[11]: $2S_k^{CD} = -(S_k^{CC} + S_{k+1}^{CC})$, accuracy is 0.5%. S_{16}^{CC} is obtained using the C3 symmetry around the C_{16}-C_{15} bond: $S_{16}^{CC} = S_{16}^{CD}/(\frac{3cos^2 111° - 1}{2}))$

$^{\text{d}}S_{mol}$, the molecular order parameter was obtained from ^{7,8} for DMPC and DMPC + 30% cholesterol. Value for NLE were extrapolated by considering a maximum of 10% cholesterol in the bilayer.

$^{\text{c}}L_{chain}$ was calculated from ^{7,8}. $\langle L_{chain} \rangle = \frac{1+\sqrt{1+8S_{mol}}}{4}\left[\langle l_{C_n - H}\rangle + 1.25 \sum_{k=2}^{n}\left(\frac{1}{2} + \frac{S_k^{CC}}{S_{mol}}\right)\right]$, where $\langle l_{C_n - H}\rangle$ was the contribution of the methyl terminus (0.81 Å).

$^{\text{f}}$Under the assumption ^{7,8} that there were no lipid interdigitation, the bilayer thickness was obtained by summing two tail-to-tail molecular lengths: $b = 2\langle L_{lipid}\rangle$, where $\langle L_{lipid}\rangle = \langle L_{chain}\rangle + \langle L_{gly}\rangle + \langle L_{head}\rangle$. $\langle L_{lipid}\rangle = \langle L_{chain}\rangle + \langle L_{gly}\rangle + \langle L_{head}\rangle$. $\langle L_{head}\rangle + \langle L_{gly}\rangle = 8.4$ Å was obtained by combining neutron diffraction data for the lipid length, 21.8Å, and NMR data for the chain length, 13.4 Å, calculated for DPPC in the fluid phase. Accuracy for L_{chain} is ± 0.4Å. Accuracy for b is estimated to be ±1Å.

Supplementary Table 2. **Simulations of ^{31}P-NMR spectra.** Experimental chemical shielding anisotropies and deformation parameters were obtained from simulation of ^{31}P-NMR spectra, at 25°C.

	NLE			POPC			
	$\Delta\sigma^{a}$		weight[b]	$\Delta\sigma^{a}$		weight[b]	$\Delta\sigma^{c}$
Assignment[d]	kHz	ppm	%	kHz	ppm		ppm
PI	15.6	-48.3	11±3				-61
PS	14.6	-45.2	1±3				-50
PC	11.5	-35.7	66±3	15.00	-46.4	100	-47
PE	8.8	-27.3	12±3				-43
PA	7.2	-22.3	9±3				-50
CL	5.4	-16.7	1±3				-33
c/a^{e}	3.0			1.0			

[a]Chemical Shielding anisotropy, $\Delta\sigma = \sigma_{//} - \sigma_{\perp}$, acquired at a Larmor frequency of 323 MHz, accuracy ±1%.

[b]Weigth of each pattern, accuracy ± 3%

[c]Literature values from isolated species: PC, PE, CL values at 50°C from Shin [12], PS value at 30°C from Tilcock & Cullis [13], PA value at 5°C, pH 7 from Cullis [14], PI value at 10°C from Zhendre [15]. It has been shown that the presence of PI and cholesterol promotes a decrease in the chemical shielding anisotropies of phospholipids [16,17]

[d]Tentative assignment using literature values and Table 1 of main text.

[e]Anisotropy ratio (c = long axis, a = short axis) defining the prolate ellipsoid, accuracy ±0.2

Theory of magnetically induced liposome deformation

Following the Helfrich theory [18,19] one may describe the magnetically induced deformation of membrane bilayer spheres of initial radius r_0 (at equilibrium, outside magnetic field) to ellipsoids of revolution of semi-long and semi-short axes c and a, respectively, as the combined effects of both the magnetic energy and the membrane elastic energy.
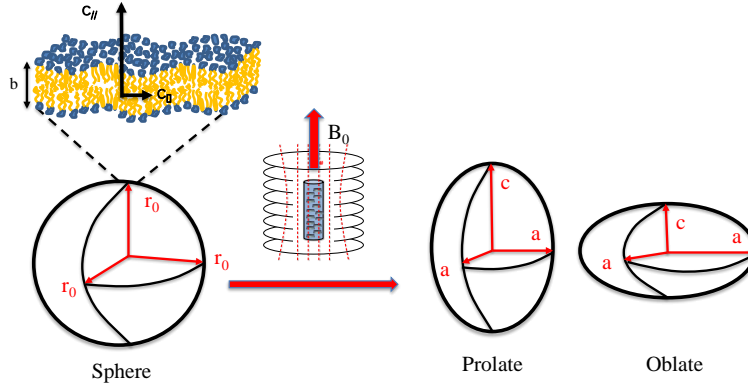
Scheme S1. **Bilayer spheres of radius r_0 (µm) deform into ellipsoids of revolution upon magnetic field action**. c and a are the semi-long and semi-short axes, respectively (expressed in µm). The bilayer thickness is denoted b (nm) and the magnetic field B_0 (T). $\chi_\parallel$ and $\chi_\perp$ are the magnetic susceptibilities for magnetic field normal (parallel) and tangential (perpendicular) to the bilayer plane.

The deformation happens when the membrane curvature-elastic energy, E_C, is smaller than the orientation energy in the magnetic field, E_H [18,19]:

$$E_C = \pi k_C \left[2(2 - r_0 c_0)^2) + \frac{\frac{9}{4}(c-a)^2}{r_0^2} \left(\frac{48}{5} - \frac{8(r_0 c_0)}{5} \right) \right]$$

$$E_H = -\pi \Delta\chi b \frac{B_0^2}{\mu_0} \left[\left(\frac{2}{3} r_0^2 - \frac{8 r_0 (c-a)}{5} \right) \right]$$

Where k_C is the membrane curvature-elastic modulus (in J), B_0 the magnetic field induction (in T) and $\Delta\chi = \chi_\parallel - \chi_\perp$, the anisotropy of the magnetic susceptibility of molecules in the membrane. Minimization in energy leads to deformation into an ellipsoid expressed as (SI System):

$$c - a \approx -f \frac{r_0^3 \Delta\chi b B_0^2}{\mu_0 k_C}$$

146

Where $f = 1/18$ for symmetric bilayers ($c_0 = 0$) and μ_0 is the vacuum permeability $= 4\pi\times10^{-7}$ (in N/A^2 or kg.m.s^{-2}.A^{-2}).

As the anisotropy ratio *c/a* can easily be obtained from NMR simulations (*vide supra*) and by considering that there is no significant variation of the liposome volume under deformation (*i.e.*, fusion between liposomes promoted by the magnetic field is limited to a few percent) one may write $r_0^3 \approx a^2c$ and hence $a \approx \left(r_0^3\frac{a}{c}\right)^{1/3}$ and $c \approx \left(r_0^3\frac{c^2}{a^2}\right)^{1/3}$. The average elasticity modulus k_C may then be calculated:

$k_C \approx -f\frac{r_0^3\Delta\chi bB_0^2}{\mu_0(c-a)}$. In the case of liposomes with *n* lamellae the calculated elasticity modulus translates into $k_C^{lip} = nk_C$ [20].

Annihilation of magnetic deformation by magic angle sample spinning.

The deformation of initially spherical liposomes by magnetic field is obtained because the magnetic energy[18]:

$$E_H = -\pi\Delta\chi b \frac{B_0^2}{\mu_0}\left[\left(\frac{2}{3}r_0^2 - \frac{8r_0(c-a)}{5}\right)\right]$$

$\Delta\chi$: anisotropy of magnetic susceptibility

b: bilayer thickness

B_0: magnetic field intensity

μ_0: vacuum permeability

r_0: radius of initial spherical liposomes

c-a: difference of ellipsoid long and short axes

is slightly greater than the membrane curvature elastic energy:

$$E_C = \pi k_C\left[2(2-r_0c_0)^2) + \frac{\frac{9}{4}(c-a)^2}{r_0^2}\left(\frac{48}{5} - \frac{8(r_0c_0)}{5}\right)\right]$$

r_0: radius of initial spherical liposomes

k_C: elastic modulus

c-a: difference of ellipsoid long and short axes

c_0: membrane curvature at rest, for symmetric bilayers ($c_0 = 0$) and for asymmetric bilayers ($c_0 = 2/r_0$).

Both energies are computed to be in the range **10^{-18}-10^{-19} J** per liposome.

When spinning the sample at a rate of 1.4 kHz and subsequently recording an NMR spectrum, the deformation is cancelled. Let us compute the mechanic energy provided by the spinning speed.

The Mechanical Energy or Kinetic Angular Energy can be written as:

$$E_K = \frac{1}{2}I\omega^2 = \frac{1}{4}mr_{cyl}^2(2\pi v_r)^2$$

I : moment of inertia

m : mass of sample ($m=\rho V$)

ρ : sample density (1030 kg.m^{-3})

V = sample volume (100 μL)

r_{cyl}: cylindrical NMR rotor inner radius (1.5 mm)

v_r : spinning speed (1400 Hz

One computes $E_K = 4.5 \ 10^{-3}$ J, which is the kinetic angular energy for N liposomes, N_{MLV}, inside the sample. Let us now compute the number of liposomes, N_{MLV}:

$$N_{MLV} = n_{mol}^{sample}/n_{mol}^{MLV}$$

n_{mol}^{sample} : total number of lipid molecules in sample

n_{mol}^{MLV} : number of lipids per spherical MLV of area, S_{sphere}, and composed of ca. $n_b \approx 10\text{-}20$ concentric bilayers

$n_{mol}^{sample} = N_a \cdot m_{lipids}/mw_{lipid} = (10 \ 10^{-3} \text{ g}/700 \text{ g.mole}^{-1}) \times 6.02 \ 10^{23} \text{ molecules.mole}^{-1} = 8.6 \ 10^{18}$ molecules. By considering that each lipid in the membrane occupies a surface of 60 Å^2, one obtains:

$n_{mol}^{MLV} = 2n_b.S_{sphere}/A_{lipid} = 40 \times 4\pi r_0^2/A_{lipid} = 40 \times 4\pi \ (0.45 \ 10^{-6} \ \mu)^2/60 \text{ Å}^2 = 4.2 \ 10^7$ molecules, and

$N_{MLV} \approx 2 \ 10^{11}$

The energy per liposome due to MAS at 1.4 kHz is then: $E_K/N_{MLV} \approx \mathbf{2 \ 10^{-14} \ J}$, a value much higher than both magnetic and curvature elastic energies (*vide supra*).

References

1   Kaffarnik, S., Ehlers, I., Grobner, G., Schleucher, J. & Vetter, W. Two-Dimensional P-31,H-1 NMR Spectroscopic Profiling of Phospholipids in Cheese and Fish. *J. Agric. Food Chem.* **61**, 7061-7069, doi:10.1021/jf4021812 (2013).

2   Meneses, P. & Glonek, T. High-Resolution P-31 NMR of Extracted Phospholipids. *J. Lipid Res.* **29**, 679-689 (1988).

3   Massiot, D. *et al.* Modelling one- and two-dimensional solid-state NMR spectra. *Magnetic Resonance in Chemistry* **40**, 70-76, doi:10.1002/mrc.984 (2002).

4   Casu, M., Anderson, G. J., Choi, G. & Gibbons, W. A. Nmr Lipid Profiles of Cells, Tissues and Body-Fluids .1. 1D and 2dD Proton NMR of Lipids from Rat-Liver. *Magnetic Resonance in Chemistry* **29**, 594-602, doi:10.1002/mrc.1260290610 (1991).

5   Edzes, H. T., Teerlink, T. & Valk, J. Phospholipid Identification in Tissue-Extracts by 2-Dimensional P-31-H-1 NMR-Spectroscopy with Isotropic Proton Mixing. *Journal of Magnetic Resonance* **95**, 387-395, doi:10.1016/0022-2364(91)90228-l (1991).

6   *https://sdbs.db.aist.go.jp (National Institute of Advanced Industrial Science and Technology,date of access).*

7   Douliez, J. P., Leonard, A. & Dufourc, E. J. Restatement of Order Parameters in Biomembranes - Calculation of C-C Bond Order Parameters from C-D Quadrupolar Splittings. *Biophys. J.* **68**, 1727-1739, doi:10.1016/s0006-3495(95)80350-4 (1995).

8   Douliez, J. P., Leonard, A. & Dufourc, E. J. Conformational order of DMPC sn-1 versus sn-2 chains and membrane thickness: An approach to molecular protrusion by solid state H-2-NMR and neutron diffraction. *J. Phys. Chem.* **100**, 18450-18457, doi:10.1021/jp961220v (1996).

9   Davis, J. H. The Description of Membrane Lipid Conformation, Order and Dynamics by 2H-NMR. *Biochimica Et Biophysica Acta* **737**, 117-171, doi:10.1016/0304-4157(83)90015-1 (1983).

10   Burnett, L. J. & Muller, B. H. Deuteron Quadrupole Coupling Constants in 3 Solid Deuterated Paraffin Hydrocarbons-C2D6, C4D10, C6D14. *J. Chem. Phys.* **55**, 5829-&, doi:10.1063/1.1675758 (1971).

11   Douliez, J. P., Leonard, A. & Dufourc, E. J. Restatement of order parameters in biomembranes: calculation of C-C bond order parameters from C-D quadrupolar splittings. *Biophysical Journal* **68**, 1727-1739 (1995).

12   Shin, K. H., Fujiwara, T. & Akutsu, H. Modulation of the Specific Interaction of Cardiolipin with Cytochrome-C by Zwitterionic Phospholipids in Binary Mixed Bilayers - A 2-H and P-31 NMR-Study. *Journal of Molecular Structure* **355**, 47-53, doi:10.1016/0022-2860(95)08866-t (1995).

13   Tilcock, C. P. S. & Cullis, P. R. The Polymorphic Phase-Behavior of Mixed Phosphatidylserine-Phosphatidylethanolamine Model Systems as Detected by P-31-NMR - Effects of Divalent-Cations and pH. *Biochimica Et Biophysica Acta* **641**, 189-201, doi:10.1016/0005-2736(81)90583-6 (1981).

14   Cullis, P. R. & Dekruyff, B. P-31 NMR-Studies of Unsonicated Aqueous Dispersions of Neutral And Acidic Phospholipids - Effects of Phase-Transitions, P2H and Divalent-Cations on Motion In Phosphate Region of Polar Headgroup. *Biochimica Et Biophysica Acta* **436**, 523-540, doi:10.1016/0005-2736(76)90438-7 (1976).

15   Zhendre, V. *et al.* Key Role of Polyphosphoinositides in Dynamics of Fusogenic Nuclear Membrane Vesicles. *PLoS One* **6**, doi:10.1371/journal.pone.0023859 (2011).

16   Pott, T. & Dufourc, E. J. Action of Melittin on the DPPC-Cholesterol Liquid-Ordered Phase - A Solid-State 2H-NMR and P-31-NMR Study. *Biophys. J.* **68**, 965-977, doi:10.1016/s0006-3495(95)80272-9 (1995).

17   Vist, M. R. & Davis, J. H. Phase-Equilibria of Cholesterol Dipalmitoylphosphatidylcholine Mixtures - 2H Nuclear Magnetic-Resonance and Differential Scanning Calorimetry. *Biochemistry* **29**, 451-464, doi:10.1021/bi00454a021 (1990).

18   Helfrich, W. Lipid Bilayer Spheres - Deformation and Birefringence in Magnetic-Fields. *Phys. Lett. A* **A 43**, 409-410, doi:10.1016/0375-9601(73)90396-4 (1973).

19   Helfrich, W. Elastic Properties of Lipid Bilayers - Theory and Possible Experiments. *Zeitschrift Fur Naturforschung C-a Journal of Biosciences* **C 28**, 693-703 (1973).

20   Boroske, E. & Helfrich, W. Magnetic-Anisotropy of Egg Lecithin Membranes. *Biophys. J.* **24**, 863-868, doi:10.1016/s0006-3495(78)85425-3 (1978).

II.   Conclusion

The more important result of our study is the discovery of very fluid and highly deformable nuclear lipid membrane. We suppose that their typical lipid composition, PC lipids, charged lipids, including PI lipids, cholesterol and a high concentration of chain unsaturation is at the origin of such phenomena. The elasticity of lipid nuclear membranes is much more important that that usually reported for plasma lipid membranes. This indicates that the nuclear lipid membrane gives this intrinsic property that would lead to large membrane fluctuations (undulations, hydrodynamic deformations, etc.), in the absence of membrane proteins and lamina proteins present in the nucleus. The time scale that is usually reported for large scale membrane undulations ranges from milliseconds to several seconds. In addition, it has been reported that the morphology of nuclear invaginations can change on a timescale of 5 minutes (199), a time scale that is close to that observed for hydrodynamics modes for membrane undulations reported herein. Such a dynamic structure suggests that its formation is regulated and that the mechanisms of regulation could be linked to nuclear invaginations function and composition. Our results can be linked with the fact that NE has to promote fusion events and/or nuclear invaginations. Even if these results are based on natural membrane lipids without proteins we may speculate that a such lipid composition is one of the requirements to promote the formation of nuclear invaginations, that is to say, the lipid matrix has the intrinsic property to deform almost at will. Of course such a dynamic membrane has to be bound to other proteins to prevent unwanted undulations; invaginations would be the result of lipid membrane plasticity and special protein anchoring. From our results, we postulate that the lipid composition of the nuclear envelope is involved in the formation of invaginations. It has also been reported that in some pathologies nuclear invaginations morphology is altered suggesting that nuclear invaginations are susceptible to be pathologically deregulated. By extension we may postulate that the deregulation of the lipid composition could lead to abnormal membrane structure and could be involved in some pathologies. In order to unraveled the role of nuclear membranes proteins on membrane dynamics properties 2H solid-state NMR experiments have been performed on nuclear membrane (*ie*, lipids plus proteins) and first results are presented in the following chapter.

Chapter V: Nuclear membranes: role of proteins, inner and outer nuclear membranes

The previous chapters have shown that the human nuclear envelope lipid extracts have a specific composition compared to other types of membranes and this confers to reconstructed lipid membranes unusual elastic properties. It is interesting to explore the complete nuclear membrane dynamics (lipids + proteins) and try to understand the role of membrane proteins in nuclear membrane dynamics.^{2}H solid-state NMR was chosen and the results show specific dynamic properties that I will detail in this chapter. As seen before the nuclear envelope is composed of two lipid bilayers, the Outer Nuclear Membrane (ONM) that is continuous with the endoplasmic reticulum (ER) and the Inner Nuclear Membrane (INM) that is linked to the lamina network inside the nucleus. In order to know whether the ONM has a specific lipid composition compared to the ER and whether the INM has the same composition of ONM. A second experiment was developed in this chapter by analyzing the phospholipid composition of INM vs. ONM once they have been isolated separately. A protocol based on a recent publication was used to separate the two membranes, and mass spectrometry analysis was done to define the phospholipid composition of the two membranes.

I. Nuclear Membrane dynamic properties

In the third and fourth chapter of this thesis the dynamic properties of reconstructed nuclear membrane vesicles were presented. We showed that the specific phospholipid composition of the nuclear envelope leads to specific dynamics properties of reconstructed nuclear envelope vesicles. The natural nuclear membrane is not only composed of phospholipids but also contains proteins. In order to have a better overview of nuclear membranes dynamic properties and to investigate the role of proteins, the dynamic properties of natural nuclear membranes (*i.e.* lipids and associated proteins) was explored by ^{2}H solid state NMR. Nuclear membranes were obtained from extracted nuclei after a large part of their chromatin was digested (see Material & Methods). Removing a part of the chromatin allows increasing the proportion of membranes packed into the rotor for solid state NMR experiment and improves spectral acquisition. To probe the dynamics of natural membrane a deuterated probe was incorporated. The incorporation mechanism was developed by Garnier *et al.* (195), where SUVs of deuterium-labelled lipid were incorporated into natural membranes by freeze/thaw cycles. Further, ^{2}H solid state NMR experiments were

performed at different temperatures in order to define whether the nuclear natural membrane behaves the same way as nuclear lipid reconstructed membrane.

1. Materials and methods

1) Materials

$^2H_{31}$ palmitoyl, 2-oleoyl-*sn*-glycero-3-phosphocholine (POPC-$^2H_{31}$) was purchased from Avanti Polar Lipids (Birmingham, AL. USA). These starting materials were used without further purification. Deuterium-depleted water and methylene chloride were obtained from Eurisotop (Saint Aubin, France) and solvents (chloroform, methanol and ethanol) were obtained from Sigma Aldrich Chemicals (Saint Quentin Fallavier, France). Other reagent such as Sucrose, $MgCl_2$, SDS (sodium dodecyl sulfate), Tris Base, Hepes, KCl, DTT, DNase, RNase and TPP were purchased from Sigma Aldrich (Saint Quentin-Fallavier, France). Cell culture reagent, Dulbecco's Modified Eagle's Medium (DMEM), Fetal Bovine Serum (FBS) and Streptomycin/Penicillin were purchased from Invitrogen, (Carlsbad, CA. USA).

2) Methods

i.   Nuclear membrane preparation

Nuclear extracts were recovered as explained in Chapter II. Based on Wilkie and Schirmer (177), nuclei were diluted in 10 % SHM buffer where DNase I and RNase A were added twice to digest the chromatin. Details are reported in the chapter II.

ii.   Probes incorporation

MLVs of ^2H-POPC were hydrated to 98% in a minimum final volume of 1 mL and transferred into a 5 mL plastic tube to be sonicated above the lipid transition temperature for at least 15 min. Vesicle size (100 nm) was determined by dynamic light scattering. (195). Details are explained in the chapter II. Nuclear membrane pellets were resuspended in deuterium-depleted Tris Buffer (x2) to remove as much as possible natural abundance deuterated water. For probe incorporation, a probe-to-nuclear membrane lipid molar ratio of 1.1:1 was used. More details are explained in the chapter II. The sample was resuspended in a final volume of 80µl to be transferred to a 4 mm rotor (195).

iii.   NMR experiments

Liquid-state ^1H- ^2H- and ^{31}P-NMR experiments were carried out on a Bruker Avance III-HD 400 MHz SB spectrometer (Wissembourg, France) equipped with a 5mm broadband SmartProbe at 25°C. ^{31}P-NMR spectra were acquired at 161.98 MHz using a one-pulse sequence with proton decoupling ($\pi/2$ pulse width of 8 µs, recycling delay of 20 s, acquisition time of 4s, spectral window of 54 ppm and between 80 and

1024 transients). ^{1}H-NMR spectra were acquired at 400.13 MHz using a single pulse sequence ($\pi/2$ pulse width of 10μs, recycling delay of 15s, acquisition time of 2s, spectral window of 20 ppm and 48 scans). ^{2}H-NMR spectra were acquired at 61.42 MHz using a single pulse sequence without lock ($\pi/2$ pulse width of 400μs, recycling delay of 20s, acquisition time of 2s, spectral window of 130 ppm and 48 scans). Solid-state Deuterium NMR were performed on a Bruker Avance III 800 MHz SB spectrometer (Wissembourg, France) equipped with a dual H/X 4-mm MAS probe. ^{2}H-NMR spectra were acquired at 122.82 MHz by means of a quadrupolar echo pulse sequence (194), with a spectral width of 500 kHz, a $\pi/2$ pulse width of 4.5 μs, a 40 μs interpulse delay and a recycle delay of 2 s. Typically, 10-50 k scans were recorded depending on temperature. The reference for solid-state deuterium powder patterns was set to zero and the position of the carrier arbitrarily placed in the middle of the symmetric pattern. A Lorentzian noise filtering of 100-500 Hz was applied prior Fourier transformation from the top of the echo signal. Quadrature detection was used in all cases. Samples were allowed to equilibrate at least 30 min at a given temperature before the NMR signal was acquired. Magic angle sample spinning (MAS) was accomplished and a spinning rate of 1.4 kHz was applied. The [1]H-decoupling-one-pulse sequence used with the following parameters: [2]H $\pi/2$ pulse width of 5.4 μs, recycling delay of 5 s, acquisition time of 40.9 ms, spectral window of 100 kHz and 100 scans, proton decoupling at 10W.

iv. NMR data treatment and spectral simulations

Liquid state ^{1}H-, ^{2}H- and ^{31}P-NMR spectra were processed using the Bruker TopSpin software. The corresponding ^{2}H-POPC peak in 1D-^{2}H NMR spectra was integrated and converted into milligrams quantities by comparison with the external standard methylene chloride. For wide-line solid-state NMR, spectral moments allow to quantitate spectral changes as function of temperature and were calculated according to Dufourc (200) and Davis (201) using a FORTRAN code developed by Erick Dufourc and implemented in a user-friendly routine, NMRFriend, by Sébastien Buchoux (30) as described in chapter II. The simulation program for wide line spectra has been developed in FORTRAN code by Erick Dufourc and implemented in a user-friendly graphical interface (Microsoft .NET) for Windows platforms by Arnaud Grélard.

2. **Results**

1) **Incorporation control**

In order to follow the dynamics of nuclear membranes a deuterated probe has to be incorporated. The incorporation was based on a fusion mechanism between ^{2}H POPC SUV and membranes (195). The aim of this experiment is to place in contact ^{2}H SUV vesicles with natural membrane. By freeze/thaw cycles the

structure of SUV is destabilized and vesicles are fusing with the natural membrane allowing the incorporation of deuterated lipids (see Figure 49).
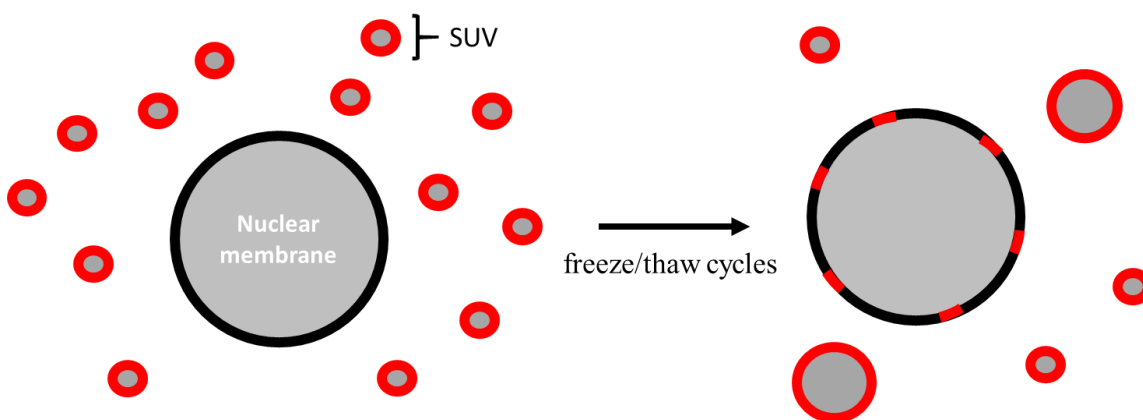
Figure 49: **^{2}H POPC incorporation mechanism**. 100µm of SUV (red rings) were place in contact with nuclei membranes, ie, lipids plus proteins (black rings). Freeze/thaw cycles were done to promote the SUV incorporation into natural membranes. Some of SUV were incorporated, some are not incorporated, and some can fuse with other SUV and form LUV (large unilamellar vesicles).

In order, to remove the non-fused ^{2}H-SUV and ^{2}H-LUV, three purification steps were done by centrifugation. Furthermore, the amount of incorporation of the deuterated probe has been investigate by the analysis of supernatants of the purification steps. Supernatants of purification steps were recovered, dried and resuspended into 500 µL of CDCl$_3$ or CHCl$_3$ and ^{1}H, ^{31}P, and ^{2}H liquid NMR experiments were performed.

i.   First control: ^{1}H liquid-state NMR experiments

Each dried supernatant has been resuspended into CDCl$_3$ and sonicated to remove some aggregates in the tube. Even with the sonication step some aggregates are still persistent in the tube indicating that one cannot solubilize completely all molecular contents. The ^{1}H liquid NMR experiment allows the characterization of ^{2}H POPC, by the presence of a choline typical chemical shift at around 3.2 ppm[202]. Figure 50 represents the ^{1}H spectrum of the four supernatant purification steps. Each supernatant spectrum is represented by a different color. By looking at the methyl region (0-1 ppm), we can observe that from the supernatant 1 to 3 the quantity of methyl groups is stable and that the quantity of methyl in the supernatant n°4 is significantly low compared to other supernatants. This result is showing that from the n°4 supernatant there is much less methyl resonances in the solution, and can be explain by the absence of phospholipid species, so this solution can be discarded. The presence of methyl groups in supernatant can come from ^{2}H POPC but they can also come from lipids from membranes or from other types of molecules. Finally, a zoom (right side of the Figure 50) shows the choline region in spectra; looking at the choline

155

region we can determinate that there is no choline from the supernatant n°2. As the choline head group is part of PC species, we can expect that there is no longer ^{2}H-POPC in the supernatant n°2. A ^{31}P liquid-state NMR experiment could define whether the methyl groups detected are coming from phospholipids or not.
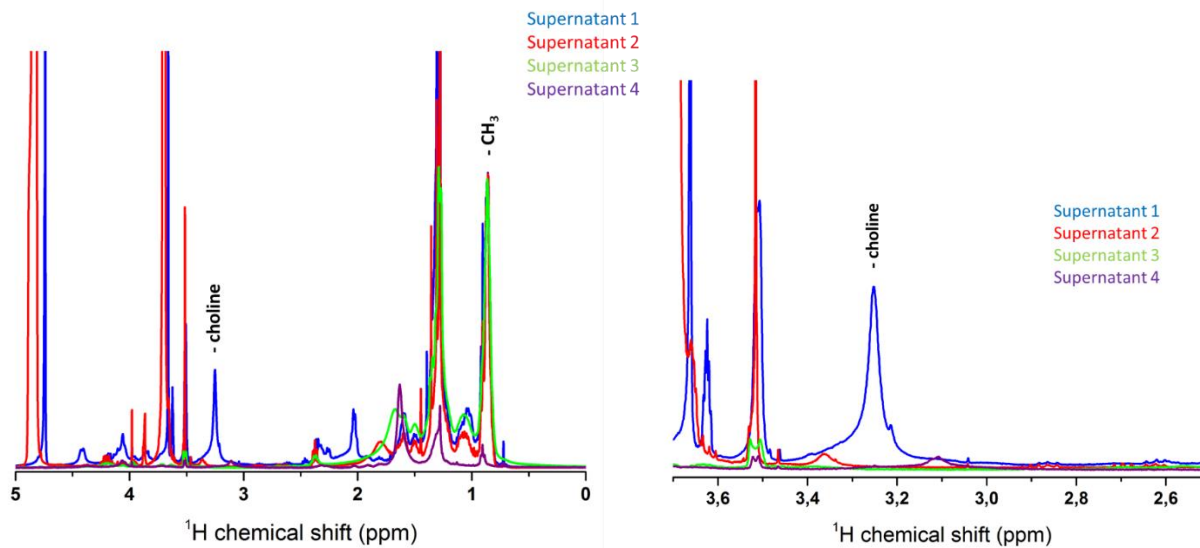
Figure 50: **^{1}H liquid-state NMR spectra of d-POPC SUV incorporation purification step**. Each colour spectrum is representing a supernatant of a purification step. The zoom is representing the choline area (3.2 ppm). Acquisition parameters were Number of scans: 48 with a recycling delay of 15 s and a Lorentzian filtering of 0.3 Hz.

ii.   Second control: ^{31}P NMR experiment

The ^{31}P experiments were done to detect the presence of phosphate groups in the purification solution and more precisely the presence of lipid phosphate groups. The recycling delay D1 was optimized for performing quantitative experiments (*i.e.,* D1=20s). Figure 51 shows the ^{31}P liquid NMR spectra of the 3 first purification step. We can observe several peaks in the phosphorus spectrum. We expect from literature that phospholipids signal is around 0 ppm, and TPP as an internal standard is at -17.95ppm. Others peaks are observed in supernatant 1 (at around -6 ppm and -20 ppm) and are coming from other types of species (possibly ATP or ADP). The unknown species are indicated by a black star at the peak. Looking at the phospholipid region we can deduce that from the third wash there is no longer any phospholipid left in

the natural membrane sample. In order to quantify ^{2}H POPC incorporated into natural membrane other experiments have been done.
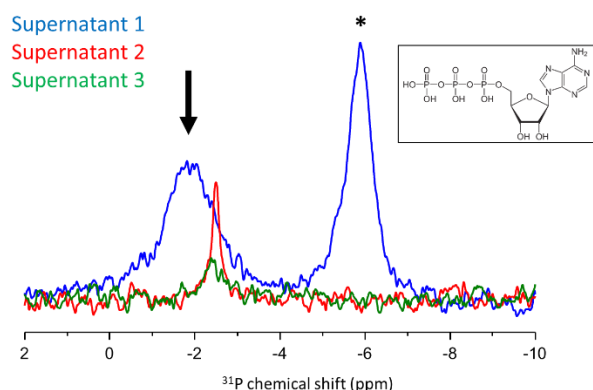
Figure 51**: ^{31}P liquid NMR spectra to follow the ^{2}H-POPC SUV incorporation**. Each coloured spectrum is representing a supernatant during the purification step that is obtained after centrifugation. Samples were dried and resuspended into CDCl$_3$ Peaks near 0 ppm (black arrow) are assigned to phospholipids species. Other peak, labelled with a black asterisk are corresponding to other phospho-compound. At-6 ppm γ of ATP and -20 ppm β of ATP. TPP: triphenyl phosphate (-17.95 ppm). ^{31}P acquisition conditions: number of scans = 2048, recycling delay = 15s, Lorentzian filtering = 10 Hz.

iii.   Third control: ^{2}H liquid-state NMR experiment

A third control was done to confirm the absence of free or non-incorporated ^{2}H POPC SUV and the quantity of ^{2}H POPC incorporated in natural membrane. Samples were dried and resuspended into CHCl$_3$. Samples were sonicated to remove aggregates in the tube. Even with this sonication step aggregates were still present in the tube. Deuterated methylene chloride was used as an internal standard. 3.18 mg of deutereted Methylene chloride in CHCl$_3$ have been added into a capillary into the NMR tube. The Figure 52, shows the ^{2}H spectrum of supernatants 1 and 2. The two spectra were normalised to the ^{2}H-methylene chloride pic (5.3ppm). We observe two pics in the supernatant n°1: ^{2}H-POPC: 1 ppm, 0.6 ppm corresponding to C^{2}H$_2$ (without the C^{2}H$_2$ in α of the carbonyl) and C^{2}H$_3$. In supernatant n°2, one no longer detected ^{2}H-POPC in solution. The result means that the other phospholipids found in supernatant 2 came from the natural membrane sample without deuterium. In order to quantify the incorporation ratio, the area under each peak was determined by the topspin software. A quick calculation led to 0.42 mg of ^{2}H-POPC as found in supernatant n°1 meaning that 2.9 mg was finally incorporated. The final ratio of incorporation was 0.9:1 (lipid probe:membrane lipids). As reported in Garnier et al. paper we were expected a ratio of 0.5:1 (33%). The quantity incorporated is therefore greater (47%) than expected and/or there is some deuterated POPC that could not be dissolved (*vide supra*) and the quantity of probe incorporated into the natural membrane is overestimated.
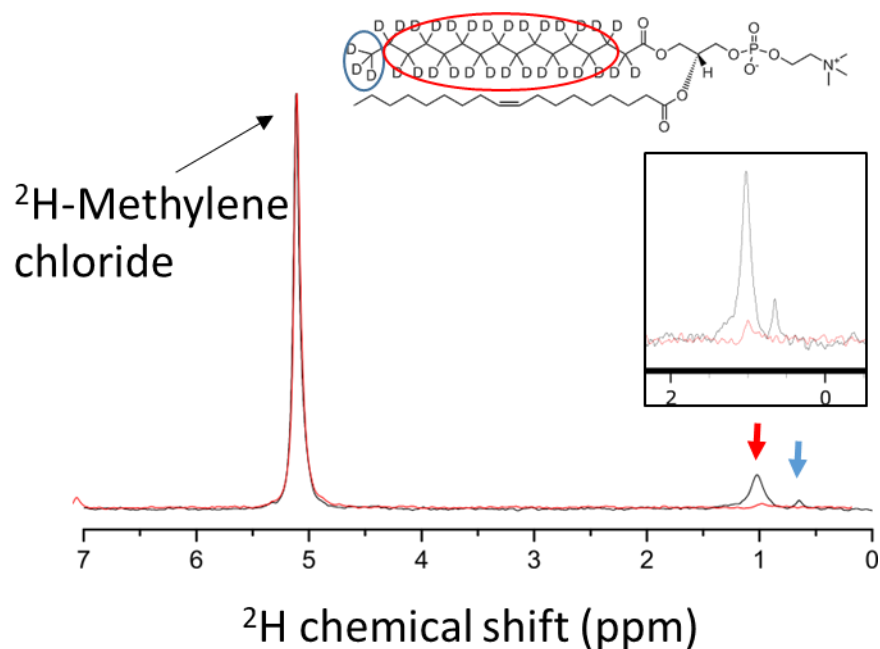
Figure 52: **²H liquid NMR spectra of ²H-POPC SUV incorporation purification step**. Samples were dried and resuspended into CHCL₃. Deuterated methylene chloride was added in a capillary in order to quantify the ²H-POPC observe in the supernatant n°1 (black line). Each colored spectrum is representing a supernatant during the purification step, supernatant n°2: red line. Acquisition conditions: number of scans = 48, recycling delay = 20s, Lorentzian filtering = 1 Hz.

2) Membrane dynamics from ²H solid-state NMR

A series of ²H solid state NMR spectra were acquired at different temperatures in order to investigate the dynamic properties of nuclear membranes. Spectra were acquired from 254K to 313K and back to 298K. Another spectrum was acquired at 298K after a short spinning, in order to see whether deformation properties of natural nuclear membranes were the same than those observed on nuclear lipid reconstructed vesicles or POPC vesicles.
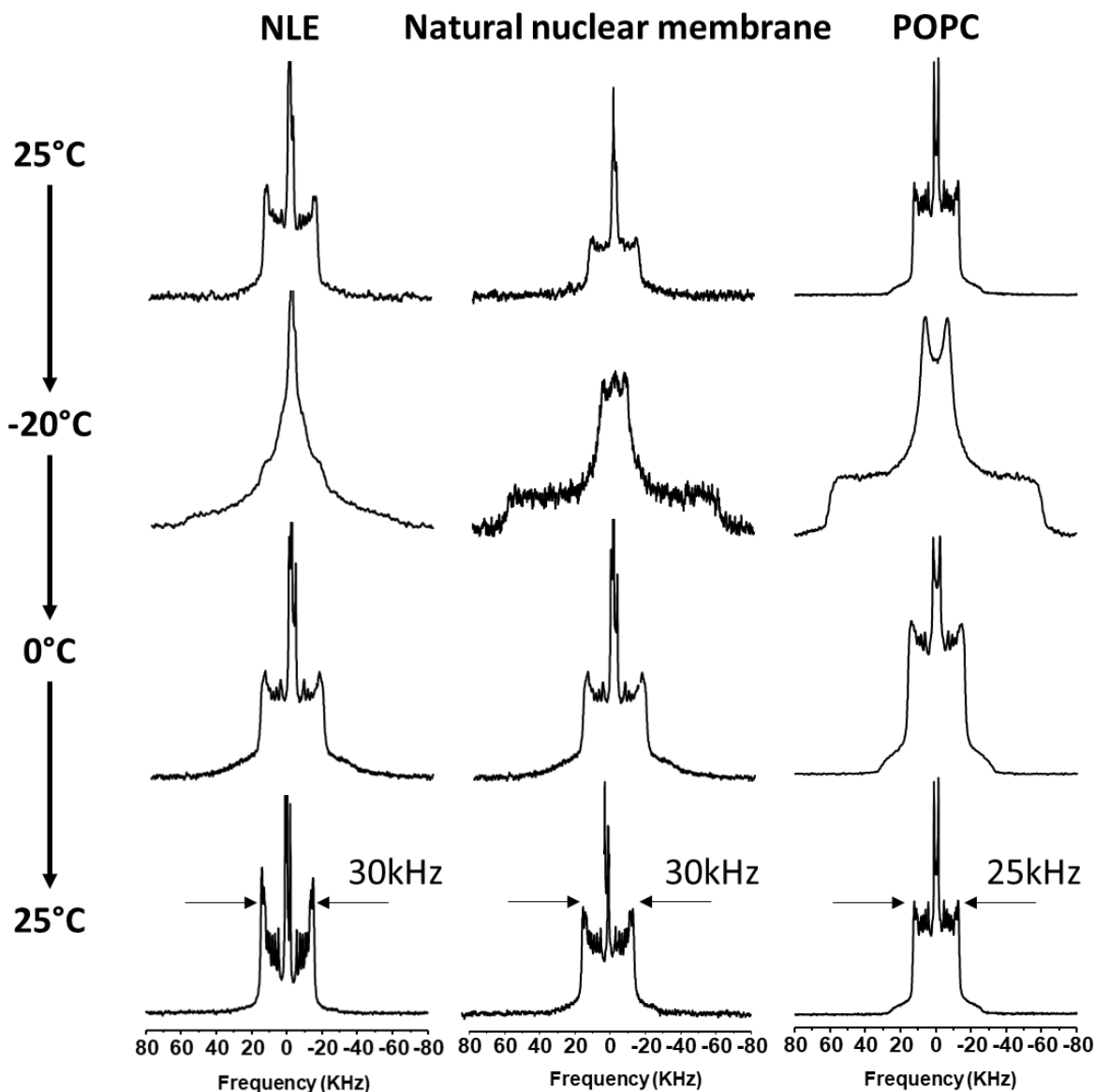
Figure 53 **Thermotropism of natural nuclear membranes and POPC controls**. Selected ^{2}H-NMR spectra of natural nuclear membrane mixed with ^{2}H$_{31}$-POPC and pure ^{2}H$_{31}$-POPC (POPC) vesicles during a thermal variation (25°C down to -20°C and back) and recorded after temperature stabilization. Spectra were obtained after Fourier transformation of solid-echo type experiments accumulated for 2-18k transients.

Natural nuclear membrane labelled with ^{2}H$_{31}$-POPC, led to a fluid phase spectrum at 25°C. The width ($\approx$ 30 kHz) was wider than for pure POPC MLV and appeared similar to that observed in reconstructed lipid nuclear membrane vesicles (Figure 53). This indicated that the lipid probe was sensing a more rigid membranous environment than in POPC vesicles and a similar environment as in NLE vesicles. Cooling

159

down to -20°C led to a composite spectrum with broad features of approximately 120, 15 kHz. This indicated a quite rigid lamellar phase. Increasing the temperature to 0°C led to an almost fluid phase spectrum with broad features detected near 36 kHz. Increasing further to 25°C resulted in a well-resolved spectrum consisting of several doublets. In this case the spectrum had almost lost some of the "powder" type distribution. This event suggested a deformation of the natural nuclear membranes in the magnetic field (*vide infra*), as was seen for lipid extracts (Chapter IV). Comparing to the spectrum of nuclear lipid extract reconstructed membrane, the deformation seemed less intense. This deformation, as seen in the Chapter IV, is due to the magnetic field action. To assess this deformation, the sample was submitted to MAS, in order to counterbalance by a mechanical force, the magnetic force. After spinning, as for reconstructed lipid nuclear membranes, the initial spectrum at 25°C was recovered without sign of deformation (see spectrum at 25°C with an asterisk in the Figure 54).

iv.   Thermotropism analysis
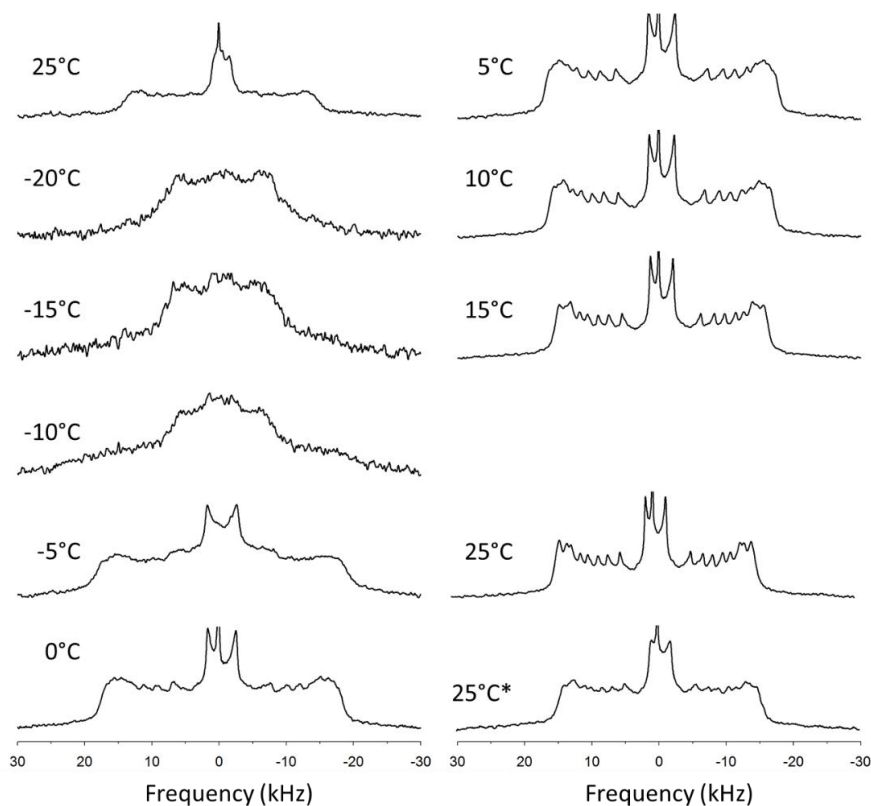
Figure 54 **Thermal variation of deuterium solid-state NMR spectra**. ^{2}H-NMR spectra of natural nuclear membrane doped with [2]H-POPC, during a thermal variation (25°C down to -20°C and back, from left top to right bottom) and recorded after temperature stabilization. Spectra were obtained after Fourier transformation of solid-echo type experiments accumulated for 10 to 50 k transients, Lorentzian line filtering of 100 to 500 Hz. The lower right spectrum (asterisk) was obtained after spinning the sample at the magic angle (1.4 kHz) and let the system stabilize at 25°C after stopping MAS.
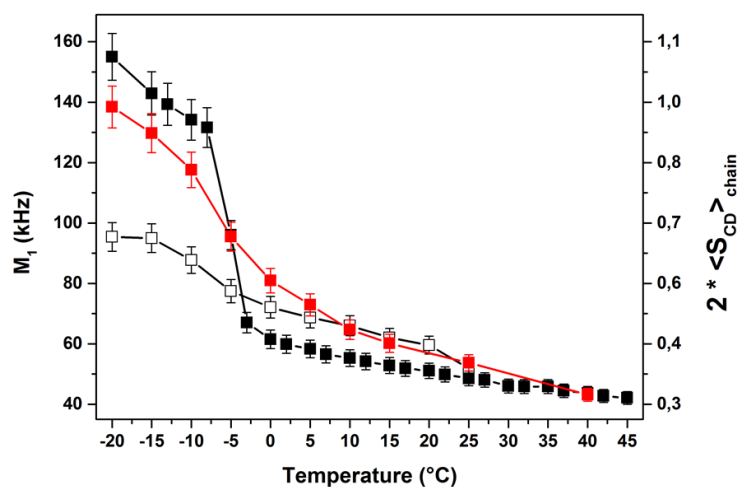
Figure 55: **Thermal variation of the first spectral moment (reporting membrane fluidity),** M_1, from ^{2}H-NMR spectra of Figure 54 of natural nuclear membrane (red squares) reconstituted NLE (white squares), and control POPC vesicles (black squares). The double y-axis plots twice the fatty acid chain order parameter to depict rigid chains (solid-ordered membranes) when $2\langle S_{CD}\rangle_{chain}$ = 1 and fully disordered systems (liquid-like) when $2\langle S_{CD}\rangle_{chain}$ = 0.

The temperature behavior of nuclear membrane systems was further quantified by calculating the first spectral moment, M_1, (41, 186). As seen in the Chapter IV, M_1 is directly proportional to the average chain order parameter. So for a $2\langle S_{CD}\rangle_{chain}$ = 1 the system is totally rigid and $2\langle S_{CD}\rangle_{chain}$ = 0 for liquid systems. Figure 55 shows both M_1 and $2\langle S_{CD}\rangle_{chain}$. At low temperatures, natural nuclear membranes samples reached $2\langle S_{CD}\rangle_{chain}$ values near 1 indicating a quite rigid nature of the hydrophobic core of the membrane. Compared to NLE vesicles, the phase transition temperature T_m was still broad and occurred between -10°C to 0°C. The chain ordering markedly decreased when the temperature was increased above T_m also indicative of the fluid phase state. Chain ordering in the fluid phase was greater than that observed with pure POPC vesicles, except for high temperatures.

v.   Chain Order parameter.

For fluid phase temperatures (*e.g.*, 25°C) a minute description of chain ordering may be obtained from ^{2}H-NMR spectra. Figure 56 shows both experimental and calculated spectra for ^{2}H$_{31}$-POPC and nuclear membrane vesicles labelled with ^{2}H$_{31}$-POPC.
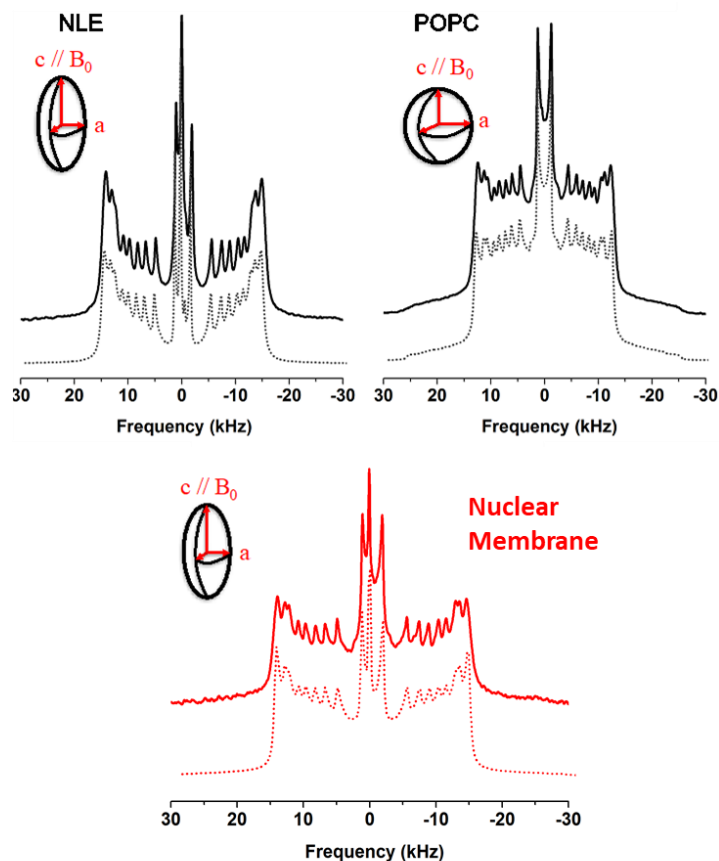
Figure 56: **Simulations of deuterium solid state spectra reveals ordering and deformability**. Experimental and simulated (dotted line) ^2H spectra of reconstructed membrane vesicles and control POPC vesicles as obtained at 25°C. Same experimental parameters as in Figure 54. Simulated spectra were calculated as described in Materials & Methods. Inserts (ellipsoid and sphere) depict the deformation that is obtained from simulations, $c/a = 3.0$ for NLE 1.8 for Nuclear Membranes and 1.0 for POPC. c and a are the long and short semi-axes with c being aligned with the B_0 magnetic field direction.

In Figure 57 the chain ordering reflects the well-known gradient of order parameters with increased rigidity near the interface and an almost liquid-like environment at the center of the membrane. As for NLE vesicles, the natural nuclear membrane has a similar ordering profile but is clearly more ordered than pure POPC. Ordering information can be correlated to bilayer thickness. At 25°C the value for the bilayer thickness of pure POPC and NLE vesicles was 42.8Å, 44.2Å. 44.1Å were found for natural nuclear membrane respectively (see Table 8), *i.e.*, very similar to NLE. The difference between POPC vesicles and natural membrane is small but notable. This could be due to the presence of cholesterol that has been shown to increase membrane ordering and hence membrane thickness (41). The membrane thickness of natural nuclear membranes is the same that reconstructed nuclear membranes, indicating that proteins may not affect much the membrane thickness.

162
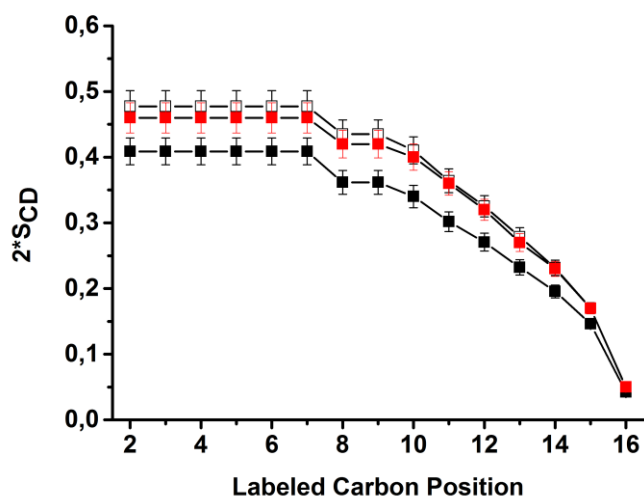
Figure 57 **Plot of S_{CD} order parameters as a function of the labelled carbon position**, $2S_{CD}$, from ^{2}H-NMR spectra obtained at 25°C of natural nuclear membrane (red squares) reconstituted NLE (white squares), and control POPC vesicles (black squares). k, along the palmitoyl acyl chain (k=16, chain end, k=2, membrane interface). Accuracy in order parameters is ±0.5%.

Table 8: **Chain order parameters from ^{2}H-NMR spectra**. Experimental quadrupolar splittings, order parameters and bilayer thickness calculation for, NLE, nuclear membrane containing ^{2}H$_{31}$-POPC and for pure ^{2}H$_{31}$-POPC liposomes, at 25°C.

	NLE			Nuclear Membrane			POPC		
#C	$\Delta v_Q{}^a$	$S_{CD}{}^b$	$S_{CC}{}^c$	$v\Delta_Q{}^a$	$S_{CD}{}^b$	$S_{CC}{}^c$	$\Delta v_Q{}^a$	$S_{CD}{}^b$	$S_{CC}{}^c$
2	29.6	-0.236	0.230	29.25	-0.233	0.233	25.6	-0.204	0.195
3	29.6	-0.236	0.242	29.25	-0.233	0.233	25.6	-0.204	0.213
4	29.6	-0.236	0.230	29.25	-0.233	0.233	25.6	-0.204	0.195
5	29.6	-0.236	0.242	29.25	-0.233	0.233	25.6	-0.204	0.213
6	29.6	-0.236	0.230	29.25	-0.233	0.233	25.6	-0.204	0.195
7	29.6	-0.236	0.242	29.25	-0.233	0.233	25.6	-0.204	0.213
8	27.10	-0.216	0.230	26.6	-0.212	0.233	22.65	-0.180	0.195
9	27.10	-0.216	0.201	26.6	-0.212	0.191	22.65	-0.180	0.166
10	25.45	-0.203	0.230	25.25	-0.201	0.233	21.30	-0.170	0.195
11	22.75	-0.181	0.175	22.5	-0.179	0.169	18.90	-0.151	0.145
12	20.50	-0.163	0.187	20.25	-0.161	0.189	16.95	-0.135	0.156
13	17.50	-0.139	0.139	17.5	-0.134	0.134	14.55	-0.116	0.114
14	14.50	-0.116	0.140	14.5	-0.116	0.145	12.25	-0.098	0.118

163

15	10.70	-0.085	0.091	10.75	-0.086	0.086	9.15	-0.073	0.077
16	3.05	-0.024	0.079	3.3	-0.026	0.086	2.65	-0.021	0.069
S_{mol}[d]	0.75			0.75			0.7		
L_{chain}[e]	13.7			13.6			13.0		
b[f]	44.2			44.1			42.8		

[a]Obtained from spectral simulations of Figure 56 of main text and represents the splitting for orientations of bilayer normals at 90° to the magnetic field, accuracy is better than 0.5 %. Assignment was based on literature (203, 204). Positions 2-9 could not be separated.

[b]Calculated from $\Delta\nu_Q^k$ using the equation $\Delta\nu_Q^k = \frac{3}{4}A_Q S_{CD}^k$ from (201) with A_Q = 167 kHz (205). Accuracy is 0.5 %.

[c]Calculated from S_k^{CD} using the recurrent equation(206): $2S_k^{CD} = -(S_k^{CC} + S_{k+1}^{CC})$, accuracy is 0.5%. S_{16}^{CC} is obtained using the C3 symmetry around the C_{16}-C_{15} bond: $S_{16}^{CC} = S_{16}^{CD}/(\frac{3cos^2 111°-1}{2})$)

[d]S_{mol}, the molecular order parameter was obtained from (203, 204) for DMPC and DMPC + 30% cholesterol. Value for NLE were extrapolated by considering a maximum of 10% cholesterol in the bilayer.

[e]L_{chain} was calculated from (203, 204). $\langle L_{chain}\rangle = \frac{1+\sqrt{1+8S_{mol}}}{4}\left[\langle l_{C_n-H}\rangle + 1.25\sum_{k=2}^{n}\left(\frac{1}{2}+\frac{S_k^{CC}}{S_{mol}}\right)\right]$, where $\langle l_{C_n-H}\rangle$ was the contribution of the methyl terminus (0.81 Å).

[f]Under the assumption (203, 204) that there were no lipid interdigitation, the bilayer thickness was obtained by summing two tail-to-tail molecular lengths: b = $2\langle L_{lipid}\rangle$, where $\langle L_{lipid}\rangle = \langle L_{chain}\rangle + \langle L_{gly}\rangle + \langle L_{head}\rangle$. $\langle L_{lipid}\rangle = \langle L_{chain}\rangle + \langle L_{gly}\rangle + \langle L_{head}\rangle$. $\langle L_{head}\rangle + \langle L_{gly}\rangle$ = 8.4 Å was obtained by combining neutron diffraction data for the lipid length, 21.8Å, and NMR data for the chain length, 13.4 Å, calculated for DPPC in the fluid phase. Accuracy for L_{chain} is ± 0.4Å. Accuracy for b is estimated to be ±1Å.

Spectral simulations were performed by considering a distribution of bilayer orientations, θ, with respect to the magnetic field as in an ellipsoid of revolution: $p(\theta) \sim \frac{sin^2\theta}{sin^2\theta+\frac{c}{a}cos^2\theta}$ (207), where c/a represents the ellipsoid long axis to short axis ratio (207). c/a values were varied until a correct agreement was obtained between experimental and calculated spectra (Figure 56). c/a was found to be near 1.0 for POPC (almost no deformation), 1.8 for Nuclear Membrane and close to 3.0 for reconstituted nuclear membrane vesicles. This indicates a small but marked prolate deformation of the initially spherical vesicles of Nuclear membranes compared to POPC and NLE. Inserts in Figure 56 (ellipsoid and sphere) depict the deformation that is obtained from simulations, with c being aligned with the B_0 magnetic field direction.

1. Discussion

As seen in the Chapter IV, the study of nuclear lipid extract reconstituted liposomes has shown atypical dynamic properties. In order to unravel whether proteins have an impact on membrane dynamic properties the study of complete natural nuclear membrane was investigated. The method used to explore the membrane dynamics was based on the incorporation of a deuterated probe and further performing ^{2}H solid-state NMR experiments.

The incorporation step is crucial: enough probe had to be incorporated in order to have a good signal to noise ratio by NMR, but the incorporation must not be too high to disturb the system analysed. We decided to follow the protocol of incorporation used by Garnier *et al.*(195) where the initial ratio was 1.1:1 (probe:membrane lipids) for a final ratio of 0.5:1 as detected by mass spectrometry. In our case, the incorporation control was based on quantitative ^{2}H liquid-state NMR experiment and we observed that the level of incorporation was too high (0.9:1). We have to note that Garnier *et al.* had done the control of the incorporation by mass spectrometry experiments directly on membrane samples (with incorporated probe) and in our case the control was done by an indirect method on non-incorporated deuterated probes (washing supernatant). Furthermore, we observed precipitates in supernatant solutions used for the control and we wonder if the deuterated POPC was completely solubilized. Moreover, in the case of Garnier *et al.* paper, the type of membrane study was much more rigid, which could explain that even with a high proportion of SUV placed in contact to liposomes, less probe was incorporated. In the case of human nuclear membrane, the initial protocol of Garnier *et al.* requires some improvement by placing less SUV in contact with natural membranes. We also have to improve the incorporation control to be sure of the incorporation level. A direct control by using membrane with incorporated probe can be performed after having done the thermotropism analysis. Membrane lipids could be extracted and analysed directly by ^{2}H liquid-state NMR or by mass spectrometry after solubilization of all lipids.

The thermotropism of the nuclear membrane system was explored by ^{2}H solid-state NMR. We observed that the behavior of nuclear membrane was between POPC and NLE vesicles. Furthermore, the ordering profile of nuclear membrane was close to that of NLE vesicles. If there is no effect of the incorporated ^{2}H-POPC we can conclude that proteins do not have a great effect on ordering parameters. This has already been reported years ago for intrinsic model membrane proteins(208): molecular order is quasi unchanged but slow molecular motions are affected. But if the ^{2}H-POPC is too concentrated, as we suspect, ordering parameters can be affected and should be higher. Finally, we observed that the deformation of nuclear

membrane is less intense than with NLE vesicles. We can deduce that the proteins or ^{2}H-POPC probe may hamper the deformation.
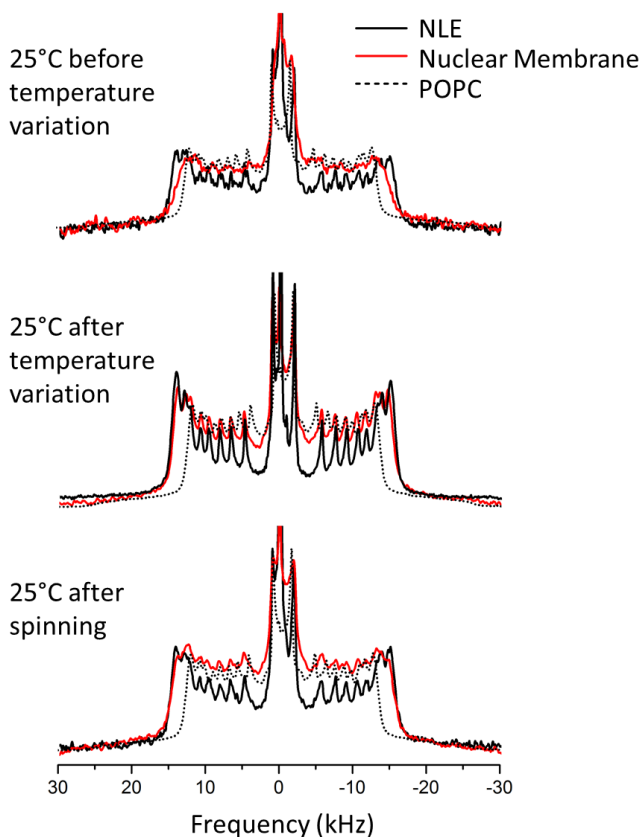
2. Conclusion

To conclude about this experiment, the incorporation process has to be optimized by putting in contact less ^{2}H SUV with natural membrane in order to obtain a maximal final incorporation ratio of 0.5:1 (lipid probe: nuclear membrane) or even much less. Furthermore, the method to control the incorporation process must be optimized too. A direct control should be performed on natural membranes after all solid-state NMR experiments. This control can be done by mass spectrometry or by liquid-state NMR. At the moment we have a hint that membrane proteins do not act on membrane thickness but do reduce the deformation by almost half. However, such a conclusion has to be postponed and more experiments be performed.

II.   Outer and inner nuclear membrane phospholipid analysis

In the Chapter III, we have presented results of the nuclear membrane phospholipid composition obtained by mass spectrometry. The typical phospholipid composition is dominated by three phospholipids types: PC, PE and PI. Furthermore, we observed that phospholipids moderate chain length with many double bonds. The nuclear membrane is a double phospholipid bilayer composed of an outer and an inner membrane (ONM and INM respectively) separated by a perinuclear space. The ONM is continuous with the ER and the INM is linked to the lamina network inside the nucleus. The proteomic study of the two membranes has been done and shows that there are composed of different kinds of proteins. In order to know the ONM composition and whether the INM (Inner Nuclear Membrane) has the same lipid composition of the ONM we decided to separate and analyze both membranes. We used a protocol published by Schindler *et al*.(176) where citraconic anhydride is used to separate the two membranes. Furthermore, the lipid extraction protocol was performed in silanized glassware in order to recovered as much of PI as possible (see Annex I).

1. Materials and methods

1) Materials

Liquid chromatography solvents, *i.e*., methanol, isopropanol, acetonitrile, and chloroform, were HPLC-grade and purchased from Sigma-Aldrich (Saint-Quentin Fallavier, France). Ammonium acetate, ethylamine, formic acid, and NH_4OH solution (28.0–30.0 % NH basis) were also purchased from Sigma-Aldrich. Synthetic internal lipid standards for mass spectrometry analysis (PE 17:0/17:0, PS 17:0/17:0, PC 17:0 /17:0, PA 17:0/17:0, PI 17:0/14:1, and PG 17:0/17:0). Other reagent as Citraconic anhydride, Sucrose, $MgCl_2$, SDS (sodium dodecyl sulphate), Tris Base, glycine, PVDF membrane, low fat milk powder, tween, antibodies, Hepes, KCl, DTT, were purchased from Sigma Aldrich (Saint Quentin-Fallavier, France). Cell culture reagent, Dulbecco's Modified Eagle's Medium (DMEM), Fetal Bovine Serum (FBS) and Streptomycin/Penicillin were purchase from Invitrogen, (Carlsbad, CA. USA).

2) Methods

i.   Protocol of separation

Nuclear extracts were recovered as explained in the chapter II. The membrane separation protocol was based on Schindler *et al.*, 1985(176). Nuclei were resuspended in 1 ml of modification buffer (200 mM HEPES, 1 mM $MgCl_2$, 0.25 M Sucrose, pH 8.5 adjusted with NaOH) and supplemented with 11 mM of

citraconic anhydride. Following the reagent addition, the reaction mixture was centrifuged at 15,000 g at 4°C for 3 min. A pellet was formed, which was then washed with modification buffer and centrifuged. The pellet corresponds to INM and the supernatant is corresponding to ONM.
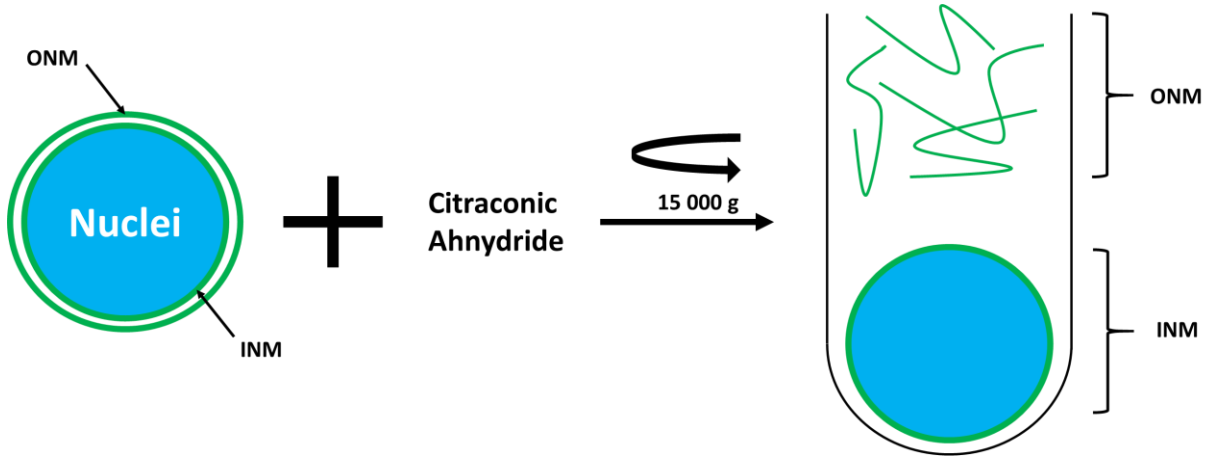
Figure 59: **Schematic view of the protocol of separation of the INM and the ONM**.

ii.   Western blot

Electrophoresis. Nuclei and membranes samples corresponding to 20 µg proteins (obtained by Bradford (209)) were mixed with 5µL of 4X SDS (Sodium Dodecyl Sulphate) loading buffer and boiled for 10 minutes at 95 °C to denature proteins. Samples were loaded into a 4–12% Bis-Tris gel (Invitrogen, city) against a protein ladder (PageRuler Plus, Thermo Scientific, Carlsbad, CA. USA). Gels were run in a running buffer (25 mM Tris Base pH 8.3, 3.5 mM SDS, 192 mM Glycine) at 145 V for approximately two hours, until the dye front had reached the bottom of the gel.

Western blotting. We used the classical method based on Towbin *et al.* (210). Proteins were transferred from the gel onto a PolyVinylidene DiFluoride (PVDF) membrane for Western blotting, pre-activated with methanol and subsequently washed by a transfer buffer (20 mM Tris, pH 8.3, 192 mM Glycine, 20 % (v/v) Methanol)) prior to use. Proteins were transferred using the Biorad Trans-Blot transfer apparatus, at 400 mA for two hours. Membranes were blocked one hour at room temperature with 5% low fat milk powder (w/v) in TBST (TBS 1 %, 0.1 % Tween 20). Following blocking, membranes were incubated with the appropriate primary antibody in 5% (w/v) low fat milk powder in PBST (PBS 1 %, 0.1 % Tween 20) at 4°C overnight. Membranes

were washed to remove the excess of primary antibody and the nonspecific binding. Membranes were subsequently incubated with HRP (horseradish peroxidase)-conjugated secondary antibody for 1 h at room temperature in 5% (w/v) low fat milk powder in PBST, followed by 5% (w/v) low fat milk powder in PBST washing steps. Amersham ECL reagents were used at a ratio of 1:1 and incubated on the membrane for 3 min. Protein were revealed under a chemiluminescent system (Thermo Scientific, Carlsbad, CA. USA).

iii.   Glassware silanization

Lipid extraction was carried out in silanized glassware(211) in order to minimize the loss of charged phosphoinositides. Glass universals, specimen tubes, chromacol screwtop tubes and Pasteur pipettes were silanized by immersion in a 3% (v/v) solution of dichlorodimethylsilane (DCMS) in toluene. Glassware was left in a fume hood for 1 hour, then rinsed twice with methanol and twice with water. The glassware was kept in a heated cabinet until dry, then stored in a cool, dark place.

iv.   Lipid extraction.

Lipids were extracted from nuclei samples using a modified Folch extraction (212). Nuclei were added to 4 mL of acidified chloroform:methanol (2.5:1), sonicated and filtered. After addition of 0.2 volumes of K_4EDTA (0.2 M, pH 6), samples were centrifuged at 800 g. The lower phase was retained and dried down completely at 55°C, under nitrogen gaz. Phospholipid concentration was determined by a Fiske Assay resulting on an indirect measurement of inorganic phosphates released from extracted lipids (199). Phospholipid characterization and quantification were provided by mass spectrometry as described below.

v.   Mass spectroscopy.

Phospholipid extracts (around 0.25 mg) were dissolved in $CHCl_3/CH_2OH$ (1:2, v/v) + 8 mM ammonium acetate and then centrifuged to remove the non-dissolved components. Each sample was infused into the TurboV electrospray source of a mass spectrometer model QTRAP® 5500 (Sciex, Concord, Ontario, Canada) at a flow rate of 7 µL/min. ESI-MS experiments were achieved in the negative (PC, PE, PS, PA, PI, PG) and positive (PC, EPC) ion modes in the mass range m/z 350-100. ESI- MS/MS experiments (Precursor Ion scans) were also performed in the negative and positive ion modes with fast polarity switching (50 ms) and a scan rate of 200 Da/s. Nitrogen was

169

used for the curtain gas (set to 15), gas1 (set to 20) and gas2 (set to 0). Needle voltage was set at -4,5 or +5,5 kV without needle heating. The de-clustering potential was either -100 V or +100 V. Calibration was achieved using an ES Tuning Mix (Sciex, Concord, Ontario, Canada). The collision gas was nitrogen and collision energy was fixed to either -50 or 50 eV. The mass range was m/z 250-1100. MS/MS experiments included one positive mode precursor ion scan and 54 negative mode precursor ion scans. Phospholipids species were identified using Lipid View software (v1.0, Sciex, Concord, Ontario, Canada).

Liquid chromatography mass spectrometry. LC-MS/MS (MRM mode) analyses were performed with the same mass spectrometer model QTRAP® 5500 (Sciex, Concord, Ontario, Canada) coupled to a LC system (LC-20AD XR pump, Shimatzu, Marne-la-Vallée, France) and PAL HTC-xt Autosampler (CTC Analytics, Zwingen, Switzerland). Phospholipid extracts (50 pg) were dissolved in CH_3CN/H_2O 80/20 and internal lipid standards were added (PA: 10 pmol, PC: 0.25 pmol, PE, PG, PI: 2.5 pmol). Analyses were achieved in the negative (PC, PE, PS, PA, PI, PG) and positive ion modes (PC, EPC) with fast polarity switching (50 ms); nitrogen was used for the curtain gas (set to 20), gas1 (set to 35) and gas2 (set to 0). Needle voltage was at -4,5 or +5,5 kV without needle heating; the de-clustering potential was adjusted to +40 V and between -180V and -85 V. The collision gas was also nitrogen; collision energy was +47 eV and varied from -62 to -48 eV. The dwell time was set to 3 ms. MS/MS experiments were performed by 19 positive and 111 negative MRM scans. Phospholipids species were identified using Lipid View software (v1.0, Sciex, Concord, Ontario, Canada) and the area of LC peaks were determined using MultiQuant software (v2.1, Sciex, Concord, Ontario, Canada). Reversed phase separations were carried out at 40 °C on a Ascentis RP Amide 150×1 mm column, with 3 µm particles (Supelco, Sigma Aldrich, St Quentin Fallavier, France)). Eluent A was H_2O+0.1 % formic acid and eluent B was CH_3CN+0.1 % formic acid. The gradient elution program was: 0 min, 30 % B; 8 min, 30 % B; 10 min, 70 % B; 35–36 min, 87 % B; 37 min, 30 % B. The flow rate was 50 µL/min; 10µL sample volumes were injected. %mol were obtained by normalization with peak area of standard.

2. Results

1) Separation of ONM and INM

In order to obtain the phospholipid composition of the ONM and the INM, both membranes have to be separated. We used a protocol from Schindler *et al*. (176) where citraconic anhydride is used to separate the two membranes. The mechanism for separation is based on interaction of the agent with amino groups of proteins. In principle, following the addition of the reagent ONM and INM can be separated. The INM was still bound to the lamina network and the DNA, so by a simple centrifugation INM form a pellet and ONM, as there are less heavy are found in the supernatant. We used western blots to confirm the separation of both membranes.
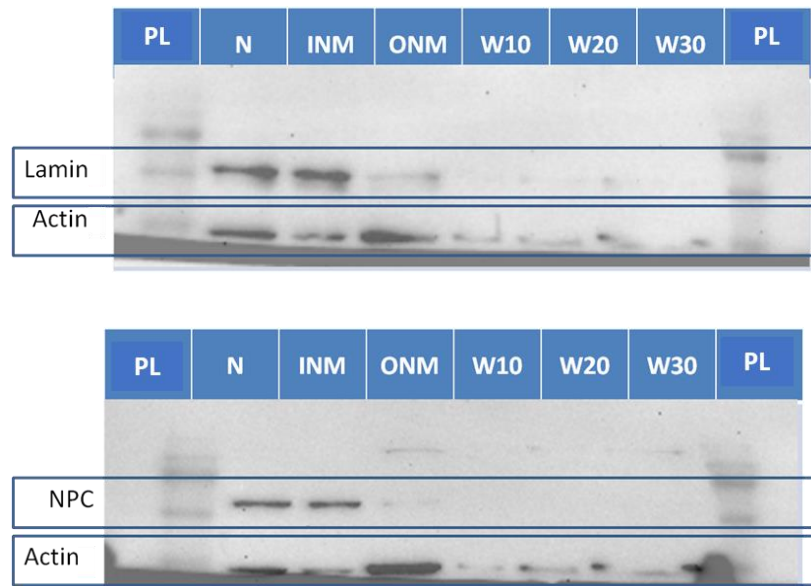
Figure 60: **Western Blot of Nuclei, ONM and INM** showing the efficiency of the separation. w: washing solution 10µL, 20µL, 30µL.PL: Protein ladder, N: Nuclei, INM: inner nuclear membrane, ONM: outer nuclear membrane. N, INM, ONM: 20µg of proteins.

We used specific nuclear proteins such as lamin, actin and NPC (Nuclear Pore Complex) to control the purity of samples. Each sample was loaded on the acrylamide gel at 20µg of proteins. Intact nuclei were used as a control. The washing solution was loaded at different concentrations (w10, w20, w30). The control, intact nuclei, shows the presence of lamin, actin and NPC. After separation of the two layers, we observed that INM are enriched in lamin but also in NPC. The

ONM is enriched in actin as it is linked to the NE by a ONM protein, nesprin (213). NPC are only present on INM membranes. The presence of a small amounts of actin in the INM sample may be due to a ONM contamination or by the remaining actin in the nucleoplasm. According to the western blot, the separation protocol is working and both membranes appear to be separated adequatley. INM and ONM samples were repared to extract lipids membranes and analysed by mass spectrometry.

2) INM/ONM phospholipid composition

The phospholipid composition experiments have been performed by mass spectrometry as the amount of lipids recovered was too low to perform by NMR experiments. The glassware was silanized as described in the Annex 1. The mass spectrometry experiments were acquired by the same method and parameters, as described in Chapter I (see Material and Methods). A shotgun analysis was done on samples in order to obtain a list of precursor ions. Then a LC/MS/MS (MRM mode) was performed to get the molar percent of each phospholipid types by using internal standard lipids. Results are presented in the Figure 61. The %mol of the washing fraction (W) is also represented in this Figure.
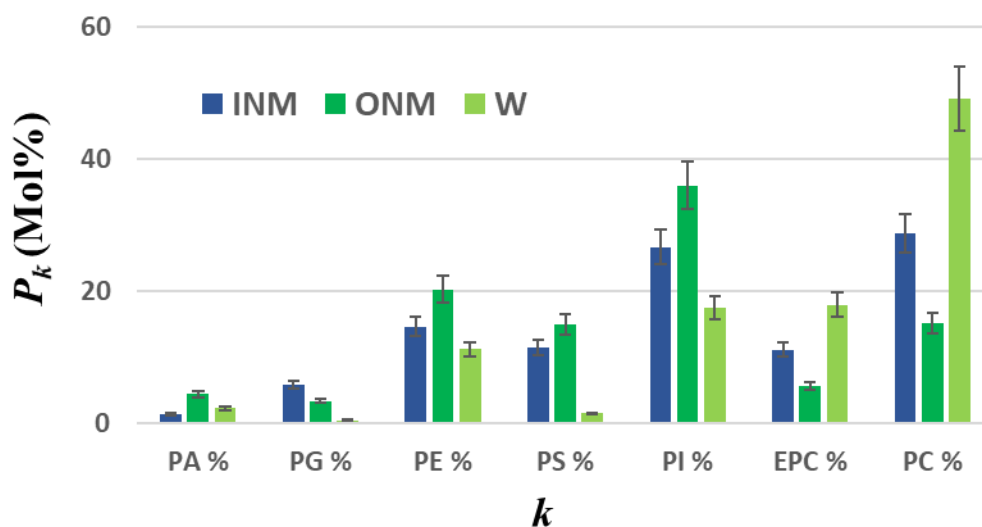
Figure 61: **INM vs ONM phospholipid composition obtained by reversed phase liquid chromatography-mass spectrometry in MRM mode**. P_k: molar proportion of k. k: PC, EPC, … Lipids were dissolved in CH_3CN/H_2O 80/20 and internal lipid standards were added (PA: 10 pmol, PC: 0.25 pmol, PE, PG, PI: 2.5 pmol). %mol are obtained by normalization with the peak area of respective internal standards. Experimental error: 10%.

At first glance, the phospholipid composition of the INM and ONM seems a little bit different. But we performed one experiment only so we defined on the graph an experimental error of 10% related to the separation process, the extraction method and the mass spectrometry analysis. Furthermore, it seems that there is as much PC than PI due to the silanization process and this is in contradiction with the results obtained in the Chapter III. As I just did one experiment we have to take these results with caution. Nonetheless, PC and EPC are lower in the ONM with 15% and 6% respectively versus 29% and 11% for the INM. On the contrary, PI, PS and PE concentrations are higher in the ONM than in the INM. But the values are in the experimental error. The concentrations are 36%, 15%, 20% in the ONM and 27%, 11%, 15% respectively at the INM. Analysis of the washing step shows the presence of phospholipids with a majority of PC and EPC. As we can observe on the western blot that in the washing solution there is very little INM proteins and still the presence of actin, we may consider that the phospholipids of the washing step may originate from the ONM. We decided to compare ONM+W and INM and have a better overview of the two membranes (Figure 62).
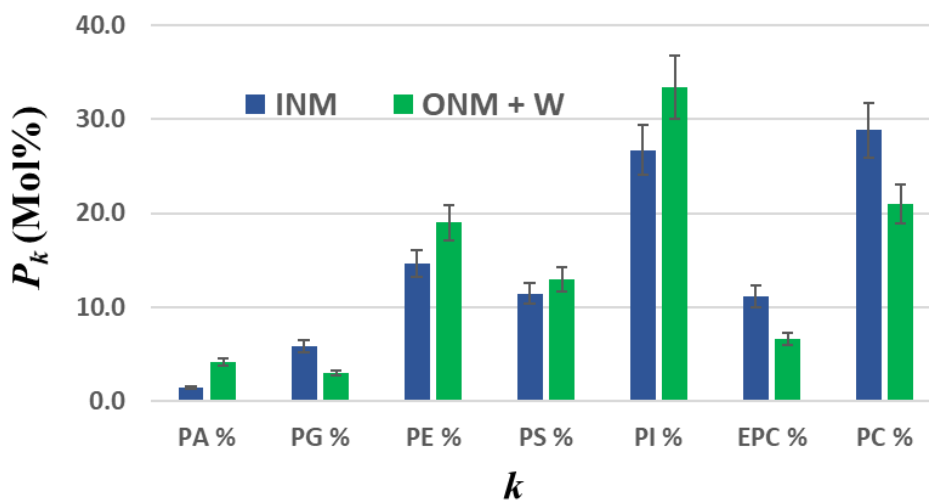
Figure 62 **:INM vs ONM phospholipid composition obtained by reversed phase liquid chromatography-mass spectrometry in MRM mode**. P_k: molar proportion of k. k: PC, EPC, … Lipids were dissolved in CH_3CN/H_2O 80/20 and internal lipid standards were added (PA: 10 pmol, PC: 0.25 pmol, PE, PG, PI: 2.5 pmol). %mol are obtained by normalization with peak area of internal standards. Experimental error: 10%.

The Figure 62 is representing the %mol of phospholipids of INM and ONM+W. Based on these results we can see that the ONM have still more of PI and PE than the INM. The INM is

dominated by PC then PI and PE species. As just one experiment has been done, other replicates have to be performed to confirm these results and see whether the small differences between the two membranes are significative or not.

From the results obtained by MRM, the phospholipids can be identified by their two fatty acid chains and double bonds information. The results are reported in the Figure 63
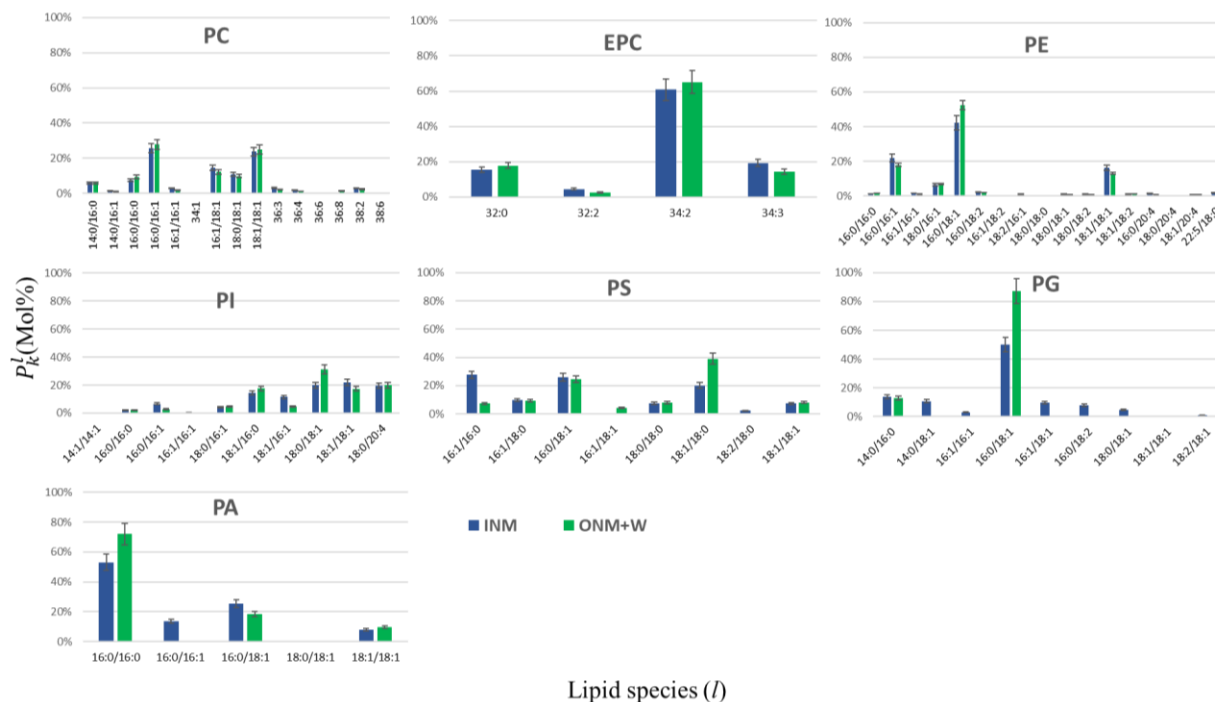
Figure 63 **INM vs ONM chain length and unsaturation distribution obtained by reversed phase liquid chromatography-mass spectrometry in MRM mode**.P_k^l: molar proportion for each lipid type (k) of lipid species (l). Lipids were dissolved in CH_3CN/H_2O 80/20 and internal lipid standards were added (PA: 10 pmol, PC: 0.25 pmol, PE, PG, PI: 2.5 pmol). %mol are obtained by normalization with peak area of internal standards

Figure 63 represents the distribution of fatty acid chains in *sn-1* and *sn-2* positions and unsaturation composing each phospholipid. The first observation leads to the conclusion that INM and ONM are composed of about the same phospholipid species. However, we can observe that some species are present in higher quantities at the ONM: PG (16:0/18:1), PI (18:0/18:1), PS (18:0/18:1), and PA (16:0/16:0).

174

3. Discussion

In the Chapter III, we presented a method to determine the nuclear membrane phospholipid composition. We discovered that this composition was atypical compared to other cell membranes with a high proportion of PC, PE and PI. We showed also that the phospholipid species were made of moderate chain length (34 carbon atoms) bearing elevated amounts of double bonds.

In this exploratory Chapter we validated a method to separate the outer from the inner nuclear membrane and extracted their lipids. Although we found that the method works, it must be repeated to assess its robustness. In addition, we used silanized glassware that favors the extraction of PI lipids and disfavours that of PC lipids (Annex I). So comparison with previous chapter may be difficult but worth doing by considering general results. We will discuss sequentially the separation method, the composition of INM *vs.* ONM and the comparison with chapter III results for the whole membrane.

In our case, and by a western blot experiment, we found that the protocol is working and the two membrane can be separated. We can deduce than there is little contamination of INM by the ONM part. Nevertheless, the control step by western blot could be improved by using other markers that are more specific of the two membranes. For example, the use of the nesprin to control the ONM (213). The efficiency of the separation could also be controlled by electron microscopy, were the presence of one or two membranes around nuclei could be observed.

After having extracted membrane lipids, we then performed the phospholipid analysis by mass spectrometry experiments. The results are reported in Table 9 and showed slight differences between the two membranes. In this table we reported also results from Schindler *et al.*(176), and Zambrano *et al.*(214), that were obtained respectively on rat liver and rat kidney tissues.

Table 9: **Phospholipid composition on nuclear membrane, ONM and INM**. In bold, the more important lipid types.

	PC	EPC	PE	PI	PS	PG	PA	SM	LPC	CL
Whole[a] nuclei	**64**	Nd	**18**	**7**	4	3	3	Nd	Nd	Nd
INM[a]	**67**	Nd	**16**	**6**	5	3	2	Nd	Nd	Nd
ONM[a]	**67**	Nd	**17**	**6**	4	2	2	Nd	Nd	Nd

ER[b]	**38.4**	Nd	**23**	**2**	**11**	Nd	1	20	4	0
NLE[c]	**54**	18	**11**	**6**	8	2	1	Nd	Nd	Nd
NLE[d]	**48**	15	**9**	**11**	4	0	7	4	0	1
INM[e]	**30**	11	**15**	**27**	11	6	1	Nd	Nd	Nd
ONM[e]	**21**	7	**19**	**33**	13	3	4	Nd	Nd	Nd

[a] Obtained from Schindler *et al.* (176) by anion exchange HPLC.
[b] Obtained from Zambrano *et al.* (214) by two-dimensional thin-layer chromatography on silicic acid. [c] Obtained in this thesis by LC/MS/MS mass spectrometry with non silanized glassware (chapter III)
[d] Obtained in my thesis by ^{31}P liquid-state NMR. (chapter III)
[e] Obtained in my thesis by LC/MS/MS mass spectrometry with silanized glassware (chapter V)

The two membranes are dominated by three phospholipid species like in NLE: PC, PE and PI. Indeed, we found that INM and ONM have a high proportion of PI following by PC and PE and that are not significantly different. We have to take in account that the protocol of lipid extraction of NLE was different as we used silanized glassware to perform the lipid extraction of INM and ONM. As expected with this new protocol we recovered more PI during the extraction (see Annex I).

In his paper, Schindler *et al.*(176) found that INM, ONM and whole nuclei are dominated by the same phospholipid species as we found in NLE (Chapter III). Furthermore, he found that INM and ONM have about the same phospholipid composition. In our case, we found that there is more PC in INM (Table 9). These results have to be taken with caution because we just analysed one sample. Furthermore, we found much more PI in ONM and INM than in the paper of Schindler for the same membrane. It is difficult to reach a firm conclusion as we performed our experiments in silanized glassware that increased the recovered proportion of PI.

We had speculated that the ONM and the ER have the same phospholipid composition. In the Chapter III, and using a non-silanized glassware, we previously found that the NE is composed with a majority of PC, PE and PI species that slightly differs than the ER composition. We could expect that the ONM and/or INM lipid composition be different to the ER composition. If we compare our results on the ONM and INM with the ER phospholipid composition performed by Zambrano *et al.*(214), we can observe that even though ONM is continuous with the ER, the two membranes seemed to have their own lipid composition. ER membranes were dominated by PC and PE while the ONM seems to be dominated by PI then PC and PE (Table 9). One again these

results need to be confirmed with further experiments as we used a silanized glassware that increased the proportion of recovered PI. As the extraction protocol used by Zambrano et al. and the one used in our chapter were different a direct comparison would be difficult to make.

The phospholipid composition analysis performed in this Chapter was done by mass spectrometry that has the advantage of recovering information about chain length and double bonds. Figures 64 and 65 represent the normalised view of chain length and double bonds for INM vs ONM. We can observe that the repartition of chain length and double bonds are a little bit different for the two membranes. The ONM is composed of long chains due to the high proportion of PI and PS species. The weighted arithmetic average chain length of ONM is 34.5 compare to 34.3 for INM, *i.e.*, within the experimental error. Furthermore, we observed a difference in the repartition of unsaturation for both membranes. There seems to be more unsaturation in the INM as the weighted arithmetic average of unsaturation is 1.5 compared to 1.4 for ONM. Again this is near the experimental error.
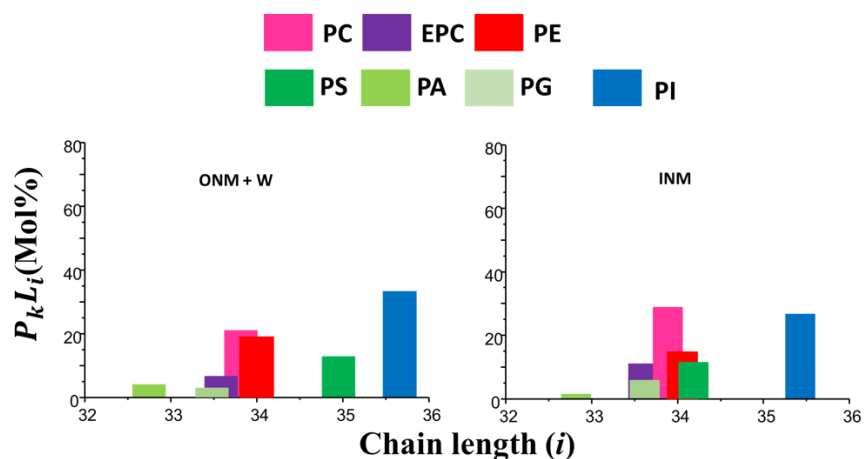
Figure 64: **Normalized view of chain length $(P_k L_i)$ for ONM+W and INM**. P_k is the proportion of lipid types, k= PC, PE, … as determined by MS, with the average chain length, $L_i = \sum (P_k^i \times i)$ with i the chain length, i = 28, 30, 32, 34, 36, 38, 40 (sum of 2 chains)
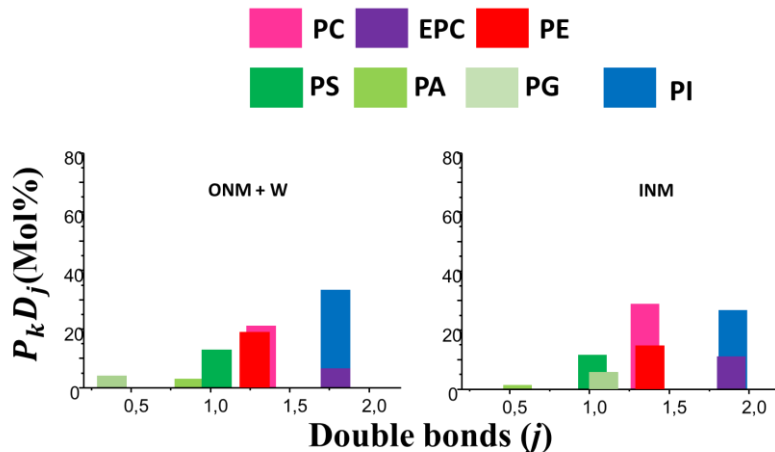
Figure 65 : **Normalized view of unsaturation number $(P_k D_j)$ for ONM+W and INM**. P_k is the proportion of lipid types, $k=$ PC, PE, … as determined by MS, with the average number of double bonds $D_j = \sum P_k^j \times j$, with j standing for the number of double bonds.

When we can compare the chain lengths and double bonds repartition of the INM+ONM *vs.* NLE (see Figures 66 and 67). The INM+ONM is composed of a length chain of 34.4 in average and 1.5 double bonds in average. By comparison, the NLE is composed of 34.1 chain length average and 1.5 double bonds. The little profile difference that is observed may be due to the modification of the extraction protocol as we used silanized glassware to extract INM and ONM but the final proportion of length chain and double bonds averages was about the same as for NLE.
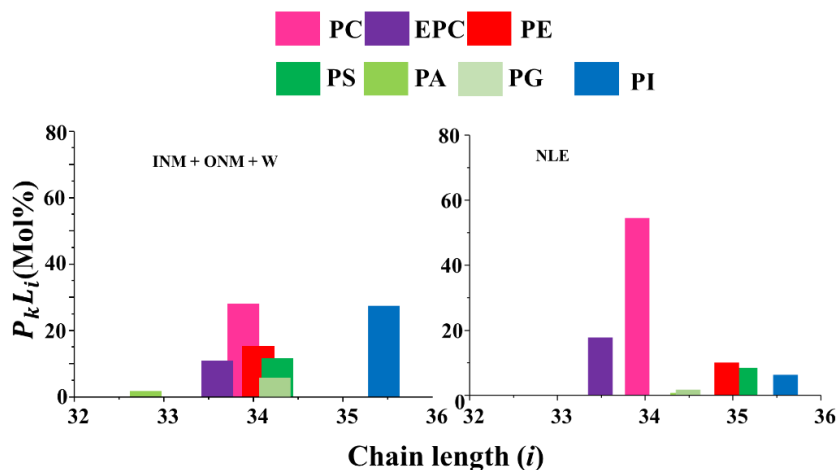
Figure 66: **Normalized view of chain length $(P_k L_i)$ for INM+ONM+W and NLE**. P_k is the proportion of lipid types, $k=$ PC, PE, … as determined by MS, with the average chain length, $L_i = \sum(P_k^i \times i)$ with i the chain length, $i = 28, 30, 32, 34, 36, 38, 40$ (sum of 2 chains).

178
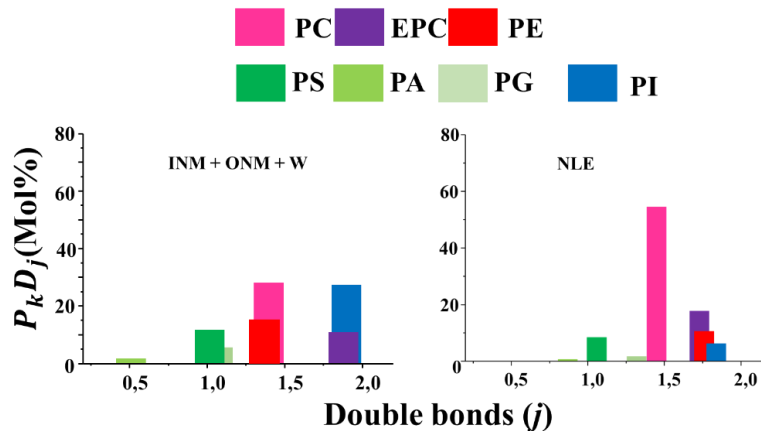
Figure 67: Normalized view of unsaturation number $(P_k D_j)$ for INM+ONM+W and NLE. P_k is the proportion of lipid types, k= PC, PE, … as determined by MS, with the average number of double bonds $D_j = \sum P_k^j \times j$, with j standing for the number of double bonds.

4. Conclusion

In this part we present an exploratory trial to separate of the two nuclear membranes: INM and ONM. The method chosen to separate both membrane appears to work but must clearly be improved, especially the method for controlling the separation. Moreover, we perform these experiments in silanized glassware that increased the proportion of recovered PI and decreased the proportion of PC extracted. Due to this this new method, it was difficult to really compare the INM and ONM phospholipid composition with the NLE phospholipid composition obtained in the Chapter III and in literature. Our preliminary results suggest that the head group composition of phospholipids in the INM and the ONM are quite similar with slight variations in the acyl chain compositions . These results require confirmation by further replication of the experiments.

III.   Conclusion

In summary the for the analysis of nuclear membrane dynamics, the interpretation of the results must be toned down because of the high incorporation of ^{2}H-POPC. However, properties of NLE still persist to a smaller extend in the natural nuclear membrane. In order to know whether the results are due to the presence of proteins or the excess of ^{2}H-POPC, other experiments with less incorporated ^{2}H-POPC SUV have to be performed. Furthermore, a second control should be taken into consideration, by directly measuring the amount of incorporated probe in extracted natural nuclear membranes.

In a second part of this Chapter analysis of INM and ONM was presented. The protocol of the two membranes seems to work even if some other controls have to be performed. The analysis of the two membranes was done by using silanized glassware that enriched the lipid extract in PI lipids and lower the PC extraction. It is therefore difficult to compare the phospholipid composition of the two membranes with results obtained in the Chapter III of the whole nuclear membrane phospholipid composition or with literature were non-silanized glassware was used. However, the analysis of INM and ONM of our preliminary results suggest that the head group composition of phospholipids in the INM and the ONM are quite similar with slight variations in the acyl chain compositions. These results require confirmation by further replication of the experiments.

Chapter VI. Conclusion and perspectives

We have shown in the Introduction that the Nuclear Envelope (NE) presents specific invaginations structures called nucleoplasmic reticulum (NRs). The role and composition of these substructure is still unknown, but we postulated that their lipids composition plays an important role in their formation. Indeed, as lipids can influence the structure and the dynamics of natural membranes, we did explore the lipid nuclear membrane composition and dynamics of human cells by quantitative methods such as NMR and Mass spectrometry in order to unravel the role of lipids in NRs formation.

One of the first challenges of this work was to develop a protocol to extract high amounts of nuclei from human kidney cells without using detergent. In fact, several protocols of nuclei extraction exist but use detergent (215). Detergent solubilizes lipids from membranes and so perturbs the lipid composition analysis. The physical method developed here, i.e., the opening of cells to free the contents under nitrogen, was improved from Blobel & Potter (216) and Domart *et al*. (217). Using a modified Folch extraction (212) milligrams of lipids were extracted and analysed by two quantitative methods: NMR and mass spectrometry (MS). The two methods report the same results and we show that nuclear membranes were composed of a greatest amount of PC lipids, very moderate PE and PI are in very important quantity. Lipid chain lengths range between 30 to 38 carbon atoms (two chains summed up) with a high proportion of 34 carbon atom length for most species, *i.e.*, C16:C18 chain length in average, except for phosphoinositides that have near 36 carbon atoms on average. The degree of unsaturation of human nuclear membranes lipid extracts was found to 1.5 double bond in average. Other lipid species have been observed by MS. The shotgun infusion mass spectrometry experiment shows the presence of a complex mixture of lipids composed of free fatty acids and sterols, lysophospholipids, diglycerides and cholesterol esters, phospholipids and triglycerides (218). Furthermore, by liquid state NMR experiments performed on the nuclear lipid extract we detected the presence of a certain amount of cholesterol.

NMR and MS are two powerful methods to characterize lipid membrane composition. Although, ^{31}P liquid-state NMR is a direct method for analysing phosphate group lipids but required milligrams of samples, MS required only nanograms of samples and is given additional information about all lipid species, and especially about lipid chain length and double bonds. However, mass spectrometry is an indirect lipid analysis method that requires the use of internal standards because molecules with different structures and charges may ionize in the mass spectrometer chamber very differently. We believe that the two methods complement each other.

In most cells the membranes of intracellular organelles may have very different lipid compositions as it is shown in Figure 68. Plasma membranes are typically enriched in PC, PE and SM. We found data on ER, which is continuous with nuclear membranes, from rat kidney cells and sea urchin eggs and spermatozoa. Data on ER membranes show larger amounts of PC whereas PE are found in similar quantities. Furthermore, there is a lot of variance for SM and for PI.
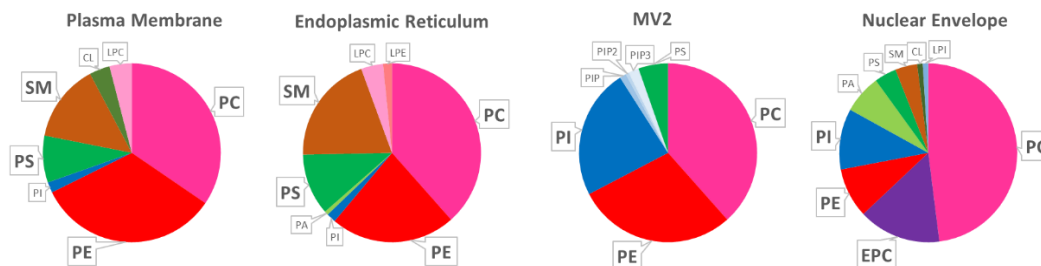
Figure 68 **Phospholipid composition of different cell membranes**. From left to right: rat kidney plasma membrane and endoplasmic reticulum (214), ER like MV2 vesicles from Sea Urchins (219), and human kidney nuclear envelope composition obtained in this thesis (chapter III).

As a way to explore deeper the nuclear envelope an analysis of INM and ONM was performed based on Schindler *et al*.(176) using a detergent-free method. The protocol of the two membranes seems to work even if some other controls have to be performed. The analysis of the two membranes was accomplished by using silanized glassware (211) that enriched the lipid extraction in PI lipids and lower the PC extraction (Annex I). It is therefore difficult to compare the phospholipid composition of the two membranes with the results obtained of the whole nuclear membrane phospholipid composition or with literature were non-silanized glassware was used. In order to validate the use of silanize glassware some other experiments have to be performed. For example, compare the extraction of PC/PI lipid standard sample in silanized and non-silanized

glassware by ^{31}P liquid-NMR and MS experiments (Figure 69). Determining the depletion of PC's on silanized glassware could be done using PC commercial samples also.
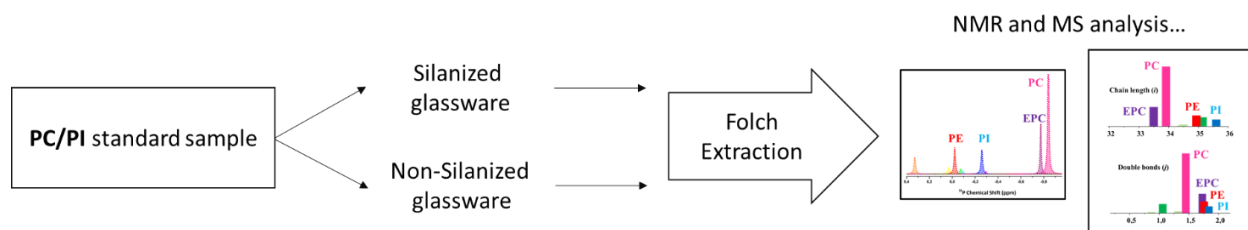
Figure 69: **Comparison of silanized and non-silanized glassware using 2 independent methods**.

However, the analysis of INM and ONM does not show, based on these preliminary results, significant difference of phospholipid composition. As just one experiment has been performed other experiments have to be done to confirm these results. Furthermore, in order to compare these results with other cell membranes, the lipid analysis of other cell membranes of the same cell type (for example as in our case HEK 293T cells) could be performed in silanized glassware (if the extraction protocol has been validated), allowing a better comparison of cell membrane types. Beside, to complete our finding about phospholipid composition, other types of lipids could be analysed by mass spectrometry, using for example the protocol of Gao *et al.* (218). This method provided a high coverage of the lipidome using an ultra-performance liquid chromatography (UPLC) that enhance the sensitivity of separation samples.

The reconstitution of lipids from human nuclear membranes into liposomes has brought several new and interesting findings. The study of thermotropism of reconstructed nuclear membranes first indicates that the gel-to-fluid transition occurs near -10°C and has a breadth of ca. 20°C. Even at the lowest temperature investigated, -20°C, the system is not completely in the solid-ordered state. This is remarkable and can be link to the presence of many charged lipids and double bonds. Also, we found that nuclear membrane reconstructed vesicles are slightly thicker than pure POPC membrane vesicles. We suggest that is related to the finding of cholesterol in the lipid composition. One of a major finding in our work is that the reconstituted nuclear membrane vesicle of initial spherical shape can be remarkably deformed by a high magnetic field (18.8T) into elongated ellipsoidal prolate. By calculation of the membrane elastic modulus it appears that its

value is very small and clearly indicates that membrane undulations are very much favoured. Such results are in favour of nuclear envelope deformation into NRs (Figure 70).
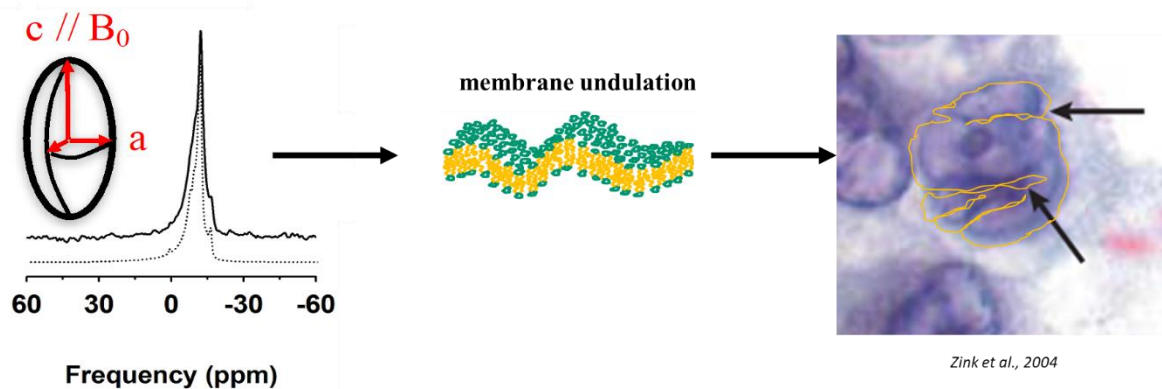
Figure 70: **Hypothesis of Nucleoplasmic Reticulum (NR) formation**. From left to the right: ^{31}P-NMR spectra (solid lines) of reconstituted nuclear lipid membrane extracts (NLE) obtained at 25°C after a thermal variation from -20°C to 25°C. In dotted line simulated spectra. Representation of membrane undulation. Cancer lung carcinoma cells image obtained from Zink *et al.(220)* . In yellow the nuclear envelope that forms several invaginations.

In order to investigate the dynamics of complete nuclear envelope (lipids + proteins) we used a protocol developed in Garnier *et.al.*(195) where a deuterated probe is incorporated in membranes to follow the dynamic properties of the membrane. Based on deuterated lipids detected in the supernatant we suspected a too high incorporation of the probe, which could perturb the analysis of nuclear membrane dynamics and the interpretation of our results have to be toned down. However, we observed that properties of NLE still persist to a smaller extend in the natural nuclear membrane. In order to validate this finding other experiments, have to be performed. Moreover, to investigate the hypothetic role of the chromatin on membrane dynamics the same protocol of incorporation could be used directly on entire nuclei and see whether the dynamics properties of the nuclear membrane varied or not in presence of chromatin.

Through the nuclei extraction protocol, we can imagine other experiments that would enhance our understanding of NRs structure and formation process. Our first results led to a typical phospholipid composition of the nuclear envelope. Using the protocol of Hagen *et al.* (221), in which the use of an anti retro-viral protease inhibitor, *i.e.*, saquinavir, induces NRs, we could explore further the NRs lipid composition. In fact, the use of saquinavir on cells (like HEK 293T) could increase the number of invaginations, nuclei extraction can be then performed followed by

a lipid extraction and quantification. We could then compare the results to normal nuclear envelope lipid composition and see whether or not there is an increase or a decrease of specific lipid types. In addition, we could also investigate the nuclear envelope lipid composition of cancerous cell types that show nuclear envelope deformation and invaginations. A difference in lipid composition may be provide an explanation for the NE disturbed structure. Another perspective could be the investigation of the NE breakdown mechanism. Based on the protocol of Collas *et al.*(222), nuclei extracts can be placed in contact with mitotic cytoplasmic solution. The hypothesis is that the NE breakdown will result in NE vesicles that can have different proteo-lipid compositions. The analysis of such vesicles can be a means to have a better understanding of NE breakdown and formation. Also, results can be compared to the sea urchin model of NE formation.

To conclude, our findings about nuclear envelope dynamics properties provide for the first time a mechanical explanation for nuclear envelope invaginations. Other experiments have to be performed to explore deeper the NE lipid composition and dynamics (INM/ONM analysis, NE in presence of proteins and chromatin). Also our adapted non-detergent protocol of nuclei extraction can result in performing other experiments in order to investigate the formation of NRs and NE breakdown and formation.

Annex I: Improvement of the protocol for the Nuclear membrane analysis.

In this part we tried to optimize the protocol of phospholipid analysis. Actually, we were supposing that we had problems to recover negative charged phospholipids with our extraction protocol. According to the paper of M. Wakelam (211), there is possibility of loss of negative phospholipids during the extraction process of lipids. We speculated that perhaps there was a loss of cetial lipid molecular species during the extraction process. Especially the loss of negatively charged lipids such as the polyphosphoinositide. The first hypothesis was that negative charged lipids interact with the glassware, which may be possible charged, used for the extraction and was adsorbed on it (211). The second hypothesis is related to the liquid-liquid extraction protocol where negative charged lipids could stay at the interface between the aqueous phase and the organic phase(211). Experiments were undertaken to explore the different hypothesis.

I.   Adsorption of negative charge lipids on the glassware

Our hypothesis was that the Si-OH group of the glassware interact with the OH group of phosphoinositol or negative charge lipids. This would reduce therefore the quantity of negative charge lipids analized by NMR and mass spectrometry. In order to remove the –OH of the glassware, glassware was treated with TMS (trimethylsulfate) and so –Me$_3$ were coated on the Si of the glassware(211). Lipid extractions were performed in silanized glassware and non-silanized glassware and analysed by mass spectrometry. The results are presented Figure 71.
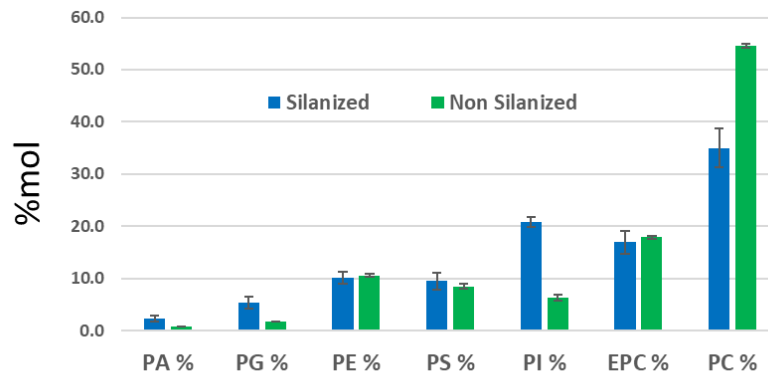
Figure 71: **Nuclear membrane phospholipid composition obtained from silanised and non-silanised glassware**. The graph represens the %mol of phospholipids with respect to internal standards. Results were obtained by reversed phase liquid chromatography-mass spectrometry in MRM mode. Lipids were dissolved in CH_3CN/H_2O 80/20 and internal lipid standards were added (PA: 10 pmol, PC: 0.25 pmol, PE, PG, PI: 2.5 pmol). %mol are obtained by normalization with peak area of internal standards.

From the Figure 71 we can see that the phospholipid composition obtained by an extraction with silanized glassware and a non silanized glassware show some differences. We obtain the same phospholipid species but with some variance in molar concentration, especially for negative charged lipid as PA and PG and especially PI and PC. With the silanized glassware the molar concentration of PI increase from 6% to 21%, PA increase from 0.7% to 2.3%, PG increase from 1.7% to 2.4% and the PC molar concentration decrease from 54% to 35%. This result confirms that negative charged lipids such as phosphoinositides adsorb on the non-silanized glassware. Moreover, we can observe that the silanization process decreases the PC recovering.

187

Figure 72: **Nuclear membrane phospholipid composition obtained from silanised and non-silaniszed glassware :chain length and unsaturation distribution obtained by reversed phase liquid chromatography-mass spectrometry in MRM mode** . Lipids were dissolved in CH_3CN/H_2O 80/20 and internal lipid standards were added (PA: 10 pmol, PC: 0.25 pmol, PE, PG, PI: 2.5 pmol). %mol are obtained by normalization with peak area of internal standards

Figure 72 represents the species repartition in function of phospholipid types. In general, we observe that the lipid species are the same when they are extracted with silanized glassware and non-silanized glassware. We can note a little difference in lipid species concentration for negative phospholipid such as PS, PG and PA. For PS with silanized glassware the most important species is PS (16:1/16:0) and for non-silanized glassware PS (18:0/18:1) is the most important species. In the case of PG different species are present in function of the silanized condition. Shorter chain lipid species are recovered with silanized glassware. For PA we observe the absence of PA (18:0/18:1) in silanized glassware.

To conclude, as suspected, we observed differences between the two glassware extraction protocol. Negative charged lipids were recovered with an increase of almost 10% with silanized glassware compare to non-silanized glassware. Furthermore, we observed that short chain species are more recovered with silanized glassware especially of negative charged lipids. The increase of negative charged lipids in the %mol phospholipid composition produces the decrease of %mol of

188

PC. A proper quantification of phospholipid analysis can be done by ^{31}P liquid state NMR experiment in order to know whether the PC proportion is well recovered with silanized glassware.

II. Lipid extraction protocol

The lipid extraction protocol is based on a liquid-liquid extraction. Lipids are amphiphilic compounds where their head are hydrophilic and their tail are hydrophobic. By adjusting the pH to 6 a majority of head groups are protonated and so the extraction can be based on the hydrophobic tail separation, ie the hydrophobic interaction will drive the separation. Most of the lipids are present in the organic phase. If the head groups are non-protonated, lipids will stay at the interface between the aqueous and the organic phase due to electrostatic/hydrophilic interactions. During the extraction process we may lose these lipids. In the case of PI, the head group is non-protonated at pH6. By decreasing the pH to 2, PI can be protonated and can be totally present into the organic phase. To see whether we can recover some more PI, a first extraction at pH6 was done following by a second extraction at pH2(211). Each organic phase was analysed by mass spectrometry and the results are presented in Figures 73 and 74.

Table 10: **pKa of phospholipid species**, data CRC handbook of lipids bilayers, D Marsh (1990) CRCpress, Boca Raton.

Phospholipids	pka
PC	1
PE	1.7; 11.25
PS	2.6; 5.5; 11.55
PA	3; 8
PG	2.9; 3.1; 3.5
PI	2.5

Figure 73: **Nuclear membrane phospholipid composition obtained from pH6 and further pH2 extraction as obtained by reversed phase liquid chromatography-mass spectrometry in MRM mode** . Lipids were dissolved in CH₃CN/H₂O 80/20 and

189

internal lipid standards were added (PA: 10 pmol, PC: 0.25 pmol, PE, PG, PI: 2.5 pmol). %mol are obtained by normalization with peak area of internal standards

Figure 73 is showing the results of the second lipid extraction at pH2. With the second extraction we recover all phospholipids types present in the first extraction at pH6, but of course to a smaller extend. Furthermore, we can observe that we recover a high proportion of PI as PS in the second extraction. All other phospholipids species were also recovered but in a smaller extend. The proportion of these lipid recovered is significate and if we add this proportion to the initial phospholipid concentration we can observe that the phospholipid composition is quite different. Especially, the PI molar concentration is increasing from 21% to 26%, and the PS is increasing from 9% to 12%.
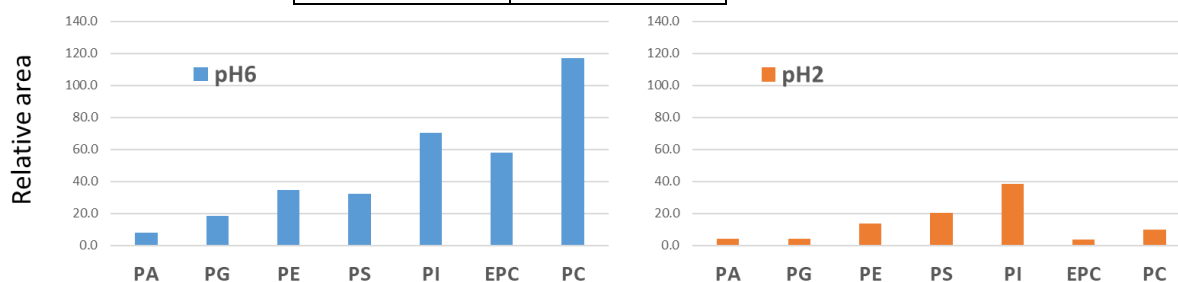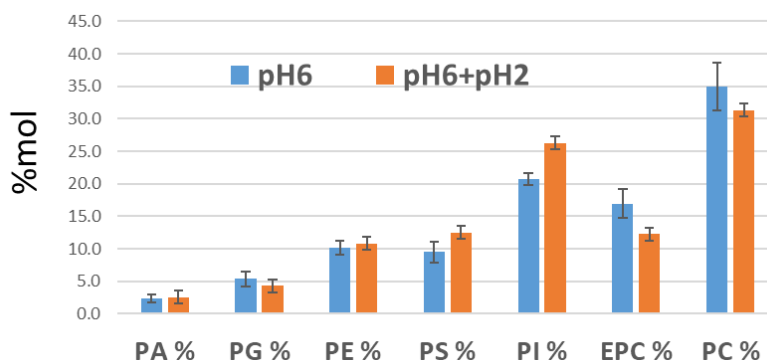

Figure 74 :**Nuclear membrane phospholipid composition obtained from pH6 and additional pH2 extraction obtained by reversed phase liquid chromatography-mass spectrometry in MRM mode** . Lipids were dissolved in CH_3CN/H_2O 80/20 and internal lipid standards were added (PA: 10 pmol, PC: 0.25 pmol, PE, PG, PI: 2.5 pmol). %mol are obtained by normalization with peak area of internal standards
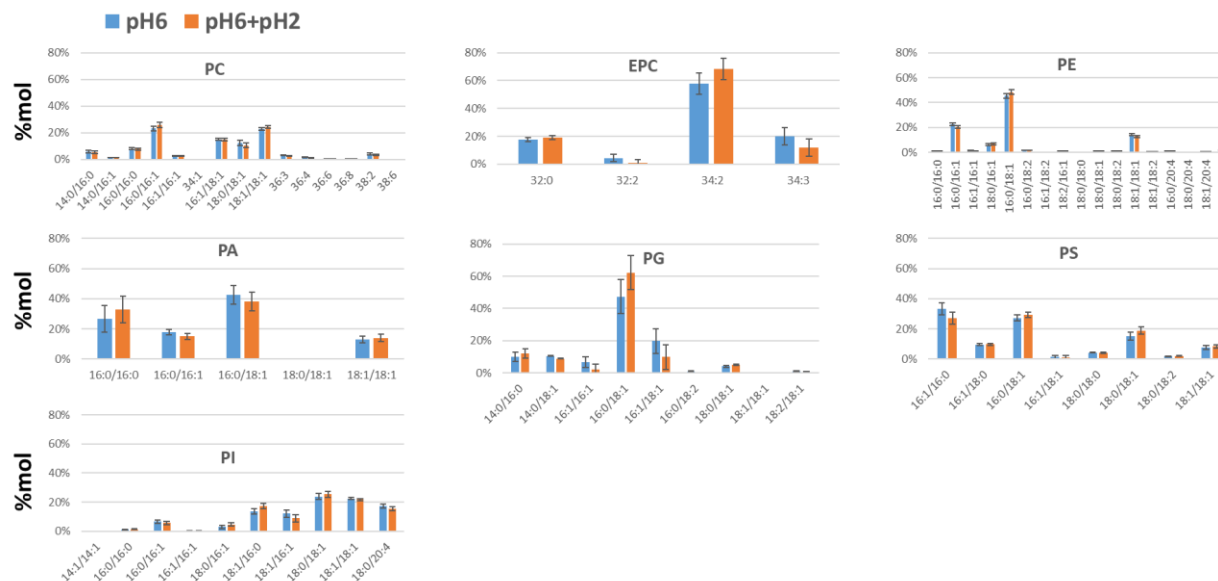
Figure 75: **Nuclear membrane phospholipid composition obtained from pH6 and additional pH2 extraction: chain length and unsaturation distribution obtained by reversed phase liquid chromatography-mass spectrometry in MRM mode** . Lipids were dissolved in CH_3CN/H_2O 80/20 and internal lipid standards were added (PA: 10 pmol, PC: 0.25 pmol, PE, PG, PI: 2.5 pmol). %mol are obtained by normalization with peak area of internal standards

As represented Figure 75, if we consider all lipid species by phospholipid types, the species recovered are not especially different.

To conclude, with a second extraction at pH2 we recovered 5% more of PI and 3%more of PS but there is no effect for the extraction of lipid species particularly.

III.   Conclusion

With the glassware silanization we are able to recover much more negative charged lipids such as PI. A decrease of PC was observed and a quantification by ^{31}P liquid state NMR has to be done in order to quantify the real PC proportion. With a second extraction at pH2 we are able to recover 5% more of PI but the other phospholipids types remain the same. To conclude, we can suggest that in experiments done during my thesis the proportion of PI has been underestimated.

References

1.   Hetzer MW. The Nuclear Envelope. Cold Spring Harbor Perspectives in Biology. 2010;2(3):16.
2.   Singer SJ, Nicolson GL. The fluid mosaic model of the structure of cell membranes. Science. 1972;175(4023):720-31.
3.   Fricker M, Hollinshead M, White N, Vaux D. Interphase nuclei of many mammalian cell types contain deep, dynamic, tubular membrane-bound invaginations of the nuclear envelope. Journal of Cell Biology. 1997;136(3):531-44.
4.   Fricker M, Hollinshead M, White N, Vaux D. The convoluted nucleus. Trends Cell Biol. 1997;7(5):181.
5.   Alberts B. Molecular biology of the cell. In: Johnson A, editor. 5th ed. ed. New York: Garland Science; 2007.
6.   Danielli JF. A contribution to the theory of permeability of thin films. In: Davson H, editor.: Journal of Cellular and Comparative Physiology; 1935. p. 495-508.
7.   Bothorel P, Lussan C. [Some new aspects of a dynamic model of biological membrane]. C R Acad Sci Hebd Seances Acad Sci D. 1970;271(7):680-3.
8.   Simons K, Ikonen E. Functional rafts in cell membranes. Nature. 1997;387(6633):569-72.
9.   Edidin M. The state of lipid rafts: from model membranes to cells. Annu Rev Biophys Biomol Struct. 2003;32:257-83.
10.   McMullen TPW. Cholesterol-phospholipid interactions, the liquid-ordered phase and lipid rafts in model and biological membranes. Current Opinion in Colloid & Interface Science; 2004. p. 459-68.
11.   Dufourc EJ. Sterols and membrane dynamics. J Chem Biol. 12008. p. 63-77.
12.   Pike LJ. The challenge of lipid rafts. J Lipid Res. 2009;50 Suppl:S323-8.
13.   Bagatolli LA, Mouritsen OG. Is the fluid mosaic (and the accompanying raft hypothesis) a suitable model to describe fundamental features of biological membranes? What may be missing? Frontiers in Plant Science. 2013;4.
14.   Jacobson K, Dietrich C. Looking at lipid rafts? Trends Cell Biol. 1999;9(3):87-91.
15.   Brown DA, London E. Structure and function of sphingolipid- and cholesterol-rich membrane rafts. J Biol Chem. 2000;275(23):17221-4.
16.   Rajendran L, Simons K. Lipid rafts and membrane dynamics. J Cell Sci. 2005;118(Pt 6):1099-102.
17.   Schechter E. Biochimie et Biophysique des Membranes : Aspects structuraux et

 fonctionnels. Masson ed. Paris1990.
18.   Cullis PR, Fenske DB. Physical properties and functional roles of lipids in membranes. In: Science E, editor. Biochemistry of lipids, Lipoproteins and Membranes1996. p. 1-33.
19.   Zhendre V. Etude de l'implication des Phosphoinositides dans la formation de l'enveloppe nucléaire: Université de Bordeaux; 2010.
20.   Schaller H. The role of sterols in plant growth and development. Progress in Lipid Research. 2003;42(3):163-75.
21.   Saito H, Suzuki N. Distributions and sources of hopanes, hopanoic acids and hopanols in Miocene to recent sediments from ODP Leg 190, Nankai Trough. Organic Geochemistry. 2007;38(10):1715-28.
22.   van Meer G, Voelker DR, Feigenson GW. Membrane lipids: where they are and how they behave. Nat Rev Mol Cell Biol. 2008;9(2):112-24.
23.   Kent C. Eukaryotic phospholipid biosynthesis. Annu Rev Biochem. 1995;64:315-43.

24.   Vance D, Vance JE, editors. Biochemistry of Lipids, Lipoproteins and Membranes: Elsevier Science; 1996.
25.   Nicole J. Y, Marlone J. H. Getting Across the Cell Membrane: An Overview for Small Molecules, Peptides, and Proteins. Methods Mol Biol. 2015;1266:29-53.
26.   Luzzati V. X-ray diffraction studies of lipid—water systems. In: Press A, editor. Biological Membranes. New York1968. p. 71-123.
27.   McIntosh TJ, Magid AD. Phospholipid Hydration. . In: Dekker M, editor. Phospholipids Handbook. New York: G. Cevc.; 1993. p. 553-77.
28.   Cullis PR, de Kruijff B. Lipid polymorphism and the functional roles of lipids in biological membranes. Biochim Biophys Acta. 1979;559(4):399-420.
29.   Israelachvili JN, Marcelja S, Horn RG. Physical principles of membrane organization. Q Rev Biophys. 1980;13(2):121-200.
30.   Buchoux S, Lai-Kee-Him J, Garnier M, Tsan P, Besson F, Brisson A, et al. Surfactin-triggered small vesicle formation of negatively charged membranes: A novel membrane-lysis mechanism. Biophys J. 2008;95(8):3840-9.
31.   Sanders CR, Oxenoid K. Customizing model membranes and samples for NMR spectroscopic studies of complex membrane proteins. Biochim Biophys Acta. 2000;1508(1-2):129-45.
32.   Fernandez C, Hilty C, Bonjour S, Adeishvili K, Pervushin K, Wuthrich K. Solution NMR studies of the integral membrane proteins OmpX and OmpA from Escherichia coli. FEBS Lett. 2001;504(3):173-8.
33.   Lau TL, Partridge AW, Ginsberg MH, Ulmer TS. Structure of the integrin beta3 transmembrane segment in phospholipid bicelles and detergent micelles. Biochemistry. 2008;47(13):4008-16.
34.   Alain Léonard, Céline Escrive, Michel Laguerre, Eva Pebay-Peyroula, Willfrid Néri, Tanja Pott, et al. Location of Cholesterol in DMPC Membranes. A Comparative Study by Neutron Diffraction and Molecular Mechanics Simulation†. 2001.
35.   Villar AV, Goni FM, Alonso A. Diacylglycerol effects on phosphatidylinositol-specific phospholipase C activity and vesicle fusion. FEBS Lett. 2001;494(1-2):117-20.
36.   Aussenac FaLMaSJMaDEJ. Detailed structure and dynamics of bicelle phospholipids using selectively deuterated and perdeuterated labels. 2H NMR and molecular mechanics study. Langmuir. 2003;19(25):10468--79.
37.   Etzkorn M, Martell S, Andronesi OC, Seidel K, Engelhard M, Baldus M. Secondary structure, dynamics, and topology of a seven-helix receptor in native membranes, studied by solid-state NMR spectroscopy. Angew Chem Int Ed Engl. 2007;46(3):459-62.
38.   Seddon JM, Cevc G. Lipid Polymorphism: Structure and stability of lyotropic mesophases of Phospholipids. In: Dekker M, editor. Phospholipids Handbook. New York: G. Cevc.; 1993. p. 553-77.
39.   Marinov R, Dufourc EJ. Thermotropism and hydration properties of POPE and POPE cholesterol systems as revealed by solid state H-2 and P-31-NMR. European Biophysics Journal with Biophysics Letters. 1996;24(6):423-31.
40.   Vist MR, Davis JH. Phase equilibria of cholesterol/dipalmitoylphosphatidylcholine mixtures: 2H nuclear magnetic resonance and differential scanning calorimetry. Biochemistry. 1990;29(2):451-64.
41.   Beck JG, Mathieu D, Loudet C, Buchoux S, Dufourc EJ. Plant sterols in "rafts": a better way to regulate membrane thermal shocks. FASEB journal : official publication of the Federation of American Societies for Experimental Biology. 2007;21(8):1714-23.
42.   Ragoonanan V, Malsam J, Bond DR, Aksan A. Roles of membrane structure and phase transition on the hyperosmotic stress survival of Geobacter sulfurreducens. Biochim Biophys Acta. 2008;1778(10):2283-90.

43.   Koynova R, Caffrey M. An index of lipid phase diagrams. Chem Phys Lipids. 2002;115(1-2):107-219.

44.   Hope MJ, Cullis PR. The role of nonbilayer lipid structures in the fusion of human erythrocytes induced by lipid fusogens. Biochim Biophys Acta. 1981;640(1):82-90.

45.   Tilcock CP, Fisher D. Interactions of glycerol monooleate and dimethylsulphoxide with phospholipids. A differential scanning calorimetry and 31P-NMR study. Biochim Biophys Acta. 1982;685(3):340-6.

46.   Epand RM. Relationship of phospholipid hexagonal phases to biological phenomena. Biochem Cell Biol. 1990;68(1):17-23.

47.   Eastman SJ, Hope MJ, Wong KF, Cullis PR. Influence of phospholipid asymmetry on fusion between large unilamellar vesicles. Biochemistry. 1992;31(17):4262-8.

48.   Gawrisch K, Parsegian VA, Hajduk DA, Tate MW, Graner SM, Fuller NL, et al. Energetics of a hexagonal-lamellar-hexagonal-phase transition sequence in dioleoylphosphatidylethanolamine membranes. Biochemistry. 1992;31(11):2856-64.

49.   Chen Z, Rand RP. The influence of cholesterol on phospholipid membrane curvature and bending elasticity. Biophys J. 1997;73(1):267-76.

50.   Szule JA, Fuller NL, Rand RP. The effects of acyl chain length and saturation of diacylglycerols and phosphatidylcholines on membrane monolayer curvature. Biophys J. 2002;83(2):977-84.

51.   Fuller N, Benatti CR, Rand RP. Curvature and bending constants for phosphatidylserine-containing membranes. Biophys J. 2003;85(3):1667-74.

52.   Luzzati V, Husson F. The structure of the liquid-crystalline phasis of lipid-water systems. J Cell Biol. 1962;12:207-19.

53.   Chernomordik L. Non-bilayer lipids and biological fusion intermediates. Chem Phys Lipids. 1996;81(2):203-13.

54.   Cullis PR, Hope MJ. Effects of fusogenic agent on membrane structure of erythrocyte ghosts and the mechanism of membrane fusion. Nature. 1978;271(5646):672-4.

55.   Vidal M, Hoekstra D. In vitro fusion of reticulocyte endocytic vesicles with liposomes. J Biol Chem. 1995;270(30):17823-9.

56.   Ahkong QF, Fisher D, Tampion W, Lucy JA. The fusion of erythrocytes by fatty acids, esters, retinol and alpha-tocopherol. Biochem J. 1973;136(1):147-55.

57.   Allan D, Thomas P, Michell RH. Rapid transbilayer diffusion of 1,2-diacylglycerol and its relevance to control of membrane curvature. Nature. 1978;276(5685):289-90.

58.   Alonso A. Structure and functional properties of diacylglycerols in. 1999;38.

59.   Chung GHC. The role of fusogenic vesicles in the regulation of nuclear envelope assembly: University college London; 2014.

60.   J Zimmerberg, S S Vogel a, Chernomordik LV. Mechanisms of Membrane Fusion. Annual Review of Biophysics and Biomolecular Structure. 1993;22:433-66.

61.   Basanez G. Membrane fusion: the process and its energy suppliers. Cell Mol Life Sci. 2002;59(9):1478-90.

62.   Chernomordik LV, Kozlov MM. Protein-lipid interplay in fusion and fission of biological membranes. Annu Rev Biochem. 2003;72:175-207.

63.   Chernomordik LV, Zimmerberg J, Kozlov MM. Membranes of the world unite! J Cell Biol. 1752006. p. 201-7.

64.   Chernomordik LV, Kozlov MM. Mechanics of membrane fusion. Nat Struct Mol Biol. 2008;15(7):675-83.

65.   Cohen FS, Melikyan GB. The energetics of membrane fusion from binding, through hemifusion, pore formation, and pore enlargement. J Membr Biol. 2004;199(1):1-14.
66.   Frolov VA, Zimmerberg J. Cooperative elastic stresses, the hydrophobic effect, and lipid tilt in membrane remodeling. FEBS Lett. 2010;584(9):1824-9.
67.   Kozlovsky Y, Kozlov MM. Stalk model of membrane fusion: solution of energy crisis. Biophys J. 2002;82(2):882-95.
68.   Larijani BaPDL. Nuclear envelope formation: mind the gaps. Annual review of biophysics. 2009;38:107--24.
69.   Chernomordik L, Kozlov MM, Zimmerberg J. Lipids in biological membrane fusion. J Membr Biol. 1995;146(1):1-14.
70.   Longo FJ, Anderson E. The fine structure of pronuclear development and fusion in the sea urchin, Arbacia punctulata. J Cell Biol. 1968;39(2):339-68.
71.   Parsons TD, Coorssen JR, Horstmann H, Almers W. Docked granules, the exocytic burst, and the need for ATP hydrolysis in endocrine cells. Neuron. 1995;15(5):1085-96.
72.   Efrat A, Chernomordik LV, Kozlov MM. Point-like protrusion as a prestalk intermediate in membrane fusion pathway. Biophys J. 92. United States2007. p. L61-3.
73.   Yang L, Huang HW. Observation of a membrane fusion intermediate structure. Science. 2002;297(5588):1877-9.
74.   Jahn R, Lang T, Sudhof TC. Membrane fusion. Cell. 2003;112(4):519-33.
75.   Wickner W, Schekman R. Membrane fusion. Nat Struct Mol Biol. 2008;15(7):658-64.
76.   Zimmerberg J, Kozlov MM. How proteins produce cellular membrane curvature. Nature Reviews Molecular Cell Biology. 2005;7(1):9.
77.   Churchward MA, Rogasevskaia T, Hofgen J, Bau J, Coorssen JR. Cholesterol facilitates the native mechanism of Ca2+-triggered membrane fusion. J Cell Sci. 2005;118(Pt 20):4833-48.
78.   Lang T, Halemani ND, Rammner B. Interplay between lipids and the proteinaceous membrane fusion machinery. Prog Lipid Res. 2008;47(6):461-9.
79.   Poccia DaLB. Phosphatidylinositol metabolism and membrane fusion. The Biochemical journal. 2009;418(2):233--46.
80.   Illustration showing the structures of an animal cell. Image credit: Genome Research Limited https://www.yourgenome.org/facts/what-is-a-cell [
81.   Frenster JH, Allfrey VG, Mirsky AE. METABOLISM AND MORPHOLOGY OF RIBONUCLEOPROTEIN PARTICLES FROM THE CELL NUCLEUS OF LYMPHOCYTES*. Proc Natl Acad Sci U S A. 1960;46(4):432-44.
82.   Nunes VS, Moretti NS. Nuclear subcompartments: an overview. Cell Biol Int. 2017;41(1):2-7.
83.   GL K. The Relative Permeability of the Surface and Interior Portions of the Cytoplasm of Animal and Plant Cells. . Biol. Bull; 1913. p. 1–7.
84.   Kite. The Relative Permeability of the Surface and Interior Portions of the Cytoplasm of Animal and Plant Cells. . Biol. Bull; 1913. p. 1–7.
85.   Bessis M, Policard A. [Not Available]. Exp Cell Res. 1956;11(2):490-2.
86.   Watson ML. The nuclear envelope; its structure and relation to cytoplasmic membranes. J Biophys Biochem Cytol. 1955;1(3):257-70.
87.   Beams HW, Tahmisian TN, Devine R, Anderson E. Ultrastructure of the nuclear membrane of a gregarine parasitic in grasshoppers. Exp Cell Res. 1957;13(1):200-4.
88.   Lammerding J, Fong LG, Ji JY, Reue K, Stewart CL, Young SG, et al. Lamins A and C but not lamin B1 regulate nuclear mechanics. J Biol Chem. 2006;281(35):25768-80.

89.   Dechat T, Pfleghaar K, Sengupta K, Shimi T, Shumaker DK, Solimando L, et al. Nuclear lamins: major factors in the structural organization and function of the nucleus and chromatin. Genes Dev. 2008;22(7):832-53.

90.   Callan HG, Tomlin SG. Experimental studies on amphibian oocyte nuclei. I. Investigation of the structure of the nuclear membrane by means of the electron microscope. Proc R Soc Lond B Biol Sci. 1950;137(888):367-78.

91.   Tran EJ, Wente SR. Dynamic nuclear pore complexes: life on the edge. Cell. 2006;125(6):1041-53.

92.   D'Angelo MA, Hetzer MW. Structure, dynamics and function of nuclear pore complexes. Trends Cell Biol. 2008;18(10):456-66.

93.   Starr DA, Han M. ANChors away: an actin based mechanism of nuclear positioning. J Cell Sci. 2003;116(Pt 2):211-6.

94.   Wilhelmsen K, Ketema M, Truong H, Sonnenberg A. KASH-domain proteins in nuclear migration, anchorage and other processes. J Cell Sci. 2006;119(Pt 24):5021-9.

95.   Wilhelmsen K, Litjens SH, Kuikman I, Tshimbalanga N, Janssen H, van den Bout I, et al. Nesprin-3, a novel outer nuclear membrane protein, associates with the cytoskeletal linker protein plectin. J Cell Biol. 1712005. p. 799-810.

96.   Fridkin A, Penkner A, Jantsch V, Gruenbaum Y. SUN-domain and KASH-domain proteins during development, meiosis and disease. Cell Mol Life Sci. 2009;66(9):1518-33.

97.   Schirmer ECaGL. The nuclear membrane proteome: Extending the envelope. Trends in Biochemical Sciences. 2005;30(10):551--8.

98.   Akhtar A, Gasser SM. The nuclear envelope and transcriptional control. Nat Rev Genet. 2007;8(7):507-17.

99.   Dorner D, Gotzmann J, Foisner R. Nucleoplasmic lamins and their interaction partners, LAP2alpha, Rb, and BAF, in transcriptional regulation. Febs j. 2007;274(6):1362-73.

100.   Schirmer EC, Foisner R. Proteins that associate with lamins: many faces, many functions. Exp Cell Res. 2007;313(10):2167-79.

101.   Mattout A, Dechat T, Adam SA, Goldman RD, Gruenbaum Y. Nuclear lamins, diseases and aging. Curr Opin Cell Biol. 2006;18(3):335-41.

102.   Heessen S, Fornerod M. The inner nuclear envelope as a transcription factor resting place. EMBO Rep. 2007;8(10):914-9.

103.   Reddy KL, Zullo JM, Bertolino E, Singh H. Transcriptional repression mediated by repositioning of genes to the nuclear lamina. Nature. 2008;452(7184):243-7.

104.   Vlcek S, Foisner R. Lamins and lamin-associated proteins in aging and disease. Curr Opin Cell Biol. 2007;19(3):298-304.

105.   Worman HJ, Bonne G. "Laminopathies": a wide spectrum of human diseases. Exp Cell Res. 2007;313(10):2121-33.

106.   Neilan EG. Laminopathies, other progeroid disorders, and aging: common pathogenic themes and possible treatments. Am J Med Genet A. 2009;149a(4):563-6.

107.   Voeltz GK, Prinz WA. Sheets, ribbons and tubules - how organelles get their shape. Nat Rev Mol Cell Biol. 8. England2007. p. 258-64.

108.   Tzur YB, Wilson KL, Gruenbaum Y. SUN-domain proteins: 'Velcro' that links the nucleoskeleton to the cytoskeleton. Nat Rev Mol Cell Biol. 7. England2006. p. 782-8.

109.   Stewart CL, Roux KJ, Burke B. Blurring the boundary: the nuclear envelope extends its reach. Science. 2007;318(5855):1408-12.

110.   Gruenbaum Y, Wilson KL, Harel A, Goldberg M, Cohen M. Review: nuclear lamins--structural proteins with fundamental functions. J Struct Biol. 2000;129(2-3):313-23.

111.   Cohen TV, Hernandez L, Stewart CL. Functions of the nuclear envelope and lamina in development and disease. Biochem Soc Trans. 2008;36(Pt 6):1329-34.

112.   Gruenbaum Y, Margalit A, Goldman RD, Shumaker DK, Wilson KL. The nuclear lamina comes of age. Nat Rev Mol Cell Biol. 2005;6(1):21-31.

113.   Mounkes LC, Kozlov S, Hernandez L, Sullivan T, Stewart CL. A progeroid syndrome in mice is caused by defects in A-type lamins. Nature. 2003;423(6937):298-301.

114.   Muchir aaWHJ. The nuclear envelope and human disease. Physiology (Bethesda). 2004;19(Journal Article):309--14.

115.   Scaffidi P, Misteli T. Lamin A-dependent nuclear defects in human aging. Science. 2006;312(5776):1059-63.

116.   D'Angelo MA, Hetzer MW. The role of the nuclear envelope in cellular organization. Cell Mol Life Sci. 2006;63(3):316-32.

117.   Fricker MaHMaWNaVD. Interphase nuclei of many mammalian cell types contain deep, dynamic, tubular membrane-bound invaginations of the nuclear envelope. Journal of Cell Biology. 1997;136(3):531--44.

118.   Schermelleh L, Carlton PM, Haase S, Shao L, Winoto L, Kner P, et al. Subdiffraction multicolor imaging of the nuclear periphery with 3D structured illumination microscopy. Science. 2008;320(5881):1332-6.

119.   Prufert K, Alsheimer M, Benavente R, Krohne G. The myristoylation site of meiotic lamin C2 promotes local nuclear membrane growth and the formation of intranuclear membranes in somatic cultured cells. Eur J Cell Biol. 2005;84(6):637-46.

120.   Bourgeois CA, Hemon D, Bouteille M. Structural relationship between the nucleolus and the nuclear envelope. J Ultrastruct Res. 1979;68(3):328-40.

121.   Broers JL, Machiels BM, van Eys GJ, Kuijpers HJ, Manders EM, van Driel R, et al. Dynamics of the nuclear lamina as monitored by GFP-tagged A-type lamins. J Cell Sci. 1999;112 (Pt 20):3463-75.

122.   Johnson N, Krebs M, Boudreau R, Giorgi G, LeGros M, Larabell C. Actin-filled nuclear invaginations indicate degree of cell de-differentiation. Differentiation. 2003;71(7):414-24.

123.   Storch KN, Taatjes DJ, Bouffard NA, Locknar S, Bishop NM, Langevin HM. Alpha smooth muscle actin distribution in cytoplasm and nuclear invaginations of connective tissue fibroblasts. Histochem Cell Biol. 2007;127(5):523-30.

124.   Hu S, Chen J, Butler JP, Wang N. Prestress mediates force propagation into the nucleus. Biochem Biophys Res Commun. 2005;329(2):423-8.

125.   Ingber DE. Cellular mechanotransduction: putting all the pieces together again. Faseb j. 2006;20(7):811-27.

126.   Houben F, Ramaekers FC, Snoeckx LH, Broers JL. Role of nuclear lamina-cytoskeleton interactions in the maintenance of cellular strength. Biochim Biophys Acta. 2007;1773(5):675-86.

127.   Crisp M, Liu Q, Roux K, Rattner JB, Shanahan C, Burke B, et al. Coupling of the nucleus and cytoplasm: role of the LINC complex. J Cell Biol. 2006;172(1):41-53.

128.   Langevin HM, Storch KN, Snapp RR, Bouffard NA, Badger GJ, Howe AK, et al. Tissue stretch induces nuclear remodeling in connective tissue fibroblasts. Histochem Cell Biol. 2010;133(4):405-15.

129.   Ji JY, Lee RT, Vergnes L, Fong LG, Stewart CL, Reue K, et al. Cell nuclei spin in the absence of lamin b1. J Biol Chem. 2007;282(27):20015-26.

130. Broers JL, Ramaekers FC, Bonne G, Yaou RB, Hutchison CJ. Nuclear lamins: laminopathies and their role in premature ageing. Physiol Rev. 2006;86(3):967-1008.

131. Gehrig K, Lagace TA, Ridgway ND. Oxysterol activation of phosphatidylcholine synthesis involves CTP:phosphocholine cytidylyltransferase alpha translocation to the nuclear envelope. Biochem J. 2009;418(1):209-17.

132. Drozdz MM, Jiang H, Pytowski L, Grovenor C, Vaux DJ. Formation of a nucleoplasmic reticulum requires de novo assembly of nascent phospholipids and shows preferential incorporation of nascent lamins. Sci Rep. 2017;7(1):7454.

133. Fischer AH, Taysavang P, Jhiang SM. Nuclear envelope irregularity is induced by RET/PTC during interphase. Am J Pathol. 2003;163(3):1091-100.

134. Fischer AHaBSaJZ. Molecular aspects of diagnostic nucleolar and nuclear envelope changes in prostate cancer. Journal of Cellular Biochemistry. 2004;91(1):170--84.

135. Sarkar D, Emdad L, Lee SG, Yoo BK, Su ZZ, Fisher PB. Astrocyte elevated gene-1: far more than just a gene regulated in astrocytes. Cancer Res. 2009;69(22):8529-35.

136. Chow K-HaFREaUKS. The nuclear envelope environment and its cancer connections. Nature reviews Cancer. 2012;12(3):196--209.

137. Fry. The nuclear envelope in mammalian cells. 1977.

138. Ledeen RW, Wu G. Nuclear lipids: key signaling effectors in the nervous system and other tissues. J Lipid Res. 2004;45(1):1-8.

139. Birnie GD. Subnuclear components, preparation and fractionation. Butterworth-Heinemann; 1976.

140. Khandwala AS, Kasper CB. The fatty acid composition of individual phospholipids from rat liver nuclear membrane and nuclei. J Biol Chem. 1971;246(20):6242-6.

141. Zambrano F, Fleischer S, Fleischer B. Lipid composition of the Golgi apparatus of rat kidney and liver in comparison with other subcellular organelles. Biochim Biophys Acta. 1975;380(3):357-69.

142. Schindler M, Holland JF, Hogan M. Lateral diffusion in nuclear membranes. J Cell Biol. 1985;100(5):1408-14.

143. Alroy J, Merk FB, Goyal V, Ucci A. Heterogeneous distribution of filipin-sterol complexes in nuclear membranes. Biochim Biophys Acta. 1981;649(2):239-43.

144. Harayama T, Riezman H. Understanding the diversity of membrane lipid composition. Nat Rev Mol Cell Biol. 2018;19(5):281-96.

145. Burke BaGL. A cell free system to study reassembly of the nuclear envelope at the end of mitosis. Cell. 1986;44(4):639--52.

146. Lohka MJ, Masui Y. Formation in vitro of sperm pronuclei and mitotic chromosomes induced by amphibian ooplasmic components. Science. 1983;220(4598):719-21.

147. Cameron LA, Poccia DL. In vitro development of the sea urchin male pronucleus. Dev Biol. 1994;162(2):568-78.

148. Zhao Y, Liu X, Wu M, Tao W, Zhai Z. In vitro nuclear reconstitution could be induced in a plant cell-free system. FEBS Lett. 2000;480(2-3):208-12.

149. Lu P, Zhai ZH. Nuclear assembly of demembranated Xenopus sperm in plant cell-free extracts from Nicotiana ovules. Exp Cell Res. 2001;270(1):96-101.

150. Prunuske AJaUKS. The nuclear envelope: Form and reformation. Current Opinion in Cell Biology. 2006;18(1):108--16.

151. Buendia B, Courvalin JC, Collas P. Dynamics of the nuclear envelope at mitosis and during apoptosis. Cell Mol Life Sci. 2001;58(12-13):1781-9.

152.   Burke B, Ellenberg J. Remodelling the walls of the nucleus. Nat Rev Mol Cell Biol. 2002;3(7):487-97.

153.   Crisp M, Burke B. The nuclear envelope as an integrator of nuclear and cytoplasmic architecture. FEBS Lett. 2008;582(14):2023-32.

154.   Webster MaWKLaC-FO. Sizing up the nucleus: nuclear shape, size and nuclear-envelope assembly. Journal of cell science. 2009;122(Pt 10):1477--86.

155.   Webster M, Witkin KL, Cohen-Fix O. Sizing up the nucleus: nuclear shape, size and nuclear-envelope assembly. J Cell Sci. 2009;122(Pt 10):1477-86.

156.   Anderson DJ, Hetzer MW. Reshaping of the endoplasmic reticulum limits the rate for nuclear envelope formation. J Cell Biol. 2008;182(5):911-24.

157.   Baur T, Ramadan K, Schlundt A, Kartenbeck J, Meyer HH. NSF- and SNARE-mediated membrane fusion is required for nuclear envelope formation and completion of nuclear pore complex assembly in Xenopus laevis egg extracts. J Cell Sci. 2007;120(Pt 16):2895-903.

158.   Gant TMaWKL. Nuclear Envelope Structure and Dynamics. 1997.

159.   Sodergren EaWGaDEHaCRaaGRaaARCaALM. The genome of the sea urchin Strongylocentrotus purpuratus. Science. 2006;314(5801):941--52.

160.   Collas P, Poccia D. Lipophilic organizing structures of sperm nuclei target membrane vesicle binding and are incorporated into the nuclear envelope. Dev Biol. 1995;169(1):123-35.

161.   Collas P, Poccia D. Distinct egg membrane vesicles differing in binding and fusion properties contribute to sea urchin male pronuclear envelopes formed in vitro. J Cell Sci. 1996;109 (Pt 6):1275-83.

162.   Dumas FaBRDaVBaHTMCaPDLaLB. Spatial regulation of membrane fusion controlled by modification of phosphoinositides. PLoS ONE. 2010;5(8):e12208.

163.   Garnier-Lhomme MaBRDaHTMCaGSaWRaPDLaDEJaL. Nuclear envelope remnants: Fluid membranes enriched in STEROLS and polyphosphoinositides. PLoS ONE. 2009;4(1):e4255.

164.   Byrne RDaBTMaGMaKGaKMaPDLaLB. Nuclear envelope assembly is promoted by phosphoinositide-specific phospholipase C with selective recruitment of phosphatidylinositol-enriched membranes. The Biochemical journal. 2005;387(Pt 2):393--400.

165.   Byrne RDaG-LMaHKaDMaMNaTNaZVaCAaPTRa. PLCγ is enriched on poly-phosphoinositide-rich vesicles to control nuclear envelope assembly. Cellular Signalling. 2007;19(5):913--22.

166.   Zhendre VaGAaG-LMaBSaLBaDEJ. Key role of polyphosphoinositides in dynamics of fusogenic nuclear membrane vesicles. PLoS ONE. 2011;6(9):e23859.

167.   Basanez G, Nieva JL, Rivas E, Alonso A, Goni FM. Diacylglycerol and the promotion of lamellar-hexagonal and lamellar-isotropic phase transitions in lipids: implications for membrane fusion. Biophys J. 1996;70(5):2299-306.

168.   Collas P, Poccia DL. Formation of the sea urchin male pronucleus in vitro: membrane-independent chromatin decondensation and nuclear envelope-dependent nuclear swelling. Mol Reprod Dev. 1995;42(1):106-13.

169.   Collas P, Pinto-Correia C, Poccia DL. Lamin dynamics during sea urchin male pronuclear formation in vitro. Exp Cell Res. 1995;219(2):687-98.

170.   Gutiérrez Lete M. Phosphoinositides: interaction with histones and their role in nuclear envelope assembly: Universidad del País Vasco (UPV/EHU); 2014.

171.   Hetzer MW. The nuclear envelope. Cold Spring Harbor perspectives in biology. 2010;2(3):a000539.

172.   Larijani BaDEJ. Polyunsaturated phosphatidylinositol and diacylglycerol substantially modify the fluidity and polymorphism of biomembranes: A solid-state deuterium NMR study. Lipids. 2006;41(10):925--32.

173.   Chung GHC, Domart MC, Peddie C, Mantell J, McLaverty K, Arabiotorre A, et al. Acute depletion of diacylglycerol from the cis-Golgi affects localized nuclear envelope morphology during mitosis. Journal of Lipid Research. 2018;59(8):1402-13.

174.   Somech R, Shaklai S, Amariglio N, Rechavi G, Simon AJ. Nuclear envelopathies--raising the nuclear veil. Pediatr Res. 2005;57(5 Pt 2):8r-15r.

175.   Zink DaFAHaNJa. Nuclear structure in cancer cells. Nature Reviews Cancer. 2004;4(9):677--87.

176.   Schindler M, Holland JF, Hogan M. LATERAL DIFFUSION IN NUCLEAR-MEMBRANES. Journal of Cell Biology. 1985;100(5):1408-14.

177.   Wilkie GS, Schirmer EC. Purification of nuclei and preparation of nuclear envelopes from skeletal muscle. Methods Mol Biol. 2008;463:23-41.

178.   Ho C, Lam C, Chan M, Cheung R, Law L, Lit L, et al. Electrospray Ionisation Mass Spectrometry: Principles and Clinical Applications. Clin Biochem Rev. 242003. p. 3-12.

179.   https://docplayer.net/49298579-Ab-sciex-triple-quad-5500-system-today-s-most-sensitive-and-selective-triple-quadrupole.html [

180.   Bure C, Ayciriex S, Testet E, Schmitter JM. A single run LC-MS/MS method for phospholipidomics. Analytical and Bioanalytical Chemistry. 2013;405(1):203-13.

181.   Abragam A, Hebel LC. The Principles of Nuclear Magnetism. American Journal of Physics 1961. p. 860-1.

182.   Loudet C. Les Biphényles: un nouveau modèle de biomembrane pour l'étude de protéines membranes par RMN des solides. . Université de Bordeaux 1: Thesis; 2006. p. 264.

183.   Mehring M. Principles of high resolution NMR in solids. Berlin: Springer-Verlag; 1983.

184.   Dufourc EJ, Mayer C, Stohrer J, Althoff G, Kothe G. Dynamics of phosphate head groups in biomembranes. Comprehensive analysis using phosphorus-31 nuclear magnetic resonance lineshape and relaxation time measurements. Biophys J. 1992;61(1):42-57.

185.   Dufourc E. La résonance magnétique nucléaire du deutérium et du phosphore dans les milieux organisés. Théorie et applications à l'étude de l'action de la mélittinine et de la delta-lysine sur les membrane biologique Bordeaux, Université de Bordeaux 1: Thèse d'état ès Sciences: 245 1986.

186.   Davis JH. The description of membrane lipid conformation, order and dynamics by 2H-NMR. Biochim Biophys Acta. 1983;737(1):117-71.

187.   Seelig J. Deuterium magnetic resonance: theory and application to lipid membranes. Q Rev Biophys. 1977;10(3):353-418.

188.   Seelig J, Borle F, Cross TA. Magnetic-Ordering of Phospholipid-Membranes. Biochimica Et Biophysica Acta. 1985;814(1):195-8.

189.   Helfrich W. Lipid Bilayer Spheres - Deformation and Birefringence in Magnetic-Fields. Physics Letters A. 1973;A 43(5):409-10.

190.   Helfrich W. Elastic properties of lipid bilayers - Theory and possible experiments. Zeitschrift Fur Naturforschung C-a Journal of Biosciences. 1973;C 28(11-1):693-703.

191.   Pott T, Dufourc EJ. Action of melittin on the DPPC-cholesterol liquid-ordered phase - A solid state H-2 NMR and P-31-NMR study. Biophysical Journal. 1995;68(3):965-77.

192.   Rance MaBRA. Obtaining high-fidelity powder spectra in anisotropic media: Phase-cycled Hahn echo spectroscopy. Journal of Magnetic Resonance. 1983;52(2):221--40.

193.   Davis JHHaJKRaBMaVMIIaHTPPaJKR. Quadrupolar echo deuteron magnetic resonance spectroscopy in ordered hydrocarbon chains. Chemical Physics Letters. 1976;42(2):390--4.

194.   Davis JH, Jeffrey KR, Bloom M, Valic MI, Higgs TP. Quadrupolar Echo Deuteron Magnetic-Resonance Spectroscopy in Ordered Hydrocarbon Chains. Chemical Physics Letters. 1976;42(2):390-4.

195.   Garnier-Lhomme M, Byrne RD, Hobday TMC, Gschmeissner S, Woscholski R, Poccia DL, et al. Nuclear Envelope Remnants: Fluid Membranes Enriched in STEROLS and Polyphosphoinositides. Plos One. 2009;4(1):12.

196.   Fischer AH, Taysavang P, Jhiang SM. Nuclear envelope irregularity is induced by RET/PTC during interphase. American Journal of Pathology. 2003;163(3):1091-100.

197.   Fischer AH, Bardarov S, Jiang Z. Molecular aspects of diagnostic nucleolar and nuclear envelope changes in prostate cancer. Journal of Cellular Biochemistry. 2004;91(1):170-84.

198.   Sarkar D, Emdad L, Lee SG, Yoo BK, Su ZZ, Fisher PB. Astrocyte Elevated Gene-1: Far More Than Just a Gene Regulated in Astrocytes. Cancer Research. 2009;69(22):8529-35.

199.   Fiske CH, Subbarow Y. The colorimetric determination of phosphorus. J Biol Chem. 1925;66(2):375-400.

200.   Beck JG, Mathieu D, Loudet C, Buchoux S, Dufourc EJ. Plant sterols in "rafts": a better way to regulate membrane thermal shocks. Faseb J. 2007;21(8):1714-23.

201.   Davis JH. The Description of Membrane Lipid Conformation, Order and Dynamics by 2H-NMR. Biochimica Et Biophysica Acta. 1983;737(1):117-71.

202.   Furlan AL, Jobin ML, Buchoux S, Grelard A, Dufourc EJ, Gean J. Membrane lipids protected from oxidation by red wine tannins: A proton NMR study. Biochimie. 2014;107:82-90.

203.   Douliez JP, Leonard A, Dufourc EJ. Restatement of Order Parameters in Biomembranes - Calculation of C-C Bond Order Parameters from C-D Quadrupolar Splittings. Biophys J. 1995;68(5):1727-39.

204.   Douliez JP, Leonard A, Dufourc EJ. Conformational order of DMPC sn-1 versus sn-2 chains and membrane thickness: An approach to molecular protrusion by solid state H-2-NMR and neutron diffraction. J Phys Chem. 1996;100(47):18450-7.

205.   Burnett LJ, Muller BH. Deuteron Quadrupole Coupling Constants in 3 Solid Deuterated Paraffin Hydrocarbons-C2D6, C4D10, C6D14. J Chem Phys. 1971;55(12):5829-&.

206.   Douliez JP, Leonard A, Dufourc EJ. Restatement of order parameters in biomembranes: calculation of C-C bond order parameters from C-D quadrupolar splittings. Biophysical Journal. 1995;68(5):1727-39.

207.   Pott T, Dufourc EJ. Action of Melittin on the DPPC-Cholesterol Liquid-Ordered Phase - A Solid-State 2H-NMR and P-31-NMR Study. Biophys J. 1995;68(3):965-77.

208.   Meier P, Sachse JH, Brophy PJ, Marsh D, Kothe G. INTEGRAL MEMBRANE-PROTEINS SIGNIFICANTLY DECREASE THE MOLECULAR-MOTION IN LIPID BILAYERS - A DEUTERON NMR RELAXATION STUDY OF MEMBRANES CONTAINING MYELIN PROTEOLIPID APOPROTEIN. Proceedings of the National Academy of Sciences of the United States of America. 1987;84(11):3704-8.

209.   Bradford MM. Rapid and Sensitive Method for Quantitation of Microgram Quantities of Protein Utilizing Principle of Protein-Dye Binding. Anal Biochem. 1976;72(1-2):248-54.

210.   Towbin H, Gordon J. Immunoblotting and Dot Immunobinding - Current Status and Outlook. Journal of Immunological Methods. 1984;72(2):313-40.

211.   Wakelam MJO, Pettitt TR, Postle AD. Lipidomic analysis of signaling pathways. Lipidomics and Bioactive Lipids: Mass-Spectrometry-Based Lipid Analysis. 2007;432:233-46.

212.   Larijani B, Poccia DL, Dickinson LC. Phospholipid identification and quantification of membrane vesicle subfractions by P-31-H-1 two-dimensional nuclear magnetic resonance. Lipids. 2000;35(11):1289-97.

213.   Crisp M, Liu Q, Roux K, Rattner JB, Shanahan C, Burke B, et al. Coupling of the nucleus and cytoplasm: role of the LINC complex. Journal of Cell Biology. 2006;172(1):41-53.

214.   Zambrano F, Fleischer S, Fleischer B. Lipid-Composition of Golgi Apparatus of Rat-Kidney and Liver in Comparison with other Subcellular Organelles. Biochimica Et Biophysica Acta. 1975;380(3):357-69.

215.   Birnie GD. Subnuclear Components. Butterworth, editor1976.

216.   Blobel G, Potter VR. Nuclei from Rat Liver - Isolation Method that Combines Purity with High Yield. Science. 1966;154(3757):1662-&.

217.   Domart MC, Hobday TMC, Peddie CJ, Chung GHC, Wang A, Yeh K, et al. Acute Manipulation of Diacylglycerol Reveals Roles in Nuclear Envelope Assembly & Endoplasmic Reticulum Morphology. Plos One. 2012;7(12):14.

218.   Gao XL, Zhang QB, Meng D, Isaac G, Zhao R, Fillmore TL, et al. A reversed-phase capillary ultra-performance liquid chromatography-mass spectrometry (UPLC-MS) method for comprehensive top-down/bottom-up lipid profiling. Analytical and Bioanalytical Chemistry. 2012;402(9):2923-33.

219.   Collas P, Poccia D. Distinct egg membrane vesicles differing in binding and fusion properties contribute to sea urchin male pronuclear envelopes formed in vitro. Journal of Cell Science. 1996;109:1275-83.

220.   Zink D, Fischer AH, Nickerson JA. Nuclear structure in cancer cells. Nature Reviews Cancer. 2004;4(9):677-87.

221.   Hagen C, Werner S, Carregal-Romero S, Malhas AN, Klupp BG, Guttmann P, et al. Multimodal nanoparticles as alignment and correlation markers in fluorescence/soft X-ray cryo-microscopy/tomography of nucleoplasmic reticulum and apoptosis in mammalian cells. Ultramicroscopy. 2014;146:46-54.

222.   Collas P. Nuclear envelope disassembly in mitotic extract requires functional nuclear pores and a nuclear lamina. Journal of Cell Science. 1998;111:1293-303.